2008

XYLARIC ACID, D-ARABINARIC ACID (D-LYXARIC ACID), L-ARABINARIC ACID (L-LYXARIC ACID), AND RIBARIC ACID-1,4-LACTONE; SYNTHESIS AND ISOLATION - SYNTHESIS OF POLYHYDROXYPOLYAMIDES THEREFROM

Michael Raymond Hinton
The University of Montana

XYLARIC ACID, D–ARABINARIC ACID (D-LYXARIC ACID), L-ARABINARIC ACID (L-LYXARIC ACID), AND RIBARIC ACID-1,4-LACTONE; SYNTHESIS AND ISOLATION – SYNTHESIS OF POLYHYDROXYPOLYAMIDES THEREFROM

By
Michael Raymond Hinton

Bachalors in Chemistry, Bellarmine University, Louisville, KY. 2003
Minor in Biology, Bellarmine University, Louisville, KY. 2003

presented in partial fulfillment of the requirements
for the degree of

Doctorate of Philosophy
in Chemistry

The University of Montana
Missoula, Montana

Autumn 2008
Approved by:

Perry Brown
Associate Provost for Graduate Education

Donald E. Kiely, Ph.D. Advisor/Chair
Chemistry

Merilyn Manley-Harris, Ph.D.
Chemistry, University of Waikato, NZ

Michael K. Dowd, Ph.D.
United States Department of Agriculture

Michael D. Degrandpre, Ph.D.
Chemistry

J. Stephen Lodmell, Ph.D.
Division of Biological Sciences

Edward E. Waali, Ph.D.
Chemistry

Hinton, Michael, Doctorate of Philosophy, 2008 Chemistry

Donald E. Kiely, Ph.D.

This dissertation describes the nitric acid oxidation of the pentoses D-xylose, L-arabinose, D-arabinose, and D-ribose to produce xylaric acid, L-arabinaric acid (L-lyxaric acid), D-arabinaric acid (D-lyxaric acid), and ribaric acid, respectively, or salts therefrom. Isolation of the aldaric acids from nitric acid has proven difficult in prior reports and an improved nitric acid oxidation and isolation method for each aldaric acid is described.

Aldaric acids are the starting monomers for a class of polymers known as polyhydroxypolyamides (PHPAs) or "hydroxylated nylons," produced through condensation polymerization of the esterified aldaric acid and a diamine of choice. In an effort to obtain larger polymers synthetic routes were varied to initially produce smaller polyamides labeled as "prepolymers." Of these prepolymers, poly (hexamethylene xylaramide) was subjected to three post production treatments to further increase their size.

Additionally, in an effort to better predict physical and chemical properties and potential applications of PHPAs, the conformation of the aldaryl monomer units in solution were investigated using ^{1}H NMR, and molecular mechanics modeling. Limitations inherent to ^{1}H NMR and MM3(96) computational modeling required the use of glutaramides and pentaramides as small molecule mimics of the PHPA's aldaryl monomer unit. A converging Monte Carlo Metropolis search coupled to MM3(96) was employed to search the conformational space afforded the diamides. A Boltzmann distribution was applied to the resultant conformational ensemble which was analyzed for structural detail. Theoretical average ^{1}H vicinal coupling constants were compared to experimental ^{1}H NMR coupling constants. Dependence of experimental ^{1}H NMR coupling constants on solvent composition was investigated. MM3(96) lowest energy conformations of the diamides had structural detail consistent with their corresponding ^{1}H NMR and x-ray crystal data.

Acknowledgements

I would like to thank my advisors Dr. Donald E. Kiely, Dr. Merilyn Manley-Harris, and Dr. Michael K. Dowd, especially Dr. Kiely for initiating my project and giving his guidance and support for my education both inside and outside the academic arena. The support was invaluable and I am forever indebted.

Dr. Merilyn Manley-Harris must be thanked for her support during my time studying at the University of Waikato in Hamilton, New Zealand. She not only guided my research but my explorations of New Zealand's wonderful culture and countryside as well.

Dr. Michael K. Dowd has given me great support and explanation of molecular modeling simulations without which my computational modeling would not have been possible.

Professor Brian Nicholson has given me the tools necessary to explore X-ray crystallography and many thanks must be bestowed upon him for helping me solve my structures.

Thank you to Professor Allister Wilkens for demonstrating the power of nuclear magnetic resonance spectroscopy.

I am especially appreciative of me colleagues in the Shafizadeh Rocky Mountain Center for Wood and Carbohydrate Research, University of Montana. They include Chrissie A. Carpenter, Tyler Smith, Kylie Presta, Kirk Hash Sr., Kendra Davis, Dan Shirley, Holly Williams, and Bevan Jarmen.

Finally my parents and family must be thanked for their support. Their encouragement to carry on through difficult times will always be remembered.

Table of Contents

List of Tables

List of Figures

PHPA	Polyhydroxypolyamide
NMR	Nuclear Magnetic Resonance
MM3	Molecular Mechanics 3
^{1}H NMR	Proton NMR
^{13}C NMR	Carbon 13 NMR
MP	Melting Point
w/w	weight by weight
HCl	Hydrochloric Acid
NaOH	Sodium Hydroxide
EtOH	Ethanol
MeOH	Methanol
GC	Gas Chromatography
FID	Flame Ionization Detector
MS	Mass Spectroscopy
NIST	National Institute of Standards and Technology
DMSO-d_6	Deuterated DMSO
1D NOESY	One dimensional Nuclear Overhauser Enhancement Spectroscopy
ACS	American Chemical Society
HPLC	High Performance Liquid Chromatography
RI	Refractive Index
IC	Ion Chromatography
h	Hour
min.	minute
mL	milliliters
L	Liter
Mg	milligram
g	gram
D_2O	Dueterated water
M	Molar
Mmol	Millimole
dec.	decompose
lit.	literature
b/w	by weight
m/z	mass to charge ratio
LRMS	Low resolution mass spectroscopy
DNA	Deoxyribonucleic Acid
RNA	Ribonucleic Acid
DP	Degrees of Polymerization
M_n	Number average molecular weight
N_i	Number of polymer chains
M_i	Molar mass of polymer chain
M_r	Molecular weight of repeating unit

n	number of repeating units
Conc.	Concentrate
TEA	Triethylamine
EG	Ethylene Glycol
DMSO	Dimethyl Sulfoxide
Chloroform-*d*	Deuterated Chloroform
TFA-*d*	Dueterated Trifluoroacetic Acid
TFA	Trifluoroacetic Acid
GPC	Gel Permeation Chromatography
NaOMe	Sodium Methoxide
ppm	parts per million
Hz	Hertz
t	triplet
m	multiplet
s	singlet
Kcal	Kilocalarie
Mol	Mole
T	*trans*
G	*gauche*
DIELEC	Dielectric Constant
E	Energy
R	Gas Constant
P	Probability
N_a	Molar ratio of conformer a
N_o	Molar ration of conformer o
P_a	Percent population of conformer a
X_i	Percent population of conformer a
J	coupling constant
Å	Angstroms
MHz	Megahertz
K	Kelvin
C	Celcius
α	alpha
β	beta
δ	delta
γ	gamma
º	degrees
H_2O	water
CCD	Cambridge Crystal Database
Mo-Ka	Molybdenum Potassium alpha radiation
r.t.	Room Temperature
RO	Reverse Osmosis

1. Nitric Acid Oxidation of D-Xylose, D-Arabinose, L-Arabinose, and D-Ribose to Xylaric, D-Arabinaric (D-Lyxaric), L-Arabinaric (L-Lyxaric), and Ribaric Acids

1.1 Introduction

The overall goal of the research in this dissertation is directed towards the synthesis of polyhydroxypolyamides (PHPAs) from monomer pentaric acids and alkylenediamines employing condensation polymerization methods. As none of the four possible stereoisomeric pentaric acids were commercially available they were targeted for synthesis from the appropriate aldopentoses. The target pentaric acids were: xylaric acid (**1**), D-arabinaric acid (D-lyxaric acid) (**2**), L-lyxaric acid (L-arabinaric acid) (**3**), and ribaric acid (**4**) (Figure 1.1). Every possible pentaric acid stereoisomer has been synthesized; xylaric acid and ribaric acid are *meso* compounds, D-arabinaric and D-lyxaric acids are identical with L-arabinaric and L-lyxaric acids, and the two identical as their respective enantiomers L-arabinaric and L-lyxaric acids. The nitric acid oxidation of the aldopentoses, D-xylose, D-arabinose, L-arabinose, and D-ribose to their pentaric acids is described in this report.

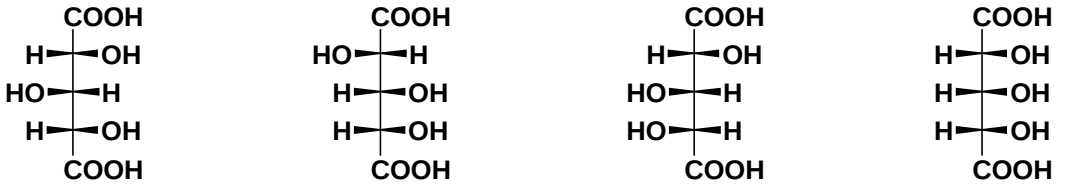

Xylaric Acid (1)

D-Arabinaric Acid (D-Lyxaric Acid) (2)

L-Lyxaric Acid (L-Arabinaric Acid) (3)

Ribaric Acid (4)

Figure 1.1 Four aldaric acids derived from aldopentoses

1.1.1 D-Xylose, L-Arabinose, D-Arabinose, and D-Ribose

D-Xylose, L-arabinose, D-arabinose, and D-ribose (Figure 1.2) are naturally occurring aldopentoses with the chemical formula $C_5H_{10}O_5$, and commonly occur in their pyranose and/or furanose ring forms as illustrated for D-xylose in Figure 1.3. Their commercial availability arises from acid, base, or enzymatic hydrolysis of hemicellulose with subsequent purification of the monosaccharide. The hemicellulose can be any of several heteropolymers present in the cell wall of plants.

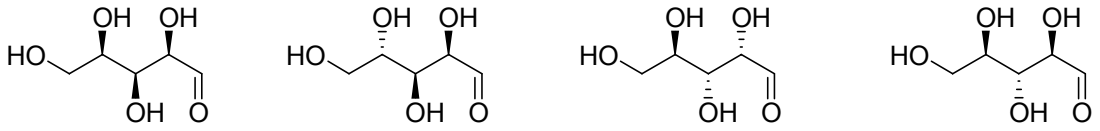

D-Xylose L-Arabinose D-Arabinose D-Ribose

Figure 1.2 Acyclic structures of D-xylose, L-arabinose, D-arabinose, and D-ribose showing differences in stereochemistry along the carbohydrate backbone

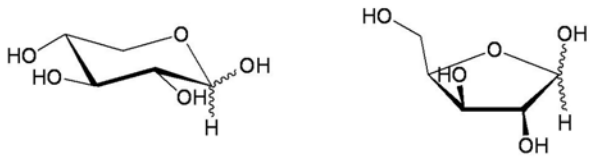

α/β D-xylopyranose α/β D-xylofuranose

Figure 1.3 Cyclic forms of D-xylose

Improved methods for the nitric acid oxidation of the aforementioned monosaccharides to their aldaric (pentaric) acid forms (Figure 1.4) or corresponding salts are described. Historically, nitric acid oxidations of monosaccharides have resulted in poor yields of aldaric acids contaminated with side products, due to the difficulty of removing the nitric acid from the aldaric acid product and to the relatively harsh reaction

conditions employed. As a result, multiple chemical transformations of the aldaric acids have been employed to eliminate impurities with subsequent regeneration of the desired pure aldaric acid or salt. The literature relating to the oxidations of aldopentoses is reviewed in sec 1.1.2. The improved methods of oxidation and isolation relative to methods reported in the literature are given in the Results and Discussion, Section 1.2 pg.24.

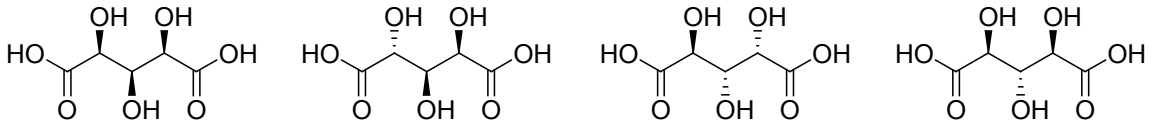

Xylaric Acid | L-Arabinaric Acid (L-Lyxaric Acid) | D-Arabinaric acid (D-Lyxaric Acid) | Ribaric Acid

Figure 1.4 Aldaric acid oxidation products of D-xylose, L-arabinose, D-arabinose, and D-ribose

1.1.2 Oxidation of Aldopentoses to Aldaric Acids

1.1.2.1 Nitric Acid Oxidation of Aldopentoses and Alditol to Aldaric Acids

Kiliani first reported the nitric acid oxidation of pentoses in 1889.[1] Both D-xylose and D-arabinose were oxidized and their respective diacids isolated as their calcium salts. Hardegger and co-workers[2] also reported nitric acid oxidation of D-arabinose; the product was isolated as 2,3,4-tri-*O*-acetyl-D-arabinaramide, following removal of the acetate groups to give D-arabinaramide. Whistler and coworkers [3] reported the nitric acid oxidation of D-xylose according to the method of N.V. Chalov (1948)[4] and xylaric acid was isolated as its crystalline zinc salt (III) in a yield of 53.5 %. Cantrell *et al.*[5] reported the nitric acid oxidation of an aqueous solution of D-xylose to yield xylaric acid in a yield of 44 %. Kiely *et al*.[6] described the nitric acid oxidation of aqueous D-xylose, wherein oxygen was bubbled into the reaction mixture during the oxidation and crude

xylaric acid was isolated as a fine powder in 83.1% yield. No assessment of purity was reported. Williams and co-workers reported the nitric acid oxidation of D-arabinitol and isolation of D-arabinaric acid, however the isolation procedure was not fully detailed and the product was heavily contaminated with oxalic acid.[7] The yield of D-arabinaric acid relative to D-arabinitol was 9.78 %.

1.1.2.2 Alkaline Oxidation of D-Xylose to Aldaric Acids

Fleche reported the preparation of xylaric acid by the degradative oxidation of 5-ketogluconic acid in alkaline medium.[8] A crude product containing sodium salts of xylaric, formic, glycolic, glyceric, tartaric, malic, and tartronic acid and disodium sulphate was isolated with a molar yield of 51.4 % sodium xylarate, relative to the 5-ketogluconate. Subsequent isolation of xylaric acid was reported as 99.2 % pure, mp 145 °C, but no yield was reported.

1.2 Results and Discussion

1.2.1 Oxidations of D-xylose, D-arabinose, L-arabinose, and D-ribose

The oxidation of monosaccharides in nitric acid is an exothermic reaction. Without a method to control the temperature of the reaction, the reaction mixture will quickly warm resulting in boiling of aqueous solvent and the violent evolution of NO_x gases. Such an uncontrolled reaction leads to extensive by-product production, especially oxalic acid. In an effort to better control the temperature of the reaction, a LabMax reactor with a jacketed reaction vessel was used for the nitric acid oxidation of D-xylose, D-arabinose, and L-arabinose. The LabMax reactor was also used to control pressure within the closed reaction vessel. The oxidation of D-ribose was performed on a smaller

scale using conventional glassware and not in the LabMax reactor due to an insufficient amount of D-ribose available and its relatively high cost.

Extensive experimentation was performed to find the experimental profiles (temperature and pressure ramps) necessary for nearly complete consumption of the starting monosaccharide with limited by-product formation. Utilization of the Labmax reactor allowed for controlled positive pressure to be applied in the closed reaction vessel and aided in the oxygen-driven oxidation of nitric oxide to nitrogen dioxide, and ultimately regeneration of nitric acid. A small amount of sodium nitrite was used as an oxidation initiator. The general progression of the oxidation is illustrated in Figure 1.5 and a generic experimental profile is given in Figure 1.6. In all cases, nitric acid oxidation of the monosaccharide to its corresponding aldonic acid was rapid and highly exothermic. Subsequent oxidation of the aldonic acid at the terminal carbon to the aldaric acid is by comparison a slower and more difficult reaction.

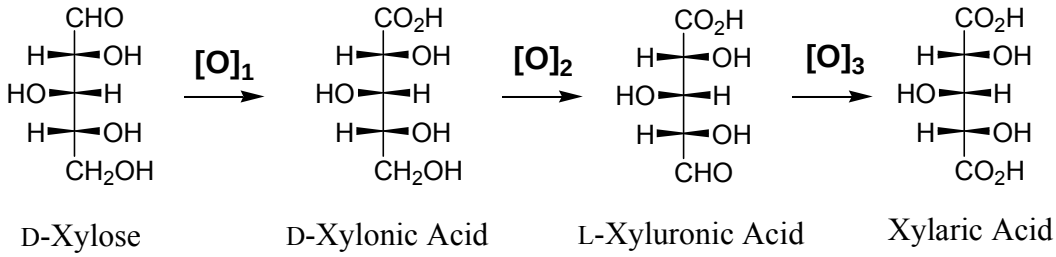

Figure 1.5 The general reaction progression of nitric acid oxidation from aldopentose to aldaric acid illustrated with D-xylose

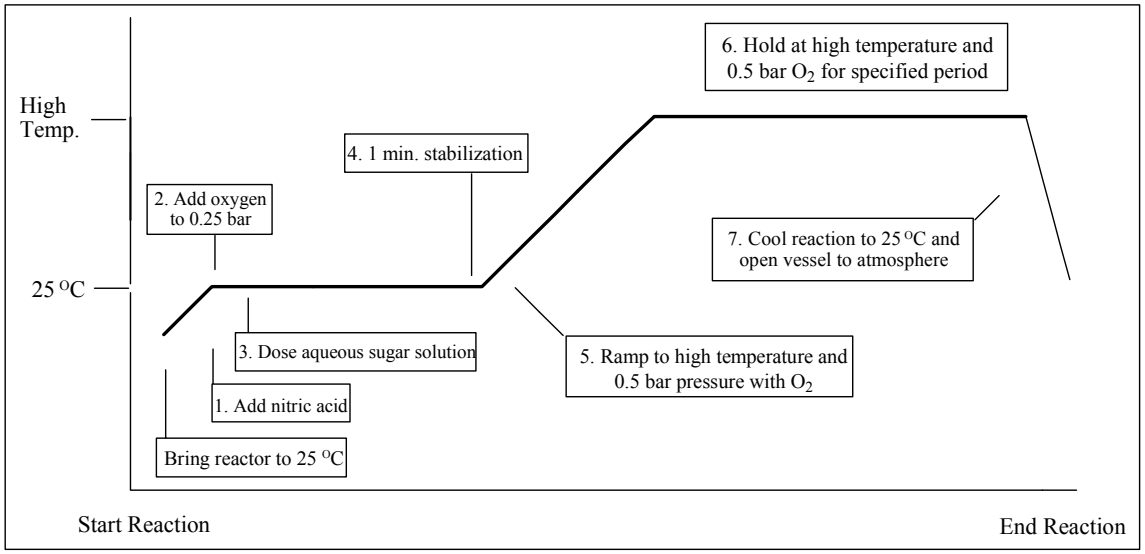

Figure 1.6 General experimental profile for a nitric acid oxidation of an aqueous sugar solution (applicable to D-xylose, D-arabinose, and L-arabinose)

The initial reactor parameters employed for the oxidation of D-xylose, D-arabinose, and L-arabinose to their corresponding aldaric acids were the same. As D-xylose has greater solubility (62.5% w/w) in water than do D-arabinose and L-arabinose (50.0% w/w), it was found that the additional water necessary to dose 750 mmol of D-arabinose and L-arabinose into the reaction vessel greatly retarded product formation due to dilution of the nitric acid. Consequently, additional nitric acid was used to offset this dilution. However, it was determined that the second oxidation of D-arabinose and L-arabinose at C-5 was much slower than with D-xylose at 35 °C and thus required a significantly higher temperature of 50 °C after the initial exotherm. The higher reaction temperature necessary for the second oxidation of D-arabinose and L-arabinose also increased the amount of NO_x gases released into the headspace of the reaction vessel resulting in pressure increases above the set pressure parameter (0.5 bar). Because the reaction vessel was not fitted with a computer controlled pressure release valve, the

vessel was vented manually. It was not possible to directly determine the composition of the headspace gases in the reactor, however, it was observed that during manual addition of oxygen an immediate pressure increase occurred followed by a subsequent pressure decrease until another gradual increase in pressure occurred. These observations suggest the headspace is comprised of NO_x gases, particularly NO, that are reactive with oxygen and that the reaction vessel is deficient in oxygen when the pressure increase begins.

Nitric acid oxidations of D-ribose were performed in a ventilated hood using a warm oil bath and conventional small scale glassware. Little experimentation was performed to optimize the reaction conditions, but fortuitously D-ribose is converted primarily to ribaric acid with relatively little by-product formation. It appears that ribaric acid and ribaric acid-1,4 (5,2)-lactone are relatively stable and do not significantly degrade under the oxidation conditions employed. Thus ribaric acid can be isolated as ribaric acid-1,4 (5,2)-lactone in yields comparable to those of xylaric acid, disodium D-arabinarate, and disodium L-arabinarate, despite the high reaction temperatures employed.

1.2.2 Isolation and Characterization of oxidation products

1.2.2.1 Xylaric Acid Isolation

The isolation of xylaric acid was performed by two different methods. In each case GC-MS and NMR results indicated a single, pure product was obtained. Both isolation methods started with the removal of the oxidation mixture from the reaction vessel and concentration of the mixture by rotary evaporation. Concentration of the reaction mixture by rotary evaporation is governed by the negative azeotrope of an aqueous nitric acid solution resulting in removal of the water and then the nitric acid. As

a result the concentrated reaction mixture is a thick syrup consisting of carbohydrate acids and residual nitric acid. The syrup can be dissolved in water and concentrated again to remove additional nitric acid, but each repeat of the process removes smaller amounts of nitric acid and does not completely remove the nitric acid.

Method 1. The syrup resulting from the rotary evaporation process was seeded with powdered xylaric acid. Upon standing it crystallized. The crystals were stirred with acetone and separated by filtration. The yield was 33% and the melting point 144-145 °C. Guy Fleche reported the isolation of xylaric acid by this method with 99.2 % purity and a melting point of 145 °C.[8] Whistler *et al.* reported a melting point range of 151-152 °C of xylaric acid.[3] Neither Whistler nor Fleche gave a percent yield based on their starting material.

Method 2. Xylaric acid may also be obtained through a method incorporating a nanofiltration step, Figure 1.7. The reaction syrup obtained from the rotary evaporation process described earlier was made basic with aqueous 5M sodium hydroxide. At pH 3.5-4.0 a solid results and can be removed by filtration. This solid was later characterized as impure disodium 2,2,3,3-tetrahydroxybutanedioate and will be discussed later in section 1.2.2.3 of this dissertation. The resulting filtrate was then taken to pH 9 with addition of sodium hydroxide to yield carbohydrate acid disodium salts and sodium nitrate. The mixture was then passed through nano-filter unit, which had been build in-house, to separate the small carbohydrate acid salts and sodium nitrate from the disodium xylarate. Although complete separation of the disodium xylarate (retentate) from the sodium nitrate (permeate) was not achieved, the retentate solution was concentrated, and dried under vacuum. The solid was stirred with ethanol to remove residual water, removed by

filtration, and dried again to give a dry solid product. This material was dissolved in water and the solution treated with acidic form ion exchange resin to give a solution of carbohydrate acids and a significantly reduced amount of residual nitric acid. The solution was concentrated to a syrup by rotary evaporation and seeded with powdered xylaric acid as before. The resulting xylaric acid was obtained in significantly higher yield (50 %) but with a slightly depressed melting point 138-140 ºC.

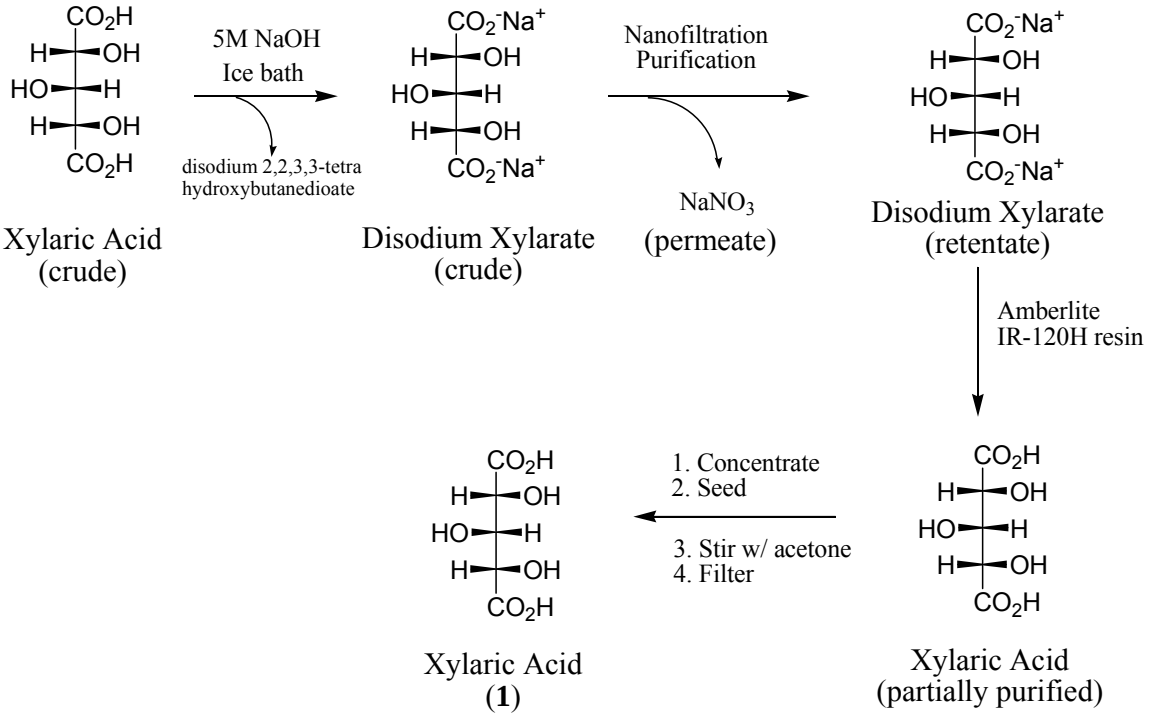

Figure 1.7 Xylaric acid isolation employing a nanofiltration step

1.2.2.2 Disodium D-Arabinarate (Disodium D-Lyxarate) and Disodium L-Arabinarate (Disodium L-Lyxarate) Isolation and Characterization

The relatively harsh reaction conditions necessary to obtain significant conversion of L(D)-arabinose to L(D)-arabinaric acid resulted in the formation of by-products in greater amounts than from D-xylose oxidation. In addition the L(D)-arabinaric acid did not

crystallize from the concentrated reaction mixture as had the xylaric acid from D-xylose oxidation, but rather formed a mixture of lactone acids which also did not crystallize. As a result isolation methods used for D-xylose were not applicable to the isolation of arabinaric acid and an alternative isolation method was developed to isolate L(D)-arabinaric acid as its disodium salt (Figure 1.8).

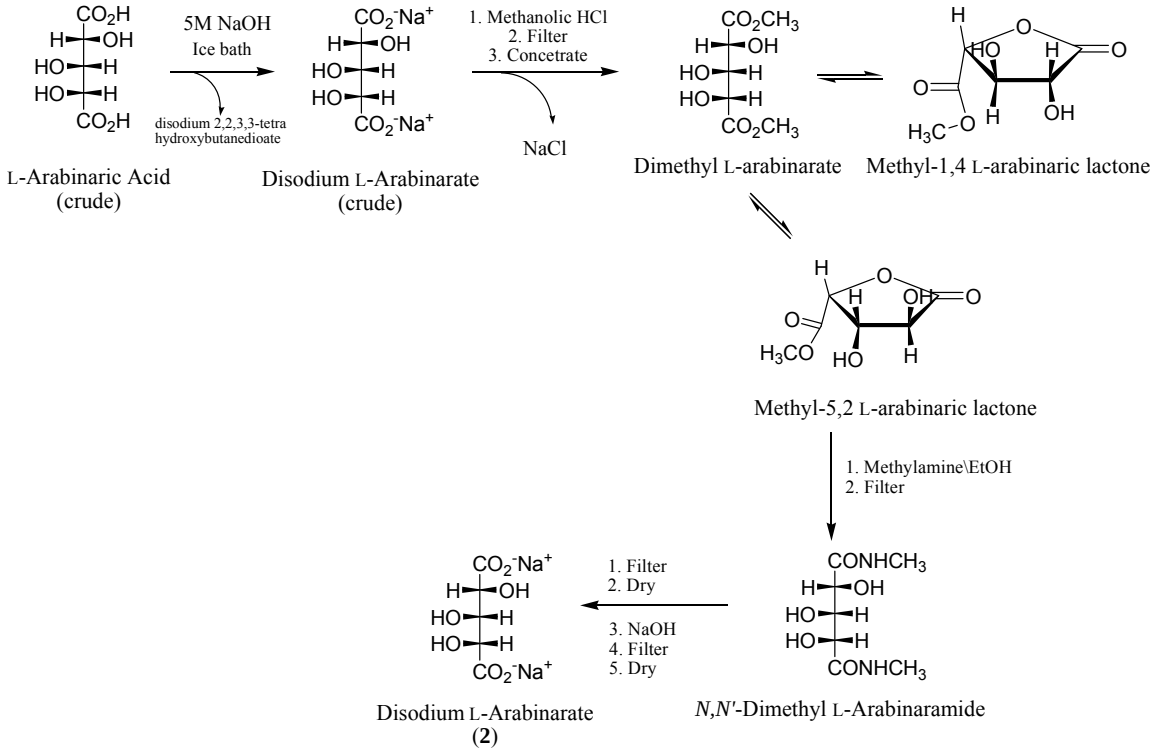

Figure 1.8 Isolation of disodium L-arabinarate (disodium L-lyxarate)

The L(D)-arabinaric acid oxidation mixture was treated in exactly the same way as the xylaric acid oxidation mixture utilizing the nanofiltration method (Method 2) up until the actual filtration. Instead of purifying the mixture utilizing the nanofilter, the disodium L(D)-arabinarate was treated with a solution of methanolic HCl to yield a crude mixture of dimethyl L(D)-arabinarate, methyl-1,4 L(D)-arabinaric lactone, methyl-5,2 L(D)-arabinaric lactone, sodium chloride, and excess methanolic HCl. The solid sodium

chloride was removed by filtration and the filtrate concentrated to a syrup thereby removing much of the excess HCl. Ethanolic methylamine was added to a methanol solution of the syrup from which *N,N'*-dimethyl L(D)-arabinaramide precipitated. Solid *N,N'*-dimethyl L(D)-arabinaramide was isolated by filtration, dried, dissolved in water, and treated with a slight excess of sodium hydroxide to give disodium L(D)-arabinarate in nearly 48 percent yield relative to L(D)-arabinose. Excess sodium hydroxide appeared trapped in the resulting material, resulting in unsatisfactory elemental analysis results. However, GC and low resolution mass spectrometry (Figure 1.10) of disodium L(D)-arabinarate as its per-*O*-trimethylsilyl derivative confirmed its identity. Observed fragments are explained in Figure 1.9. The ^{1}H NMR spectrum of the material was consistent with the assigned structure and also indicated a lack of organic impurities. Further purification of the material was not needed for the purposes of subsequent experimentation. However in an effort to obtain L(D)-arabinarate salts with satisfactory elemental analysis, calcium L and D-arabinarate were synthesized from disodium L and D-arabinarate. Both L and D salts gave almost identical carbon and hydrogen analysis but still did not meet calculated values even when hydration was included. The calcium salts were also analyzed by ion chromatography and found to have one slight impurity of undetermined structure and composition.

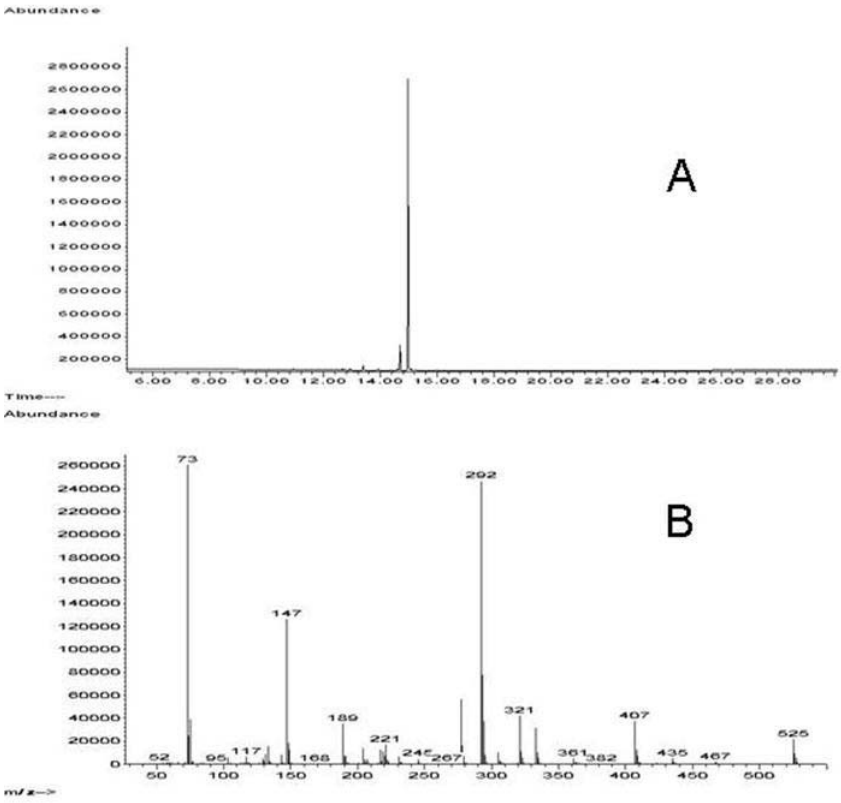

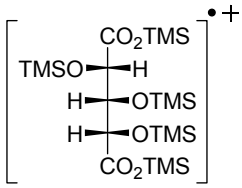

$[M]^+$ = 540
$[M - 15]^+$ = 525

per-*O*-trimethylsilyl D-Arabinaric Acid

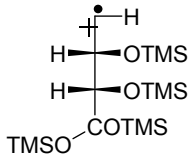

m/z = 407

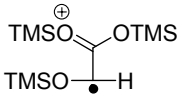

m/z = 292

McLafferty Rearrangement

m/z = 73

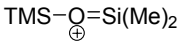

m/z = 147

Fragmentations common to Silylated Carboxylic Acids

Figure 1.9 GC-MS chromatogram and observed fragments of GC-FID chromatogram (A) and MS fragmentation pattern (B) of per-*O*-trimethylsilyl D-arabinarate

1.2.2.3 Isolation and Characterization of Disodium 2,2,3,3-tetrahydroxybutanedioate (8)

A reaction mixture of either nitric acid oxidized D-xylose or L(D)-arabinose was concentrated by rotary evaporation and the resulting syrup dissolved in water. Sodium hydroxide was added dropwise to pH 4.5. A colorless gas was emitted from the solution as evidenced by the evolution of bubbles, while a white solid precipitated from solution. This solid material was isolated through filtration and subjected to GC/MS analysis as its per-*O*-trimethylsilyl derivative. A mass fragmentation pattern search in a NIST library tentatively identified the material as the per-*O*-trimethylsilyl derivative of 2,2,3,3-tetrahydroxybutanedioic acid. Consequently, the insoluble white solid was tentatively identified as disodium 2,2,3,3-tetrahydroxybutanedioate.

To confirm this structure, disodium 2,2,3,3-tetrahydroxybutanedioate (**8**) was synthesized through bromine oxidation of dihydroxyfumaric acid with subsequent basification, as reported by Burnett *et al.*[9] GC retention times and mass fragmentation pattern, Figure 1.10, of the per-*O*-trimethylsilyl derivatives of the synthesized (**8**) and the side-product from nitric acid oxidations of D-xylose and L(D)-arabinose were identical. Additionally, decomposition of disodium 2,2,3,3-tetrahydroxybutanedioate upon heating matched the observation as reported by Lachman.

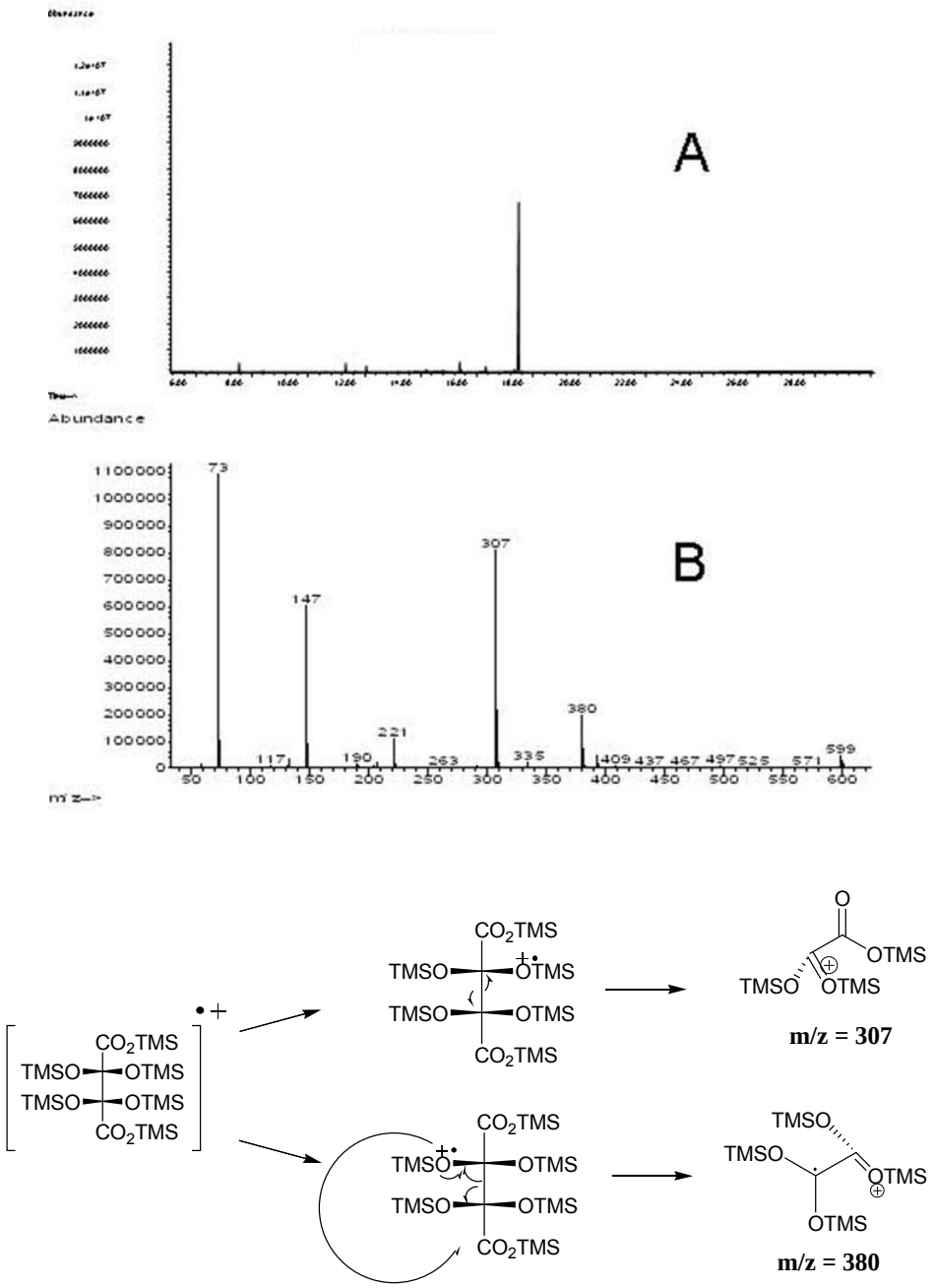

Figure 1.10 GC-FID chromatogram (A) and MS fragmentation pattern (B) of per-*O*-trimethylsilyl disodium 2,2,3,3-tetrahydroxybutanedioate

1.2.2.4 Disodium Ribarate Isolation and Characterization

The nitric acid oxidation of D-ribose was performed under much harsher conditions then those employed to D-xylose and L(D)-arabinose oxidations. A mixture of

nitric acid, solid D-ribose, and solid sodium nitrite was stirred and refluxed in an oil both set to 65 °C for 7 h. Evolution of NO_x gases was initially violent and persisted in a vigorous fashion for approximately 1 h. At the end of the 7 h oxidation the solution was concentrated by rotary evaporation to yield a white solid. To remove residual oxalic acid and nitric acid the solid was extracted by stirring with ether and filtered (five times). The resulting solid [ribaric acid-5,2 (1,4)-lactone (**6**)], from which an x-ray crystal structure was obtained, was then made basic with sodium hydroxide to yield disodium ribarate. As with the disodium salt of arabinaric acid, residual sodium hydroxide was present and contributed to unsatisfactory elemental analysis of the disodium salt. However, GC-MS of per-*O*-trimethylsilyl disodium ribarate showed a single peak with a mass fragmentation pattern matching the per-*O*-trimethylsilyl derivative of per-*O*-trimethylsilyl D-arabinarate as shown in Figure 1.9.

1.2.2.5 X-Ray Analysis of Ribaric Acid-5,2 (1,4)-Lactone (6)

The geometry of monoclinic crystalline ribaric acid-5,2-monolactone (**6**) with atom labeling is shown in Figure 1.11.

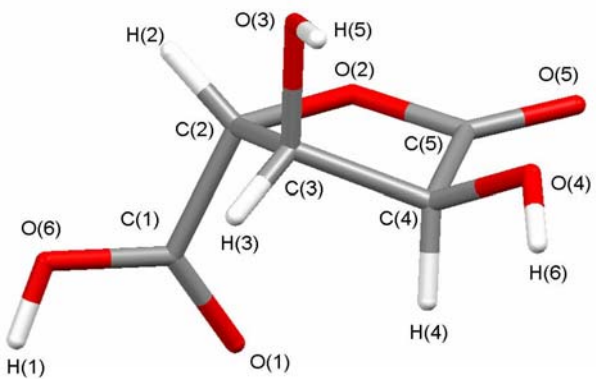

Figure 1.11 The geometry of ribaric acid-5,2 (1,4)-lactone (**6**) showing atom labeling

Figure 1.12 displays the hydrogen bonding schematic of monoclinic crystalline **6** which has a crystal density of 1.761 g cm^{-3}. Compound **6** has one hydrogen bond acceptor [O5···H5-O3, 2.078Å, 155.41º] bonded to the hydroxyl hydrogen of an adjacent molecule. The hydroxyl group oxygen of O(4) [O4-H6···O3, 1.942Å, 167.50 º] is acting as a hydrogen bond donor to the O(3) hydroxyl group of an adjacent molecule. The carboxylic acid group hydrogen (H1) is hydrogen bonded [O6-H1···O1, 1.873Å, 178.88 º] to the carboxylic acid group carboxyl oxygen of an adjacent molecule.

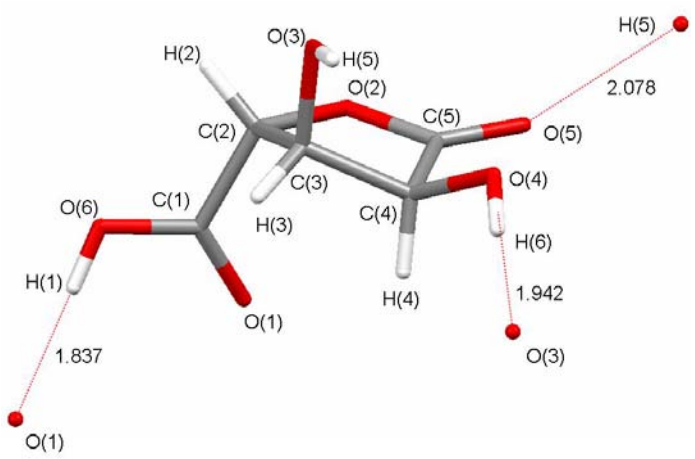

Figure 1.12 Hydrogen bonding schematic of ribaric acid-5,2-monolactone (**6**) with hydrogen bond distances in angstroms

Summary of Nitric Acid Oxidations

Oxidations of D-xylose, D-arabinose, L-arabinose, and D-ribose using nitric acid oxidation were employed to give all four of the possible stereoisomeric pentaric acids; xylaric acid, D-arabinaric acid (D-lyxaric acid), L-lyxaric acid (L-arabinaric acid), and ribaric acid, respectively. Isolation methods were developed for xylaric acid, disodium D-arabinarate (disodium D-lyxarate) and disodium L-lyxarate (disodium L-arabinarate), and ribaric acid-5, 2-lactone with typical yields of roughly 50 percent.

1.2.2.6 ^{1}H NMR Assignment of *N,N'*-Dihexyl-D-Arabinaramide

A small scale nitric acid oxidation of D-[2-^{2}H]-arabinose was carried out in order to obtain deuterium labeled D-arabinaric acid for correct ^{1}H NMR assignment of the C2-C4 protons. *N,N'*-Dihexyl-D-arabinaramide (**11**) was chosen as an appropriate D-arabinaric acid derivative for this study.

The nitric acid oxidation of D-[2-^{2}H]-arabinose and synthesis of *N,N'*-dihexyl-D-arabinaramide is described in the experimental section, section 1.3. The ^{1}H NMR experiments described here were performed on a Varian 500 MHz spectrometer using DMSO-d_6 as NMR solvent. Figure 1.13 and Figure 1.14 are ^{1}H NMR spectra of *N,N'*-dihexyl-D-arabinaramide and *N,N'*-dihexyl-D-[2-H2]-arabinaramide (**11**). The signal at δ 4.04 (Figure 1.13) is missing in Figure 1.14 and demonstrates the chemical shift of the proton on C2. Selective 1D NOESY ^{1}H NMR experiments were performed using *N,N'*-dimethyl-L-arabinaramide. The equivalence of amide and aldaryl protons between *N,N'*-dihexyl-D-arabinaramide and *N,N'*-dimethyl-L-arabinaramide can be seen in NMR spectra of each, Figures 1.13 and 1.15, respectively. Amide protons H8 and H9 are not equivalent and interact through "through space" interactions with the nearby protons (H2, H3, H4) of the aldaryl unit. Thus selective 1D NOESY ^{1}H NMR experiments can be used to assign the ^{1}H NMR spectrum of *N,N'*-dihexyl-D-arabinaramide and *N,N'*-dimethyl-L-arabinaramide. Both H8 and H9 were irradiated individually and NMR spectra recorded, Figure 1.15 and Figure 1.16, respectively. The selective 1D NOESY ^{1}H NMR spectra show the proximity of H8 and H2 and the proximity of H9 and H4, Figures 1.17 and 1.18, respectively.

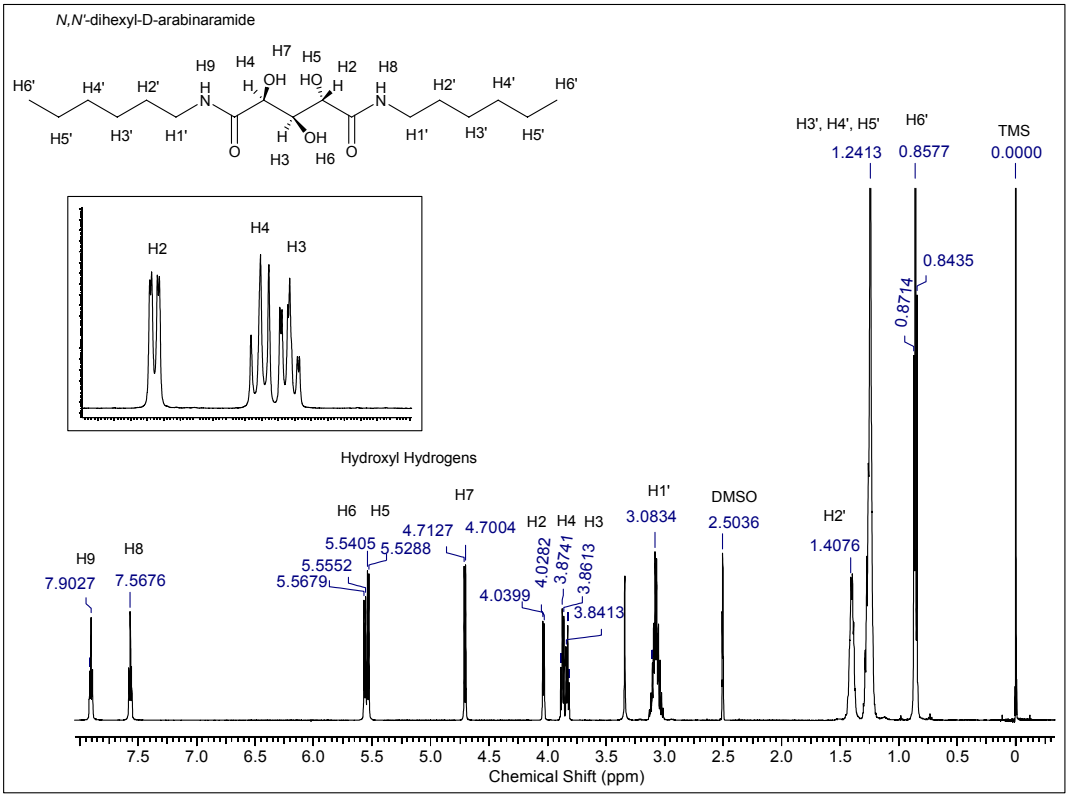

Figure 1.13 ^{1}H NMR spectrum of *N,N'*-dihexyl-D-arabinaramide

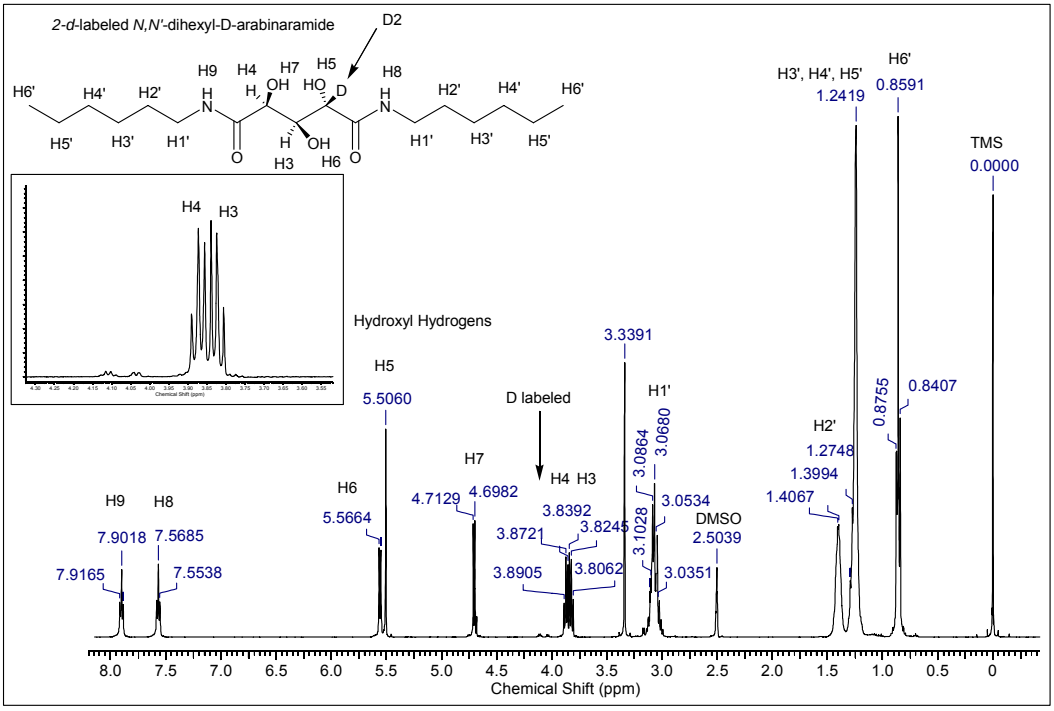

Figure 1.14 ^{1}H NMR spectrum of *N,N'*-dihexyl-D-[2-H2]-arabinaramide (**11**)

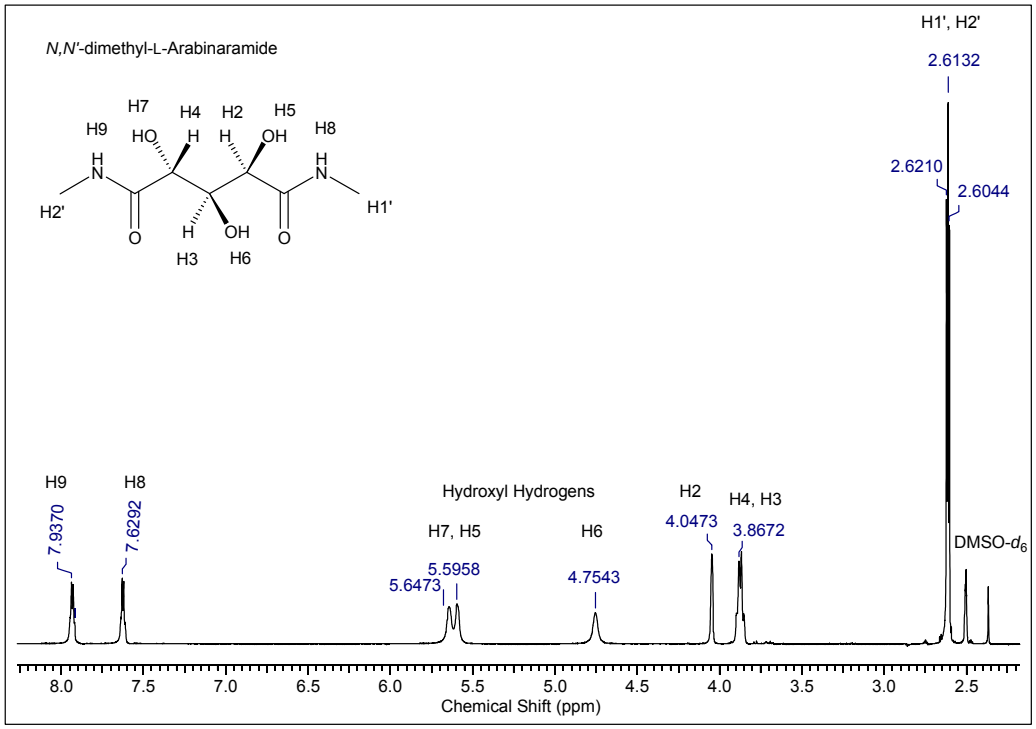

Figure 1.15 ^{1}H NMR spectrum of *N,N'*-dimethyl-L-arabinaramide

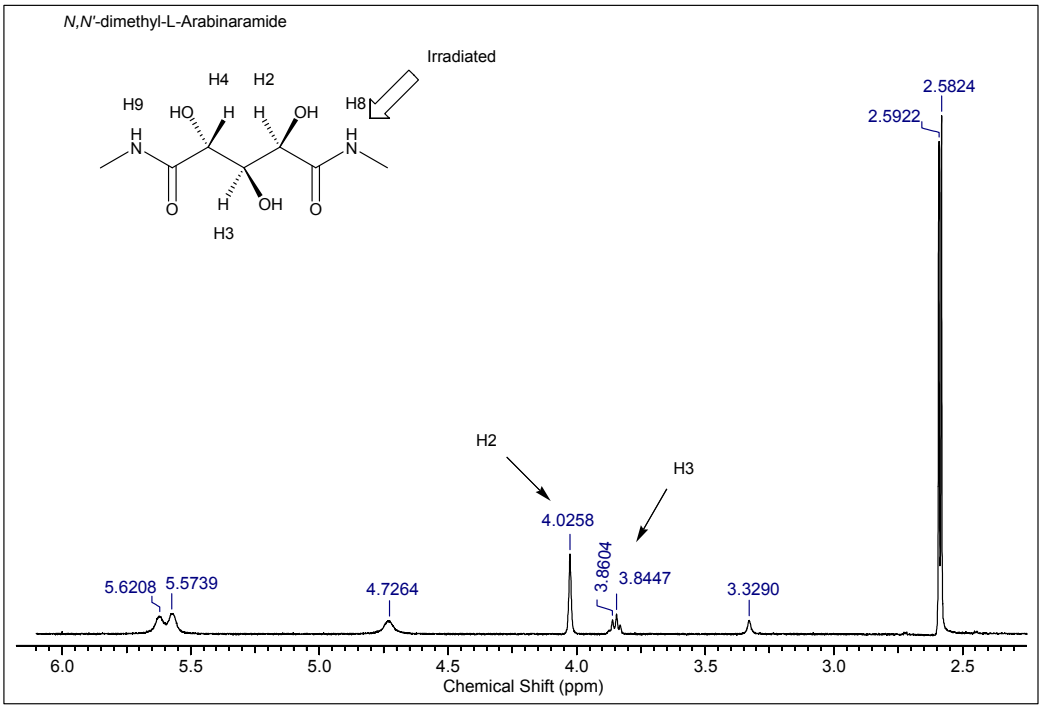

Figure 1.16 Selective 1D NOESY ^{1}H NMR spectrum of *N,N'*-dimethyl-L-arabinaramide with H8 irradiated

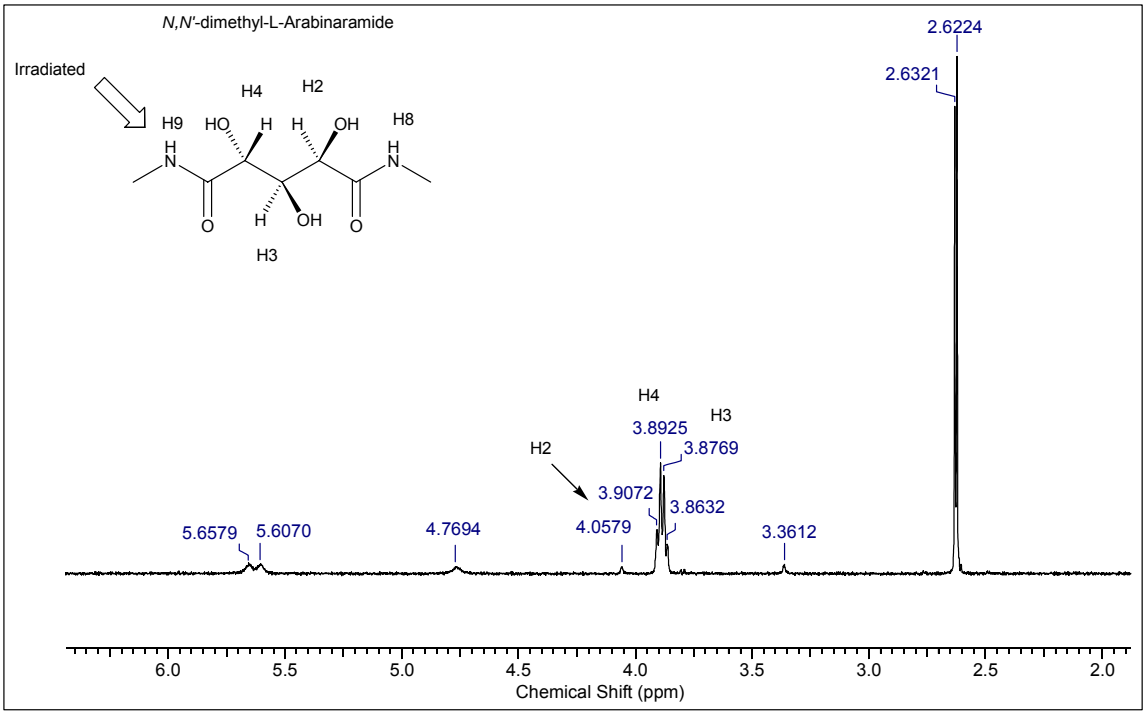

Figure 1.17 Selective 1D NOESY ^{1}H NMR spectrum of *N,N'*-dimethyl-L-arabinaramide with H9 irradiated

1.3 Experimental

Materials and General Methods

D-Xylose, D-arabinose, and L-arabinose were purchased from Hofmann International, ACS grade nitric acid (70% w/w) and HPLC grade methanol from EMD Biosciences, Inc, ACS grade sodium nitrite from Acros, acetyl-chloride (99+ %) from Alfa Aesar, Tri-Sil Reagent from Pierce, NMR solvents from Cambridge Isotope Laboratories, Inc. Sodium hydroxide was purchased from J.T. Baker. All other chemicals were purchased from Aldrich and used without further purification. X-ray crystal analysis was performed as specified in Chapter 4.

Concentrations of solutions were carried out under reduced pressure. Drying of samples was carried out under vacuum using a Fischer Scientific Isotemp Vacuum Oven

Model 280A at room temperature. Elemental analyses were performed by Atlantic Microlab, Inc., Norcross, Georgia. Melting points were obtained with a Fisher-Johns melting point apparatus and are reported uncorrected.

Oxidations of D-xylose, D-arabinose, and L-arabinose were performed using a Mettler Toledo RC-1 LabMax fitted with a Mettler Toledo PG5002-S Delta Range top-loading balance, ProMinent Fluid Controls Inc. Model G/4b1201TT1 liquid feed pump, Sierra 830/840/860 Series Side-Trak & Auto-Trak Mass Flow Meter and Controller flow valve, FTS Maxi Cool recirculation chiller, and appropriate gas bubbler, pressure manifold with safety valves and gauges, condenser, pH meter, stir rod, thermometer, and temperature controlled jacketed reaction flask. The system is operator controlled through Camile TG v1.2 software enabling temperature and pressure control within the 2L reaction vessel. Concentration of nitric acid was carried out under reduced pressure with a system consisting of a Buchi Rotovapor R-205, Buchi Vacuum Controller V-800, Buchi Heating Bath B-490, Brinkmann Model B-169 Vacuum Aspirator, and a Thermo Haake compact refrigerated circulator DC30-K20 in conjunction with a Thermo Haake EK45 immersion circulator cooling coil.

Nanofiltration was performed on a unit built in-house consisting of the necessary valves, pump, tubing, pressure gauge, and an appropriate membrane such as GE DL2540F using reverse osmosis purified water obtained in-house.

GC-MS analyses were performed on an Agilent 6890N GC interfaced to an Agilent 5973 MS detector. A Phenomenex ZB-5 GC column, 30 m x 0.25 mm x 0.25 μm, composed of 5%-phenyl 95% dimethylpolysiloxane was used for all GC-MS analysis. Samples for GC-MS analyses were prepared as per-*O*-trimethylsilyl derivatives. Tri-Sil

Reagent (1.0 mL) was added to dried sample (5.0 mg) in a 7 mL vial and the mixture heated at 50 °C for 60 min. The sample was cooled to room temperature and heptane (6 mL) added. The mixture was centrifuged and the liquid portion (3 mL) transferred to a 7 mL vial. Heptane (3 mL) was added to the liquid portion and an aliquot taken for GC-MS analysis.

High-Performance Liquid Chromatography (HPLC) was performed on two Aminex® HPX-87H columns in series where used with a refractive index (RI) detector. The first column was heated to 35˚C and the second column to heated to 85˚C. A 0.005 M H_2SO_4 eluent heated to 70˚C under an argon atmosphere and samples run isocratically at a 0.5 mL/min flow rate.

One dimensional ^1H NMR spectra were obtained using a 400 MHz Varian Unity Plus spectrometer or a 500 MHz Varian spectrometer. NMR spectra were processed using ACD/SpecManager 1D NMR software Version 9.13. Chemical Shifts were expressed in parts per million relative to *t*-BuOH (1.203 ppm) for D_2O.

IC was performed on a Dionex ICS-2000 Ion Chromatography system consisting of a Dionex IonPac AS II analytical column and a sodium hydroxide EluGen cartridge in conjunction with Chromeleon software. Samples were analyzed using a 35mM sodium hydroxide isocratic elution method with a flow rate of 1.5 mL/min running with the suppressor current at 186 mA. IC method development was carried out by Cara-Lee Davey from the University of Waikato, Hamilton, New Zealand.

1.3.1 Xylaric Acid (1) - Nitric Acid Oxidation of D-Xylose

The oxidation was carried out using the LabMax reactor. The parameters were programmed in a series of stages for the oxidation. Stage 1. The reactor vessel was set at

25 ºC, the stirring rod speed was set at 200 rpm (held constant throughout the remaining stages), concentrated nitric acid (70%, 3 mol, 187 mL) was added, the vessel was closed to the atmosphere, and time set for 3 min. Stage 2. Oxygen was added to the reaction vessel to increase the pressure to 0.25 bar. Stage 3. D-Xylose [181.16 g of an aqueous 62.5% solution containing sodium nitrite (1.16 g, 16.8 mmol)] was added over 120 min. Stage 4. A one minute stabilization period, i.e. no change in reaction conditions. Stage 5. Reactor temperature was raised to 35 ºC and the pressure raised by addition of oxygen to 0.5 bar over 60 min. Stage 6. Reaction was held at 35 ºC and 0.5 bar of pressure for 210 min. Stage 7. Reaction mixture was cooled to 25 ºC over 10 min and the vessel opened to the atmosphere.

1.3.2. Isolation of Xylaric Acid (1) – Concentration Method

The D-xylose oxidation mixture, taken directly from the Mettler Toledo LabMax reactor, was concentrated to a thick syrup at 50 ºC. Water (200 mL) was added to dissolve the syrup and the resulting solution concentrated to a syrup. This concentration process was repeated twice. The resulting syrup was seeded with xylaric acid (< 1.0 mg) and left undisturbed at room temperature for three days. Cold acetone (300 mL) was added to the semi-solid mixture and the mixture stirred at room temperature for 12 h. The mixture was cooled (ice bath) and white solid xylaric acid was obtained by filtration. (**1**, 44.58 g, 247.5 mmol, 33.00 % yield): mp 144-145 ºC (Lit. 151 ºC),[3] ^{1}H NMR (D_2O) δ 4.45(d, 2H, *J* 4.33 *Hz,* H-1, H-3) δ 4.22(t, 1H, H-2) Anal. Calcd for $C_5H_8O_7$ (180.11): C, 33.34; H, 4.48. Found C, 33.31; H, 4.34. GCMS (ESI) *m/z* Calcd for $C_{20}H_{48}O_7Si_5$ [M – $C_{11}H_{28}O_3Si_3$, $C_9H_{20}O_4Si_2^+$] 292.6 Found 292; GCMS (ESI) *m/z* Calcd for $C_{20}H_{48}O_7Si_5$ [M – 15, $C_{19}H_{45}O_7Si_5]^+$ 525.2. Found 525.

1.3.3. Isolation of Xylaric Acid (1) – Nanofiltration Method

The D-xylose oxidation mixture, taken directly from the LabMax reactor, was concentrated to a thick syrup at 50 °C. Water (200 mL) was added to dissolve the syrup, the solution cooled (ice bath), and sodium hydroxide (5M) added with stirring to bring the mixture to pH 4.5. A white precipitate formed, which was removed by filtration, and characterized as 2,2,3,3-tetrahydroxybutanedioate (**8**, 8.39 g, 37.1 mmol, 4.94 % yield, dec. 142 °C). The filtrate was cooled (ice bath) and sodium hydroxide (5M) added with stirring to bring the solution to pH 10. The solution was concentrated under reduced pressure at 50 °C to dryness to give a brown solid to which absolute ethanol (300 mL) was added and the mixture stirred at room temperature for 12 h. The solid was removed by filtration and dried to yield a crude brown solid of disodium xylarate (156.9 g). The solid was dissolved in reverse osmosis water (3,500 mL) and the solution passed through a G.E. Water & Process Technologies, model # DL2540F1072 nanopore filter. When the permeate volume reached 1,000 mL, reverse osmosis (RO) water (1,000 mL) was added to the feedstock. The typical rate of permeate flow was 48 mL/min. After 2,000 mL of permeate had been removed another 1,000 mL of RO water was added to the feedstock. This was repeated until 4,000 mL of RO water had been added to the feedstock. Filtration continued until the permeate flow slowed to a trickle. The retentate contained predominantly organic acid sodium salts and the permeate predominately inorganic sodium nitrate, as determined by HPLC analyses. The retentate of disodium xylarate was concentrated at 50 °C to 200 mL and treated with an excess of Amberlite IR-120H^+ resin (1.32 L, 2.5 mol, 3 h) to give aqueous diacid. The resin was removed by filtration and rinsed with water (500 mL). The combined filtrate and rinse was concentrated at 50 °C to

a thick syrup, seeded with xylaric acid (< 1 mg), and allowed to remain undisturbed at room temperature for 3 days. Cold acetone (300 mL) was added to the near solid product and the mixture stirred at room temperature for 12 h. The mixture was cooled (ice bath) and white solid xylaric acid was separated by filtration. (**1**, 67.10 g, 372.55 mmol, 49.67 % yield): mp 138-140 ºC (lit. 151 ºC),[3] ^{1}H NMR (D_2O) δ 4.45(d, 2H, H-1, H-3) δ 4.22(t, 1H, H-2).

1.3.4 L-Arabinaric Acid (L-Lyxaric Acid), (2) -Nitric Acid Oxidation of L-Arabinose

The oxidation was carried out using the LabMax reactor as described for D-xylose. The following reaction parameters for the oxidation were programmed into the Recipe Menu accessed on the LabMax Camile TG v1.2 software in the following series of stages. Stage 1. The reactor vessel was set at 25 ºC, the stirring rod speed was set at 200 rpm (held constant throughout the remaining stages), concentrated nitric acid (70%, 5.13 mol, 320 mL) was added, the vessel was closed to the atmosphere, and time set for 3 min. Stage 2. Oxygen was added to the reaction vessel to increase the pressure to 0.25 bar. Stage 3. L-arabinose [226.62 g of an aqueous 50.0% solution containing sodium nitrite (1.76 g, 25.5 mmol)] was added over 90 min. Stage 4. A one minute stabilization period, i.e., no change in reaction conditions. Stage 5. Reactor temperature was raised to 50 ºC and the pressure raised by addition of oxygen to 0.5 bar over 45 min. Stage 6. Reaction was held at 50 ºC and 0.5 bar of pressure for 180 min. Stage 7. Reaction mixture was cooled to 25 ºC over 10 min and the vessel opened to the atmosphere.

1.3.5. Isolation of Disodium L-Arabinarate (Disodium L-Lyxarate) (3)

The L-arabinose oxidation mixture was taken directly from the LabMax reactor, concentrated to a syrup at 50 °C and dissolved in cold (ice bath) water (200 mL). Sodium hydroxide (5M) was added with stirring to bring the mixture to pH 4.5. A white precipitate formed, was removed by filtration and identified as disodium 2,2,3,3-tetrahydroxybutanedioate (**8**, 7.95 g, 35.2 mmol, 4.69%, mp (dec.) 142 °C). The filtrate was cooled (ice bath) and sodium hydroxide (5M) added with stirring to bring the mixture to pH 10. The solution was concentrated at 50 °C to give a brown solid which was stirred with absolute ethanol (300 mL) at room temperature for 12 h. The solid was removed by filtration and dried, to yield a crude brown solid of disodium L-arabinarate (**3**) (148.83 g). Acetyl chloride (118.7 g, 1.52 mol) was added to cold methanol and the resulting solution was added with stirring to a mixture of crude solid disodium L-arabinarate and cold (ice bath) methanol (100 mL). The reaction mixture was stirred at room temperature (4 h) after which a white, insoluble precipitate, sodium chloride was removed by filtration, and the filtrate concentrated to a thick syrup at 40 °C. The thick syrup was dissolved in methanol (100 mL), a solution of methylamine in ethanol (33% b/w, 87.01 g, 265 mL, 2.80 mol) was added dropwise to the cold (ice bath) solution, and the resulting reaction mixture stirred at room temperature (24 h). A white solid was removed by filtration and dried. Aqueous sodium hydroxide (2M, 0.760 mmol, 380.1 mL) was added at room temperature and the mixture stirred 3 days, after which it was concentrated at 40 °C and the resultant solid stirred with absolute ethanol (300 mL). The solid wa removed by filtration and the stirring process with ethanol was repeated three times to give a final white amorphous solid of disodium L-arabinarate (**3**, 79.88 g, 356.5

mmol, 47.53%) ^{1}H NMR (D_2O) δ 4.15(d, 1H, *J* 1.47 *Hz*) δ 4.03(d, 1H) δ 3.99 (d, 1H). ^{13}C NMR (D_2O): 180.60, 180.05, 74.20, 74.16, 72.94 ppm. Anal. Calcd for $C_5H_6Na_2O_7$ (224.08): C, 26.80; H, 2.70. Found C, 23.69; H, 2.97. GCMS (ESI) *m/z* Calcd for $C_{20}H_{48}O_7Si_5$ [M – $C_{11}H_{28}O_3Si_3$, $C_9H_{20}O_4Si_2^+$] 292.6 Found 292; GCMS (ESI) *m/z* Calcd for $C_{20}H_{48}O_7Si_5$ [M – 15, $C_{19}H_{45}O_7Si_5]^+$ 525.2. Found 525. Optical rotation -0.80°

1.3.6 D-Arabinaric Acid (D-Lyxaric acid) (4) -Nitric Acid Oxidation of D-Arabinose

The oxidation was carried out using the LabMax reactor as described for L-arabinose. Stage 1. The reactor vessel was set at 25 °C, the stirring rod speed was set at 200 rpm (held constant throughout the remaining stages), concentrated nitric acid (70%, 5.13 mol, 320 mL) was added, the vessel was closed to the atmosphere, and time set for 3 min. Stage 2. Oxygen was added to the reaction vessel to increase the pressure to 0.25 bar. Stage 3. D-arabinose [226.62 g of an aqueous 50.0% solution containing sodium nitrite (1.76 g, 25.5 mmol)] was added over 90 min. Stage 4. A one minute stabilization period, i.e. no change to reaction conditions. Stage 5. Reactor temperature was raised to 50 °C and the pressure raised by addition of oxygen to 0.5 bar over 45 min. Stage 6. Reaction was held at 50 °C and 0.5 bar of pressure for 180 min. Stage 7. Reaction mixture was cooled to 25 °C over 10 min and the vessel opened to the atmosphere.

1.3.7. Isolation of Disodium D-Arabinarate (Disodium D-Lyxarate) (5)

The D-arabinose oxidation mixture was taken directly from the LabMax reactor, concentrated to a syrup at 50 °C and dissolved in cold (ice bath) water (200 mL). Sodium hydroxide (5M) was added with stirring to bring the mixture to pH 4.5. A white precipitate formed and was removed by filtration and identified as disodium 2,2,3,3-

tetrahydroxybutanedioate (**8**, 6.25 g, 27.7 mmol, 3.69%, mp (dec.) 142 °C). The filtrate was cooled (ice bath) and sodium hydroxide (5M) added with stirring to bring the mixture to pH 10. The solution was concentrated at 50 °C to give a brown solid which was stirred with absolute ethanol (300 mL) at room temperature for 12 h. The solid was removed by filtration and dried, to yield a crude brown solid of disodium D-arabinarate (142.45 g). Acetyl chloride (118.7 g, 1.52 mol) was added dropwise to cold methanol and the resulting solution was added with stirring to a mixture of crude solid disodium D-arabinarate and cold (ice bath) methanol (100 mL). The reaction mixture was stirred at room temperature for 4 h after which white insoluble sodium chloride, was removed by filtration and the filtrate concentrated to a thick syrup at 40 °C. The thick syrup was dissolved in methanol (100 mL), a solution of methylamine in ethanol (33% b/w, 87.01 g, 265 mL, 2.80 mol) was added dropwise to the cold (ice bath) solution, and the resulting reaction mixture stirred at room temperature (24 h). A white solid was removed by filtration and dried. Aqueous sodium hydroxide (2M, 0.760 mmol, 380.1 mL) was added at room temperature and the mixture stirred 3 days, after which it was concentrated at 40 °C and the resultant solid stirred with absolute ethanol (300 mL), before filtration. This process with ethanol was repeated three times to give a final white amorphous solid of disodium D-arabinarate (disodium D-lyxarate) (**5**, 77.34 g, 345.16 mmol, 46.02%) ^{1}H NMR (D_2O) δ 4.15(d, 1H, *J* 1.47 *Hz*) δ 4.03(d, 1H) δ 3.99 (d, 1H). ^{13}C NMR (D_2O): 180.60, 180.05, 74.20, 74.16, 72.94 ppm. GCMS (ESI) *m/z* Calcd for $C_{20}H_{48}O_7Si_5$ [M – $C_{11}H_{28}O_3Si_3$, $C_9H_{20}O_4Si_2^+$] 292.6 Found 292; GCMS (ESI) *m/z* Calcd for $C_{20}H_{48}O_7Si_5$ [M – 15, $C_{19}H_{45}O_7Si_5]^+$ 525.2. Found 525. Optical rotation +0.95°.

1.3.8 Ribaric Acid-1,4 (5,2)-Lactone (6) - Nitric Acid Oxidation of D-Ribose

To a 500 mL round bottom flask was added concentrated nitric acid (70%, 75 mL, 1.80 mol) to which solid D-ribose (30.372 g, 202.32 mmol) and solid sodium nitrite (< 1 mg) were added. The flask was immediately fitted with a water-cooled Liebig condenser and the resulting solution warmed with stirring in an oil bath (65 °C, 7 h). Within one minute the solvent warmed to boiling and brown gases were violently evolved. At the end of the reaction process the resulting solution was concentrated under reduced pressure to yield a white solid, which was dissolved in water (100 mL) and the solution concentrated to dryness. The resultant solid was redissolved in water and concentrated to dryness, and then the process was repeated. The solid product was stirred with ethyl ether (300 mL, 1 h) and the solid removed by filtration; the trituration and filtration procedure was repeated five times. The filtrate for each iteration was tested for acidity using pH paper. The fifth filtrate having a neutral pH. The white solid was dried under vacuum overnight to yield ribaric acid-1,4 (5,2)-lactone (**6**, 16.25 g, 100.2 mmol, 49.54 % yield) ^{1}H NMR (D_2O) δ 5.01(s, 1H) δ 4.66(d, 1H) δ 4.62 (d, 1H) mp 163-166 ºC. Calcd for $C_5H_6O_6$ (162.10): C, 37.05; H, 3.73; Found C, 36.87; H, 3.71.

1.3.9 Isolation of Disodium Ribarate (7)

To a solution of ribaric acid-1,4 (5,2)-lactone (**6**, 10.01 g, 61.78 mmol) in water (50 mL) was added sodium hydroxide (5M, 30.0 mL, 150 mmol) dropwise with stirring at room temperature. The solution was stirred at room temperature for 12 h and then concentrated at 35 °C to a white solid. The solid was stirred with methanol (100 mL, 1 h) and a white solid isolated by filtration. This process was repeated three times. The resulting white solid was dried to yield disodium ribarate (**7**, 13.24 g, 59.08 mmol, 95.65%). ^{1}H NMR

(D_2O) δ 4.062(s, H2,3,4). ^{13}C NMR (D_2O): 179.84, 75.42, 74.03 ppm. Anal. Calcd for $C_5H_6Na_2O_7$ (224.08): C, 26.80; H, 2.70. Found C, 25.55; H, 2.99. GCMS (ESI) *m/z* Calcd for $C_{20}H_{48}O_7Si_5$ [M – $C_{11}H_{28}O_7Si_{13}$, $C_9H_{20}O_4Si_2^+$] 292.6 Found 292; GCMS (ESI) *m/z* Calcd for $C_{20}H_{48}O_7Si_5$ [M – 15, $C_{19}H_{45}O_7Si_5^+$] 525.2. Found 525.

1.3.10 Synthesis of Disodium 2,2,3,3-tetrahydroxybutanedioate (8)

The procedure described by Fenton and modified by Burnett was used for the preparation of disodium 2,2,3,3-tetrahydroxybutanedioate.[9]

To a solution of dihydroxyfumaric acid (0.193 g, 1.300 mmol) in water (5 mL) was added glacial acetic acid (1 mL) dissolved in cold (ice bath) water (1 mL). Bromine (0.276 g, 1.727 mmol) was added dropwise with stirring to cold (ice bath) glacial acetic acid (1.5 mL) and the resulting bromine/glacial acetic acid solution was added dropwise to the cooled dihydroxyfumaric acid/acetic acid solution over 3 h. Solid sodium bicarbonate was added until bubble formation stopped and a precipitate was formed and removed by filtration. The solid was washed with acetone (3 x 2 mL), isolated by filtration and the solid dried to give disodium 2,2,3,3-tetrahydroxybutanedioate dihydrate (**8**, 0.2399 g, 0.915 mmol, 70.41%): mp (dec.) 142 °C (lit. 150-160 °C) [9] (Calcd for $C_4H_8Na_2O_{10}$ (262.08): C, 18.33; H, 3.08. Found C, 18.12; H, 3.07. LRMS (ESI) *m/z* Calcd for $C_{22}H_{54}O_8Si_6$ [M – $C_{11}H_{27}O_4Si_3$, $C_{11}H_{27}O_4Si_3^+$] 307.59. Found 307; LRMS (ESI) *m/z* Calcd for $C_{22}H_{54}O_8Si_6$ [M – $C_8H_{18}O_4Si_2$, $C_{14}H_{36}O_4Si_4^+$] 380.7 Found 380.

Disodium 2,2,3,3-tetrahydroxybutanedioate (**8**) obtained from nitric acid oxidation of D-xylose and L(D)-arabinose yielded (**8**, 0.2399 g, 0.915 mmol, 70.41%): mp (dec.) 142 °C (lit. 150-160 °C) [9] LRMS (ESI) *m/z* Calcd for $C_{22}H_{54}O_8Si_6$ [M – $C_{11}H_{27}O_4Si_3$,

$C_{11}H_{27}O_4Si_3^+$] 307.59. Found 307; LRMS (ESI) *m/z* Calcd for $C_{22}H_{54}O_8Si_6$ [M – $C_8H_{18}O_4Si_2$, $C_{14}H_{36}O_4Si_4^+$] 380.7 Found 380.

1.3.11 Synthesis of Calcium L-Arabinarate (Calcium L-Lyxarate) (9)

To a solution of disodium L-arabinarate (0.502 g, 2.240 mmol) in water (4 mL) was added saturated calcium chloride (2 mL) and the solution stirred 1h. A precipitate was formed and removed by filtration. The solid was washed with water (3 x 2 mL), isolated by filtration, and the solid dried to give calcium L-arabinarate (calcium L-lyxarate) (**9**, 0.381 g, 1.748 mmol, 78.40%) (Calcd for $C_5H_6CaO_7$ (217.97): C, 27.53; H, 2.77. Found C, 22.59; H, 3.18.

1.3.12 Synthesis of Calcium D-Arabinarate (Calcium D-Lyxarate)(10)

To a solution of disodium D-arabinarate (0.517 g, 2.240 mmol) in water (4 mL) was added saturated calcium chloride (2 mL) and the solution stirred 1h. A precipitate was formed and removed by filtration. The solid was washed with water (3 x 2 mL), isolated by filtration, and the solid dried to give calcium D-arabinarate (calcium D-lyxarate) (**10**, 0.360 g, 1.652 mmol, 73.74%) (Calcd for $C_5H_6CaO_7$ (217.97): C, 27.53; H, 2.77. Found C, 22.73; H, 3.13.

1.3.13 *N,N'*-Dihexyl-D-[2-^{2}H]-Arabinaramide - Nitric Acid Oxidation of D-[2-2H]-Arabinose (11)

To a 25 mL round bottom flask was added concentrated nitric acid (70%, 0.4 mL, 6.710 mmol) to which solid D-[2-2H]-arabinose (0.124 g, 0.819 mmol) and solid sodium nitrite (< 1 mg) were added. The flask was immediately fitted with a water-cooled Liebig condenser and the resulting solution warmed with stirring in an oil bath (60 °C, 6 h). Within one minute the solvent warmed to boiling and brown gases were violently

evolved. At the end of the reaction process the resulting solution was concentrated under reduced pressure to yield a clear syrup. To methanol (1.5 mL) was added acetyl-chloride (0.029 mL, 0.410 mmol) and the syrup dissolved in the methanolic HCl then stirred for 2 h. The solution was concentrated to a thick syrup, dissolved in methanol (1 mL), and hexylamine (0.249g, 0.325 mL, 2.457 mmol) added dropwise with stirring. A solid precipitated within 30 min. and the mixture was allowed to stir for another 3 h. The mixture was pipetted into an 8 dram vial and centrifuged; the supernant was decanted and the solid washed with methanol (3x, 0.5 mL) then dried under vacuum overnight to yield *N,N'*-dihexyl-D-[2-^{2}H]-arabinaramide (**11**, 0.091 g, 0.262 mmol, 31.93 % yield) ^{1}H NMR (DMSO-d_6) δ 7.90 (s, 1H, N**H**) δ 7.53(s, 1H, N**H**) δ 5.56 (d, 1H, *J* 5.08, O**H**) δ 5.51 (s, 1H, O**H**) δ 4.71 (d, 1H, *J* 5.88, O**H**) δ 3.87 (1H) δ 3.82 (1H) δ 3.06 (m, 2H, CONHC**H$_2$**) δ 1.40 (m, 2H, CONHCH$_2$C**H$_2$**) δ 1.23 (6H, C**H$_2$**) δ 0.85 (t, 3H, C**H$_3$**)

1.3.14 Ribaric acid-5,2 (1,4)-lactone (**6**)

Crystals were obtained by dissolving ribaric acid-5,2-lactone (**6**) in methanol and allowing the methanol to evaporate. The resulting crystals were colorless needles, mp 164-166 ºC.

References

1. Kiliani, H. Oxydation der Arabinose durch Salpetersaure, Berichte, **1889**, 21, 3006-3009

2. Hardegger, E.; Kreis, K.; Spitz, D. The oxidative degradation of uronic acids and derivatives of trihydroxyglutaric acids. Helvetica Chimica Acta, **1952**, 35, 958-63

3. Whistler, R. L., Wolfrom, M. L.; D-Glucaric Acid. In Methods in Carbohydrate Chemistry, Academic Press, New York, **1962**, 2, 46-48

4. Chalov, N. V.; Preparation of trihydroxyglutaric acid by oxidation of xylose by nitric acid. Zhurnal Prikladnoi Khimii (Sankt-Peterburg, Russian Federation) **1948**, 21, 486-95

5. Cantrell, Charles E.; Kiely, Donald E.; Abruscato, Gerald J.; Riordan, James M.; Dicarbonyl sugars. A novel synthesis of a branched-chain cyclitol. Journal of Organic Chemistry, **1977**, 42(22), 3562-7

6. Kiely, D. E., Carter, A., Shrout, D. P.; Oxidation Process, U.S. Patent 5,599,977, **1997**

7. Williams, LaKenya; Nguyen, Tinh; Li, Yingchun; Porter, Tamiko N.; Raushel, Frank M. Uronate Isomerase: A Nonhydrolytic Member of the Amidohydrolase Superfamily with an Ambivalent Requirement for a Divalent Metal Ion. Biochemistry **2006**, 45(24), 7453-7462.

8. Fleche, G.; Process for the manufacture of xylaric acid and uses thereof. U.S. Patent 5,731,467, **1998**

9. Burnett, Christopher A.; Lagona, Jason; Wu, Anxin; Shaw, Jennifer A.; Coady, Daniel; Fettinger, James C.; Day, Anthony I.; Isaacs, Lyle. Preparation of glycoluril monomers for expanded cucurbit[n]uril synthesis. Tetrahedron, **2003**, 59(11), 1961-1970.

2. Synthesis of Polyhydroxypolyamides from Xylaric Acid, L-Arabinaric Acid (L-Lyxaric Acid), and Ribaric Acid

2.1 Introduction

The focus of the work presented here was the synthesis of polyhydroxypolyamides (PHPAs) derived from three pentaric acids, *meso*-xylaric acid, L-arabinaric acid (L-lyxaric acid), and *meso*-ribaric acid, Figure 2.1.

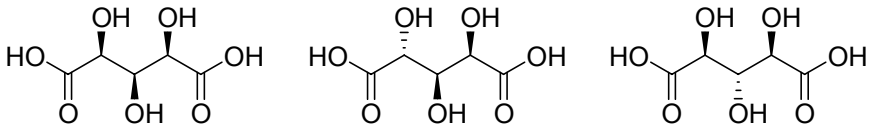

meso-Xylaric Acid L-Arabinaric Acid *meso*-Ribaric Acid

Figure 2.1 *meso*-Xylaric acid, L-Arabinaric acid, and *meso*-Ribaric acid

Natural polymers are ubiquitous throughout nature. Cellulose, starch, proteins, DNA, RNA, collagen, rubber, chitin, and silk are all naturally occurring polymers making up the backbone upon which biological systems operate. Cellulose is a structural polysaccharide for plants built from 1,4-β-D-glucopyranose linked monomers, whereas the polysaccharide starch employs α-D-glucopyranose units in 1,4-α- and 1,6-α-glycosidic linkages. Sources of cellulose other than cotton include sugar beets, trees, and agricultural waste such as corn husks and wheat stalks. Starch, is the primary food polysaccharide, and is obtained from corn, wheat, rice, potatoes, and other food crops.

Hemicellulose is a collective term for a variety of naturally occurring plant polysaccharides composed of different sugar residues, especially those of the D-pentose series of monosaccharides and to a lesser extent L-pentose monosaccharides. Unlike cellulose, hemicellulose consists of branched and unbranched polymers that prevent efficient packing within the polymer matrix and result in an amorphous material that is

more easily hydrolyzed than cellulose. The hydrolysis products of hemicellulose are the main source of D-xylose and L-arabinose, two of the base starting materials for the PHPAs presented here. D-Ribose is a carbohydrate constituent of nucleic acids found in plant and animal cells and is obtained from hydrolysis of yeast nucleic acids.

Polyhydroxypolyamides (PHPAs) are step growth polymers synthesized through polymerization of multifunctional monomers resulting in ABAB co-block polymers, Figure 2.2. As the polymerization progresses growing chains may react with each other to form even longer chains of varying length. The chemical and physical properties of a polymer changes as a function of its size, referred to as degree of polymerization (DP). The DP value is the number of repeating units (n) in the polymer chain, Figure 2.2.

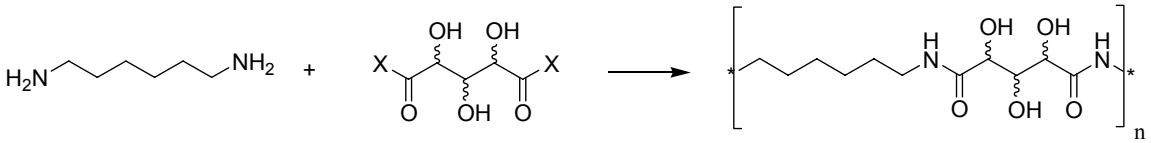

Figure 2.2 An example of a step-growth polymerization

In this work the average DP is calculated by ^{1}H NMR end group analysis as discussed later. The number average molar mass (M_n) of a polymer is calculated from the average DP. M_n is defined in equation 1.1, where N_i is the number of polymer chains of a molar mass M_i. Alternatively, M_n can be calculated by multiplying the average DP by the molecular weight of the repeating unit, M_r, as in equation 1.2.

$$M_n = \frac{\sum N_i \times M_i}{\sum N_i} \qquad (1.1)$$

$$M_n = DP \times M_r \qquad (1.2)$$

Because the chemical and physical properties of a polymer are dependent on molecular weight, considerable effort has been undertaken by polymer chemists to increase and control polymer molecular weights. Wallace Carothers, in an effort to obtain larger polymers of Nylon 6,6, the first commercially successful synthetic polymer, separated the polymerization of adipic acid (1,6-hexanedioic acid) with hexamethylenediamine (1,6-hexanediamine)[1,2] into two steps: Step 1, the formation of a diammonium salt (hexamethylenediammonium adipate) to obtain a 1:1 molar ratio of starting monomers; Step 2, polymerization at elevated temperatures (ca. 250 °C). Use of hexamethylenediammonium adipate as the source of monomers for Nylon 6,6 overcame the "stoichiometric problem" which until then prevented the synthesis of large polymers (> 10,000 Daltons) produced by step-growth polymerizations.

PHPAs are structurally analogous to Nylon 6,6 and Nylon 5,6, Figure 2.3, and similarly are synthesized from diacids and diamines. Unlike polymerizations yielding Nylons, PHPA's do not require the high temperatures necessary for polymerization. Hoagland demonstrated the polymerization of diethyl xylarate with hexamethylenediamine at room temperature.[3, 4] Diethyl xylarate underwent an intramolecular condensation reaction to form a γ-lactone which subsequently reacted with hexamethylenediamine through an intermolecular condensation reaction to generate the polyamide.

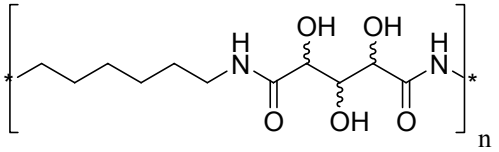

Poly(hexamethylene pentaramide)

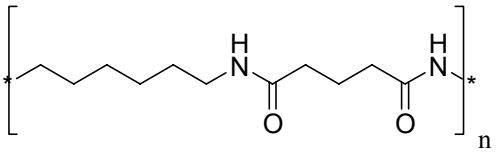

Nylon 5,6

Figure 2.3 An example of a poly(hexamethylene pentaramide) and Nylon 5,6

Ogata *et. al.* in the 1970's reported PHPAs synthesized by esterification of an aldaric acid with subsequent addition of a diamine to yield a PHPA.[5-16] Kiely *et. al.* have more recently contributed knowledge in this area through preparations of PHPAs from unprotected esterified aldaric acids derived from nitric acid oxidation of D-glucose, D-mannose, D-galactose and D-xylose.[17-30] Some attention has been given to D-xylose derived PHPAs but there has been no report of PHPAs derived from D-arabinose, L-arabinose, D-lyxose, L-lyxose and D-ribose using the synthetic strategies described in these earlier reports.

Kiely and co-workers have successfully synthesized a variety of poly(alkylene aldaramides) including poly(alkylene xylaramides).[17,18,20,21,23-26,28-30] The primary structural differences between different PHPAs are the number of carbons and stereochemistry in the aldaryl monomer unit as well as the length of the diamine unit. These structural differences result in significantly different chemical and physical properties within the class of PHPAs.

In an effort to obtain large PHPAs from starting pentaric acids and diamines of choice, three sets of reaction conditions, falling into two general synthetic routes, Figure

2.4, were employed. Route 1 proceeds through an esterified aldaric acid which is then reacted with a diamine of choice. Route 2 proceeds through a diammonium aldarate salt which is esterfied with methanolic HCl to produce a mixture of *bis*-ammonium dichloride salt, dimethyl aldarate, and methyl aldarate-1,4 (5,2)-lactone which is then neutralized and allowed to polymerize. The diammonium aldarate salts utilized in this study are depicted in Figure 2.5.

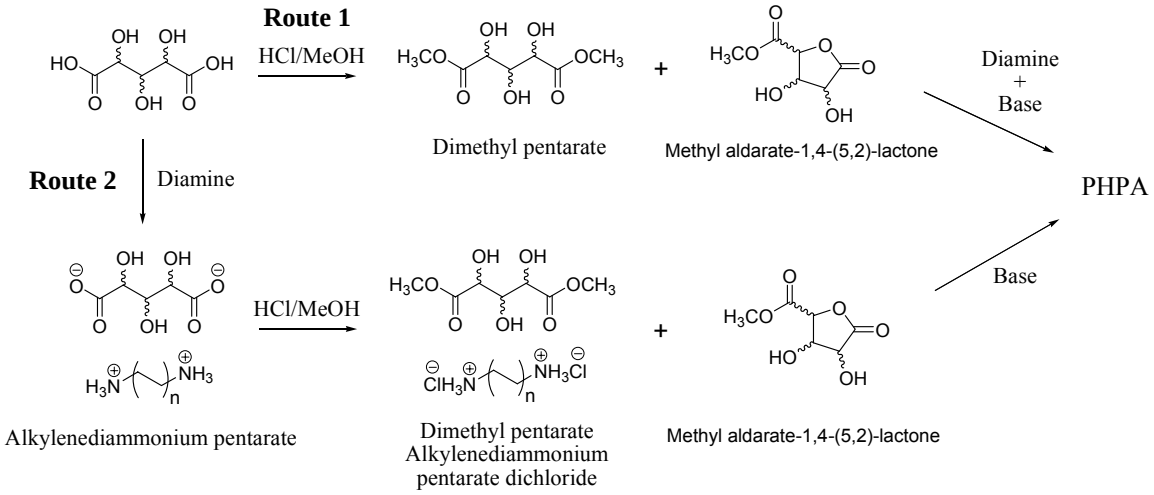

Figure 2.4 Synthetic routes 1 and 2 to obtain PHPAs derived from pentaric acids

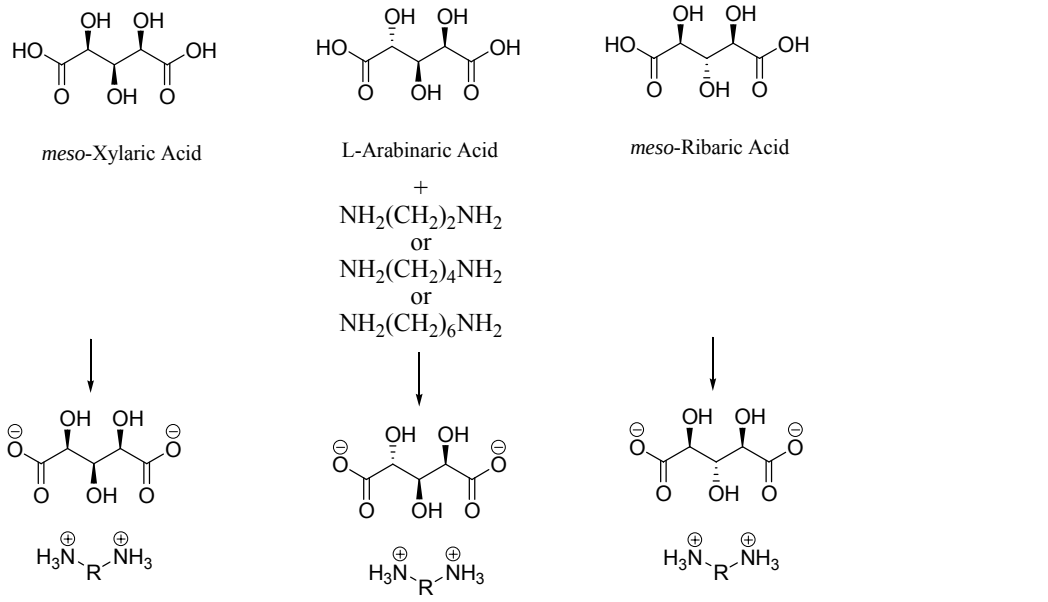

Figure 2.5 Ethylenediammonium, tetramethylenediammoium, and hexamethylenediammonium salts of xylaric acid, L-arabinaric acid, and ribaric acid

2.2 Results and Discussion

Xylaric acid, disodium L-arabinarate (disodium L-lyxarate), and disodium ribarate were used as starting diacid monomer sources for polymerizations with three diamine monomers (ethylenediamine, tetramethylenediamine, and hexamethylenediamine) using three different reaction conditions. Because disodium D-arabinarate and disodium L-arabinarate are enantiomers and thus have the same chemical properties, only one of these salts (disodium L-arabinarate) was used in the following polymerization experiments.

Because disodium L-arabinarate (disodium L-lyxarate) and disodium ribarate were used as starting materials for the polymerization experiments an additional acidification step not shown in Figure 2.4 was applied. In route 1, after esterification of the disodium salt with methanolic HCl, the mixture was filtered to remove the sodium chloride. In route 2, the disodium salt was dissolved in water, treated with a slight excess of acid form cation exchange resin for 5 minutes, the resin removed by filtration followed by addition of the diamine to form the diammonium aldarate salt.

In the triethylamine method, method (1), route 2 (Figure 2.4), a 3.0 molar excess of triethylamine as base was employed to neutralize the ammonium chloride salt. The sodium methoxide/triethylamine method, method (2), route 2 (Figure 2.4), utilized a 1.6 molar equivalent of sodium methoxide and 0.8 molar equivalent of triethylamine as base. A sodium methoxide/triethylamine mixture was used to neutralize the ammonium chloride salt because sodium methoxide is a much stronger base and the ability of triethyamine to neutralize a primary ammonium ion was in question. The ester/amine method, method (3), utilized route 1 (Figure 2.4), and a 0.5 molar equivalent of

triethylamine as a base to neutralize any residual HCl left over from the concentration step. The twenty seven resulting PHPAs are referred to as "prepolymers" and were isolated and characterized. The different prepolymer reaction conditions yielded polymers of varying size and chemical and physical properties, discussed later in this section. Additionally, in an effort to obtain larger polymers in a post-production treatment, and ascertain the best reaction conditions to do so, poly(hexamethylene xylaramide) prepolymers resulting from the three different prepolymer reaction conditions were stirred in three different postpolymer solvent mixtures [Mixture 1, MeOH/TEA/EG; Mixture 2, MeOH/TEA/DMSO; Mixture 3, MeOH/TEA].

All diammonium aldarate salts were soluble in water and consequently their NMR spectra were recorded in D_2O with chemical shifts referenced to *t*-butanol. The ^1H NMR spectrum of hexamethylenediammonium xylarate (**3**) is typical of these spectra and is shown in Figure 2.6. Hydroxyl and ammonium protons are not seen due to the rapid exchange of protons with deuterium in the D_2O. The methylene groups alpha (H1', H6', triplet, δ 2.95 ppm) and beta (H2', H5', multiplet, δ 1.63 ppm) to the ammonium groups have baseline separation and are shifted downfield of the internal methylene (H3', H4', δ 1.37 ppm) protons of the hexamethylenediammonium unit. The symmetrical nature of the example *meso* compound **3** can be seen as there are only two proton signals for the three protons on the xylarate unit. The protons alpha to the carboxylate groups (H2 and H4, δ 4.08 ppm) are split into a doublet by the inner triplet proton (H3, δ 4.03 ppm).

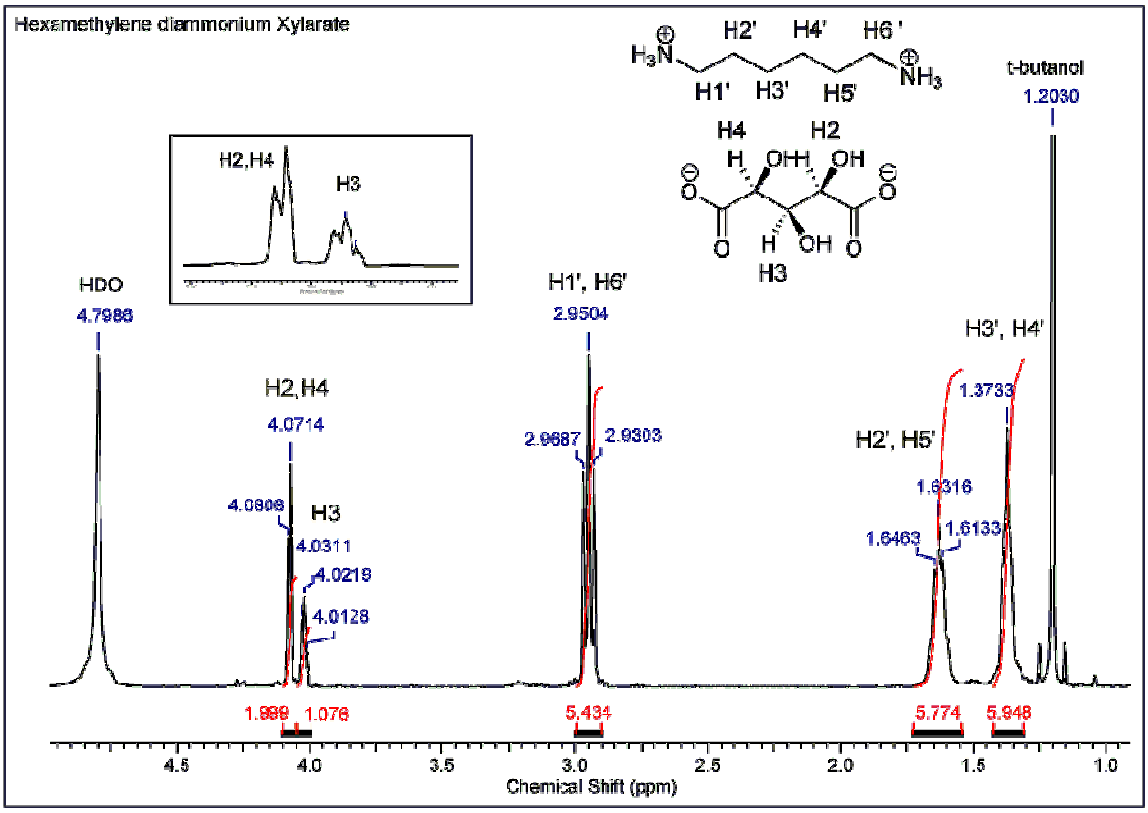

Figure 2.6 ^{1}H NMR spectra of hexamethylenediammonium xylarate (**3**)

^{1}H NMR spectra from all mixtures of alkylenediammonium dichloride salts, dimethyl aldarates, and methyl aldarate-1,4 (5,2)-lactones (Route 2, Figure 2.3) were recorded in DMSO-d_6 with chemical shifts referenced to TMS. DMSO-d_6, unlike D_2O, is a non-exchangeable solvent and the hydroxyl and ammonium protons should be visible and relatively sharp. However, broad ^{1}H NMR signals from the hydroxyl and ammonium groups of alkylenediammonium dichloride salt mixtures are observed, resulting most likely from OH and NH proton exchange due to residual methanol used in the esterification reaction. Figure 2.7 shows the ^{1}H NMR spectra of the mixture of hexamethylenediammonium dichloride, dimethyl xylarate, methyl xylarate-1,4-lactone, and methyl xylarate-5,2-lactone. The ^{1}H NMR spectrum of methyl xylarate-5,2-lactone is identical to methyl xylarate-1,4-lactone which is depicted in Figure 2.7. This mixture was

made from the methanolic HCl esterification of hexamethylenediammonium xylarate in accordance with the experimental procedure for **12**, except that after the mixture was concentrated under a stream of nitrogen and dried overnight, the ^{1}H NMR spectrum was obtained in DMSO-d_6 without further manipulation.

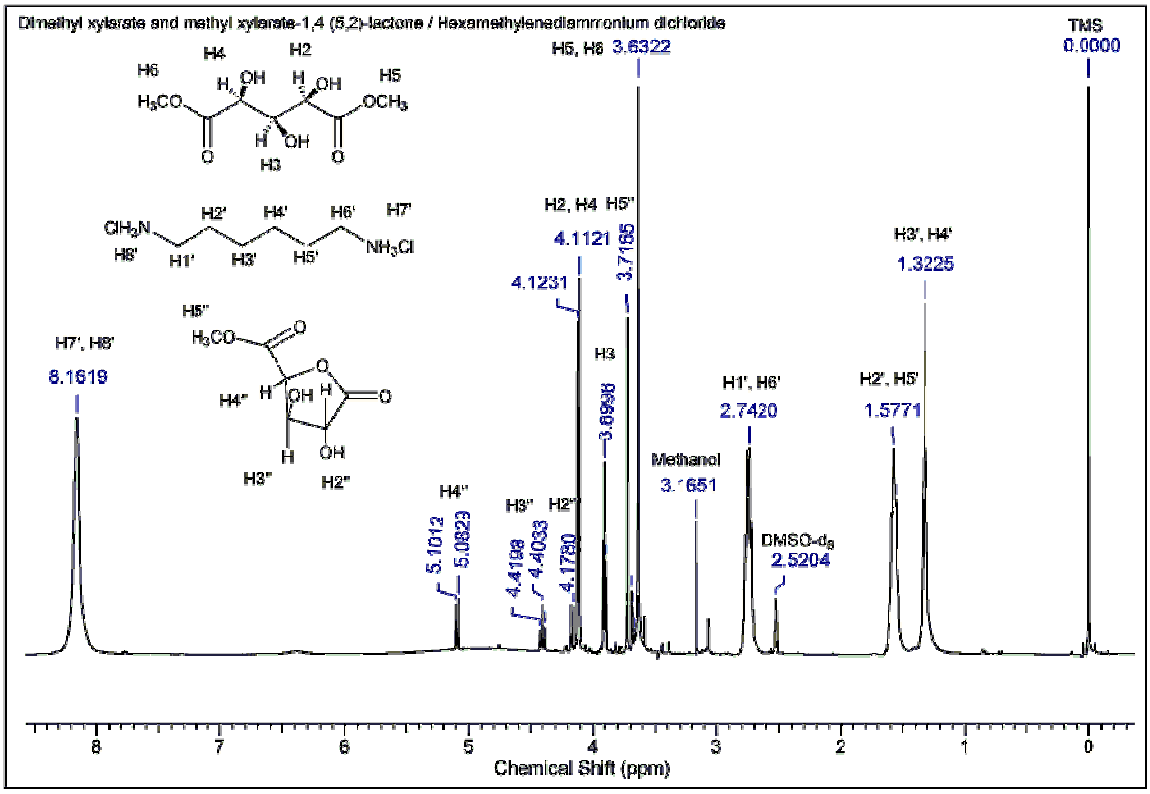

Figure 2.7 ^{1}H NMR spectrum of a mixture of hexamethylenediammonium dichloride, dimethyl xylarate, and the equivalent methyl xylarate-1,4-lactone and methyl xylarate-5,2-lactone

PHPAs synthesized through routes 1 and 2 exhibited variable solubility in different solvents, the solubility being dependent upon the aldaryl monomer and the length of the diamine unit. Because ^{1}H NMR end group analysis is used to determine the polymer's size, baseline resolution of proton signals used in the analysis was necessary and the NMR solvent choice is critical. ^{1}H NMR end group analysis was performed in

D_2O, a mixture of DMSO-d_6 (0.6-0.7 mL) and TFA-*d* (< 0.10 mL), or neat TFA-*d*, with D_2O as the preferred solvent. Polymers not soluble in water were typically soluble in DMSO-d_6 although the ^{1}H NMR proton signals necessary for end group analysis often overlapped with the residual DMSO-d_6 signal. Therefore, a solvent mixture of DMSO-d_6 and TFA-*d* was sometimes employed. This solvent mixture separated the ^{1}H NMR signals of the methylene group alpha to the terminal amine from the residual DMSO-d_6 solvent peak, and the terminal amine unit was converted into an ammonium group. TFA-*d* was used as a solvent only when the polymer was insoluble in D_2O or a mixture of DMSO-d_6 and TFA-*d*. PHPAs are unstable over time in TFA-*d*, thus requiring that ^{1}H NMR spectra be obtained as quickly as possible when TFA-*d* was used as the NMR solvent.

The size of the polymers in this work is reported as an average degree of polymerization (DP) and as a number average molar mass (M_n). DP calculations were performed in this investigation utilizing ^{1}H NMR end group analysis by setting the integration value of the methylene protons alpha to the terminal amine or its corresponding ammonium salt to a value of 0.5. The resulting ratio of integration value of the methylene protons alpha to the amide to that of the methylene protons alpha to the terminal amine or ammonium unit is a good approximation of the DP value, Figure 2.8.

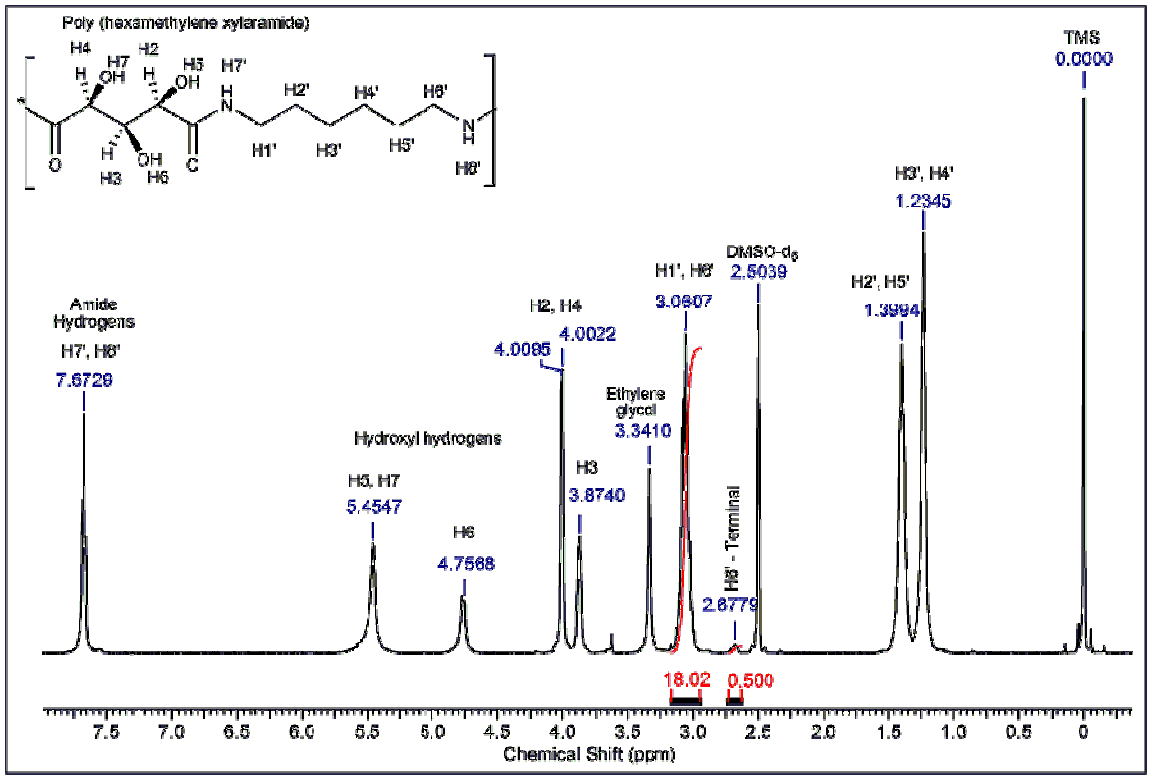

Figure 2.8 Assigned ^{1}H NMR spectra of poly(hexamethylene xylaramide) (**37**) DP = 18.0

Pre-polymerizations

In an effort to compare the relative size of PHPAs starting from pentaric acids and diamines of choice, three sets of reactions conditions were employed to investigate the best reaction conditions for each polymer. Prepolymer polymerization results for poly(alkylene aldaramides) with DP, M_n, and percent yields are reported in Table 2.1. There is a corresponding trend between increasing percent yields and larger DP values. Additionally, independent of the method employed the ethylenediamine polymers gave the smallest DP values while the hexamethylene polymers were typically the largest.

The three methods employed were method (1), route 2 (Figure 2.4); sodium methoxide/triethylamine method, method (2), route 2 (Figure 2.4); ester/amine method,

method (3), utilized route 1 (Figure 2.4). The triethylamine method which used three molar equivalents of triethylamine as base and gave the largest pre-polymers for ribaric and L-arabinaric acid derived PHPAs. The ester/amine method gave higher DP values for xylaric acid derived pre-polymers. The poly(alkylene xylaramide)s synthesized using the triethylamine method have percent yields and DP values similar to those of the other poly(alkylene L-arabinaramide)s and poly(alkylene ribaramide)s synthesized which were considerable higher than for the sodium methoxide/triethylamine and ester/amine methods.

The sodium methoxide/triethylamine method generally had the smallest DP values and percent yields for the three methods, with the exception of poly(ethylene L-arabinaramide). A sodium methoxide/triethylamine mixture was used because the ability of triethylamine to neutralize a primary ammonium chloride ion was in question. Sodium methoxide, a much stronger base, was considered a good candidate for the neutralization of the ammonium chloride salt although the experimental results refute this assertion. Because the reactions were not carried out in dry methanol, it is possible that the methanol had absorbed a significant amount of water from the air which could allow the esterified aldaric acids to undergo hydrolysis in the basic solvent system, thereby preventing polymerization.

As Carothers demonstrated, step-wise polymerizations produce the largest polymers when there are equal molar equivalents of monomers A and B in the reaction mixture as was the case in the prior two methods. The ester/amine method does not incorporate a 1:1 salt and is therefore sensitive to unequal molar amounts of monomers A and B. The poly(alkylene xylaramide) pre-polymers synthesized by the ester/amine

method were significantly larger than poly(alkylene xylaramide) pre-polymers synthesized by the other two methods and also larger than the poly(alkylene L-arabinaramide) and poly(alkylene ribaramide) pre-polymers synthesized by the ester/amine method. In this study, the ester/amine polymerizations of esterified xylaric acid were less sensitive to laboratory measurements because they were on a larger scale than those of esterified L-arabinaric and esterified ribaric acids. The sensitivity to 1:1 molar ratios of monomers A and B is most likely the cause for these observations.

Table 2.1 Results of Pre-polymerizations - Degree of polymerization, molar average molecular weights, and percent yield using three different reaction conditions

Results for poly(alkylene pentaramide) prepolymers using TEA Method (1)[(a)]

Polymer	DP	M_n	Yield %
Poly(ethylene xylaramide)	3	720	79.9
Poly(tetramethylene xylaramide)	9.4	2520	69.6
Poly(hexamethylene xylaramide)	7.9	2330	85.5
Poly(ethylene-L-arabinaramide)	2.9	690	42.7
Poly(tetramethylene-L-arabinaramide)	6.7	1790	73.6
Poly(hexamethylene-L-arabinaramide)	18.4	5440	69.5
Poly(ethylene ribaramide)	4.3	1030	87.1
Poly(tetramethylene ribaramide)	17.8	4770	90.0
Poly(hexamethylene ribaramide)	30.8	9110	90.9

Results for poly(alkylene pentaramide) prepolymers using NaOMe/TEA Method (2)[(b)]

Polymer	DP	M_n	Yield %
Poly(ethylene xylaramide)	4.4	1050	37.4
Poly(tetramethylene xylaramide)	4.3	1150	61.6
Poly(hexamethylene xylaramide)	5.0	1480	41.5
Poly(ethylene-L-arabinaramide)	7.2	1730	96.6
Poly(tetramethylene-L-arabinaramide)	3.0	800	59.1
Poly(hexamethylene-L-arabinaramide)	9.6	2840	35.4
Poly(ethylene ribaramide)	3.3	790	82.3
Poly(tetramethylene ribaramide)	8.2	2190	88.9
Poly(hexamethylene ribaramide)	12.1	3580	83.7

Table 2.1 Continued

Results for poly(alkylene pentaramide) prepolymers using Ester/Amine Method (3)[(c)]

Polymer	DP	M_n	Yield %
Poly(ethylene xylaramide)	9.1	2210	89.3
Poly(tetramethylene xylaramide)	4.8	1280	81.2
Poly(hexamethylene xylaramide)	18.6	5500	48.5
Poly(ethylene-L-arabinaramide)	2.0	480	25.7
Poly(tetramethylene-L-arabinaramide)	3.5	930	27.0
Poly(hexamethylene-L-arabinaramide)	2.9	850	31.1
Poly(ethylene ribaramide)	4.4	1050	92.8
Poly(tetramethylene ribaramide)	9.3	2490	87.7
Poly(hexamethylene ribaramide)	12.1	3580	85.7

a. Route 2, Figure 2.3, 3.0 molar excess of triethylamine
b. Route 2, Figure 2.3, 1.6 molar equivalence of sodium methoxide, 0.8 molar equivalent of triethylamine
c. Route 1, Figure 2.3, 0.5 molar equivalence of triethylamine

Post-polymerizations

In an effort to understand the reaction conditions necessary to increase the solubility of PHPAs and produce even larger polymers, pre-polymers of poly(hexamethylene xylaramide) from each pre-polymer method underwent three different post-polymermerization treatments. In each solvent mixture triethylamine was used as a base to neutralize any remaining ammonium chloride salt that may be present in the pre-polymer material. Figure 2.9 depicts the post-polymerization treatment. Results for poly(hexamethylene xylaramide) post-polymers are reported in Table 2.2.

Poly(hexamethylene xylaramide) post-polymers derived from pre-polymer route 2 (utilizing a 1:1 salt mixture) had significantly larger gains in average DP than those of route 1 utilizing the ester/amine method. Signficant post-polymerization gains in the DP values of PHPAs synthesized through pre-polymer route 2 (utilizing a 1:1 salt mixture) illustrates that within the pre-polymer material there are significant quanitites of

ammonium chloride salts that prevent further polymerization. Additionally, the size of the post-polymer was independent of solvent composition as all post-polymers of poly(hexamethylene xylaramide) showed DP values of approximately 21 and average molecular weights of 6220. This is most likely due to reaching the limitations in solubility with increasing DP value.

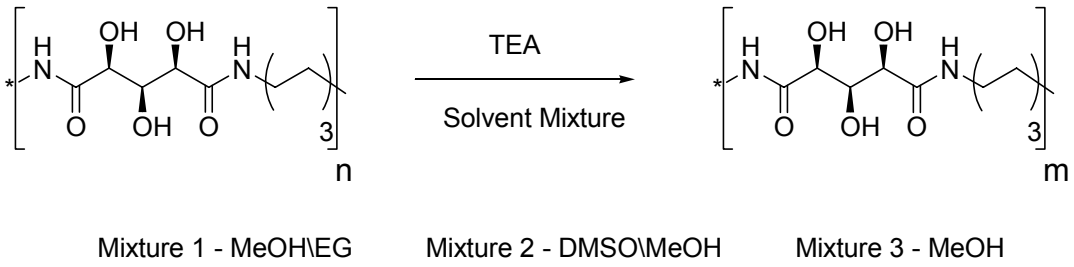

Figure 2.9 Post-polymerization using triethylamine as base and varying solvent mixtures

Table 2.2 Poly(hexamethylene xylaramide) postpolymer results from three postpolymerization methods

Prepolymer Method	Postpolymer Method	Starting DP	Starting M_n	New DP	New M_m	Yield %	Change in DP/M_n
TEA Method 1	MeOH\TEA\EG Mixture 1	7.83	2320	18.0	5330	97.1	10.2 , 3010
TEA/NaOMe Method 2	MeOH\TEA\EG Mixture 1	5.04	1490	12.7	3760	93.1	7.7 , 2270
Ester/Amine Method 3	MeOH\TEA\EG Mixture 1	18.6	5510	21.0	6220	98.3	2.4 , 710
TEA Method 1	DMSO\TEA\MeOH Mixture 2	7.83	2320	18.5	5480	97.4	10.7 , 3160
TEA/NaOMe Method 2	DMSO\TEA\MeOH Mixture 2	5.04	1490	15.9	4710	85.5	10.9 , 3220
Ester/Amine Method 3	DMSO\TEA\MeOH Mixture 2	18.6	5510	20.0	5920	47.1	1.4 , 410
TEA Method 1	TEA\MeOH Mixture 3	7.83	2320	23.2	6870	86.0	15.4 , 4550
TEA/NaOMe Method 2	TEA\MeOH Mixture 3	5.04	1490	21.7	6420	65.3	16.7 , 4930
Ester/Amine Method 3	TEA\MeOH Mixture 3	18.6	5510	18.2	5390	77.8	-0.4 , -120

2.3 Experimental

General Methods

One dimensional ^{1}H NMR spectra were obtained using a 400 MHz Varian Unity Plus spectrometer or a 500 MHz Varian spectrometer. NMR spectra were processed using ACD/SpecManager 1D NMR software Version 9.13. Chemical Shifts were expressed in parts per million relative to tertiary-butyl alcohol (1.203 ppm) for D_2O, tetramethylsilane (0.00 ppm) for DMSO-d_6 and chloroform-*d*, and to the solvent peak (11.50 ppm) for TFA-*d*. All NMR solvents were obtained from Cambridge Isotope Laboratories, Inc. NMR solvent listed as "DMSO/TFA" signifies a mixture of deuterated DMSO (0.6-0.7 mL) and deuterated TFA (< 0.03 mL). NMR data is presented in the first experimental procedure reported for a given molecule. All chemicals were purchased from Aldrich and used without further purification. Solvent concentrations were performed under reduced pressure. Samples were dried under vacuum at room temperature. In all instances deionized water was used.

2.3.1 Synthesis and Characterization of Diammonium Salts

Ethylenediammonium xylarate (**1**).

To a solution of xylaric acid (5.541 g, 30.77 mmol) in methanol (20 mL) was added ethylenediamine (2.219 g, 36.92 mmol) in methanol (5 mL) and the resulting reaction mixture stirred at room temperature for 1 h. The solid was isolated by filtration and washed with methanol (3 x 5 mL). The final solid was isolated by filtration and dried 12 h to yield ethylenediammonium xylarate (**1**, 6.340 g, 26.39 mmol, 85.8%). ^{1}H NMR (D_2O) δ 4.11 (d, 2H, *J* 2.93 Hz, H-2, H-4), 4.04 (t, 1H, H-3), 3.26 (s, 4H,). Anal. Calcd for $C_7H_{16}N_2O_7$ (240.21): C, 35.00; H, 6.71; N, 11.66. Found C, 34.69; H, 6.77; N, 12.47.

Tetramethylenediammonium xylarate (**2**).

Prepared according to the procedure for **1**: xylaric acid (5.336 g, 29.79 mmol) in methanol (20 mL) was added tetramethylenediamine (3.152 g, 35.75 mmol) in methanol, then reaction mixture then stirred at r.t. for 1 h. The solid was isolated, washed with methanol (3 x 5 mL), and dried (12 h) to yield tetramethylenediammonium xylarate (**2**, 6.432 g, 23.98 mmol, 80.5%).^{1}H NMR (D_2O) δ 4.09 (d, 2H, *J* 2.93 Hz), 4.03 (t, 1H) 2.99 (s, 4H), 1.70 (s, 4H). Anal. Calcd for $C_9H_{20}N_2O_7$ (268.26): C, 40.29; H, 7.51; N, 10.44. Found C, 40.34; H, 7.68; N, 10.43

Hexamethylenediammonium xylarate (**3**).

Prepared according to the procedure for **1**: xylaric acid (6.288 g, 34.91 mmol) in methanol (20 mL) was added hexamethylenediamine (4.869 g, 41.90 mmol) in methanol (5 mL), the reaction mixture then stirred at room temperature for 1 h. The solid was isolated, washed with methanol (3 x 5 mL), and dried (12 h) to yield hexamethylenediammonium xylarate (**3**, 8.390 g, 28.31 mmol, 81.09%).^{1}H NMR (D_2O) δ 4.08 (d, 2H, *J* 2.93 Hz), 4.02 (t, 1H), 2.95 (t, 4H), 1.63 (s, 4H), 1.37 (s, 4H). Anal. Calcd for $C_{13}H_{30}N_2O_7$ (296.32): C, 44.59; H, 8.16; N, 9.45. Found C, 44.04; H, 8.08; N, 9.31.

Ethylenediammonium L-arabinarate (ethylenediammonium L-lyxarate) (**4**).

To a solution of disodium L-arabinarate (1.011 g, 4.315 mmol) in water (7 mL) was added Dowex 50WX cation exchange resin (7 mL, 14.7 mmol) and the mixture was stirred at r.t. for 5 min. The resin was removed by filtration and a solution of ethylenediamine (0.3257 g, 5.419 mmol) in water (3 mL) was added to the filtrate. The solution was stirred at room temperature 1 h and concentrated to nearly a tacky solid. The tacky solid was stirred with ethanol (25 mL) at r.t. for 3 days, The resulting solid was

isolated by filtration and dried overnight to yield ethylenediammonium L-arabinarate (ethylenediammonium L-lyxarate). (**4**, 0.850 g, 4.169 mmol, 96.5%). ^{1}H NMR (D_2O) δ 4.14 (s, 2H), 3.99 (s, 1H), 2.70 (s, 4H). Anal. Calcd for $C_7H_{16}N_2O_7$ (240.21): C, 35.00; H, 6.71; N, 11.66. Found C, 31.79; H, 5.42; N, 7.86.

Tetramethylenediammonium L-arabinarate (tetramethylenediammonium L-lyxarate) (**5**).

Prepared according to the procedure for **4**: disodium L-arabinarate (1.004 g, 4.285 mmol) in water (7 ml), Dowex 50WX (7 mL, 14.7 mmol), the mixture stirred at r.t. for 5 min. The resin was removed, tetramethylenediamine (0.4737 g, 5.374 mmol) in water (3 mL) was added, the solution stirred for 1 h, and concentrated. The tacky solid product was stirred with ethanol (25 mL), at r.t. for 3 h, the resulting solid was isolated, and dried overnight to yield tetramethylenediammonium L-arabinarate (tetramethylenediammonium L-lyxarate) (**5**, 0.8862 g, 3.305 mmol, 77.14%). ^{1}H NMR (D_2O) δ 4.15 (s, 1H) 3.98 (s, 2H) 2.99 (s, 4H) 1.71 (s, 4H). Anal. Calcd for $C_9H_{20}N_2O_7$ (268.26): C, 40.29; H, 7.51; N, 10.44. Found C, 40.32; H, 7.59; N, 10.55.

Hexamethylenediammonium L-arabinarate (hexamethylenediammonium L-lyxarate) (**6**).

Prepared according to the procedure for **4**: disodium L-arabinarate (1.019 g, 4.351 mmol) in water (10 mL), Dowex 50WX (10 mL, 21.0 mmol), the mixture was stirred at r.t. for 5 min. The resin was removed, hexamethylenediamine (0.634 g, 5.457 mmol) in water (5 mL) was added, the solution stirred at r.t. for 1 h, and concentrated. The tacky product was stirred with ethanol (3 x 25 mL) for 4 h, isolated, and dried to yield hexamethylenediammonium L-arabinarate (hexamethylenediammonium L-lyxarate) (**6,**

0.8735 g, 2.954 mmol, 67.81%). ^{1}H NMR (D_2O) δ 4.14 (s, 2H), 3.98 (s, 2H), 2.92 (t, 4H), 1.62 (s, 4H), 1.37 (s, 4H). Anal. Calcd for $C_{13}H_{30}N_2O_7$ (296.32): C, 44.59; H, 8.16; N, 9.45. Found C, 42.75; H, 8.39; N, 8.98.

Ethylenediammonium ribarate (**7**).

To a solution of disodium ribarate (1.092 g, 5.279 mmol) in water (10 mL) was added Dowex 50WX cation exchange resin (10 mL, 21.0 mmol) and the mixture was stirred at r.t. for 5 min. The resin was removed by filtration and a solution of ethylenediamine (0.381 g, 6.335 mmol) in water (3 mL) was added to the filtrate. The solution was stirred at r.t. for 1 h and concentrated to a tacky solid. The tacky solid was stirred with ethanol (3 x 25 mL) for 4 h and isolated by filtration. The resulting solid was dried 12 h to yield ethylenediammonium ribarate (**7**, 0.9588 g, 4.545 mmol, 86.13%). ^{1}H NMR (D_2O) δ 4.07 (s, 3H, H-2, H-3, H-4), 3.27 (s, 4H,). Anal. Calcd for $C_7H_{16}N_2O_7$ (240.21): C, 35.00; H, 6.71; N, 11.66. Found C, 31.61; H, 5.34; N, 7.51.

Tetramethylenediammonium ribarate (**8**).

Prepared according to the procedure of **7**: disodium ribarate (1.025 g, 4.574 mmol) in water (7mL), Dowex 50WX (7 mL, 14.7 mmol), the mixture stirred at r.t. for 5 min. The resin was removed, tetramethylenediamine (0.484 g, 5.489 mmol) in water (3mL) was added. The solution was stirred 1 h, and concentrated to a tacky solid which was triturated with ethanol (3 x 25 mL). The resulting solid was dried 12 h to yield tetramethylenediammonium ribarate (**8,** 0.9588 g, 3.574 mmol, 78.14%). ^{1}H NMR (D_2O) δ 4.06 (s, 3H, H-2, H-3, H-4), 2.99 (s, 4H,), 1.70 (s, 4H). Anal. Calcd for $C_9H_{20}N_2O_7$ (268.26): C, 40.29; H, 7.51; N, 10.44. Found C, 40.41; H, 7.70; N, 10.47.

Hexamethylenediammonium ribarate (**9**).

Prepared according to the procedure for **7**: disodium ribarate (1.553 g, 6.930 mmol) in water (10 mL), Dowex 50wx (10 mL, 21.0 mmol), the mixture stirred at r.t. for 5 min. The resin was removed, hexamethylenediamine (1.127 g, 9.702 mmol) in water (3 mL). The solution stirred at r.t. for 1 h and concentrated. The tacky product was stirred with methanol (50 mL) at r.t. for 2 h and isolated, stirred with ethanol (50 mL) for 2 h, and isolated. The solid stirred with acetone (25 mL) for 2 h, isolated, dried 12 h to yield hexamethylenediammonium ribarate (**9,** 1.495 g, 5.048 mmol, 72.85%). ^{1}H NMR (D_2O) δ 4.06 (s, 3H, H-2, H-3, H-4), 2.95 (t, 4H,), 1.63 (s, 4H), 1.37 (s, 4H). Anal. Calcd for $C_{13}H_{30}N_2O_7$ (296.32): C, 44.59; H, 8.16; N, 9.45. Found C, 40.00; H, 7.36; N, 10.39.

2.3.2 Polymerizations of Diammonium Salts – Method 1 – Triethylamine Method

Poly(ethylene xylaramide) Prepolymer (**10**).

To a solution of acetyl chloride (0.537 mL, 7.599 mmol) in methanol (4 mL) was added ethylenediammonium xylarate (**6,** 0.608 g, 2.533 mmol) and the mixture was stirred at room temperature for 3 h. The reaction mixture was concentrated under a stream of nitrogen and dried overnight. The resulting syrup was dissolved in methanol (7.2 mL) to which triethylamine (1.058 mL, 7.599 mmol) was added dropwise and the mixture was stirred at room temperature for 24 h. The solid was isolated by centrifugation, rinsed with cold methanol (3x 2 mL), isolated by centrifugation and dried overnight to yield poly(ethylene xylaramide) prepolymer (**10**, 0.414 g, 2.026 mmol, 79.9%, dp 3.0). ^{1}H NMR (D_2O) δ 4.27 (s, 2H), 4.09 (s, 1H), 3.38 (s, 4H).

Poly(tetramethylene xylaramide) Prepolymer (**11**).

Prepared according to the procedure for **10**: acetyl chloride (0.478 mL, 6.759 mmol) in methanol (4 mL), tetramethylenediammonium xylarate (**7,** 0.604 g, 2.253 mmol), stirred at r.t. for 3 h, reaction mixture concentrated, and dried overnight. The resulting syrup was dissolved in methanol (7.0 mL), triethylamine (0.941 mL, 6.759 mmol) was added dropwise and the mixture stirred at r.t. for 24 h. The solid was isolated, rinsed with cold methanol (3 x 2 mL), isolated, and dried to yield poly(tetramethylene xylaramide) prepolymer (**11**, 0.364 g, 1.567 mmol, 69.6%, dp 9.4). ^{1}H NMR (TFA) δ 4.85 (s, 2H), 4.74 (s, 1H), 3.45 (s, 4H), 1.70 (s, 4H).

Poly(hexamethylene xylaramide) Prepolymer (**12**).

Prepared according to the procedure for **10**: acetyl chloride (0.363 mL, 5.131 mmol) in methanol (4 mL), hexamethylenediammonium xylarate (**8,** 0.507 g, 1.710 mmol) stirred at r.t. for 3 h, reaction mixture concentrated and dried overnight. The resulting syrup was dissolved in methanol (7.3 mL), triethylamine (0.714 mL, 5.131 mmol) was added dropwise, and the mixture stirred at r.t. for 24 h. The solid was isolated, rinsed with cold methanol (3 x 2 mL), isolated, and dried to yield poly(hexamethylene xylaramide) prepolymer (**12**, 0.380 g, 1.460 mmol, 85.5%, dp 7.93). ^{1}H NMR (DMSO/TFA) δ 4.14 (d, 2H), 4.00 (s, 1H), 3.16 (s, 4H), 1.49 (d, 4H), 1.32 (s, 4H).

Poly(ethylene L-arabinaramide) [Poly(ethylene L-lyxaramide)] Prepolymer (**13**).

To a solution of acetyl chloride (0.186 mL, 2.626 mmol) in methanol (2 mL) was added ethylenediammonium L-arabinarate (**4,** 0.210g, 0.875 mmol) and the mixture was stirred at room temperature for 3 h. The reaction mixture was concentrated under a stream of nitrogen and dried overnight. The resulting syrup was dissolved in methanol

(3.5 mL) to which triethylamine (0.366 mL, 2.625 mmol) was added dropwise and the mixture was stirred at room temperature for 24 h. The solid was isolated by centrifugation, rinsed with cold methanol (3 x 2 mL), isolated by centrifugation and dried overnight to yield poly(tetramethylene L-arabinaramide) [Poly(ethylene L-lyxaramide)] prepolymer (**13,** 0.077 g, 1.389 mmol, 43.0%, dp 4.38). ^{1}H NMR (DMSO/TFA) δ 4.24 (s, 1H), 4.13 (s, 1H), 3.94 (m, 1H), 3.24 (s, 4H).

Poly(tetramethylene L-arabinaramide) [Poly(tetramethylene L-lyxaramide)] Prepolymer (**14**).

Prepared according to the procedure for **13**: acetyl chloride 0.400 mL, 5.662 mmol) in methanol (4 mL), tetramethylenediammonium L-arabinarate (**5,** 0.506g, 1.887 mmol) and the mixture stirred at r.t. for 3 h, concentrated, and dried overnight. The resulting syrup was dissolved in methanol (7 mL), triethylamine (0.788 mL, 5.662 mmol) was added dropwise, and the mixture stirred at r.t for 24 h. The solid was isolated, rinsed with cold methanol (3 x 2 mL), isolated and dried to yield poly(tetramethylene L-arabinaramide) [Poly(tetramethylene L-lyxaramide)] prepolymer (**14,** 0.323 g, 1.389 mmol, 73.6%, dp 6.74). ^{1}H NMR (DMSO/TFA) δ 4.14 (d, 1H), 3.91 (dd, 2H), 3.12 (s, 4H), 1.43 (s, 4H).

Poly(hexamethylene L-arabinaramide) [Poly(hexamethylene L-lyxaramide)] Prepolymer (**15**).

Prepared according to the procedure for **13**: acetyl chloride (0.366 mL, 5.181 mmol) in methanol (4 mL), hexamethylenediammonium L-arabinarate (**6,** 0.511g, 1.727 mmol) and the mixture stirred at r.t. for 3 h, concentrated, and dried overnight. The resulting syrup was dissolved in methanol (7 mL), triethylamine (0.721 mL, 5.181 mmol)

was added dropwise, and the mixture stirred at r.t. for 24 h. The solid was isolated, rinsed with cold methanol (3 x 2 mL), isolated, and dried to yield poly(hexamethylene L-arabinaramide) [Poly(hexamethylene L-lyxaramide)] prepolymer (**15,** 0.312 g, 1.201 mmol, 69.5%, dp 18.4). ^{1}H NMR (DMSO/TFA) δ 4.08 (s, 1H), 3.91 (dd, 2H), 3.11 (s, 4H), 1.43 (s, 4H), 1.27 (s, 4H).

Poly(ethylene ribaramide) Prepolymer (**16**).

To a solution of acetyl chloride (0.244 mL, 3.456 mmol) in methanol (4 mL) was added ethylenediammonium ribarate (**7,** 0.275 g, 1.152 mmol) and the mixture was stirred at room temperature for 3 h. The reaction was concentrated under a stream of nitrogen and dried overnight. The resulting syrup was dissolved with methanol (4.0 mL) to which triethylamine (0.481 mL, 3.456 mmol) was added dropwise and the mixture was stirred at room temperature for 24h. The solid was isolated by centrifugation, rinsed with cold methanol (3 x 2 mL), isolated by centrifugation and dried overnight to yield poly(ethylene ribaramide) prepolymer (**16,** 0.205 g, 1.004 mmol, 87.1%, dp 4.34). ^{1}H NMR (DMSO/TFA) δ 4.06 (s, 2H, H-3, H-4), 4.00 (s, 1H, H-3), 3.24 (s, 4H).

Poly(tetramethylene ribaramide) Prepolymer (**17**).

Prepared according to the procedure for **16**: acetyl chloride (0.158 mL, 2.241 mmol) in methanol (4 mL), tetramethylenediammonium ribarate (**8,** 0.200 g, 0.747 mmol) and the mixture stirred at r.t. for 3 h, concentrated, and dried overnight. The resulting syrup was dissolved in methanol (4.0 mL), triethylamine (0.312 mL, 2.241 mmol) was added dropwise, and the mixture stirred at r.t. for 24h. The solid was isolated, rinsed with cold methanol (3 x 2 mL), isolated, and dried to yield poly(tetramethylene

ribaramide) prepolymer (**17,** 0.158 g, 0.679 mmol, 90.9%, dp 17.8). ^{1}H NMR (DMSO) δ 4.01 (s, 3H, H-2, H-3, H-4), 3.11 (s, 4H), 1.43 (s, 4H).

Poly(hexamethylene ribaramide) Prepolymer (**18**).

Prepared according to the procedure of **16**: acetyl chloride (0.180 mL, 2.553 mmol) in methanol (4 mL), hexamethylenediammonium ribarate (**9,** 0.252 g, 0.851 mmol), the mixture stirred at r.t. for 3 h, concentrated, and dried overnight. The resulting syrup was dissolved in methanol (4.0 mL), triethylamine (0.356 mL, 2.553 mmol) was added dropwise, and the mixture stirred at r.t. for 24h. The solid was isolated, rinsed with cold methanol (3 x 2 mL), isolated, and dried to yield poly(hexamethylene ribaramide) prepolymer (**18,** 0.198 g, 0.760 mmol, 89.3%, dp 30.8). ^{1}H NMR (DMSO/TFA) δ 3.99 (s, 3H, H-2, H-3, H-4), 3.11 (s, 4H), 1.42 (s, 4H), 1.25 (s, 4H).

2.3.3 Polymerizations of Diammonium Salts – Method 2 – Sodium Methoxide/Triethylamine Method

Poly(ethylene xylaramide) Prepolymer (**19**).

To a solution of acetyl chloride (0.561 mL, 7.921 mmol) in methanol (4 mL) was added ethylenediammonium xylarate (**1,** 0.317 g, 1.320 mmol) and the mixture was stirred at room temperature for 3 h. The reaction mixture was concentrated under a stream of nitrogen and dried overnight. The resulting syrup was dissolved in methanol (1 mL) to which sodium methoxide in methanol (4.22 mL, 2.112 mmol) and triethylamine (0.147 mL, 1.056 mmol) were added dropwise and the mixture was stirred at room temperature for 24 h. The solid was isolated by centrifugation, rinsed with cold methanol (3 x 2 mL), isolated by centrifugation and dried overnight to yield poly(ethylene xylaramide) prepolymer (**19,** 0.101 g, 0.494 mmol, 37.4%, dp 4.42).

Poly(tetramethylene xylaramide) Prepolymer (**20**).

Prepared according to the procedure of **19**: acetyl chloride (0.500 mL, 7.054 mmol) in methanol (4 mL), tetramethylenediammonium xylarate (**2,** 0.631 g, 2.351 mmol), stirred at r.t. 3 h, concentrated, dried overnight, treated with sodium methoxide in methanol (7.525 mL, 3.762 mmol) and triethylamine (0.262 mL, 1.881 mmol), and stirred at r.t. for 24 h. The solid was isolated, rinsed with cold methanol (3 x 2 mL), isolated, and dried overnight to yield poly(tetramethylene xylaramide) prepolymer (**20,** 0.337 g, 1.449 mmol, 61.6%, dp 4.31).

Poly(hexamethylene xylaramide) Prepolymer (**21**).

Prepared according to the procedure for **19**: acetyl chloride (0.736 mL, 10.39 mmol) in methanol (4 mL), hexamethylenediammonium xylarate (**3,** 0.513 g, 1.730 mmol), stirred at r.t. for 3 h, concentrated, dried overnight, treated with sodium methoxide in methanol (5.542 mL, 2.771 mmol) and triethylamine (0.193 mL, 1.390 mmol), and stirred ar r.t. for 24 h. The solid was isolated, rinsed with cold methanol (3 x 2 mL), isolated, and dried overnight to yield poly(hexamethylene xylaramide) prepolymer (**21,** 0.187 g, 0.717 mmol, 41.5%, dp 5.04).

Poly(ethylene L-arabinaramide) [Poly(ethylene L-lyxaramide)] Prepolymer (**22**)**.**

Prepared according to the procedure for **19**: acetyl chloride (0.202 mL, 2.592 mmol) in methanol (4 mL), ethylenediammonium L-arabinarate (**4,** 0.208 g, 0.864 mmol), stirred at r.t. for 3 h, concentrated, dried overnight, treated with sodium methoxide in methanol (2.766 mL, 1.383 mmol) and triethylamine (0.091 mL, 0.691 mmol), and stirred at r.t. for 24 h. The solid was isolated, rinsed with cold methanol (3 x 2 mL),

isolated, and dried to yield poly(ethylene L-arabinaramide) [Poly(ethylene L-lyxaramide)] prepolymer (**22,** 0.171 g, 0.835 mmol, 96.62%, dp 7.22).

Poly(tetramethylene L-arabinaramide) [Poly(tetramethylene L-lyxaramide)] Prepolymer (**23**).

Prepared according to the procedure for **19**: acetyl chloride (0.186 mL, 2.388 mmol) in methanol (4 mL), tetramethylenediammonium L-arabinarate (**5,** 0.213 g, 0.796 mmol), stirred at r.t. for3 h, concentrated, dried overnight, dissolved with methanol (2 mL), treated with sodium methoxide in methanol (2.547 mL, 1.273 mmol) and triethylamine (0.084 mL, 0.637 mmol), and stirred at r.t. for 24 h. The solid isolated, rinsed with cold methanol (3 x 2 mL), isolated, and dried to yield poly(tetramethylene L-arabinaramide) [Poly(tetramethylene L-lyxaramide)] prepolymer (**23,** 0.109 g, 0.470 mmol, 59.08%, dp 3.06).

Poly(hexamethylene L-arabinaramide) [Poly(hexamethylene L-lyxaramide)] Prepolymer (**24**).

Prepared according to the procedure for **19**: acetyl chloride (0.172 mL, 2.214 mmol) in methanol (4 mL), hexamethylenediammonium L-arabinarate (**6,** 0.219 g, 0.738 mmol), stirred at r.t. for 3 h, concentrated, dried overnight, dissolved with methanol (2 mL), treated with sodium methoxide in methanol (2.236 mL, 1.181 mmol) and triethylamine (0.078 mL, 0.591 mmol), and stirred at r.t. for 24 h. The solid was isolated, rinsed with cold methanol (3 x 2 mL), isolated, and dried to yield poly(hexamethylene L-arabinaramide) [Poly(hexamethylene L-lyxaramide)] prepolymer (**24,** 0.068 g, 0.261 mmol, 35.40%, dp 9.56).

Poly(ethylene ribaramide) Prepolymer (**25**).

Prepared according to the procedure for **19:** acetyl chloride (0.49 mL, 6.921 mmol) in methanol (4 mL), ethylenediammonium ribarate (**7,** 0.277 g, 1.152 mmol), stirred at r.t. for 3 h, concentrated, dried overnight, dissoleved in methanol (1.0 mL), treated with sodium methoxide in methanol (3.69 mL, 1.846 mmol) and triethylamine (0.128 mL, 0.923 mmol), and stirred at r.t. for 24 h. The solid was isolated, rinsed with cold methanol (3 x 1 mL), isolated, and dried to yield poly(ethylene ribaramide) prepolymer (**25,** 0.194 g, 0.949 mmol, 82.3%, dp 3.29).

Poly(tetramethylene ribaramide) Prepolymer (**26**).

Prepared according to the procedure for **19**: acetyl chloride (0.325 mL, 4.497 mmol) in methanol (4 mL), tetramethylenediammonium ribarate (**8,** 0.201 g, 0.751 mmol), stirred at r.t. for 3 h, concentrated,dried overnight, dissolved in methanol (1.6 mL), treated with sodium methoxide in methanol (2.401 mL, 1.201 mmol) and triethylamine (0.082 mL, 0.600 mmol), and stirred at r.t. for 24 h. The solid was isolated, rinsed with cold methanol (3 x 2 mL), isolated, and dried to yield poly(tetramethylene ribaramide) prepolymer (**26,** 0.155 g, 0.667 mmol, 88.9%, dp 8.16).

Poly(hexamethylene ribaramide) Prepolymer (**27**).

Prepared according to the procedure for **19**: acetyl chloride (0.360 mL, 5.086 mmol) in methanol (4 mL), hexamethylenediammonium ribarate (**9,** 0.251 g, 0.848 mmol), stirred at r.t. 3 h, concentrated, dried overnight, dissolved in methanol (2.25 mL), treated with sodium methoxide in methanol (2.713 mL, 1.267 mmol) and triethylamine (0.128 mL, 0.923 mmol), and stirred at r.t. for 24 h. The solid was isolated, rinsed with cold methanol (3 x 2 mL), isolated, and dried to yield poly(hexamethylene ribaramide) prepolymer (**27,** 0.185 g, 0.710 mmol, 83.69%, 12.09).

2.3.4 Polymerization of dimethyl aldarates, and methyl aldarate-1,4 (5,2) lactone with Diamines – Method 3

Poly(ethylene xylaramide) Prepolymer (**28**).

To a solution of acetyl chloride (0.747 mL, 10.56 mmol) in methanol (4 mL) was added xylaric acid (0.459 g, 2.551 mmol) and the mixture was stirred at room temperature for 3 h. The solution was concentrated under a stream of nitrogen and dried overnight. The resulting syrup was dissolved in methanol (7.8 mL) to which triethylamine (0.178d mL, 1.276 mmol) and ethylenediamine (0.153 g, 2.551 mmol) were added dropwise and the mixture was stirred at r.t. for 24 h. The solid was isolated by centrifugation, rinsed with cold methanol (3 x 2 mL), isolated by centrifugation and dried overnight to yield poly(ethylene xylaramide) prepolymer (**28**, 0.465 g, 2.277 mmol, 89.29 %, dp 9.15).

Poly(tetramethylene xylaramide) Prepolymer (**29**).

Prepared according to the procedure for **28**: acetyl chloride (0.184 mL, 2.612 mmol) in methanol (4 mL), xylaric acid (0.314 g, 1.741 mmol), stirred at r.t. for 3 h, concentrated, dried overnight, dissolved in methanol (7.8 mL), treated with triethylamine (0.182 mL, 1.306 mmol) and tetramethylenediamine (0.153 g, 1.437 mmol), and stirred at r.t. for 24 h. The solid was isolated, rinsed with cold methanol (3 x 2 mL), isolated and dried to yield poly(tetramethylene xylaramide) prepolymer (**29,** 0.328 g, 1.413 mmol, 81.19 %, dp 4.82).

Poly(hexamethylene xylaramide) Prepolymer (**30**).

Prepared according to the procedure for **28**: acetyl chloride (0.175 mL, 2.478 mmol) in methanol (4 mL), xylaric acid (0.149 g, 0.826 mmol), stirred at r.t. for 3 h,

concentrated, dried overnight, dissolved in methanol (4.5 mL), treated with triethylamine (0.172 mL, 1.239 mmol) and hexamethylenediamine (0.100 g, 0.826 mmol), and stirred at r.t. for 24 h. The solid was isolated, rinsed with cold methanol (3 x 2 mL), isolated, and dried to yield poly(hexamethylene xylaramide) prepolymer (**30,** 0.104 g, 0.400 mmol, 48.47 %, dp 18.61).

Poly(ethylene L-arabinaramide) Prepolymer (**31**).

To a solution of dimethyl L-arabinarate and lactones (**47**, 137.48 mg mL^{-1}, 15 mL, 11.45 mmol) in methanol were added triethylamine (0.797 mL, 5.725 mmol) and ethylenediamine (0.688 g, 11.45 mmol) dropwise with stirring. The reaction mixture stirred at r.t. for 24 h. The solid was isolated by centrifugation, rinsed with cold methanol (3 x 2 mL), isolated by centrifugation and dried overnight to yield poly(ethylene L-arabinaramide) prepolymer (**31,** 0.600 g, 2.941 mmol, 25.7 %, dp 1.96).

Poly(tetramethylene L-arabinaramide) Prepolymer (**32**).

Prepared according to the procedure for **31**: solution of dimethyl L-arabinarate and lactones (**47**, 137.48 mg mL^{-1}, 15 mL, 11.45 mmol) in methanol, triethylamine (0.797 mL, 5.725 mmol), tetramethylenediamine (1.009 g, 11.45 mmol), stirred at r.t. for 24 h. The solid was isolated, rinsed with cold methanol (3 x 2 mL), isolated, and dried to yield poly(tetramethylene L-arabinaramide) prepolymer (**32,** 0.718 g, 3.093 mmol, 27.0 %, dp 3.53).

Poly(hexamethylene L-arabinaramide) Prepolymer (**33**).

Prepared according to the procedure for **31**: solution of dimethyl L-arabinarate and lactones (**47**, 137.48 mg mL^{-1}, 15 mL, 11.45 mmol) in methanol, triethylamine (0.797 mL, 5.725 mmol), hexamethylenediamine (1.331 g, 11.45 mmol), stirred at r.t. for 24 h.

The solid was isolated, rinsed with cold methanol (3 x 2 mL), isolated, and dried to yield poly(hexamethylene L-arabinaramide) prepolymer (**33,** 0.926 g, 3.560 mmol, 31.1 %, dp 2.91).

Poly(ethylene ribaramide) Prepolymer (**34**).

To a solution of acetyl chloride (0.200 mL, 2.829 mmol) in methanol (4 mL) was added ribaric acid-1,4-lactone (0.437 g, 2.693 mmol) and the mixture was stirred at room temperature 3 h. The reaction mixture was concentrated under a stream of nitrogen and dried overnight. The resulting syrup was dissolved in methanol (7.0 mL) to which triethylamine (0.187 mL, 1.347 mmol) and ethylenediamine (0.162 g, 2.693 mmol) were added dropwise and the mixture was stirred at r.t. for 24 h. The solid was isolated by centrifugation, rinsed with cold methanol (3 x 2 mL), isolated by centrifugation and dried overnight to yield poly(ethylene ribaramide) prepolymer (**34,** 0.510 g, 2.500 mmol, 92.8 %, dp 4.44).

Poly(tetramethylene ribaramide) Prepolymer (**35**).

Prepared according to the procedure for **34**: acetyl chloride (0.200 mL, 2.829 mmol)in methanol (4 mL), ribaric acid-1,4-lactone (0.459 g, 2.833 mmol), stirred at r.t. for 3 h, concentrated, dried overnight, dissolved in methanol (7.0 mL), treated with triethylamine (0.197 mL, 1.417 mmol) and tetramethylenediamine (0.250 g, 2.833 mmol), stirred at r.t. for 24 hours. The solid was isolated, rinsed with cold methanol (3 x 2 mL), isolated, and dried to yield poly(tetramethylene ribaramide) prepolymer (**35,** 0.577 g, 2.485 mmol, 87.7 %, dp 9.32).

Poly(hexamethylene ribaramide) Prepolymer (**36**).

Prepared according to the procedure for **34**: acetyl chloride (0.200 mL, 2.829 mmol) in methanol (4 mL), ribaric acid-1,4-lactone (0.478 g, 2.946 mmol), stirred at r.t. for 3 h, concentrated, dried overnight, dissolved in methanol (7.0 mL), treated with triethylamine (0.205 mL, 1.473 mmol) and hexamethylenediamine (0.432 g, 2.946 mmol), stirred at r.t. for 24 h. The solid was isolated, rinsed with cold methanol (3 x 2 mL), isolated, and dried to yield poly(hexamethylene ribaramide) prepolymer (**36,** 0.657 g, 2.524 mmol, 85.7 %, dp 12.1).

2.3.5 Post-Polymerizations of Poly(hexamethylene xylaramide) Prepolymers – Comparison of Methods

Poly(hexamethylene xylaramide) Postpolymer (**37**).

The procedure to prepare **12** was utilized to obtain poly(hexamethylene xylaramide) prepolymer with a dp 7.83. To DMSO (1.0 mL), triethylamine (0.40 mL), and ethylene glycol (0.50 mL) was added **12** (0.099 g), and the mixture stirred at 50 ºC for 48 h. The solid was isolated by centrifugation, rinsed with cold methanol (3 x 1 mL), isolated by centrifugation and dried overnight to yield poly(hexamethylene xylaramide) postpolymer (**37,** 0.096 g, 97.1 %, dp 18.02)

Poly(hexamethylene xylaramide) Postpolymer (**38**).

Prepared according to the for **37**: the procedure to prepare **21** was utilized to obtain poly(hexamethylene xylaramide) prepolymer with a dp 5.04. To DMSO (1.0 mL), triethylamine (0.40 mL), and ethylene glycol (0.50 mL) was added **21** (0.101 g), and the mixture stirred at 50 ºC for 48 h. The solid was isolated, rinsed with cold methanol (3 x 1 mL), isolated, and dried overnight to yield poly(hexamethylene xylaramide) postpolymer (**38,** 0.094 g, 93.1 %, dp 12.66).

Poly(hexamethylene xylaramide) Postpolymer (**39**).

Prepared according to the procedure **37**: the procedure to prepare **30** was utilized to obtain poly(hexamethylene xylaramide) prepolymer with a dp 18.66. To DMSO (1.0 mL), triethylamine (0.40 mL), and ethylene glycol (0.50 mL) was added **30** (0.103 g), the mixture stirred at 50 ºC for 48 h. The solid was isolated, rinsed with cold methanol (3 x 1 mL), isolated, and dried overnight to yield poly(hexamethylene xylaramide) postpolymer (**39,** 0.107 g, 103%, dp 117.6)

Poly(hexamethylene xylaramide) Postpolymer (**40**).

Prepared according to the procedure for **37**: the procedure to prepare **12** was utilized to obtain poly(hexamethylene xylaramide) prepolymer with a dp 7.83. To DMSO (1.0 mL), triethylamine (0.40 mL), and methanol (1.0 mL) was added **12** (0.099 g), the mixture stirred at 50 ºC for 48 hours. The solid was isolated, rinsed with cold methanol (3 x 1 mL), isolated, and dried overnight to yield poly(hexamethylene xylaramide) postpolymer (**40,** 0.098 g, 97.4%, dp 18.45)

Poly(hexamethylene xylaramide) Postpolymer (**41**).

Prepared according to the procedure for **37**: the procedure to prepare **21** was utilized to obtain poly(hexamethylene xylaramide) prepolymer with a dp 5.04. To DMSO (0.5 mL), triethylamine (0.20 mL), and methanol (0.50 mL) was added **21** (0.048 g), the mixture stirred at 50 ºC for 48 h. The solid was isolated, rinsed with cold methanol (3 x 1 mL), isolated, and dried overnight to yield poly(hexamethylene xylaramide) postpolymer (**41,** 0.041 g, 85.5%, dp 15.86)

Poly(hexamethylene xylaramide) Postpolymer (**42**).

Prepared according to the procedure for **37**: the procedure to prepare **30** was utilized to obtain poly(hexamethylene xylaramide) prepolymer with a dp of 18.66. To DMSO (0.25 mL), triethylamine (0.10 mL), and methanol (0.25 mL) was added **30** (0.028 g), the mixture stirred at 50 ºC for 48 h. The solid was isolated, rinsed with cold methanol (3 x 1 mL), isolated, and dried overnight to yield poly(hexamethylene xylaramide) postpolymer (**42,** 0.013 g, 47.14 %, dp 20.01)

Poly(hexamethylene xylaramide) Postpolymer (**43**).

Prepared according to the procedure for **37**: the procedure to prepare **12** was utilized to obtain poly(hexamethylene xylaramide) prepolymer with a dp 7.83. To triethylamine (0.20 mL) and methanol (0.50 mL) was added **12** (0.049 g), the mixture stirred at 50 ºC for 48 hours. The solid was isolated, rinsed with cold methanol (3 x 0.5 mL), isolated, and dried overnight to yield poly(hexamethylene xylaramide) postpolymer (**43,** 0.042 g, 86.0%, dp 23.24)

Poly(hexamethylene xylaramide) Postpolymer (**44**).

Prepared according to the procedure for **37**: the procedure to prepare **21** was utilized to obtain poly(hexamethylene xylaramide) prepolymer with a dp 5.04. To triethylamine (0.15 mL) and methanol (0.40 mL) was added **21** (0.035 g), the mixture stirred at 50 ºC for 48 h. The solid was isolated, rinsed with cold methanol (3 x 0.5 mL), isolated, and dried overnight to yield poly(hexamethylene xylaramide) postpolymer (**44,** 0.023 g, 65.33 %, dp 21.73)

Poly(hexamethylene xylaramide) Postpolymer (**45**).

Prepared according to the procedure for **37**: the procedure to prepare **30** was utilized to obtain poly(hexamethylene xylaramide) prepolymer with a dp 18.66. To triethylamine (0.10 mL) and methanol (0.25 mL) was added **30** (0.019 g), the mixture stirred at 50 ºC for 48 h. The solid was isolated, rinsed with cold methanol (3 x 0.25 mL), isolated, and dried overnight to yield poly(hexamethylene xylaramide) postpolymer (**45,** 0.015 g, 77.8 %, dp 18.18)

Dimethyl xylarate (**46**), **Methyl xylarate-1,4-lactone** (**47**), **Methyl xylarate-5,2-Lactone** (**48**).

Xylaric acid (0.501g, 2.781mmol) was dissolved in methanol (4 mL). Acetyl-chloride (0.424 mL, 6.000 mmol) was added dropwise to cold (ice bath) methanol (3 mL). The solution was added dropwise to the methanolic xylaric acid and stirred for 3 hours at room temperature. The mixture was concentrated under a stream of nitrogen and dried overnight to yield a mixture of dimethyl xylarate, methyl xylarate-1,4-lactone, and methyl xylarate-5,2-lactone (**46-48**, 0.569 g, 2.731 mmol, 98.2%). ^{1}H NMR (DMSO) δ 4.12-4.11 (d,2H, *J* 4.39 Hz) 3.91-3.89 (t, 1H)

Dimethyl-L-arabinarate (**49**), **Methyl-L-arabinarate-1,4-lactone** (**50**), **and Methyl-L-arabinarate-5,2-lactone** (**51**).

Disodium L-arabinarate (1.091 g, 4.556 mmol) was charged into a 100 ml round bottom flask to which dry methanol (15 mL) was added. Acetyl chloride (1.215 g, 15.57 mmol) was added dropwise to cold (ice bath) methanol (5 mL). The solution was added to the mixture and stirred 30 min at room temperature. A white precipitate resulted and was isolated by filtration. The filtrate was concentrated and dried for 4 hours to yield a

mixture of dimethyl L-arabinarate, methyl-L-arabinarate-1,4-lactone, and methyl-L-arabinarate-5,2-lactone (**49**-**51**, 1.0363 g, 4.98 mmol, 109.3%). ^{1}H NMR (DMSO) δ 5.12 (d,1H, *J* 3.52 Hz), 4.52 (b, 1H), 4.28 (b, 1H), 3.74 (s, 6H).

References

1. Seymour, R.B., *Introduction to Polymer Chemistry,* **1971**, New York, McGraw-Hill Book Company

2. Billmeyer, Fred W. Jr. Textbook of Polymer Science. **1984,** New York, John Wiley & Sons

3. Hoagland, P. D. The Formation of Intermediate Lactones during Aminolysis of Diethyl Galactarate. Carbohydrate Research **1981**, 98: 203-208.

4. Hoagland, P. D.; Pessen, H. and Mc Donald, G. G. The Formation of Intermediate Lactones during Aminolysis of Diethyl Xylarate. Journal of Carbohydrate Chemistry **1987**, 6(3): 495-499.

5. Ogata, N. And Hosoda, Y. Synthesis of Hydrophilic Polyamide from L-Tartarate and Diamines by Active Polycondensation. Journal of Polymer Science, Polymer Chemistry Edition **1975**, 13: 1793-1801.

6. Ogata, N. New Polycondensation Systems. Polymer Reprints **1976**, 17(1): 151-162

7. Ogata, N. And Hosoda, Y. Active Polycondensation of Methylene Tartarate with Hexamethylenediamine. Journal of Polymer Science, Polymer Letters Edition **1976**, 14: 409-412.

8. Ogata, N., Sanui, K. And Kayamo, Y. Copolycondensation of Hydroxyl Diesters and Active Diesters with Hexamethylenediamine. Journal of Polymer Science, Polymer Chemistry Edition **1977**, 15: 1523-1526.

9. Ogata, N., Sanui, K., Tanaka, H. And Suzuki, T. Active Polycondensation of alpha, alpha'-Disubstituted Adipate with Hexamethylenediamine. Journal of Polymer Science, Polymer Chemistry Edition **1977**, 15: 2531-2534.

10. Ogata, N. Synthesis of Polyamides and Polyesters Having Various Functional Groups. Journal of Macromolecule Science-Chemistry **1979**, A13(4): 177-501.

11. Ogata, N., Sanui, K., Nakamura, H. And Kishi H. Polycondensation of Diethyl Mucate with Hexamethylenediamine in the Presence of Poly(Vinyl Pyridine). Journal of Polymer Science, Polymer Chemistry Edition **1980**, 18: 933-938.

12. Ogata, N., Sanui, K., Nakamura, H. And Kuwahara, M Polycondensation Reaction of Dimethyl Tartrate with Hexamethylenediamine in the Presence of Various matrices. Journal of Polymer Science, Polymer Chemistry Edition **1980**, 18: 939-948.

13. Ogata, N., Sanui, K., Tanaka, H. And Matsuo, H. Molecular Weight Control in Polycondensation of Hydroxyl Diesters with Hexamethylenediamine by Polymer Matrices. Journal of Polymer Science, Polymer Chemistry Edition **1981**, 19: 2609-2617.

14. Ogata, N., Sanui, K. And Kato, A. Polycondensation of Diesters with Hetero Atom Groups with Hexamethylenediamine in the Presence of Polyme Matrix. Journal of Polymer Science, Polymer Chemistry Edition **1982**, 20: 227-231.

15. Ogata, N., Sanui, K., Iwaki, F. And Nomiyama, A. Matrix Polycondensation through Hydrogen Bonding Interaction. Journal of Polymer Science, Polymer Chemistry Edition **1984**, 22: 793-800.

16. Ogata, N. And Hosoda, Y. Synthesis of Hydrophilic Polyamide by Active Polycondensation. Journal of Polymer Science, Polymer Letters Edition **1974**, 12: 355-358.

17. Kiely, Donald E.; Lin, Tsu Hsing Aldaric acid-based polyhydroxypolyamides and their manufacture. U.S. **1989**, Patent 4833230, May 23.

18. Chen, Liang; Kiely, Donald E. D-Glucaric acid esters/lactones used in condensation polymerization to produce hydroxylated nylons - a qualitative equilibrium study in acidic and basic alcohol solutions. Journal of Carbohydrate Chemistry **1994**, 13(4): 585-601.

19. Kiely, D.E., Chen, L. And Lin, T. Hydroxylated Nylons Based on Unprotected Esterified D-Glucaric Acid by Simple Condensation Reactions. J. Am. Chem. Soc. **1994**, 116(2): 571-8.

20. Kiely, D.E., Chen, L. And Lin, T-H. Simple Preparation of Hydroxylated Nylons - Polyamides Derived From Aldaric Acids. ACS Symposium Series 575, **1994**, Washington.

21. Kiely, Donald E.; Chen, Liang; Morton, David W. Glucaric acid monoamides and their use to prepare poly(glucaramides). **1994**.

22. Kiely, Donald E.; Chen, Liang; Morton, David W. Process for making activated aldarate esters, ester/lactones and lactones. US. **1994**, Patent 5329044, July 12.

23. Kiely, Donald E.; Chen, Liang; Morton, David W. polyaldaramide polymers useful for films and adhesives. U.S. **1995**. US Patent 5434233, July 18

24. Chen, L. And Kiely D. E. Synthesis of Stereoregular Head,Tail - Hydroxylated Nylons Derived from D-Glucose. J. Org. Chem. **1996**, 61(17): 3847-51.

25. Kiely, Donald E. Carbohydrate diacids: Potential as commercial chemicals and hydrophilic polyamide precursors. 218th ACS National Meeting, **1999**, New Orleans, American Chemical Society, Washington, D. C.

26. Kiely, Donald E., Chen, Liang and Lin, Tsu-Hsing Synthetic Polyhydroxypolyamides from Galactaric, Xylaric, D-Glucaric and D-Mannaric Acid and

Alkylenediamine Monomers - Some Comparisons. J. Polym. Sci.; Polym Chem. Ed **2000**, 38: 594-603.

27. Morton, David W., and Kiely, Donald E. Evaluation of the Film and Adhesive Properties of Some Block Copolymer Polyhydroxypolyamides from Esterified Aldaric Acids and Diamines. J. Applied Polym. Sci. **2000**, 77: 3085-92.

28. Morton, David W., and Kiely, Donald E. Synthesis of Poly(azaalkylene aldaramides) and Poly(oxaalkylenealdaramides) Derived from D-Glucaric and D-Galactaric Acids. J. Polym. Sci.; Polym. Chem. Ed. **2000**, 38: 404.

29. Kiely, Donald E. Carbohydrate Diacids: Potential as Commercial Chemicals and Hydrophobic Polyamide Precursors. ACS Symposium Series 784, Chemicals and Materials from Renewable Resources, **2001**.

30. Styron, Susan D.; Kiely, Donald E.; Ponder, Glenn Alternating stereoregular head, tail-tail, head-poly(alkylene D-glucaramides) derived from a homologous series of symmetrical diamido-di-D-glucaric acid monomers. Journal of Carbohydrate Chemistry **2003**, 22(2): 123-142.

3. A computational study directed to understanding the conformational preferences of pentaric acids and their corresponding polyamides

3.1 Introduction

Polyhydroxypolyamide (PHPA) preparation by condensation polymerization of unprotected, esterified aldaric acids with primary diamines was discussed in chapter 2 of this dissertation. Of interest is the conformational preference of these polyamides, and particularly, the aldaryl monomer unit in solution. Thus, the driving force of this study was to determine how steric and electrostatic interactions influence the conformational preferences of the aldaryl monomer unit thereby resulting in a better understanding of the chemical and physical properties and potential applications of PHPAs. To this end, we report here a Monte Carlo MM3(96) investigation of four classes of compounds: Class 1 - glutaramide (**1**) and *N*,*N*'-dimethylglutaramide (**2**); Class 2 - xylaramide (**3**), *N*,*N*'-dimethylxylaramide (**4**), xylaric acid (**5**), dimethyl xylarate (**6**), and 2,3,4-tri-*O*-acetyl-*N*,*N*'-dimethylxylaramide (**7**); Class 3 - L-arabinaramide (**8**), *N*,*N*'-dimethyl-L-arabinaramide (**9**), L-arabinaric acid (**10**), and 2,3,4-tri-*O*-acetyl-*N*,*N*'-dimethyl-L-arabinaramide (**11**); Class 4 - ribaramide (**12**), *N*,*N*'-dimethylribaramide (**13**), ribaric acid (**14**), and 2,3,4-tri-*O*-acetyl-*N*,*N*'-dimethylribaramide (**15**). The pentaramides **3**, **4**, **7**, **8**, **9**, **11**, **12**, **13**, and **15** are good model compounds for PHPAs because they incorporate the chiral moiety of the aldaryl monomer as well as the amide bond present in the polyamides, Figure 3.1.

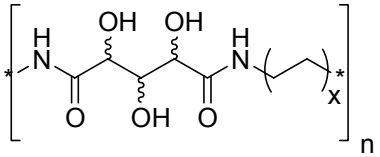

Polyhydroxypolyamide

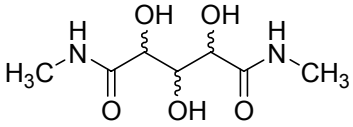

N,N'- Dimethylpentaramide

Figure 3.1 Depiction of polyhydroxypolyamide and an *N,N'*-dimethylpentaramide (aldaramide) model for the aldaradiamido unit

Additionally, compounds **1**-**15**, Figure 3.2, afford the opportunity to computationally compare the glutaramides (**1** and **2**) and pentaramides (**3**, **4**, **7**, **8**, **9**, **11**, **12**, **13**, and **15**), the latter diamides being more conformationally restricted due to the presence of pendant hydroxyl or acetoxyl groups. Computational modeling of diacids (**5**, **10**, and **14**) and the dimethyl ester of xylaric acid (**6**) provides an opportunity to compare steric and electrostatic interactions of the carboxylic acid and ester groups of these molecules to the influence of the amido and N-methyl amido groups of the pentaramides.

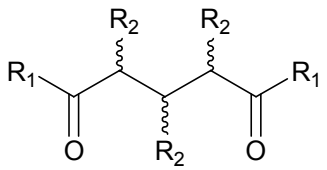

Aldaryl Monomer Unit

Compound (**1**)	$R_1 = NH_2$	, $R_2 = H$
Compound (**2**)	$R_1 = NHCH_3$	$R_2 = H$
Compound (**6**)	$R_1 = OCH_3$	, $R_2 = H$
Compound (**3, 8, 12**)	$R_1 = NH_2$	, $R_2 = OH$
Compound (**4, 9, 13**)	$R_1 = NHCH_3$	, $R_2 = OH$
Compound (**5, 10, 14**)	$R_1 = OH$	, $R_2 = OH$
Compound (**7, 11, 15**)	$R_1 = NHCH_3$	, $R_2 = OAc$

Figure 3.2 Aldaryl monomer unit illustrating varying pendent groups

The *O*-acetylated pentaramides (**7**, **11**, and **15**) are of interest because the somewhat bulky pendent acetyl groups serve to conformationally restrict the molecules as well as prevent intramolecular hydrogen bonding associated with the pendant hydroxyl groups.

This conformational restriction also allows a better comparison of computationally calculated ^{1}H NMR vicinal coupling constants with experimental values than from the conformationally more flexible unprotected diamides.

A starting point for this study was to determine the preferred conformations of the polymethylene unit in the glutaryl unit of glutaramide (**1**) and *N*,*N*'-dimethylglutaramide (**2**). As background for the evaluation the conformation of the simple hydrocarbons butane and pentane were first considered. Applying quantum mechanical calculations, During and coworkers established that the experimental energies for the *trans* (*anti*)-*gauche* (T-G) rotamers, Figure 3.3, of butane differed from 0.5-0.9 kcal/mol[1] and that the T conformation is favored by 0.75 kcal/mol.[2]

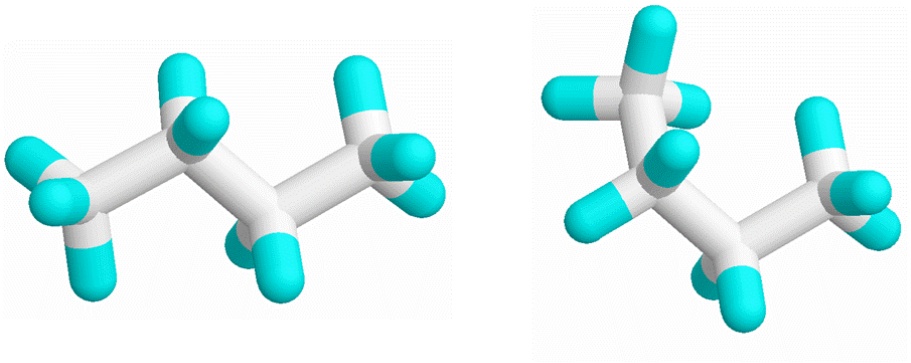

trans (T) rotamer of butane *Gauche* (G) rotamer of butane

Figure 3.3 *Trans* and *gauche* conformations of butane

The same conformational result was found for *n*-pentane where the TT-to-GG energy change experimentally ranges from 0.46[3] to 0.56[4] kcal/mol, compared to 0.76 kcal/mol derived from quantum mechanical calculations.[5] An investigation of a series of X-ray crystallographic studies of oligomeric models of polyamides indicated that the central methylene carbons of the diacyl unit usually adopted a *trans* (*anti*) conformation.[6] This was reinforced in early studies of crystalline phase Nylon 6,6 that established the

conformational preference for the methylene carbons was an all *trans* (*anti*) relationship based upon a comparison of results from molecular dynamics computer simulations and experimental NMR spectroscopy.[7] However, Navarro *et. al.* established that the preference for an all *trans* (*anti*) conformation may decrease for some acyclic amides.[6-8] When a small number of methylene carbons are present in the diacyl unit, a repulsive interaction between parallel dipoles of the amide groups can induce folding of the molecule into a *gauche* conformation. This results in a more favorable orientation of the dipoles despite the *gauche* orientation of the methylene carbon atoms. Navarro and co-workers performed ab Initio HF/6-31G* quantum mechanical calculations on glutaramide (**1**) and found the TTTTTT or fully extended conformation to be less stable than the TTGGTT or folded (sickle) conformation by 2.7 kcal/mol, Figure 3.4.[6] Thus we were interested in applying molecular mechanics to investigate the influence of the dipole-dipole interaction on the conformations of glutaramide (**1**) and *N,N'*-dimethylglutaramide (**2**), and their hydroxylated derivatives (**3**, **4**, **8**, **9**, **12**, and **13**).

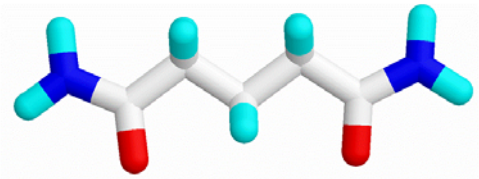

trans (T) rotamer of glutaramide

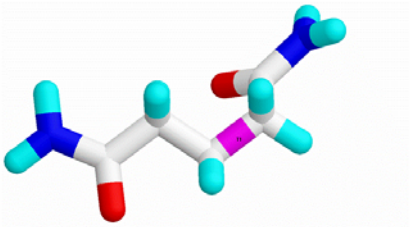

gauche (G) rotamer of glutaramide

Figure 3.4 Glutaramide depicted in a *trans* (T) or TTTTTT and *gauche* (G) or TTGGTT rotamers

It has been suggested that unfavorable steric interactions resulting from hydroxyl group oxygens that are in eclipsed 1,3-parallel arrangements cause acyclic carbohydrates, in an extended conformation, to undergo a 120° rotation about a C-C bond to alleviate this interaction resulting in a sickle conformation.[9] For such molecules these interactions are similar to a 1,3-*syn*-diaxial interaction (1.9 kcal/mol) of hydroxyl groups in chair conformations of *cis*-1,3-cyclohexanediol.[10] Vicinal coupling constant data were used by Sweeting *et al.* as a means of computational comparison of six per-acetylated hexonitriles.[11] The hexononitriles conformationally preferred an extended conformation except when an eclipsed 1,3- parallel interaction was present, as with penta-*O*-acetyl-D-gluconononitrile, wherein a sickle conformation was preferred. Hexa-*O*-acetyl-D-glucitol also preferred a sickle conformation as determined from ^{1}H NMR conformational studies carried out by Angyal and co-workers.[12] Molecular modeling of *N,N'*-dimethylxylaramide and *N,N'*-dihexyl xylaramide using MacroModel V2.0[13] found, for both molecules, that two sickle conformations were lower in energy than the extended conformation. The sickle conformations allowed for the alleviation of the eclipsed 1,3-parallel interaction present in the extended conformation between hydroxyls at C(2) and C(4).

MM3 and MM3(96) conformational analyses of a series of D-glucaric acid derivatives were performed by Zhang *et al*. [14, 15] and Styron *et. al.*, respectively.[16] D-Glucaramide modeling was carried out at a dielectric constant of 3.5 and 6.5,[10] and 2,3,4,5-tetra-*O*-acetyl-*N,N'*-dimethyl-D-glucararamide was carried out at a dielectric constant of 2.0.[14-15]

A model building approach was used by Zhang *et al.* to calculate the low energy conformations of 2,3,4,5-tetra-*O*-acetyl-*N,N'*-dimethyl-D-glucararamide.[14] Calculations were performed in Alchemy 2000 using MM3. Based upon ^{1}H NMR vicinal coupling constant data some angular restrictions were assumed and all other unknown conformational preferences were computed individually using model compounds as mimics, the results of which were combined to obtain the lowest energy conformations. In all cases, the lowest energy conformations have no eclipsing 1,3-parallel acetyl group interactions present.[14,15] All low energy conformers were in sickle conformations suggesting that eclipsing 1,3-parallel acetyl group interactions are energetically unfavorable.

In the MM3(96) modeling of D-glucaramide, nine torsional angles were varied; five in the aldaryl unit backbone and four for the hydroxyl groups.[16] At dielectric constant 3.5, ten conformations were found within 1 kcal/mol of the global minimum. 45-50% of the population were in sickle conformations where there were no eclipsing 1,3-parallel hydroxyl group interactions. Five conformations comprising an insignificant percent of the total population had eclipsing 1,3-parallel hydroxyl group interactions. Styron suggested that conformations having an eclipsed 1,3-parallel hydroxyl group interaction were stabilized by intramolecular hydrogen bonding between hydroxyl groups.

At dielectric constant 6.5, thirty-five conformations were found within 1 kcal/mol of the global minimum. 52-59% of the population had no eclipsing 1,3-parallel hydroxyl group interactions. Eclipsing 1,3-parallel hydroxyl interactions were displayed in ~28% of the population and 13% had two pairs of eclipsing hydroxyl group interactions. Styron

concluded that at lower dielectric constants eclipsing 1,3-parallel hydroxyl interactions were increasingly more destabilizing and less favored.

In light of these findings, a Monte Carlo MM3(96) program written by Dr. Michael K. Dowd[17] was applied to calculate the low-energy conformations of each molecule (**1**-**15**) at dielectric constants ranging from 1.5-10.0. By varying dielectric constant, the strength of intramolecular electrostatic interactions is varied thereby implicitly accounting for solvent effects. To test convergence of the computational simulation and thereby support the validity of the computational results, six different starting conformations of each molecule were simulated at each dielectric constant. By starting simulations with conformers from different regions of conformational space and obtaining the same result each time, one can be reasonably assured that all conformational space had been searched. Thus, a conformational ensemble comprised of hundreds or thousands of conformers and considered to be representative of the global population is generated. The percent population for each conformer was then calculated according to a Boltzmann distribution and standardized to 100%. This was necessary due to the number of conformers found in each conformational ensemble and the relatively small contribution of high energy conformers to the total percent population. The percent population (PPA) analyzed is therefore reported for each simulation and is typically greater than 90 percent. Individual conformers not analyzed did not contribute significantly to the global population. The conformers were then grouped into conformational families consisting of rotamers with the same backbone conformations, and analyzed for structural detail. Theoretical average ^{1}H vicinal coupling constants for each molecule were compared to experimental values obtained by ^{1}H NMR.

Experimental ^{1}H NMR vicinal coupling values of 2,3,4-tri-*O*-acetyl-*N*,*N*'-dimethyl-L-arabinaramide were calculated with varying NMR solvent mixtures and found to be highly dependent on solvent composition.

3.1.1 MM3(96) as a Molecular Force Field

MM3(96) was the force field chosen for this study because of the wide use with carbohydrate molecules, including previous studies from this lab.[13-16] Prior studies have utilized MM3(96) as the preferred empirical force field method for mono- and disaccharide molecules because of the functional groups present and the large number of calculations necessary for the study. MM3(96) does have some limitations. Chains of hydrogen bonding (donor-acceptor-donor-acceptor) and explicit solvent effects cannot be taken into account. MM3(96) does allow for the changing of the dielectric constant to alter the strength of hydrogen bonding. By raising the value of the dielectric constant, the contribution of hydrogen bonding to the overall steric energy decreases exponentially; therefore simulations at higher dielectric constants model solvation in more polar solvents. Smaller dielectric constant values (< or = 1.0) are suitable for simulating molecules in vacuum and, a value of 1.5 for comparison to non-polar solvents.

3.1.2 Modifications to MM3(96)

Because MM3(96) like all other molecular mechanics programs treats bonds as springs, empirical data must be used to determine individual force constants and equilibrium values for geometries. MM3(96) does this by defining an atom type according to each atoms hybridization and molecular environment. Thus atom type, bond angle, bond length, torsion parameters, and atom connectivity are all very important. The atom types employed in this study are listed in Table 3.1.

Table 3.1 Atom types in MM3 (96)

ATOM	TYPE	DESCRIPTION	AT WT	LTG	LT3	LT4	LT5	LTP	MPL	CRD
1	C	CSP3	12.000	0	0	0	0	0	0	0
3	C	CSP2 CARBONYL	12.000	0	0	0	0	0	3	0
5	H	EXCEPT ON N,O,S	1.008	0	0	0	0	0	0	0
9	N	NSP2	14.003	0	0	0	0	0	9	0
28	H	H-N-C=O (AMIDE)	1.008	0	0	0	0	0	0	0
75	O	O-H, O-C (CARBOXYL)	15.995	6	6	6	6	0	0	0
78	O	O=C-O-C (ESTER)	15.995	7	0	0	0	7	0	0
79	O	O=C-N< (AMIDE)	15.995	7	0	0	0	7	0	0
21	H	O-H (HYDROXYL)	1.008	0	0	0	0	0	0	0

AT WT = ATOMIC WEIGHT
LTG = REPLACABLE ATOM TYPE FOR GENERAL LOCALIZED (LTYPEG)
LT3 = REPLACABLE ATOM TYPE FOR 3-MEM LOCALIZED (LTYPE3)
LT4 = REPLACABLE ATOM TYPE FOR 4-MEM LOCALIZED (LTYPE4)
LT5 = REPLACABLE ATOM TYPE FOR 5-MEM LOCALIZED (LTYPE5)
LTP = REPLACABLE ATOM TYPE DELOCALIZED (LTYPEP)
MPL = ATOM HAVING OUT-OF-PLANE BENDING IF NOT ZERO (KOUTP)
CRD = ATOM HAVING 4-COORDINATE BOND IF NOT ZERO (ITCOORD)

The majority of torsion parameters required in this study were included in MM3(96) although two torsion angle parameters present in aldaramides and their acetylated derivatives were not present. The atom type sequence associated with an ester group or a hydroxyl group adjacent to an amide (9-3-1-75) was input in the constant file of MM3(96) as V1= -2.157, V2= -0.592 and V3= 0.466. The sequence of an ester group adjacent to a carbonyl group (3-1-75-3) was input into the constant file as V1=0.7246, V2=-0.6033 and V3=0.2583. These were performed according to the suggestion of Dr. Jenn-Huei Lii at the Center for Computational Chemistry, The University of Georgia.[16] A full list of torsion parameters is given in Table 3.2.

Table 3.2 Selected torsion parameters of MM3 (96)*

W	ANGLE	V1	V2	V3	
0	1001001001	0.1850	0.1700	0.5200	(1 T1)
0	1001001003	0.0000	0.4000	0.0100	(11 T1)
0	1001001005	0.0000	0.0000	0.2800	(42 T1)
0	1001075003	-2.2800	1.0000	0.0000	(93 T1)
0	1003075001	1.0500	7.5000	-0.2000	(95 T1)
0	1001003009	0.7000	-1.1000	0.3000	(178 T1)
0	1003009001	1.1000	3.8000	0.0000	(180 T1)
1	1003009028	0.0000	3.8000	0.0000	(468 T1)
1	5001009028	0.0000	0.0000	0.0800	(470 T1)
0	3001001005	0.0000	0.0000	0.1800	(51 T1)
0	5001001005	0.0000	0.0000	0.2380	(69 T1)
0	5001003075	0.2500	0.8500	0.0000	(118 T1)
0	5001075003	0.0100	0.0000	0.0000	(120 T1)
0	5001009003	0.0000	0.0000	0.0100	(191 T1)
0	78003075001	-2.6600	7.5000	0.2000	(142 T1)
2	75001003009	-2.1570	-0.5920	-0.4660	
2	3001075003	0.7246	-0.6033	0.2583	

* W = RELIABILITY
0 : FINAL
1 : RELIABLE, BUT NOT FINAL (*)
2 : CRUED (TEMPORARY) (**)
ANGLE = TORSIONAL ANGLE
V1,V2,V3 = TORSIONAL CONST

Energy change optimizations where terminated using the default Alchemy2000 value of 0.0003*n, where *n* is the number of atoms. An energy change optimization termination value of 0.00008*n was used for the computational analysis of xylaric acid (**3**).

3.1.3 Establishing Convergence of the Simulation

A concern to any investigator performing computational simulations, especially when employing a directed random search method, is how to obtain a valid representative dataset, also known as achieving convergence, while limiting the computational resources expended in the endeavor. The Monte Carlo search method employed here is an inherently incomplete search method as the computational search is intentionally biased toward the lower energy conformations. Therefore conformations of higher energy were considered less important in this simulation and were often not found during the

computational search. Convergence of Monte Carlo based searches is usually ‘tested’ by either (1) extending a run to see if additional low-energy structures are found or (2) by conducting multiple runs in parallel with different initial structures to see if consistent populations of low-energy structures are found. In this computational investigation both ‘tests’ were performed. In test (1) the lack of having identified any new “important” structures is generally taken as an indication that the search has found the low-energy conformations and thus converged. In test (2) the results from multiple runs starting in different areas of conformational space should be identical or to it. Additionally, test (3), symmetric molecules or enantiomers should show (+/-) gauche interactions equally populated.

In this work more low-energy conformers were found at higher dielectric constants, thus the convergence test (1) was performed with 100,000 steps at the highest dielectric constant of interest for each molecule. Six conformations of each molecule (e.g., Figure 3.5) were also analyzed at each dielectric constant to meet the requirements for test (2). Acetylated and unprotected molecules were run at 40,000 and 20,000 steps, respectively. At 40,000 and 20,000 steps usually ~90% of the global population had been found and any conformer found past this value did not contribute significantly to the global population. Test (3) for symmetric molecules or enantiomers, which should show (+/-) gauche interactions equally populated, was also achieved.

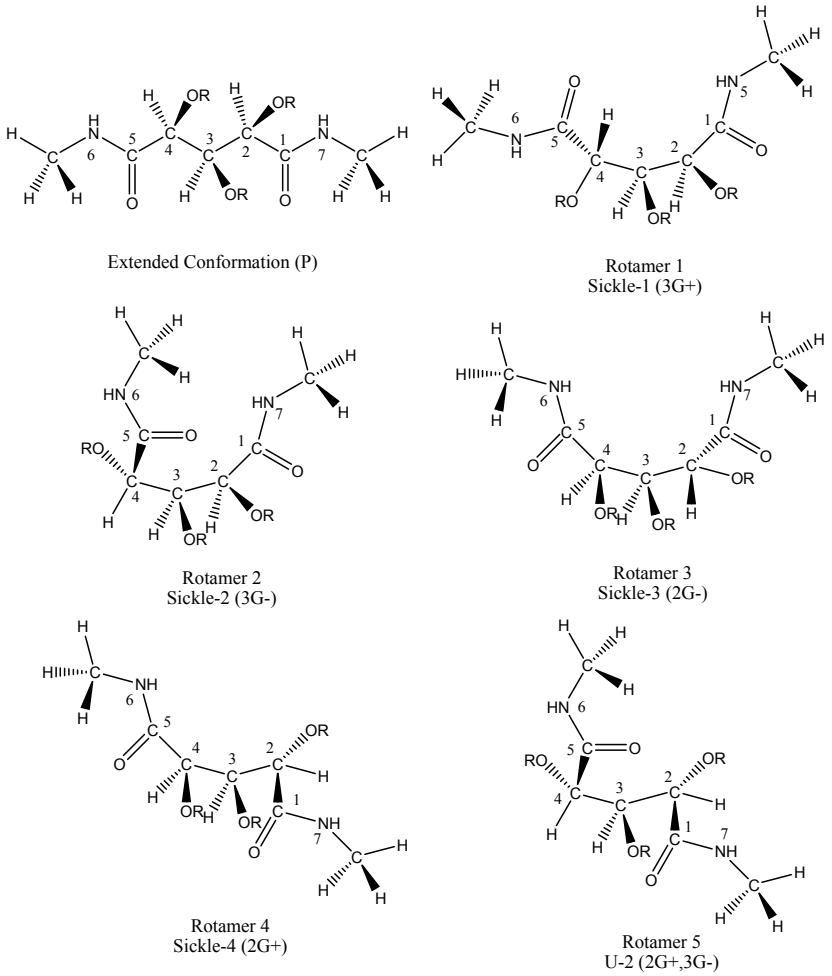

Figure 3.5 An example of six starting rotamers corresponding to different areas of conformational space illustrated using *N,N'*-dimethylxylaramide (**4**)

Additionally, the ability to model at high temperatures is needed to ensure the simulation is capable of jumping from one region of conformational space to another. This is accomplished by a process called temperature shaking. In the temperature shaking process a Boltzmann factor [P = (-ΔE/RT)] is calculated, where P stands for probability and E is the energy of the new conformer and the conformer of the last step in the simulation. A random number generator called EFACT then produces a number between 0 and 1. When the value of the Boltzmann factor is larger than the randomly generated number, the conformation is accepted as a starting conformation for the next step. 10,000

K is a sufficiently high temperature to make the value of the Boltzmann factor near 1 resulting in a high probability of the conformation being accepted for the next step.

3.1.4 Statistical Analysis of Molecules Simulated

The global population was used to calculate the percent population of each conformer using the following equations.

$$N_a/N_o = \exp(\Delta E/RT) \qquad \text{(eq 1)}$$

$$P_a = [(N_a/N_o) / \Sigma(N_i/N_o)] \times 100 \qquad \text{(eq 2)}$$

N_a/ N_o is the molar ratio of some conformer "a" to the most stable conformer *o*. ΔE represents the energy difference between conformer "a" and conformer *o*. P_a is the percent population of conformer "a" among all the other conformers *i*. The summation of P_a will always equal 100 %.

For each molecule simulated proton vicinal coupling constants corresponding to the protons on C2, C3, and C4 (H13-C2-C3-H14 and H14-C3-C4-H15) were calculated for each conformer using Haasnoot's adaptation of the Karplus equation.[18] The theoretical average coupling constant for $J_{13,14}$ and $J_{14,15}$ was calculated based on the equation:

$$\text{Jcalcd} = \sum P_a \cdot J_i \qquad \text{(eq 3)}$$

P_a is the percent population of each conformation and J_i is the corresponding calculated coupling constant for that particular conformation. Computational vicinal coupling constants values were compared between chosen dielectric constants and with experimentally determined ^{1}H NMR in an appropriate solvent (D_2O and/or chloroform-*d*).

3.2 Results and Discussion

3.2.1 Simulation of Glutaramide (1) and *N,N'*-Dimethylglutaramide (2) – Class 1

The compounds in Class 1 have an axis of symmetry through carbon C3 meaning a 120 degree rotation about the C2-C3 bond corresponds to a -120 degree rotation of the C3-C4 bond producing two different conformations that are energetically equivalent and have (+/-) *gauche* interactions. Only one conformation from the two energetically equivalent conformations with (+/-) *gauche* interactions will be discussed.

Glutaramide (1)

Six rotamers of glutaramide (**1**) were searched at a dielectric constant of 1.5, 3.5, 6.0, and 10.0 to a coefficient of variance of 0.98, 1.61, 0.00, and 1.37 with an average of 83, 91, 75, and 80 conformations found, respectively. Figures 3.7-3.10 depict the lowest energy conformations from various backbone families for **1** at dielectric constants 1.5, 3.5, 6.0, and 10.0. The energy range of the lowest energy conformer from the least populated family relative to the lowest energy conformer was 1.759, 1.599, 0.449, and 1.369 kcal/mol, respectively. The calculated percent populations are shown in Table 3.3. The number scheme for **1** is shown in Figure 3.6.

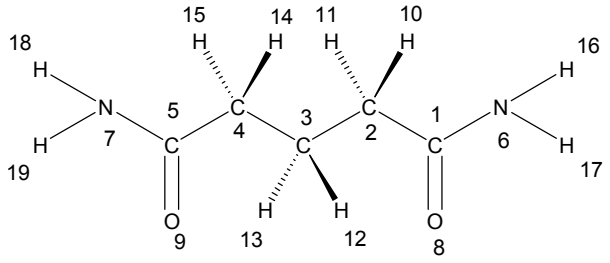

Figure 3.6 Numbering scheme for glutaramide (**1**)

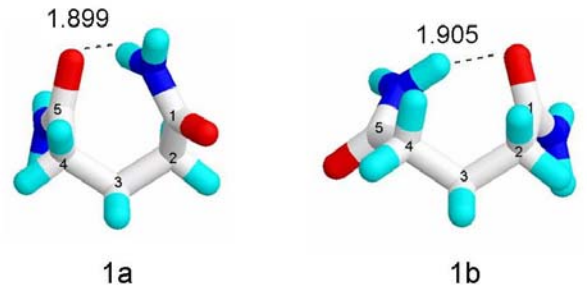

Figure 3.7 The two lowest energy conformations **1a** (2G+3G+) and **1b** (2G-3G+) and hydrogen bond length in angstroms at DIELEC 1.5

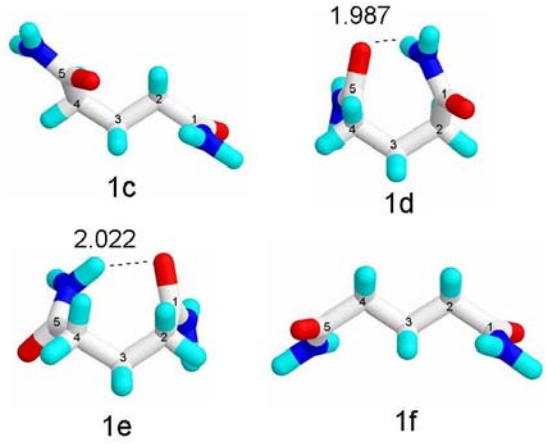

Figure 3.8 The four lowest energy conformations **1c** (3G-), **1d** (2G+,3G+), **1e** (2G-,3G+), and **1f** (extended) and hydrogen bond length in angstroms at DIELEC 3.5

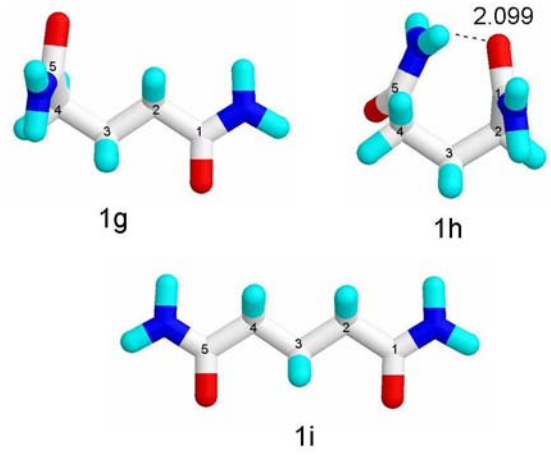

Figure 3.9 The three lowest energy conformations **1g** (3G-), **1h** (2G+3G+), and **1i** (extended) and hydrogen bond length in angstroms at DIELEC 6.0

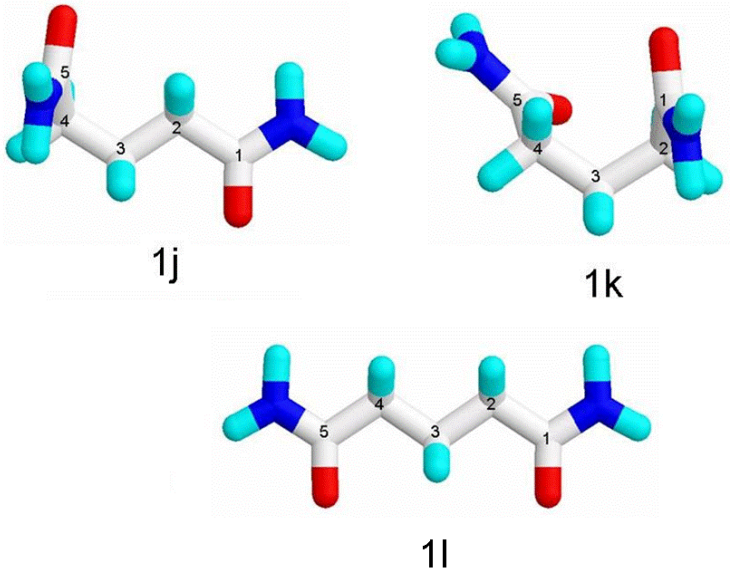

Figure 3.10 The four lowest energy conformations **1j** (3G-), **1k** (2G+3G+), and **1l** (extended) at DIELEC 10.0

Table 3.3 Calculated percent population for **1** at dielectric constant 1.5, 3.5, 6.0, and 10.0 and the percent population analysis (PPA)

DIELEC	3G-	2G-3G+	2G+3G+	Extended	PPA
1.5	0.000	15.75 (**1b**)	84.24 (**1a**)	0.000	96.13
3.5	31.62 (**1c**)	0.000	47.20 (**1d**)	21.18 (**1f**)	91.15
6.0	51.60 (**1g**)	0.000	9.728 (**1h**)	38.67 (**1i**)	90.84
10.0	52.00 (**1j**)	2.142 (**1e**)	1.215 (**1k**)	44.64 (**1l**)	90.34

The sickle 2G+3G+ is the dominant conformation (ca. 84%) at dielectric constant 1.5 and progressively decreases with increasing dielectric constant were eventually at dielectric constant 10.0 it is the least populated conformation at 1.2% of the population. The hydrogen bond (1.899 Å) at dielectric constant 1.5 is no longer present at higher dielectric constants, thereby allowing the observation of the parallel dipole-dipole

interaction at dielectric constants 3.5, 6.0 and 10.0. This illustrates the decreasing strength of electrostatic interactions with increasing dielectric constant. The increasing population of the extended conformation with increasing dielectric constant is not surprising due to the decreaseing influence of the destabilizing electrostatic parallel dipole-dipole interaction with increasing dielectric constant. However, in agreement with prior work by Novarro,[6] the sickle 3G- or TTGGTT (*gauche*) conformation is of lower energy than the extended or *anti* conformation at all dielectric constants simulated above 1.5.

N,N'-Dimethylglutaramide (**2**)

Six rotamers of *N,N'*-dimethylglutaramide (**2**) were searched at dielectric constant 1.5, 3.5, 6.0, and 10.0 to a coefficient of variance of 2.29, 2.12, 1,96, and 1.46 with an average of 321.6, 343.5, 371.6, and 384.7 conformations found, respectively. Figures 3.12-3.15 depict the lowest energy conformations from various backbone families for **2** at dielectric constants 1.5, 3.5, 6.0, and 10.0. The energy range of the lowest energy conformer from the least populated family relative to the lowest energy conformer was 0.000, 1.523, 1.071, and 0.751 kcal/mol, respectively. The calculated percent populations are shown in Table 3.4. The number scheme for **2** is shown in Figure 3.11.

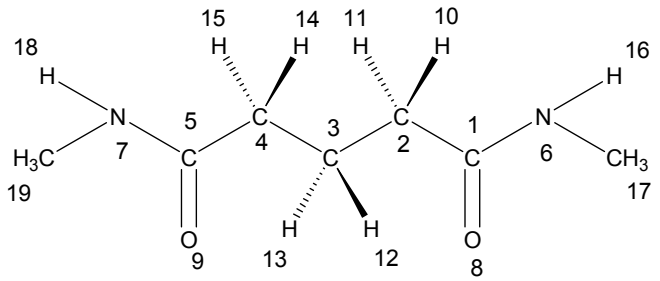

Figure 3.11 Numbering scheme for *N,N'*-dimethylglutaramide (**2**)

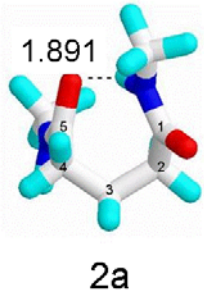

Figure 3.12 The one lowest energy conformation is **2a** (sickle 2G+3G+) and hydrogen bond length in angstroms at DIELEC 1.5

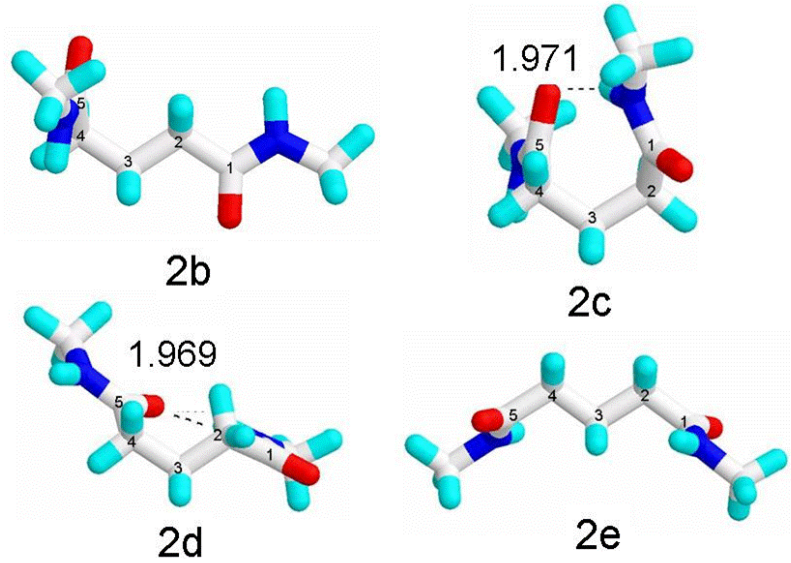

Figure 3.13 The four lowest energy conformations **2b** (3G-), **2c** (2G+3G+), **2d** (2G-3G+), and **2e** (extended) and hydrogen bond length in angstroms at DIELEC 3.5

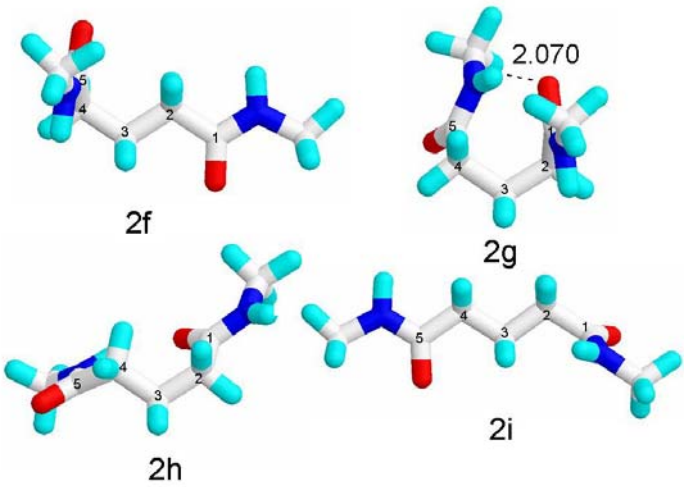

Figure 3.14 The four lowest energy conformations **2f** (3G-), **2g** (2G+3G+), **2h** (2G-3G+), and **2i** (extended) and hydrogen bond length in angstroms at DIELEC 6.0

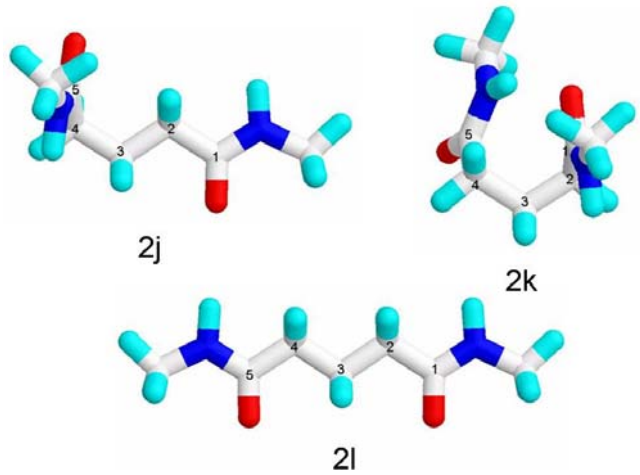

Figure 3.15 The three lowest energy conformations **2j** (3G-), **2k** (2G+3G+), and **2l** (extended) at DIELEC 10.0

Table 3.4 Calculated percent population for **2** at DIELEC 1.5, 3.5, 6.0, and 10.0 and percent population analyzed (PPA)

DIELEC	3G-	2G-3G+	2G+3G+	Extended	PPA
1.5	0.000	0.000	100 (**2a**)	0.000	99.48
3.5	26.43 (**2b**)	11.78 (**2d**)	49.10 (**2c**)	12.69 (**2e**)	89.13
6.0	47.89 (**2f**)	0.699 (**2h**)	18.90 (**2g**)	32.51 (**2i**)	89.30
10.0	49.96 (**2j**)	0.000	8.489 (**2k**)	41.00 (**2l**)	87.27

Glutaramide (**1**) and *N,N'*-dimethylglutaramide (**2**) differ in that **1** has primary amide groups and **2** has secondary N-methyl amido groups. The two compounds were found to have similar percent populations for the observed conformations at each dielectric constant. In addition, the conformational preference of each molecule similarly changes from the preferred sickle (*gauche*) rotamer at low (1.5) dielectric constant to the increasingly populated extended rotamer (*anti*) with increasing dielectric constant. With increasing simulated dielectric constant the conformational change can be attributed to the decrease in the stabilizing, intramolecular hydrogen bonding betweening the terminal amido functions as well as a decrease in the magnitude of the repulsive dipole-dipole interaction. In agreement with Aleman[5] and Novarro,[6] the *gauche* (TTGGTT) or sickle 3G- conformation is lower in energy than the extended conformation for these diamides.

3.2.2 Simulations of Xylaramide (3), *N,N'*-Dimethylxylaramide (4), Xylaric acid (5), Dimethyl Xylarate (6), and 2,3,4-Tri-*O*-acetyl-*N,N'*-dimethylxylaramide (7) – Class 2

All compounds in Class 2 are similar to Class 1 in that they have an axis of symmetry through the C3 carbon. The compounds in class 2 and 4 are *meso* compounds

because they have stereocenters and have energetically equivalent (+/-) *gauche* interactions. Again, only one conformation of the energetically equivalent (+/-) *gauche* interactions will be depicted.

Xylaramide (**3**)

Six rotamers of xylaramide (**3**) were searched at dielectric constant 3.5, 6.0, and 10.0 to a coefficient of variance of 1.36, 2.61, and 2.21 with an average of 345, 487, and 596 conformations found, respectively. Figures 3.17-3.19 depict the lowest energy conformations from various backbone families for **3** at dielectric constants 3.5, 6.0, and 10.0. The energy range of the lowest energy conformer from the least populated family relative to the lowest energy conformer was 2.304, 2.187, and 0.826 kcal/mol, respectively. The calculated percent populations are shown in Table 3.7. The number scheme for **3** is shown in Figure 3.16. Because the results of **3** and *N,N'*-dimethylxylaramide (**4**) are very similar, discussion of **3** and **4** follows the computational results of **4**.

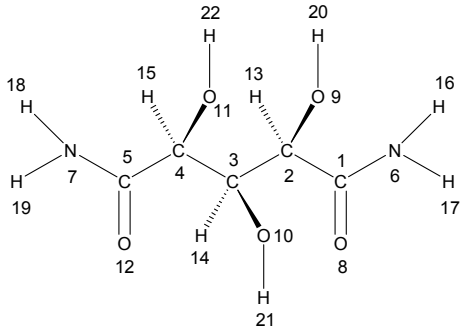

Figure 3.16 Numbering scheme for xylaramide (**3**)

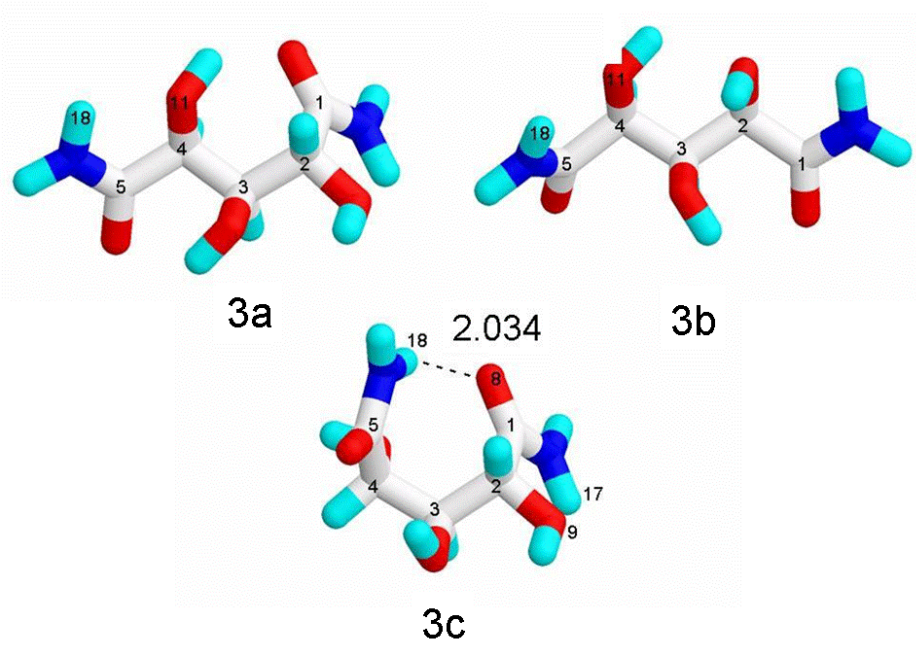

Figure 3.17 The three lowest energy conformations **3a** (2G-), **3b** (extended), and **3c** (2G-,3G-) and hydrogen bond length in angstroms at DIELEC 3.5

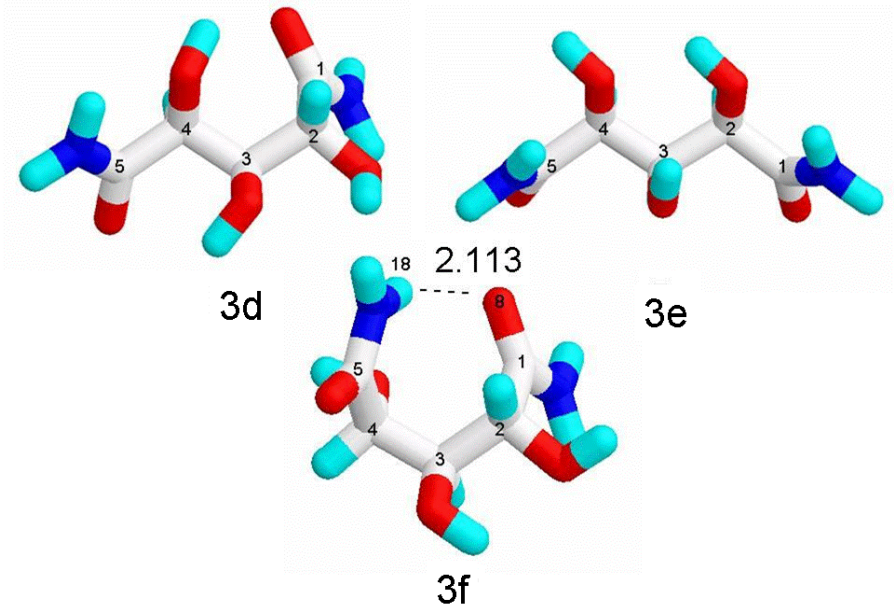

Figure 3.18 The three lowest energy conformations **3d** (2G-), **3e** (extended), and **3f** (2G-,3G-) and hydrogen bond length in angstroms at DIELEC 6.0

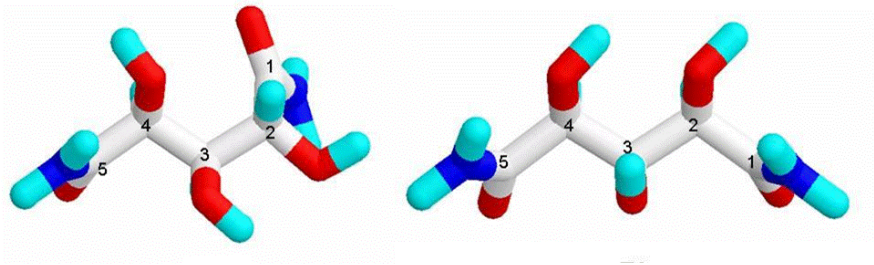

3g 3h

Figure 3.19 The two lowest energy conformations **3g** (2G-) and **3h** (extended) at DIELEC 10.0

Table 3.7 Calculated percent population for **3** at DIELEC 3.5, 6.0, and 10.0

DIELEC	**2G-**	**2G-, 3G-**	**Extended**	**PPA**
3.5	79.07 (**3a**)	0.626 (**3c**)	20.30 (**3d**)	93.87
6.0	81.46 (**3d**)	0.026 (**3f**)	18.51 (**3e**)	95.72
10.0	83.86 (**3g**)	0.000	16.14 (**3h**)	92.01

***N,N'*-Dimethylxylaramide (4)**

Six rotamers of *N,N'*-dimethylxylaramide (**4**) were searched at dielectric constant 3.5, 6.0, and 10.0 to a coefficient of variance of 0.93, 2.48, and 2.49 with an average of 345, 552, and 621 conformations found, respectively. Figures 3.21-3.23 depict the lowest energy conformations from various backbone families for **4** at dielectric constants 3.5, 6.0, and 10.0. The energy range of the lowest energy conformer from the least populated family relative to the lowest energy conformer was 1.281, 0.904, 0.849 kcal/mol, respectively. The calculated percent populations are shown in Table 3.8. The number scheme for **4** is shown in Figure 3.20.

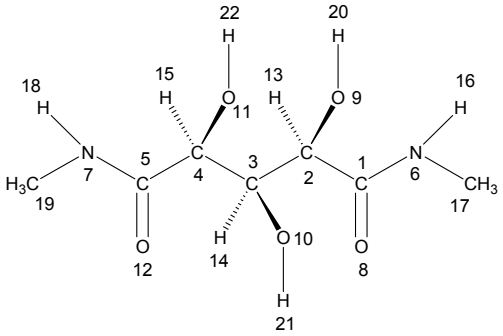

Figure 3.20 Numbering scheme for *N*,*N*'-dimethylxylaramide (**4**)

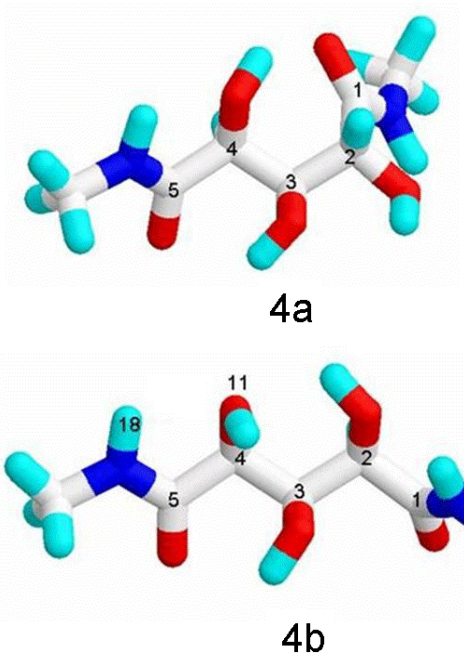

Figure 3.21 The two lowest energy conformations **4a** (2G-) and **4b** (extended) at DIELEC 3.5

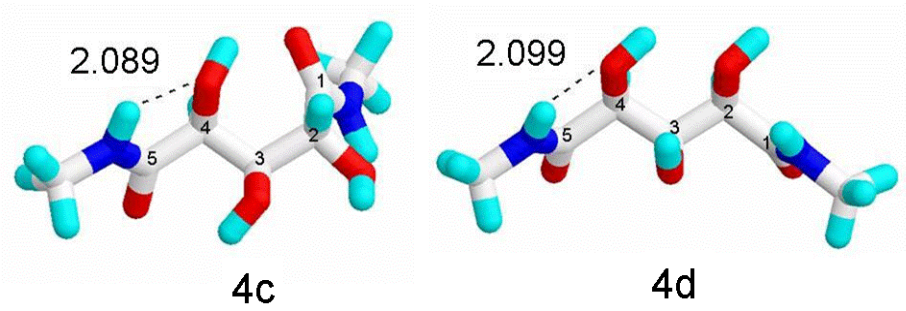

Figure 3.22 The two lowest energy conformations **4c** (2G-) and **4d** (extended) and hydrogen bond length in angstroms at DIELEC 6.0

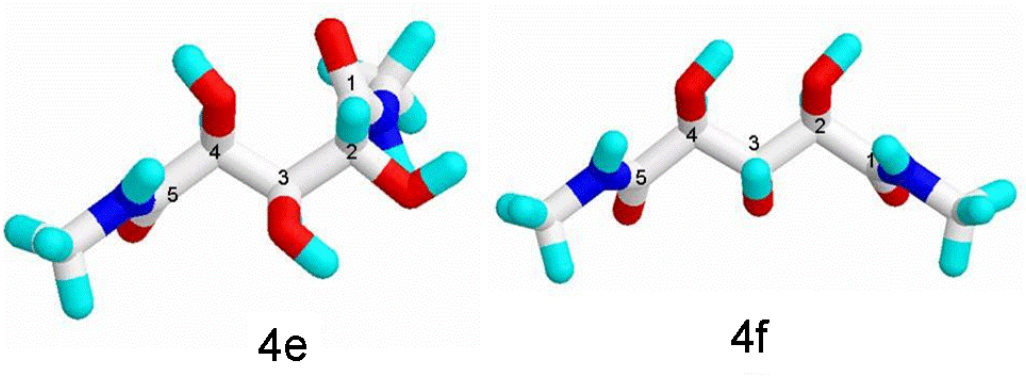

Figure 3.23 The two lowest energy conformations **4e** (2G-) and **4f** (extended) at DIELEC 10.0

Table 3.8 Calculated percent population for **4** at dielectric constant 3.5, 6.0, and 10.0

DIELEC	**2G-** (**4a**, **4c**, **4e**)	**Extended** (**4b**, **4d**, **4f**)	**PPA**
3.5	78.54 (**4a**)	21.46 (**4b**)	91.65
6.0	84.46 (**4c**)	15.54 (**4d**)	90.61
10.0	82.63 (**4e**)	17.37 (**4f**)	91.73

Xylaramide (**3**) and *N*,*N*'-dimethylxylaramide (**4**) structurally differ from one another in the same way as glutaramide (**1**) and *N*,*N*'-dimethylglutaramide (**2**), **3** has primary diamide groups while **4** has secondary N-methyl amido groups. Compounds **3** and **4** preferred the same conformations, sickle 2G- and extended, in almost identical percentages at each dielectric constant simulated. Therefore the N-methyl pendent group has little to no effect on the preferred conformations of **3** and **4**. The lower energy sickle 2G- conformation (ca. 80%) had no evidence of intramolecular hydrogen bonding and was stabilized by the alleviation of the eclipsed 1,3-parallel hydroxyl interaction that is present in the extended conformation (ca.20%). Unlike **1** and **2**, the preferred conformations of **3** and **4** did not change significantly with increasing dielectric constant

signifying, a lack of hydrogen bonding at all dielectric constants simulated. Additionally, the destabilizing parallel amide dipole interaction present in **1** and **2** could not be observed in simulations of **3** and **4**.

Kiely *et al.*[14] performed Macromodel V.2 energy minimizations of **4** at dielectric constant 8.6 and found the preferred conformations to be sickle 2G- (1.94 kcal/mol, 36.7%), sickle 3G+ (2.14 kcal/mol, 26.2%), and extended (3.08 kcal/mol, 16.4%). As discussed earlier, **4** is a *meso* compound and the sickle 2G- and sickle 3G+ conformations should be calculated as energetically equivalent. By addition of the sickle 2G- (36.7%) and sickle 3G+ (26.2%) percent population found using MacroModel V.2, one reaches a percent population value for the sickle 2G- conformation of 62.9% compared to the ~82% value calculated in this study. MacroModel V.2 results for the extended conformation agree with the calculated results by MM3(96).

Xylaric Acid (**5**)

Six rotamers of xylaric acid (**5**) were searched at dielectric constant 3.5 to a coefficient of variance of 5.18 and an average of 921.2 conformations found. The four lowest energy conformations **5a-5e** with an energy range of 1.582 kcal/mol are shown in Figure 3.25. The calculated percent populations for each conformation are given in Table 3.5. The number scheme for **5** is shown in Figure 3.24.

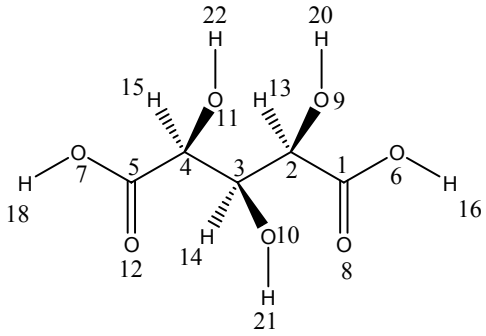

Figure 3.24 Numbering scheme for xylaric acid (**5**)

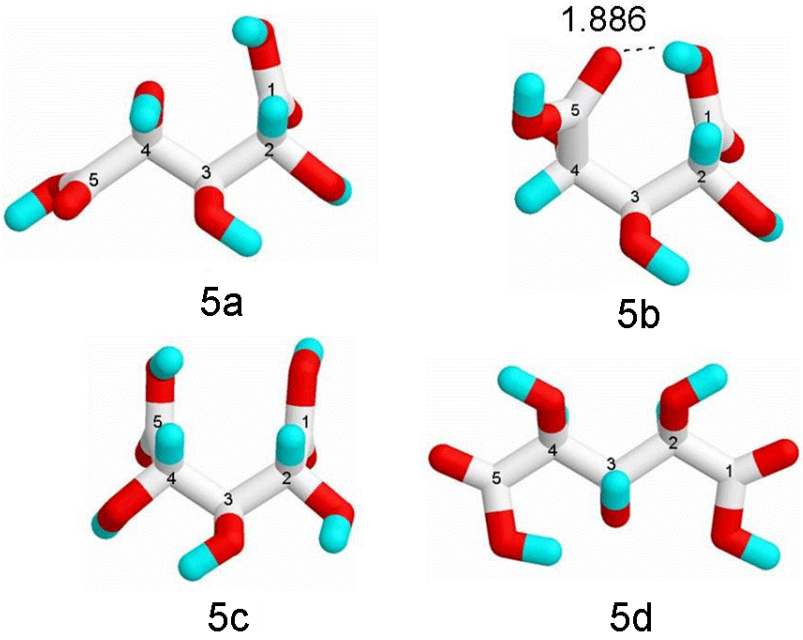

Figure 3.25 The four lowest energy conformations **5a** (2G-), **5b** (2G-3G-), **5c** (2G-3G+), and **5d** (extended) and hydrogen bond length in angstroms at DIELEC 3.5

Table 3.5 Calculated percent population and percent population analyzed (PPA) for the conformational families of **5** at DIELEC 3.5

DIELEC	2G-	2G-3G-	2G-3G+	Extended	PPA
3.5	92.54(**5a**)	1.588 (**5b**)	1.538 (**5c**)	4.329 (**5d**)	84.21

The computational results of xylaric acid (**5**) are in agreement with the results for xylaramide (**3**) and *N*,*N*'-dimethylxylaramide (**4**) which prefer conformations without eclipsed 1,3-parallel hydroxyl interactions. The overwhelming preferred and therefore lowest in energy conformation was the sickle 2G- conformation (ca. 93%) which has undergone a –120 degree rotation about the C2-C3 bond to alleviate the eclipsed 1,3-parallel hydroxyl interaction. The three other conformational states are not significantly populated and will not be discussed.

Dimethyl xylarate (**6**)

Six rotamers of dimethyl xylarate (**6**) were searched at dielectric constant3.5 to a coefficient of variance of 0.95 with an average of 837.3 conformations found. The three lowest energy conformations **6a-6c** with an energy range of 1.516 kcal/mol are shown in Figure 3.27 and the calculated percent populations are given in Table 3.6. The number scheme for **6** is shown in Figure 3.26.

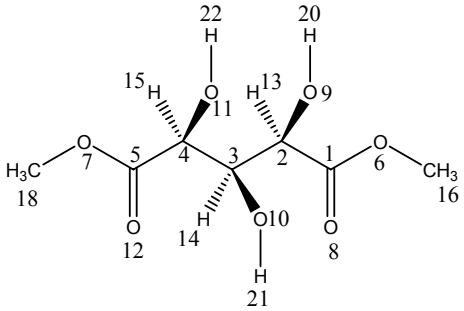

Figure 3.26 Numbering scheme for dimethyl xylarate (**6**)

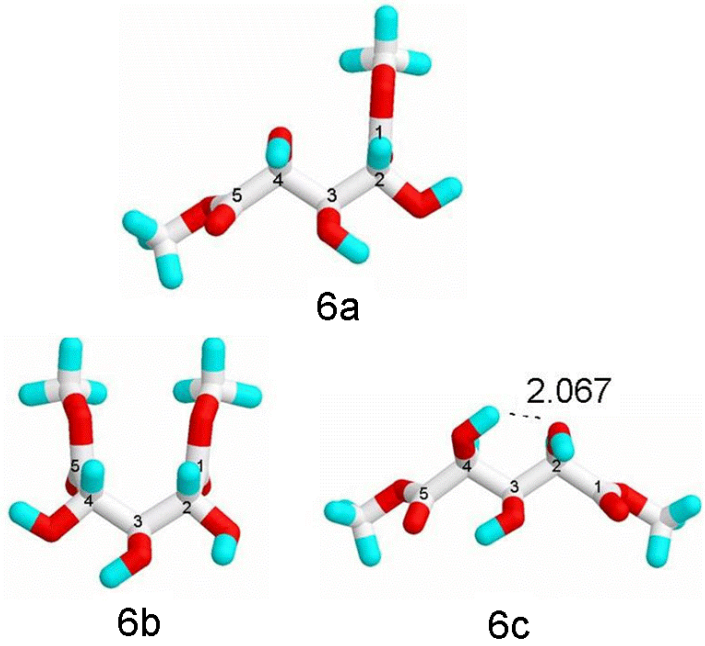

Figure 3.27 The three lowest energy conformations **6a** (2G-), **6b** (2G-3G+), and **6c** (extended) and hydrogen bond length in angstroms at DIELEC 3.5.

Table 3.6 Calculated percent population and percent population analyzed (PPA) for **6** at DIELEC 3.5

DIELEC	**2G-**	**2G-3G+**	**Extended**	**PPA**
3.5	94.24 (**6a**)	4.571 (**6b**)	1.196 (**6c**)	80.61

Dimethyl xylarate (**6**) like that of xylaramide (**3**), *N*,*N*'-dimethylxylaramide (**4**), and xylaric acid (**5**) preferred the sickle 2G- conformation (ca. 94%) overwhelmingly at dielectric constant 3.5. As with compounds **3**, **4**, and **5** this corresponds to the alleviation of the destabilizing eclipsed 1,3-parallel hydroxyl group interaction with no evidence of stabilizing intramolcular hydrogen bonding. Xylaric acid (**5**) and dimethyl xylarate (**6**) structurally differ from the **3** and and **4** in that they are a diacid and diester, respectively, and therefore lack the same ability of the amido functionality to hydrogen bond. Compounds **3** and **4** were modeled because the ability of the terminal amido groups to

intramolecularly hydrogen bond was unknown. Interestingly, the extended conformation in compounds **5** and **6** is less populated than for the diamides **3** and **4,** ~1.2% vs ~20%, respectively. This indicates that the terminal amido groups have weak electrostatic interactions (hydrogen bonds) falling outside the definition of a hydrogen bond. With the latter most likely the case because there could be a stabilizing hydrogen bond between the amide hydrogen and the hydroxyl oxygen which is alpha to the amide carbonyl with a hydrogen bond angle (donor-hydrogen····acceptor) that falls below 110 degrees.

2,3,4-Tri-*O*-acetyl-*N,N'* dimethylxylaramide (**7**)

Six rotamers of 2,3,4-tri-*O*-acetyl-*N,N'*-dimethylxylaramide (**7**) were searched at dielectric constants 1.5 and 3.5 to a coefficient of variance of 2.33 and 3.03 with an average of 1942 and 2290 conformations found, respectively. Figures 3.29 and 3.30 depict the lowest energy conformations from various backbone families for **7** at dielectric constants 1.5 and 3.5. The energy range of the lowest energy conformer from the least populated family relative to the lowest energy conformer was 2.446 and 1.302 kcal/mol, respectively. The calculated percent populations are shown in Table 3.9. The number scheme for **7** is shown in Figure 3.28.

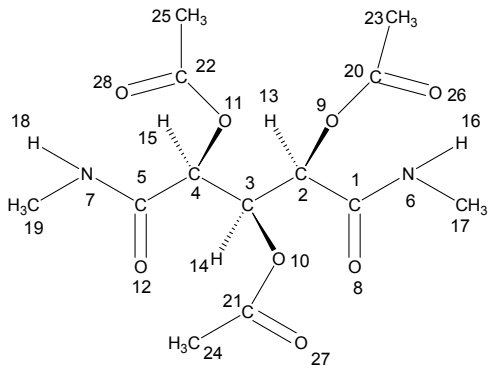

Figure 3.28 Numbering scheme for 2,3,4-tri-*O*-acetyl-*N,N'*-dimethylxylaramide (**7**)

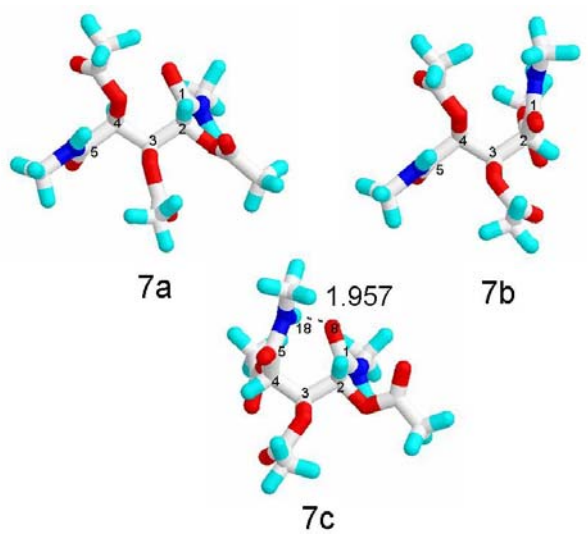

Figure 3.29 The three lowest energy conformations **7a** (2G-), **7b** (2G+), and **7c** (2G-,3G-) and hydrogen bond length in angstroms at DIELEC 1.5

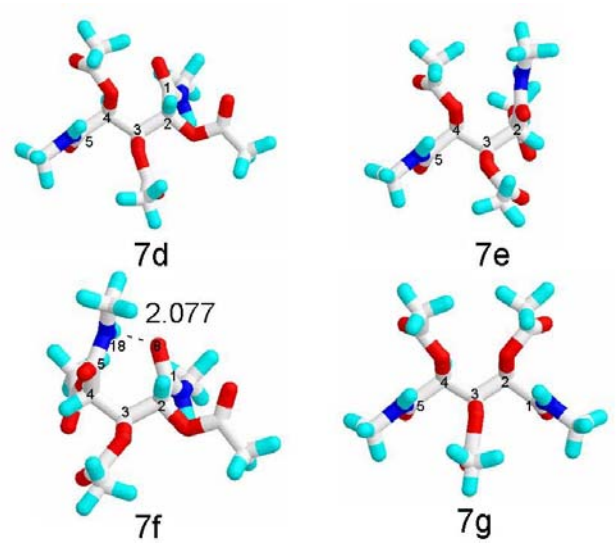

Figure 3.30 The four lowest energy conformations **7d** (2G-), **7e** (2G+), **7f** (2G-,3G-), and **7g** (extended) and hydrogen bond length in angstroms at DIELEC 3.5

Table 3.9 Calculated percent population for **7** at DIELEC 1.5 and 3.5

DIELEC	2G-	2G+	2G-,3G-	Extended	PPA
1.5	8.064 (**7a**)	1.935 (**7b**)	90.00 (**7c**)	0.000	95.55
3.5	45.08 (**7d**)	10.07 (**7e**)	30.45 (**7f**)	14.40 (**7g**)	87.27

2,3,4-Tri-*O*-acetyl-*N,N'*-dimethylxylaramide (**7**) unlike compounds **3-6** was simulated at dielectric constant 1.5 in an effort to understand the preferred conformations of the aldaryl monomer unit in a nonpolar solvent where intramolecular hydrogen bonding would be more likely to be observed. The preferred sickle 2G-3G- conformation (90.0%) shows an intramolecular hydrogen bond between amide hydrogen, H18, and carbonyl oxygen, O8, but no eclipsed 1,3-parallel interactions. This preferred sickle 2G-3G- conformation at dielectric constant 1.5 was no longer the preferred conformation at dielectric constant 3.5 with only a 30.45 percent population value indicating a decrease in the stabilizing effects of electrostatic interactions. Instead the sickle 2G- conformation, which does not have a hydrogen bond or steric eclipsed 1,3-parallel interactions, became the preferred conformation at dielectric constant 3.5 with a percent population value of 45% compared to 8% at dielectric constant 1.5. Compound **7** is the *O*-acetylated derivative of *N,N'*-dimethylxylaramide (**4**) and consequentially significant differences in the preferred conformations at dielectric constant 3.5 result between the two compounds. At dielectric constant 3.5, **7** populated the sickle 2G-3G- and 2G+ conformations (30% and 10% respectively) whereas **4** did not. The sickle 2G-3G- conformation of **7** was stabilized by an intramolecular hydrogen bond between O8 and H18 at dielectric constants 1.5 and 3.5, 1.957 and 2.077 angstroms, respectively, with the longer hydrogen bond at dielectric constant 3.5 signifying a weaker hydrogen bond. The extended

conformations of **4** and **7** were nearly equally preferred indicating that the hydroxyl groups ability to hydrogen bond in **4** did not influence the preferred conformation at dielectric constant 3.5 and that steric interactions were the main driving force determining the conformational preference.

3.2.3 Simulations of L-Arabinaramide (8), *N,N'*-Dimethyl-L-arabinaramide (9), L-Arabinaric Acid (10), and 2,3,4-Tri-*O*-acetyl-*N,N'*-dimethyl-L-arabinaramide (11) – Class 3

L-Arabinaramide (8)

Six rotamers of L-arabinaramide (**8**) were searched at dielectric constants 3.5, 6.0, and 10.0 to a coefficient of variance of 1.68, 1.41, and 1.95 with an average of 325, 491, and 618 conformations found, respectively. Figures 3.32-3.34 depict the lowest energy conformations from various backbone families for **8** at dielectric constants 3.5, 6.0, and 10.0. The energy range of the lowest energy conformer from the least populated family relative to the lowest energy conformer was 1.459, 1.459, and 0.945 kcal/mol, respectively. The calculated percent populations are shown in Table 3.11. The number scheme for **8** is shown in Figure 3.31.

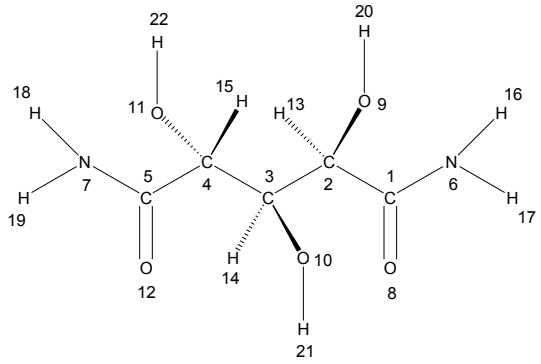

Figure 3.31 Numbering scheme for L-arabinaramide (**8**)

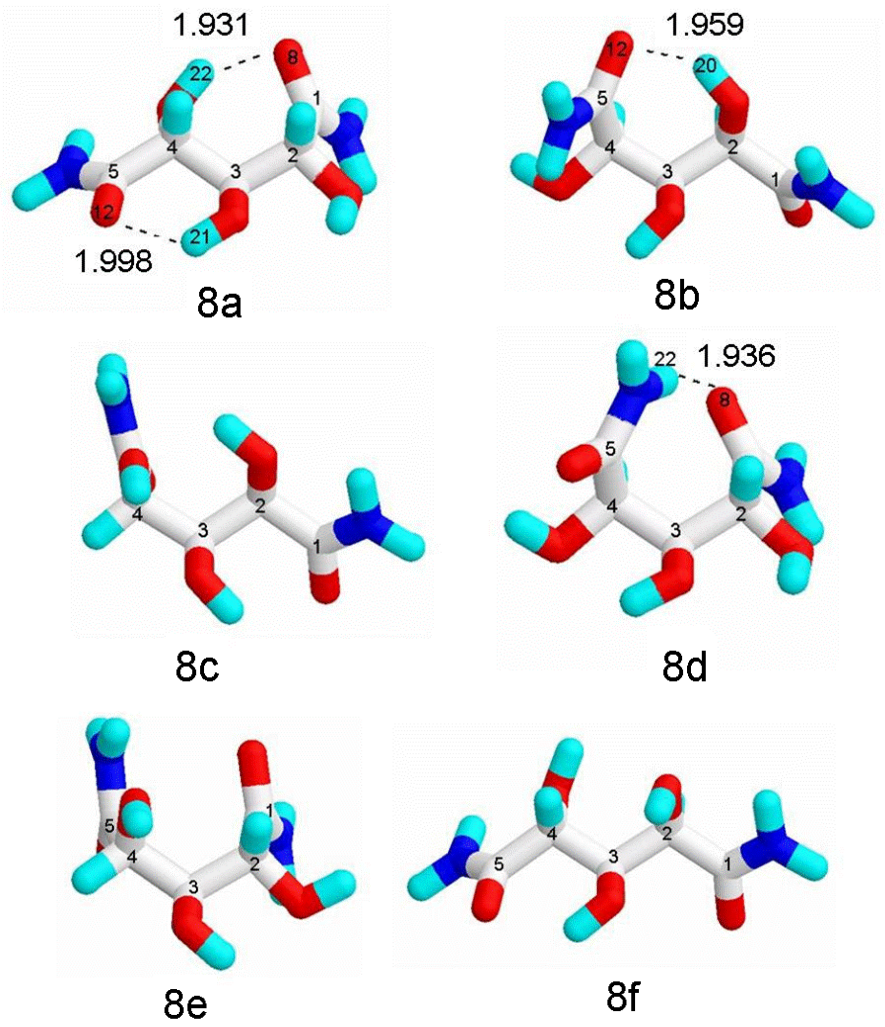

Figure 3.32 The six lowest energy conformations **8a** (2G-), **8b** (3G-), **8c** (3G+), **8d** (2G-,3G-), **8e** (2G-3G+), **8f** (extended) and hydrogen bond length in angstroms at DIELEC 3.5

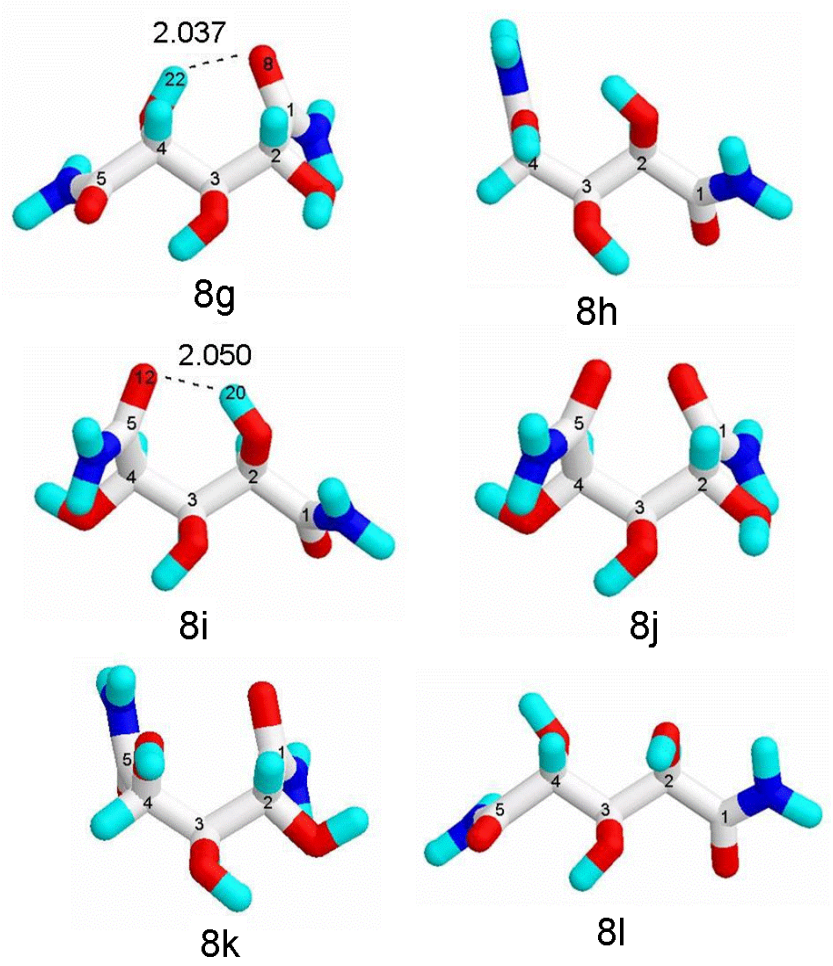

Figure 3.33 The six lowest energy conformations **8g** (2G-), **8h** (3G+), **8i** (3G-), **8j** (2G-,3G-), **8k** (2G-3G+), **8l** (extended) and hydrogen bond length in angstroms at DIELEC 6.0

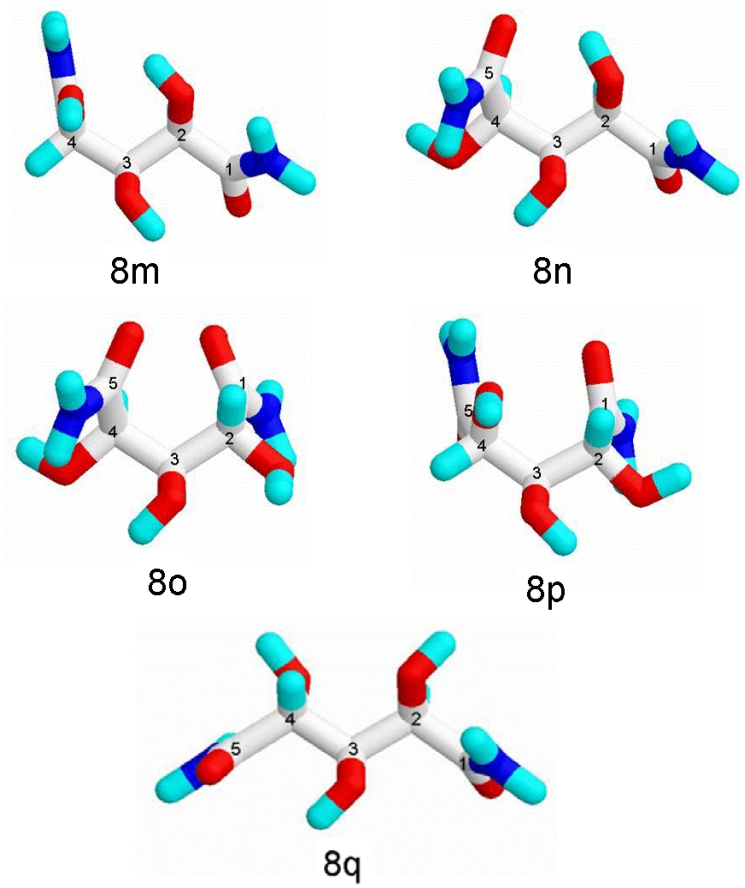

Figure 3.34 The six lowest energy conformations **8m** (3G+), **8n** (3G-), **8o** (2G-3G-), **8p** (2G-3G+), and **8q** (extended) at DIELEC 10.0

The sickle 3G+ conformation (ca. 45%) of L-arabinaramide (**8**) is the dominant conformation at simulated dielectric constants 3.5, 6.0, and 10.0 despite having an eclipsed 1,3-parallel hydroxyl interaction in this conformation. However, the sickle 3G+ conformation became less preferred with increasing dielectric constant suggesting that intramolecular hydrogen bonding is stabilizing this conformation. The sickle 2G-3G- conformation was also well populated (ca. 28%) across the dielectric constants studied. The sickle 2G-3G- conformation did not have the destabilizing eclipsed 1,3-parallel hydroxyl interaction and at dielectric constant 3.5 had a stabilizing hydrogen bond of 1.936 angstroms between an amide hydrogen (H18) and a carbonyl oxygen (O8). Despite

having computed the sickle 3G+ conformation as the lowest energy conformation when there is a destabilizing eclipsed 1,3-parallel hydroxyl interaction in this conformation, the observed trend is that with increasing dielectric constant the sickle 3G+ conformation becomes less favored, i.e. higher in energy. This result is in agreement with the literature as well as the results reported earlier in this study.

Table 3.10 Calculated percent population for **8** at DIELEC 3.5, 6.0, 10.0

DIELEC	2G-	3G+	3G-	2G-,3G-	2G-,3G+	Extended	PPA
3.5	6.963(**8a**)	47.34(**8c**)	47.85(**8b**)	25.02(**8d**)	6.708(**8e**)	6.112(**8f**)	90.21
6.0	0.839(**8g**)	46.06(**8k**)	10.32(**8i**)	27.17(**8j**)	6.416(**8l**)	9.187(**8l**)	84.04
10.0	0.000	43.07(**8m**)	9.701(**8n**)	31.50(**8o**)	9.200(**8p**)	6.538(**8q**)	80.76

***N,N'*-Dimethyl-L-arabinaramide** (**9**)

Six rotamers of *N,N'*-dimethyl-L-arabinaramide (**9**) were searched at dielectric constant 3.5, 6.0, and 10.0 to a coefficient of variance of 2.39, 2.68, and 2.99 with an average of 358, 522, and 655 conformations found, respectively. Figures 3.36-3.38 depict the lowest energy conformations from various backbone families for **9** at dielectric constants 3.5, 6.0, and 10.0. The energy range of the lowest energy conformer from the least populated family relative to the lowest energy conformer was 1.425, 1.442, and 0.946 kcal/mol, respectively. The calculated percent populations are shown in Table 3.12. The number scheme for **9** is shown in Figure 3.35.

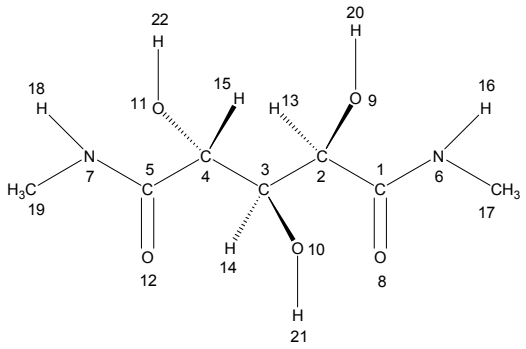

Figure 3.35 Numbering scheme for *N*,*N*'-dimethyl-L-arabinaramide (**9**)

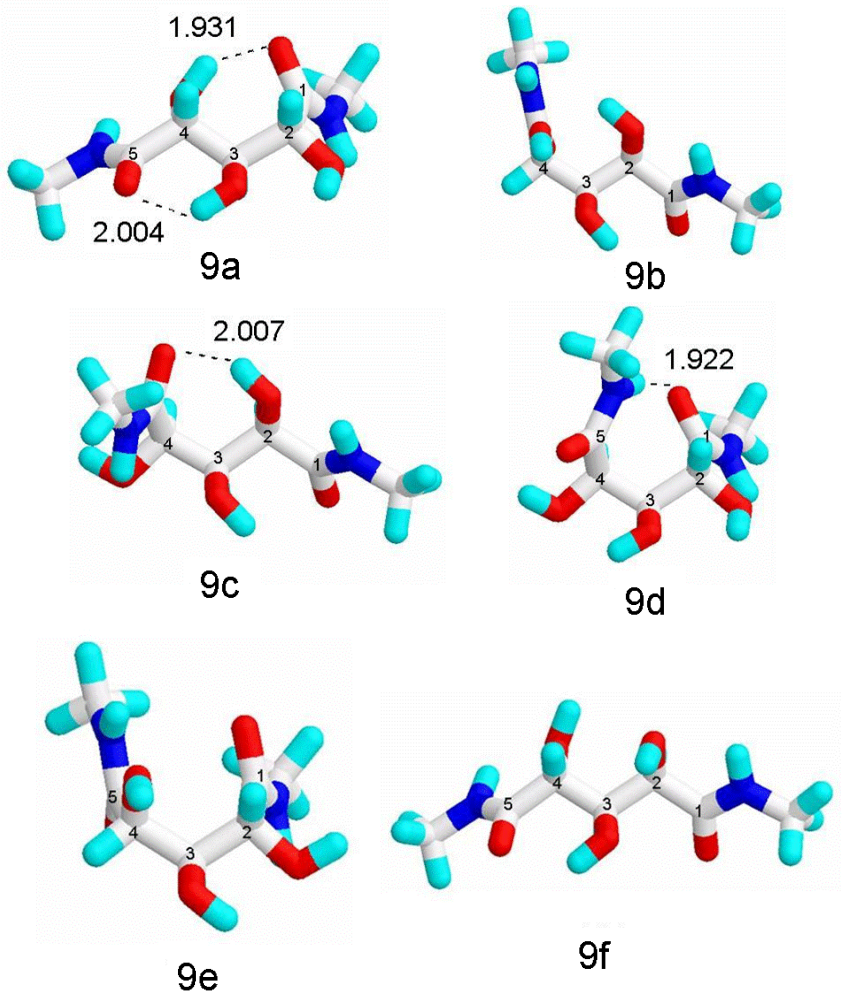

Figure 3.36 The six lowest energy conformations **9a** (2G-), **9b** (3G+), **9c** (3G-), **9d** (2G-3G-), **9e** (2G-3G+), and **9f** (extended) and hydrogen bond length in angstroms at DIELEC 3.5

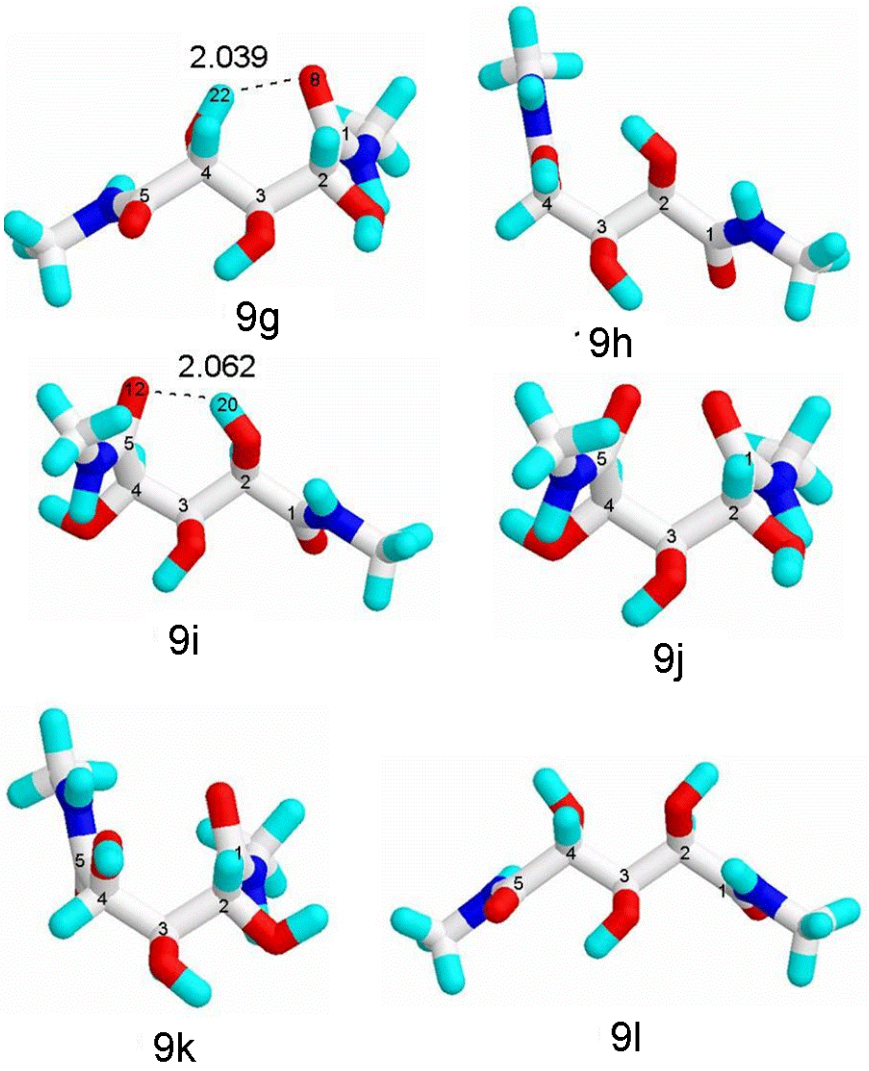

Figure 3.37 The six lowest energy conformations **9g** (2G-), **9h** (3G+), **9i** (3G-), **9j** (2G-3G-), **9k** (2G-3G+), and **9l** (extended) and hydrogen bond length in angstroms at DIELEC 6.0

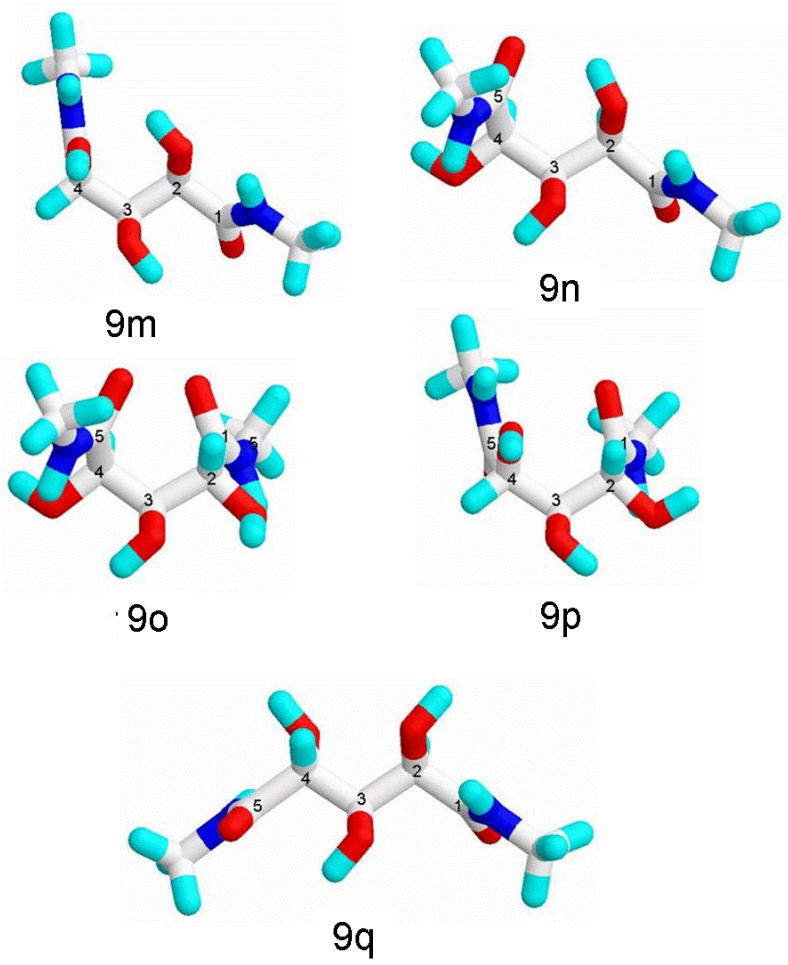

Figure 3.38 The five lowest energy conformations **9m** (3G+), **9n** (3G-), **9o** (2G-3G-), **9p** (2G-3G+), and **9q** (extended) at DIELEC 10.0

Table 3.11 Calculated percent population for **9** at DIELEC 3.5, 6.0, 10.0

DIELEC	2G-	3G+	3G-	2G-,3G-	2G-,3G+	Extended	PPA
3.5	5.471(**9a**)	48.64(**9b**)	7.560(**9c**)	20.42(**9d**)	11.50(**9e**)	6.405(**9f**)	91.28
6.0	0.835(**9g**)	40.11(**9m**)	11.29(**9i**)	26.83(**9j**)	14.58(**9k**)	6.354(**9l**)	83.63
10.0	0.000	38.94(**9h**)	5.959(**9n**)	29.87(**9o**)	17.42(**9p**)	7.804(**9q**)	75.39

The computational results of *N,N'*-dimethyl-L-arabinaramide (**9**) were almost identical to that of L-arabinaramide (**8**). The sickle 3G+ conformation is the

overwhelmingly preferred conformation at each dielectric constant despite having an eclipsed 1,3-parallel hydroxyl interaction and like **8** the percent population of the sickle 3G+ conformation decreases with increasing dielectric constant. Additionally, the sickle 3G+ conformer at dielectric constant 3.5 showed a stabilizing hydrogen bond of 1.959 angstroms length which was not present at higher dielectric constants, 6.0 and 10.0, indicating the decreasing influence of electrostatic interactions with increasing dielectric constant. The sickle 2G-3G- conformation which has no obvious steric interactions becomes increasingly preferred from ~20% to ~30% population with increasing dielectric constant. These results illustrate that intramolecular hydrogen bonding is stabilizing conformations with destabilizing eclipsed 1,3-parallel hydroxyl interactions. By increasing the dielectric constant, the stabilizing effect of the intramolecular hydrogen bond decreases and steric interactions become the driving force behind the preferred conformation.

L-Arabinaric Acid (**10**)

Six rotamers of L-arabinaric acid (**10**) were searched at dielectric constant 3.5 to a coefficient of variance of 3.07 with an average of 675.5 conformations found. The six lowest energy conformations, **10a-10f**, with an energy range of 1.396 kcal/mol are shown in Figure 3.40. The calculated percent populations for each conformation are given in Table 3.10. The number scheme for **10** is shown in Figure 3.39.

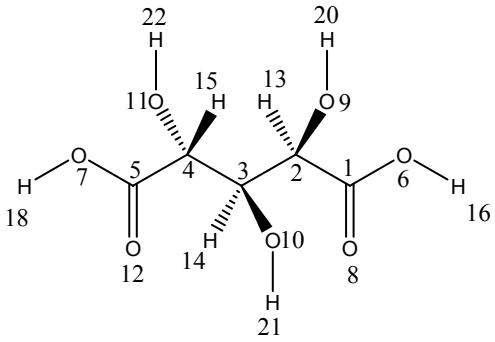

Figure 3.39 Numbering scheme for L-arabinaric acid (**10**)

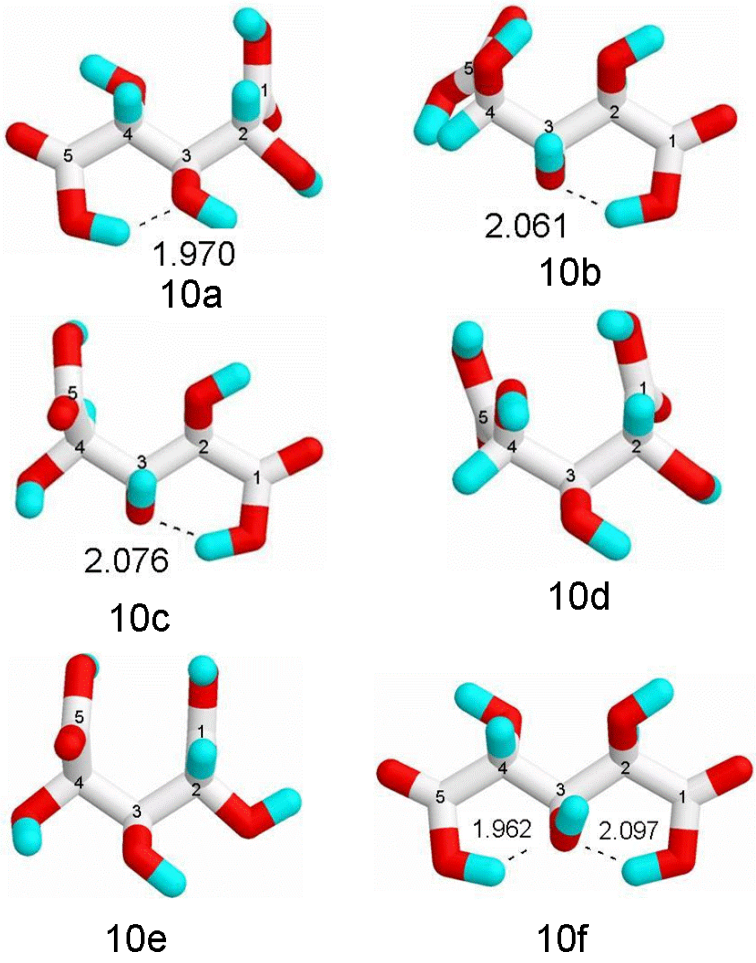

Figure 3.40 The six lowest energy conformations **10a** (2G-), **10b** (3G+), **10c** (3G-), **10d** (2G-3G+), **10e** (2G-3G-), and **10f** (extended) and hydrogen bond length in angstroms at DIELEC 3.5

Table 3.12 Calculated percent population and percent population analyzed PPA for **10** at DIELEC 3.5

DIELEC	2G-	3G+	3G-	2G-3G+	2G-3G-	Extended	PPA
3.5	2.414(**10a**)	7.105(**10b**)	10.18(**10c**)	0.773(**10d**)	46.11(**10e**)	33.41(**10f**)	75.69

Whereas the sickle 3G+ and sickle 2G-3G- conformations are the dominant conformations L-arabinaramide (**8**) and *N,N'*-dimethyl-L-arabinaramide (**9**), the conformational preference, i.e. lowest energy conformation, for L-arabinaric acid (**10**) is the extended (33%) and sickle 2G-3G+ (46%) conformations, of which neither have eclipsed 1,3-parallel hydroxyl interactions as was the case in the sickle 3G+ conformation preferred by **8** and **9**. The extended conformation of **10** is stabilized by two intramolecular hydrogen bonds between the acid protons and the hydroxyl group on C3 and does not have steric interactions.

2,3,4-Tri-*O*-acetyl-*N,N'*-dimethyl-L-arabinaramide (**11**)

Six rotamers of 2,3,4-tri-*O*-acetyl-*N,N'*-dimethyl-L-arabinaramide (**11**) were searched at dielectric constant 1.5 and 3.5 to a coefficient of variance of 0.88 and 2.69 with an average of 2426 and 2352 conformations found, respectively. Figures 3.42 and 3.43 depict the lowest energy conformations from various backbone families for **11** at dielectric constants 1.5 and 3.5. The energy range of the lowest energy conformer from the least populated family relative to the lowest energy conformer was 1.025 and 1.296 kcal/mol, respectively. The calculated percent populations are shown in Table 3.13. The number scheme for **11** is shown in Figure 3.41.

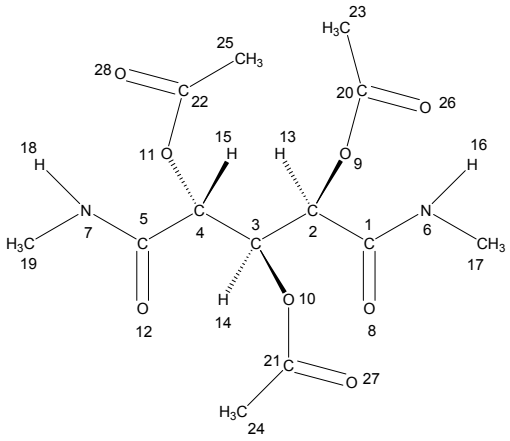

Figure 3.41 Numbering scheme for 2,3,4-tri-*O*-acetyl-*N*,*N*'-dimethyl-L-arabinaramide (**11**)

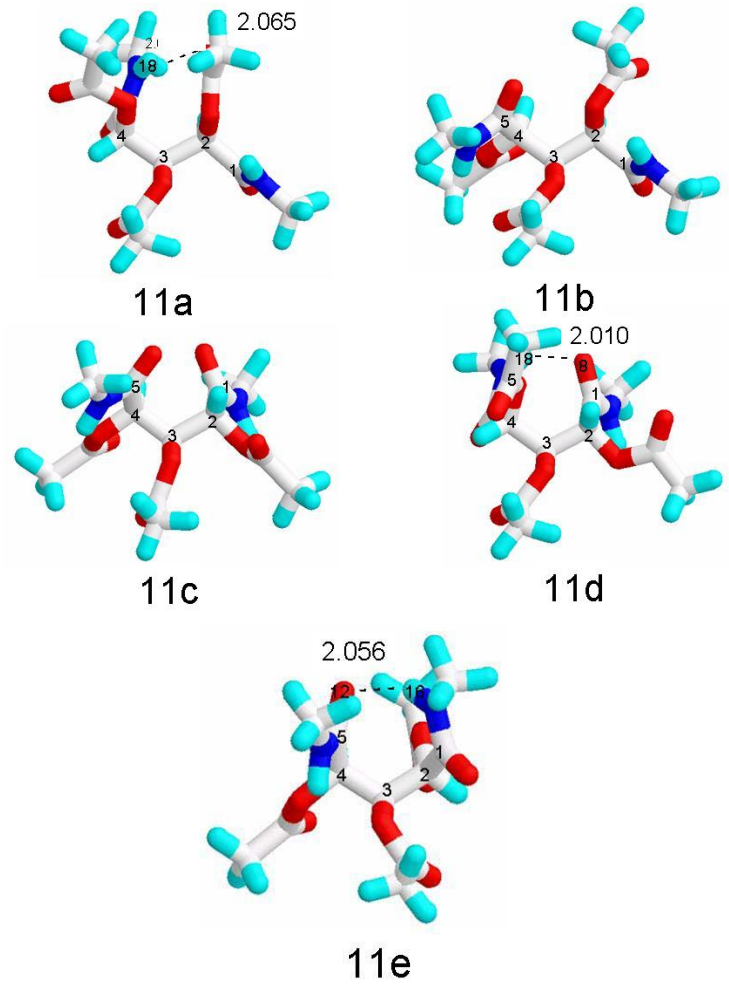

Figure 3.42 The five lowest energy conformations **11a** (3G+), **11b** (3G-), **11c** (2G-3G-), **11d** (2G-3G+), **11e** (2G+3G-) and hydrogen bond length in angstroms at DIELEC 1.5

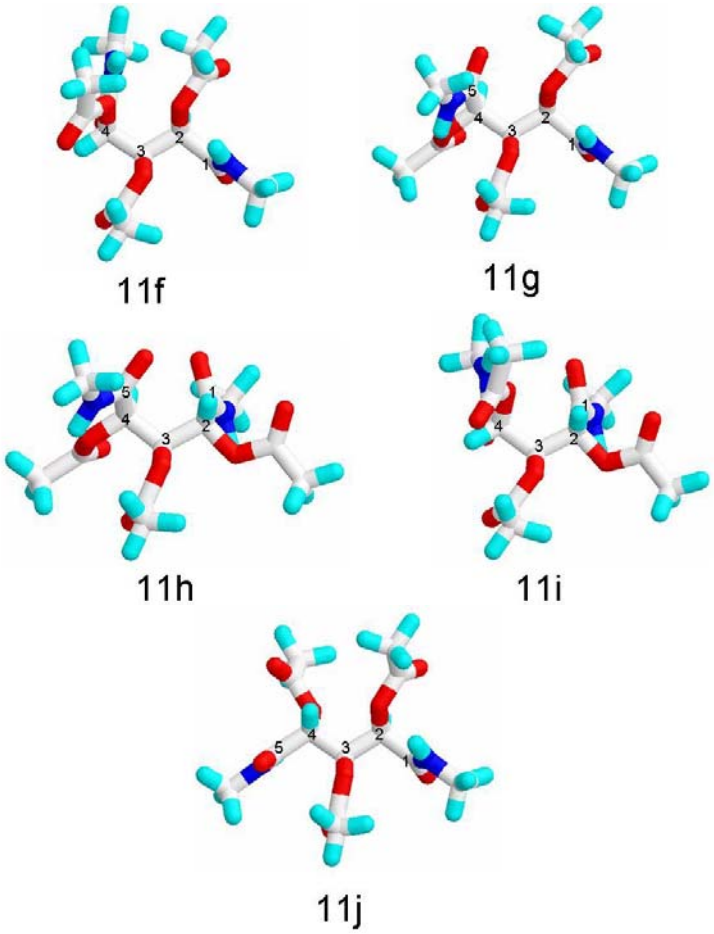

Figure 3.43 The five lowest energy conformations **11f** (3G+), **11g** (3G-), **11h** (2G-3G-), **11i** (2G-3G+), and **11j** (extended) at DIELEC 3.5

Table 3.13 Calculated percent population for **11** at DIELEC 1.5 and 3.5

DIELEC	3G+	3G-	2G-,3G-	2G-,3G+	2G+,3G-	Extended	PPA
1.5	50.65(**11a**)	8.133(**11b**)	9.582(**11c**)	27.59(**11d**)	4.042(**11c**)	0.000	82.22
3.5	32.04(**11f**)	23.49(**11g**)	13.75(**11h**)	25.56(**11i**)	0.000	5.152(**11j**)	80.68

2,3,4-Tri-*O*-acetyl-*N,N'*-dimethyl-L-arabinaramide (**11**) unlike compounds **8**-**10** was simulated at dielectric constant 1.5 in an effort to understand the preferred conformations in a nonpolar solvet where intramolecular hydrogen bonding was more likely to be observed. The two preferred conformations at dielectric constant 1.5, sickle 2G-3G+ and sickle 3G+, each showed intramolecular hydrogen bonding between an amide hydrogen, H18, and carbonyl oxygen, O8, with hydrogen bond lengths of 2.010 and 2.065 angstroms, respectively. The sickle 3G+ conformation (ca. 51%) has an eclipsed 1,3-parallel acetoxyl interaction which was stabilized by an intramolecular hydrogen bond of 2.065 angstroms at dielectric constant 1.5 that is no longer observed at dielectric constant 3.5. Instead the sickle 3G- conformation having no obvious steric interaction, increased in percent population value from 8.1% at dielectric constant 1.5 to 23.5% at dielectric constant 3.5. Compound **11** is the acetylated derivative of *N,N'*-dimethyl-L-arabinaramide (**9**) and consequentially significant differences in the preferred conformations between the two compounds result at dielectric constant 3.5. At dielectric constant 3.5, **11** populated the sickle 3G- and 3G+ conformations (23% and 32% respectively) where as **9** did not. This suggests that intramolecular hydrogen bonding of **9** was a significant stabilizing force and contributed to the population of conformations that were less energetically favored in the acetylated derivative, **11**.

3.2.4 Simulations of L-Ribaramide (12), *N,N'*-Dimethylribaramide (13), Ribaric Acid (14), and 2,3,4-Tri-*O*-acetyl-*N,N'*-dimethylribaramide (15) – Class 4

All compounds in Class 4 are similar to Class 2 in that they are *meso* compounds and have energetically equivalent (+/-) *gauche* interactions. Again only one conformation of the energetically equivalent (+/-) *gauche* interactions will be depicted.

Ribaramide (**12**)

Six rotamers of ribaramide (**12**) were searched at dielectric constant 3.5, 6.0, and 10.0 to a coefficient of variance of 1.82, 2.66, and 1.10 with an average of 336, 486, and 633 conformations found, respectively. Figures 3.45 and 3.47 depict the lowest energy conformations from various backbone families for **12** at dielectric constants 3.5, 6.0, and 10.0. The energy range of the lowest energy conformer from the least populated family relative to the lowest energy conformer was 2.291, 0.914, and 0.837 kcal/mol, respectively. The calculated percent populations are shown in Table 3.14. The number scheme for **12** is shown in Figure 3.44.

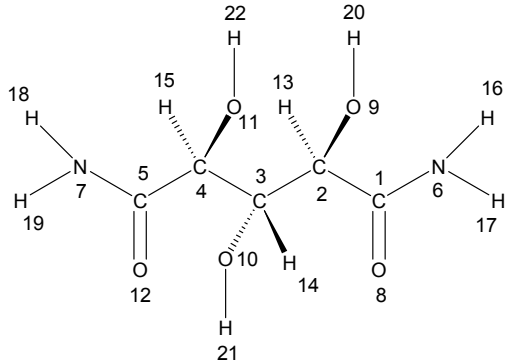

Figure 3.44 Numbering scheme for ribaramide (**12**)

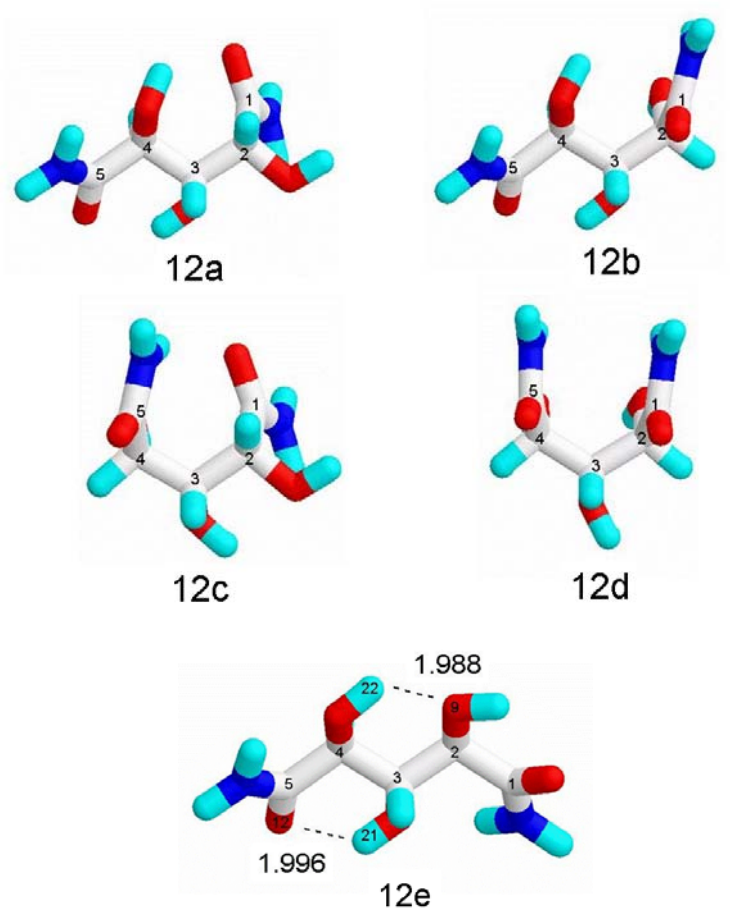

Figure 3.45 The five lowest energy conformations **12a** (2G-), **12b** (2G+), **12c** (2G-3G-), **12d** (2G+3G-), **12e** (extended) and hydrogen bond length in angstroms at DIELEC 3.5

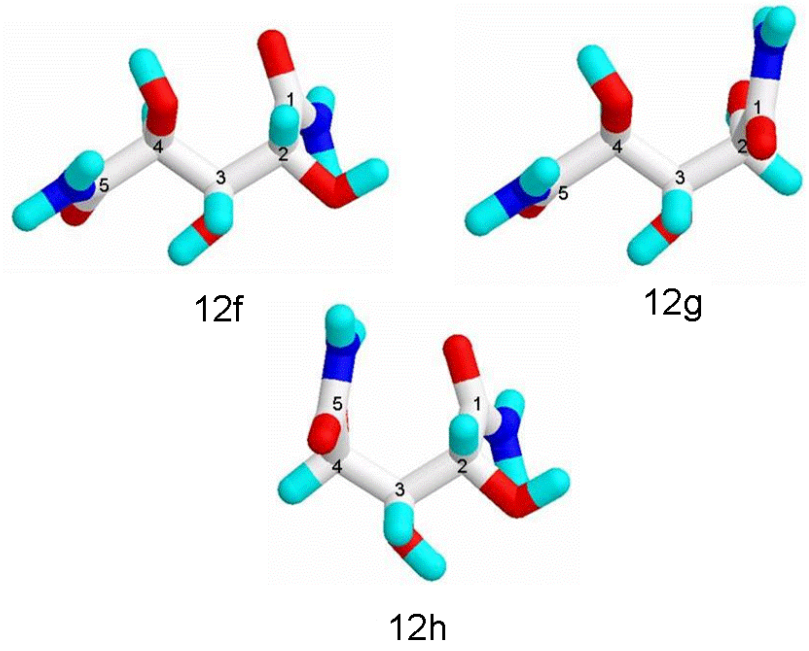

Figure 3.46 The three lowest energy conformations **12f** (2G-), **12g** (2G+), and **12h** (2G-3G-) at DIELEC 6.0

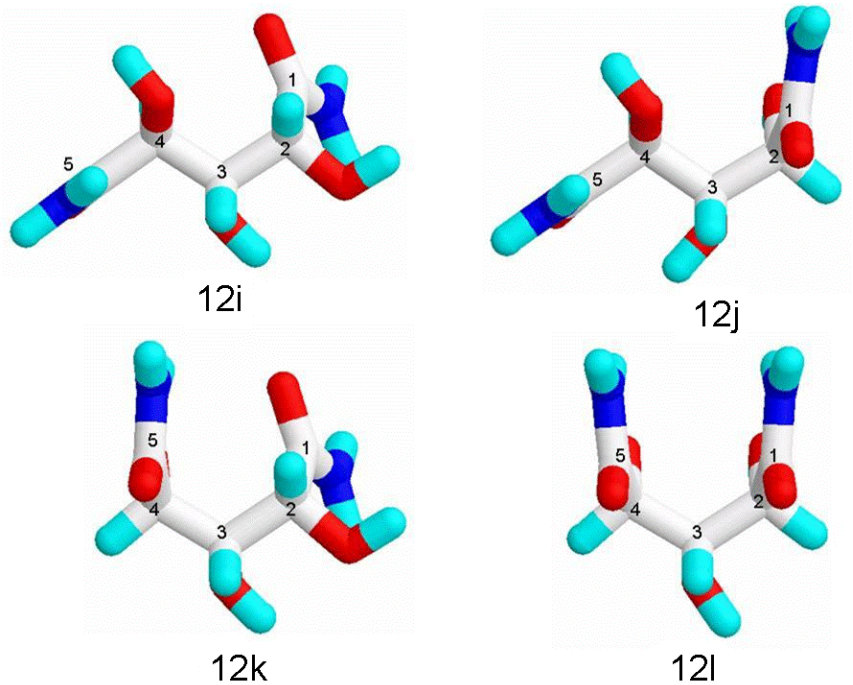

Figure 3.47 The four lowest energy conformations **12i** (2G-), **12j** (2G+), **12k** (2G-3G-), and **12l** (2G+3G-) at DIELEC 10.0

Table 3.14 Calculated percent population for **12** at DIELEC 3.5, 6.0, and10.0

DIELEC	2G-	2G+	2G-,3G-	2G+,3G-	Extended	PPA
3.5	21.10(**12a**)	12.56(**12b**)	52.10(**12c**)	13.88(**12d**)	0.361(**12e**)	88.87
6.0	45.84(**12f**)	8.311(**12g**)	45.84(**12h**)	0.000	0.000	77.17
10.0	18.69(**12i**)	9.848(**12j**)	54.88(**12k**)	11.76(**12l**)	0.000	79.45

Ribaramide (**12**) populated the sickle 2G-3G- conformation at approximately 50 percent at dielectric constants 3.5, 6.0, and 10.0. The sickle 2G-3G- and the sickle 2G- conformations do not have obvious electrostatic and steric interactions. The sickle 2G- conformation was populated ~20 percent at dielectric constants 3.5 and 10.0, and 45.84% at dielectric constant 6.0. Because the preferred conformations did not have eclipsed 1,3-parallel hydroxyl interactions it suggest that steric interactions are the driving force for the preferred conformations. Observation of a populated sickle 2G+3G- conformation is surprising in that it has an eclipsed 1,3-hydroxyl interaction and parallel amide dipoles in relatively close proximity, however this conformation comprises ~10% of the population which is quite insignificant.

In the computational results prior to ribaramide (**12**), excluding glutaramide (**1**) and *N,N'*-dimethylglutaramide, there was no direct observation of a parallel amide dipole-dipole interaction which was not surprising when the relative strength of electrostatic and steric interactions is considered. However at dielectric constant 3.5, the extended conformation of **12e**, which has a very high energy, displays a twist of the C1-C2 bond to give opposing amide dipoles. This result suggest that parallel amide dipole-dipole interactions do influence the preferred conformation of the moleculed studied but

in such small magnitude that the main driving forces are steric and electrostatic interactions.

N,N'-Dimethylribaramide (**13**)

Six rotamers of *N,N'*-dimethylribaramide (**13**) were searched at dielectric constant 3.5, 6.0, and 10.0 to a coefficient of variance of 1.00, 1.81, and 1.81 with an average of 375, 517, and 517 conformations found respectively. Figures 3.49 and 3.51 depict the lowest energy conformations from various backbone families for **13** at dielectric constants 3.5, 6.0, and 10.0. The energy range of the lowest energy conformer from the least populated family relative to the lowest energy conformer was 1.697, 1.152, and 1.152 kcal/mol, respectively. The calculated percent populations are shown in Table 3.15. The numbering scheme for **13** is shown in Figure 3.48.

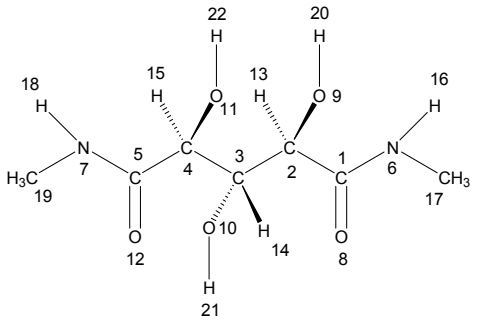

Figure 3.48 Numbering scheme for *N,N'*-dimethylribaramide (**13**)

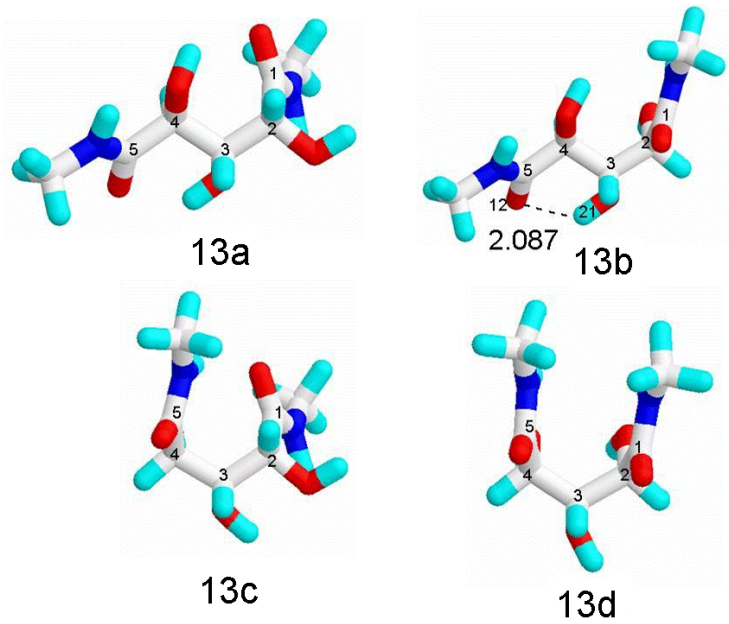

Figure 3.49 The four lowest energy conformations **13a** (2G-), **13b** (2G+), **13c** (2G-3G-), and **13d** (2G+3G-) and hydrogen bond length in angstroms at DIELEC 3.5

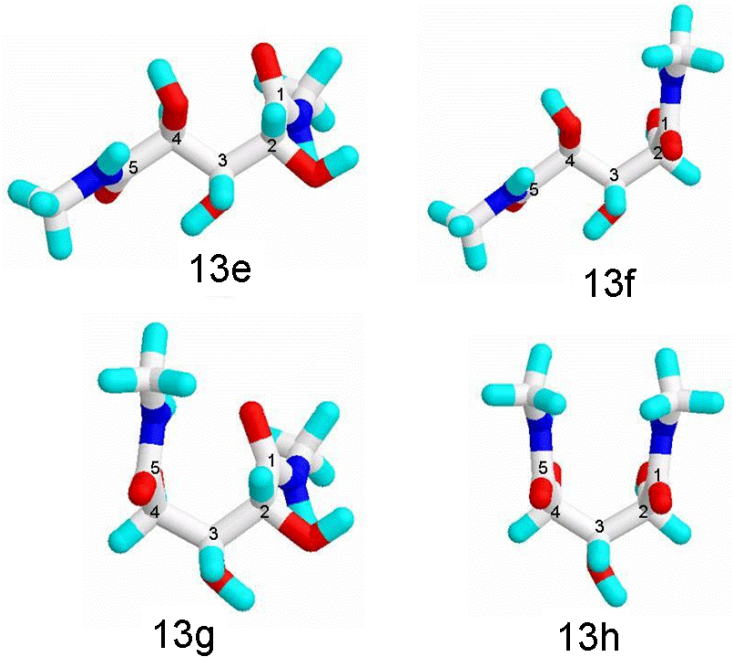

Figure 3.50 The four lowest energy conformations **13e** (2G-), **13f** (2G+), **13g** (2G-3G-), and **13h** (2G+3G-) at DIELEC 6.0

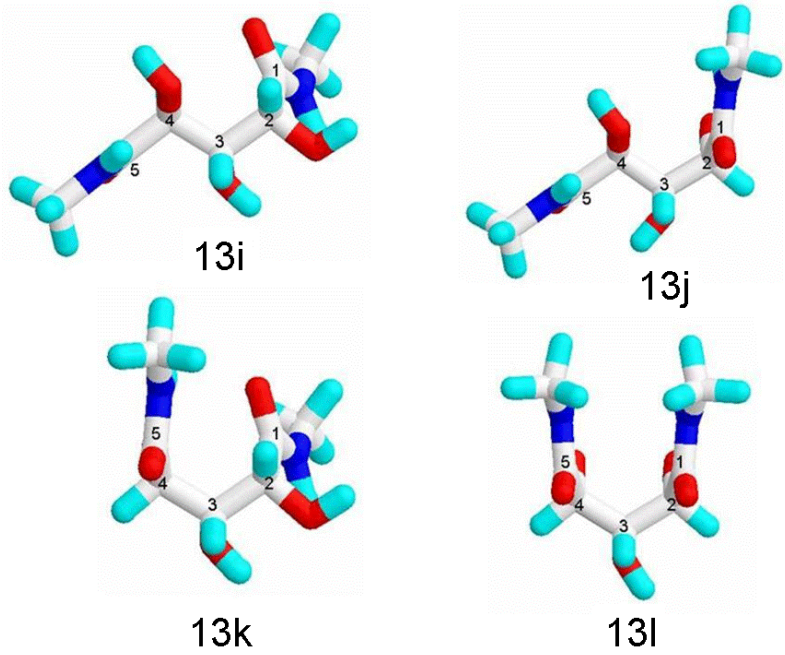

Figure 3.51 The four lowest energy conformations **13i** (2G-), **13j** (2G+), **13k** (2G-3G-), and **13l** (2G+3G-) and hydrogen bond length in angstroms at DIELEC 10.0

Table 3.15 Calculated percent population for **13** at DIELEC 3.5, 6.0, and10.0

DIELEC	**2G-**	**2G+**	**2G-,3G-**	**2G+,3G-**	**PPA**
3.5	8.301(**13a**)	10.46(**13b**)	70.10(**13c**)	11.14(**13d**)	91.33
6.0	23.83(**13e**)	9.407(**13f**)	58.20(**13g**)	6.977(**13h**)	81.53
10.0	25.35(**13i**)	6.106(**13j**)	54.56(**13k**)	13.99(**13l**)	76.97

N,N'-Dimethylribaramide (**13**) had the same conformational preferences as ribaramide (**12**) which overwhelmingly preferred the sickle 2G-3G- (ca. 60%) conformation and the sickle 2G- conformation (ca. 20%). As expected, the sickle 2G-3G- and sickle 2G- conformations do not have steric eclipsed 1,3-parallel hydroxyl interactions. This result is in agreement with the observation that **12** and **13** differ structurally in the same way as xylaramide (**3**) and *N,N'*-dimethylxylaramide (**4**), and L-arabinaramide (**8**) and *N,N'*-dimethyl-L-arabinaramide (**9**), in that **12** has primary amide

groups and **13** has secondary N-methyl amido groups, and all prefer the same conformations as their corresponding partner. **12** and **13** differ from **3** and **4** by inverted stereochemistry on C3 and similarly significantly populated the sickle 2G- conformation which alleviates steric interactions between the hydroxyl on C2 and hydroxyl on C3. Compounds **12** and **13** also populated the sickle 2G-3G- conformation which does not have obvious electrostatic or steric interactions. The C3 epimers, **3** and **4**, did not populate the sickle 2G-3G- conformation presumably due to an electrostatic interaction that is not readily observable.

Ribaric Acid (**14**)

Six rotamers of ribaric acid (**14**) were searched at dielectric constant 3.5 to a coefficient of variance of 1.16 with an average of 698.5 conformations found. The four lowest energy conformations **14a-14d** with an energy range of 1.893 kcal/mol are shown in Figure 3.53. The calculated percent populations for each conformation are given in Table 3.16. The number scheme for **14** is shown in Figure 3.52.

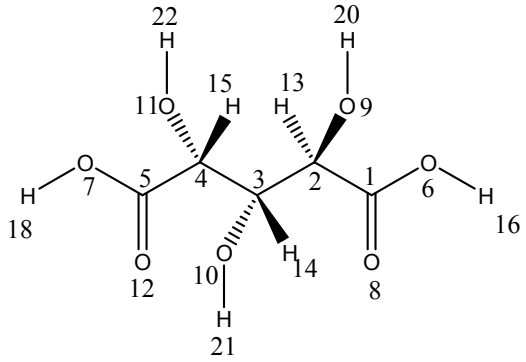

Figure 3.52 Numbering scheme for ribaric acid (**14**)

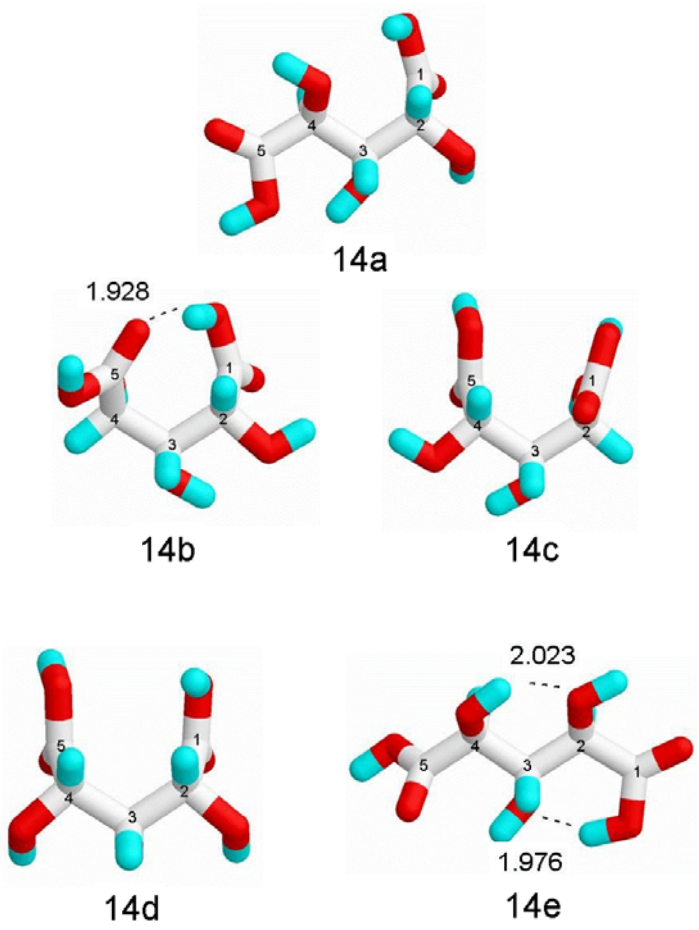

Figure 3.53 The five lowest energy conformations **14a** (2G-), **14b** (2G-3G-), **14c** (2G+3G+), **14d** (2G-,3G+) and **14e** (extended) and hydrogen bond length in angstroms at DIELEC 3.5

Table 3.16 Calculated percent population and percent population analyzed (PPA) for **14** at DIELEC 3.5

DIELEC	**2G-**	**2G-3G-**	**2G+3G+**	**2G-3G+**	**Extended**	**PPA**
3.5	37.19(**14a**)	45.41(**14b**)	8.536(**14c**)	8.212(**14d**)	0.643(**14e**)	81.00

Ribaric acid (**14**) prefers the sickle 2G-3G- and sickle 2G- conformations like that of *N,N'*-dimethylribaramide (**13**). The sickle 2G-3G- conformation has an intramolecular hydrogen bond of 1.928 angstroms which further stabilizes a conformation devoid of

obvious steric interactions. The sickle 2G- conformation also does not have obvious steric or electrostatic interactions and is significantly populated (ca. 37%). These results indicate that both electrostatic interactions (sickle 2G-3G-) and steric interactions (sickle 2G-) are influencing the conformational preference of **14** at dielectric constant 3.5.

2,3,4-Tri-*O*-acetyl-*N,N'*-dimethylribaramide (**15**)

Six rotamers of 2,3,4-tri-*O*-acetyl-*N,N'*-dimethylribaramide (**15**) were searched to a coefficient of variance of 3.91 and 2.09 with an average of 2817 and 2886 conformations found, respectively. Figures 3.55 and 3.56 depict the lowest energy conformations from various backbone families for **15** at dielectric constants 1.5 and 3.5. The energy range of the lowest energy conformer from the least populated family relative to the lowest energy conformer was 3.030 and 1.346 kcal/mol, respectively. The calculated percent populations are shown in Table 3.17. The number scheme for **15** is shown in Figure 3.54.

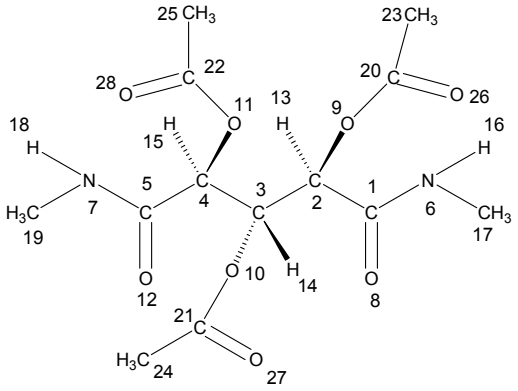

Figure 3.54 Numbering scheme for 2,3,4-tri-*O*-acetyl-*N,N'*-dimethylribaramide (**15**)

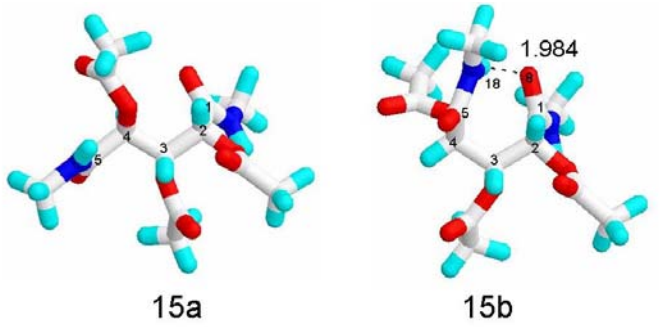

Figure 3.55 The two lowest energy conformations **15a** (2G-) and **15b** (2G-3G-) and hydrogen bond length in angstroms at DIELEC 1.5

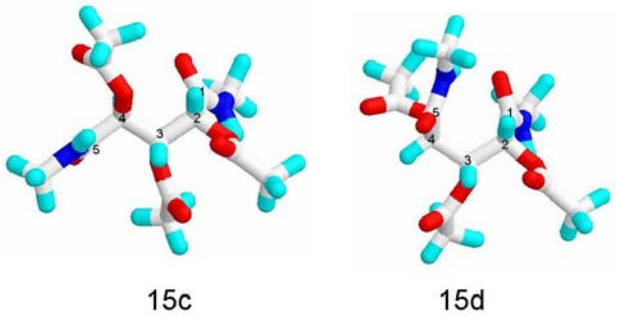

Figure 3.56 The two lowest energy conformations **15c** (2G-) and **15d** (2G-3G-) at DIELEC 3.5

Table 3.17 Calculated percent population for **15** at DIELEC 1.5 and 3.5

DIELEC	**2G-**	**2G-3G-**	**PPA**
1.5	0.261(**15a**)	99.74(**15b**)	98.10
3.5	3.143(**15c**)	96.86(**15d**)	90.86

2,3,4-Tri-*O*-acetyl-*N,N'*-dimethylribaramide **15** is a C3 epimer of 2,3,4-tri-*O*-acetyl-*N,N'*-dimethylxylaramide (**7**) and the acetylated derivative *N,N'*-dimethylribaramide (**13**). Compounds **15** and **7** each overwhelmingly prefer the sickle 2G-3G- conformation (>90%) with **15** having a stabilizing intramolecular hydrogen bond between amide hydrogen H18 and carbonyl oxygen O8 of 1.984 angstroms at dielectric

constant 1.5. The hydrogen bond present at dielectric constant 1.5 is not obvious at dielectric constant 3.5. This result is in agreement with the prior observations that with increasing dielectric constant, the influence of electrostatic interactions decreases. *O*-Acetylated compounds **7**, **11**, and **15** preferred to a greater extent the conformations that were preferred by the unprotected derivative. This demonstrates that the while the unprotected hydroxyl groups did stabilize some conformations through electrostatic interactions, steric interactions were the main driving force determining the lowest energy conformations.

3.2.5 Comparison of ^{1}H NMR and MM3(96) Proton Vicinal Coupling Constant Values

In prior MM3 and MM3(96) studies, the values of ^{1}H NMR vicinal coupling constants were used to support the validity of the computational model. Although rarely was the calculated ^{1}H NMR vicinal coupling constant value within 1 *Hz* of the experimentally derived ^{1}H NMR vicinal coupling constant value, calculated results could be used to predict the preference for a sickle or extended conformation based upon the magnitude of the calculated coupling constant. These studies used 5-45 conformers within 1 kcal/mol of the lowest energy conformer to calculate the average vicinal coupling constant. In this report the entire conformational ensemble consisting of hundreds to thousands of individual conformers were included in the calculation of the average ^{1}H NMR vicinal coupling constants. Moreover, computationally calculated ^{1}H NMR vicinal coupling constants were calculated over a range of dielectric constants enabling the observation of coupling constant trends with varying dielectric constant. This is important due to the fact that no single dielectric constant simulates a particular

solvent. So while absolute values of vicinal coupling constants are of value for predicting the conformational preference of a molecule, comparison of the ^{1}H NMR vicinal coupling constants at different dielectric constants can give important information as to the validity of the computational model and selection of the dielectric constant value that best models a particular molecule in polar or non-polar solvents.

Computationally calculated and ^{1}H NMR vicinal coupling constants are given in Table 3.19. Xylaramide (**3**) the only compound with experimental ^{1}H NMR coupling constant values not modeled at various dielectric constants had $J_{13\text{-}14}$ and $J_{14\text{-}15}$ value of 4.53 and 4.53 and nearly identical experimental ^{1}H NMR $J_{13\text{-}14}$ and $J_{14\text{-}15}$ value of 4.40 and 4.40. Compounds **3**, **4**, **7**, **9**, **11**, **13**, and **15** had ^{1}H NMR vicinal coupling constants and vicinal coupling constants calculated over a range of dielectric constants, 1.5-10.0. The $J_{13\text{-}14}$ and $J_{14\text{-}15}$ coupling constant values for compounds **3**, **7**, **11**, and **13** had trends towards agreement with experimental ^{1}H NMR vicinal coupling constant values indicating that the computational model with varying dielectric constant was becoming more accurate at modeling the molecule in the particular NMR solvent. Compounds **4** and **15** did not have $J_{13\text{-}14}$ and $J_{14\text{-}15}$ values trending towards the ^{1}H NMR $J_{13\text{-}14}$ and $J_{14\text{-}15}$ values. However the calculated $J_{13\text{-}14}$ and $J_{14\text{-}15}$ (4.27) values were within 1 *Hz* of the ^{1}H NMR coupling constants (3.66). *N,N'*-Dimethyl-L-arabinaramide (**9**) had a $J_{13\text{-}14}$ value trending away and a $J_{14\text{-}15}$ value trending towards the ^{1}H NMR $J_{13\text{-}14}$ and $J_{14\text{-}15}$ values indicating the ability of MM3(96) to accurately model the (R) stereochemistry of the C(1) end of *N,N'*-dimethyl-L-arabinaramide and not the (R) stereochemistry of the C(5) end. Overall the computationally derived vicinal coupling constants generally agreed with the experimental ^{1}H NMR vicinal coupling constants.

The prior work in this study demonstrated the computationally calculated vicinal coupling constants are dependent on dielectric constant. In an effort to understand the dependence of ^{1}H NMR vicinal coupling constant values on solvent dielectric constant, ^{1}H NMR spectra were recorded of 2,3,4-tri-*O*-acetyl-*N,N'*-dimethyl-L-arabinaramide (**11**) in chloroform-*d*, DMSO- d_6,and D_2O. Somewhat surprisely, the vicinal coupling constants of $J_{13\text{-}14}$ and $J_{14\text{-}15}$ had changed from 8.79, 2.20, respectively, in D_2O to 4.40, 7.33, respectively, in chloroform-*d*. Subsequently the chloroform-*d* sample was serially diluted with DMSO-d_6 and a gradual change in vicinal coupling constant observed. This indicates that the conformational preferences of acyclic carbohydrate derivatives are highly dependent on solvent composition and solvent chemical properties. The ^{1}H NMR experimental vicinal coupling constant data is reported in Table 3.18.

MM3(96) computational analysis of **11** agrees with the observed change in conformational preference with changing dielectric constant. Calculated average vicinal coupling constant values at dielectric constant 3.5 for $J_{13\text{-}14}$ and $J_{14\text{-}15}$, 2.38 and 4.75, respectively, agree best with the experimental results in an NMR solvent mixture of 17.6% DMSO-d_6 and 82.4% chloroform-*d*; $J_{13\text{-}14}$ *and* $J_{14\text{-}15}$, 6.59 and 4.40, respectively.

Table 3.18 Changing ^{1}H NMR vicinal proton coupling constant of 2,3,4-tri-*O*-acetyl-*N,N'*-dimethyl-L-arabinaramide (**11**) with changing solvent composition

Solvent (DMSO-d_6 / $CDCl_3$)	**Observed $J_{13\text{-}14\ ,\ 14\text{-}15}$ (*Hz*)**
100%	7.83, 2.74
50 / 50	7.33, 3.66
37.5 / 62.5	7.33, 3.66
27.3 / 72.7	7.33, 4.40
17.6 / 82.4	6.59, 4.40
100%	4.40, 7.33
100% D_2O	8.79, 2.20

Table 3.19 MM3(96) Calculated vicinal proton coupling constants (*Hz*) for the total population of molecules (**3**)-(**15**) at dielectric constants 1.5, 3.5, 6.0, and 10.0. NMR Solvent - (a) D_2O (b) $CDCl_3$

	DIELEC = 1.5	**DIELEC = 3.5**	**DIELEC = 6.0**	**DIELEC = 10.0**	**Experimental NMR**
Compound	$J_{13\text{-}14,\ 14\text{-}15}$	$J_{13\text{-}14,\ 14\text{-}15}$	$J_{13\text{-}14,\ 14\text{-}15}$	$J_{13\text{-}14,\ 14\text{-}15}$	$J_{13\text{-}14,\ 14\text{-}15}$
(**3**)[a]	-	5.33, 5.33	4.46, 4.46	4.43, 4.43	3.66, 3.66
(**4**)[a]	-	4.27, 4.27	4.42, 4.42	4.56, 4.56	3.66, 3.66
(**5**)[a]	-	4.53, 5.29	-	-	4.40, 4.40
(**6**)	-	4.72, 4.72	-	-	-
(**7**)[b]	5.85, 5.63	4.02, 3.98	-	-	5.13, 5.13
(**8**)	-	3.56, 4.12	3.05, 4.10	2.87, 4.60	-
(**9**)[a]	-	3.34, 4.09	2.83, 4.38	2.82, 4.93	7.33, 7.33
(**10**)	-	-	4.70**,** 5.08	-	-
(**11**)[b]	1.76, 4.65	2.38, 4.75	-	-	4.40, 7.33
(**12**)	-	3.76, 3.72	3.99, 4.09	3.65, 3.65	-
(**13**)[a]	-	3.16, 3.04	3.67, 3.50	3.65, 3.77	5.13, 5.13
(**14**)	-	4.52, 4.80	-	-	-
(**15**)[b]	2.81, 2.81	2.63, 2.73	-	-	5.84, 5.84

Summary

A Monte Carlo MM3(96) analysis of glutaramides (**1** and **2**), pentaramides (**3**, **4**, **7**, **8**, **9**, **11**, **12**, **13**, and **15**), diacids (**5**, **10**, and **14**), and the dimethyl ester of xylaric acid (**6**) was carried out at multiple dielectric constants. Computationally calculated proton vicinal coupling constants were compared to experimental ^{1}H NMR proton vicinal coupling constants which generally agreed with the ^{1}H NMR proton vicinal coupling constant experimental results and were more accurate than results previously reported for similar compounds. Additionally, it has been demonstrated that the conformational preference of the relatively flexible acyclic carbohydrate derivative is dependent not only on the dielectric constant in computational simulations but the ^{1}H NMR solvent composition as well. Therefore it has been demonstrated that any investigator modeling relatively flexible molecules should take special care to consider solvation effects.

Computational results for glutaramide (**1**) and *N*,*N*'-dimethylglutaramide (**2**) preferred sickle conformations agreed with previously reported quantum mechanical calculated results by Alman and Novarro.[5-6] For both **1** and **2** at dielectric constants 3.5, 6.0, and 10.0 the sickle 3G- conformation was lower in energy than the extended or *anti* conformation. Unlike earlier reports, this study investigated the change in preferred conformation with increasing dielectric constant and found that at higher dielectric constants the extended conformation became increasingly populated. This suggests that at sufficiently high dielectric constants the influence of the parallel dipole-dipole interaction would no longer be significant and an extended or *anti* conformation would be preferred.

The preferred conformations of compounds **3-15** vary depending upon stereochemistry and the strength of electrostatic and steric interactions at the simulated

dielectric constant. The unprotected molecules preferred conformations without destabilizing, eclipsing 1,3-parallel hydroxyl interactions. These conformations were then further stabilized by intramolecular hydrogen bonding between the unprotected hydroxyl groups. The lowest energy conformations of *O*-acetylated compounds **7**, **11**, and **15** at dielectric constant 1.5 had intramolecular hydrogen bonding between an amide hydrogen and carbonyl oxygen. However, upon increasing the dielectric constant to 3.5 the preferred conformations were less influenced by electrostatic interactions and more influenced by steric interactions. This was evidenced by the lack of obvious intramolecular hydrogen bonding in simulations at dielectric constant 3.5 and the greater preference for conformations without obvious steric interactions.

Steric interactions were the main driving force behind the conformational preference of all the molecules studied. The primary steric interaction driving the conformational preference of unprotected and protected diamides, diacids, and the dimethyl ester of xylaric acid in this study was the alleviation of eclipsed 1,3-parallel hydroxyl/acetoxyl interactions.

3.3 Experimental

3.3.1 General Methods

One dimensional ^{1}H NMR spectra were obtained using a 400 MHz Varian Unity Plus spectrometer. Selective pulse experiments, 1D seltocsy and 1D selnosey, were performed on a 500 MHz Varian spectrometer. NMR spectra were processed using ACD/SpecManager 1D NMR software Version 9.13. Chemical Shifts were expressed in parts per million relative to tertiary-butyl alcohol (1.203 ppm) for D_2O and tetramethylsilane (0.00 ppm) for DMSO-d_6 and chloroform-*d*. All NMR solvents were

obtained from Cambridge Isotope Laboratories, Inc. All chemicals were purchased from Aldrich and used without further purification. Melting points were obtained with a Fisher-Johns melting point apparatus and are reported uncorrected. Elemental analyses were performed by Atlantic MicroLab Inc. Norcross, GA.

3.3.2 Computational Experimental

Alchemy 2000 was used to generate the coordinate files of the six rotamers of each molecule for input into MM3(96). The Alchemy 2000 default values were used except in the simulation of xylaric acid. An energy change optimization termination value of 0.00008*n was used for the computational analysis of xylaric acid. MM3(96) energy optimizations were performed using the block diagonal full matrix optimization option. Computations for *O*-acetylated molecules were performed at dielectric constant values of 1.5 and 3.5. Computations of unprotected aldaramides, acids, and ester were performed at dielectric constant values of 3.5, 6.0, and 10.0. Computations of compounds **1** and **2** were carried out at dielectric constant value of 1.5, 3.5, 6.0, and 10.0.

Force constants for the atom type sequence associated with an ester group adjacent to an amide (9-3-1-75) were input in the constant file of MM3(96) as V1= -2.157, V2= -0.592 and V3= 0.466. The atom type sequence of an acetylated hydroxyl group adjacent to a carbonyl group (3-1-75-3) was input into the constant file as V1=0.7246, V2=-0.6033 and V3=0.2583. In carrying out simulations of acetylated molecules **7**, **11**, and **15**, 10 torsion angles were varied; four associated with the aldaryl backbone corresponding to atom numbers 6-1-2-3, 1-2-3-4, 2-3-4-5, and 3-4-5-7, and six corresponding to the ester groups; 13-2-9-20, 2-9-20-23, 14-3-10-21, 3-10-21-24, 15-4-11-22, and 4-11-22-25. The unprotected aldaramides, acids, and ester had 7 torsion

angles varied; four associated with the carbohydrate backbone (6-1-2-3, 1-2-3-4, 2-3-4-5, and 3-4-5-7) and three associated with the hydroxyl groups (13-2-9-20, 14-3-10-21, and15-4-11-22. The glutaramide compounds **1** and **2** had six torsion angles varied about the heavy atoms corresponding to atoms 17-6-1-2, 6-1-2-3, 1-2-3-4, 2-3-4-5, 3-4-5-7, 4-5-7-19. Temperature shaking was performed after the number of search steps had reached 20 times the number of torsion angles varied and at a temperature of 10000 K. The number of steps within the temperature shaking routine equaled two times the number of torsion angles varied.

The Monte Carlo program is written as a UNIX script that coordinates multiple subroutines with MM3(96). In general a coordinate file is input into the simulation. The program then chooses a random torsion angle from a user defined list of torsion angles to be varied. The torsion angle is varied between ± 60-300º and the resulting conformation is input into MM3(96) for energy minimization. After energy minimization the output conformation is analyzed to determine if the structure is a true local minima or a transition state by looking for imaginary vibrational frequencies. The output conformation is also compared to all other previously found conformers and deemed to be a new conformer if any one torsion angle differs from all other previously found conformers by more than 2.5º. If the conformation is new and a true local minima the information associated with that conformer is stored. This process is defined as a step. This new conformer is then used as the coordinate file to be input back into the simulation and is treated in exactly the same manner as before. After a user defined number of steps has occurred the simulation undergoes a temperature shaking process after the energy minimization step. The temperature shaking process enables the program

to vary more than one torsion angle and then the new conformer is input back into the simulation. The number of steps in the temperature shaking process is user defined and corresponds to the number of times a torsion angle is randomly selected and varied. Any unrealistic conformations that may be produced during this process fail to optimize in MM3(96) and are discarded. The simulation then inputs the input coordinate file in that step and the process is repeated. The simulation terminates itself after a user defined number of steps has been reached.

The conformational ensemble generated by the Monte Carlo MM3(96) simulation was sorted in ascending order and the contribution of each conformer to the global population calculated according to a Boltzmann distribution. The vicinal coupling constants were calculated according to Haasnoot's adaptation of the Karplus equation.

3.3.3 Synthesis of Diamides 1, 2, 3, 4, 7, 10, 9, 11, 13, and 15

Glutaramide (**1**)

To a solution of glutaric acid (1.025 g, 7.761 mmol) in cold (ice bath) methanol (25 mL) was added thionyl chloride (1.024 g, 8.531 mmol) and the solution stirred at room temperature for 3 days. The solution was concentrated, the syrup residue was dissolved in cold (ice bath) methanol (10mL), and 7M methanolic ammonia (35 mL, 245 mmol) added dropwise, followed by stirring of the reaction mixture at room temperature for 6 days. A solid was isolated by filtration, rinsed with cold methanol (2 x 1 mL) and dried to yield glutaramide. (**1**, 0.370 g, 2.842 mmol, 36.6%): mp 179 ºC, lit mp 175.[20] ^{1}H NMR (DMSO-d_6) δ 7.25 (s, 2H), 6.75 (s, 4H), 2.04 (t, 2H, J 7.25 Hz), 1.71-1.64 (m, 2H). Crystals were obtained by dissolving glutaramide (**1**) in methanol and allowing the

methanol to slowly evaporate. Anal. Calcd for $C_5H_{10}N_2O_2$ (130.15): C, 46.14; H, 7.74; N, 21.52. Found C, 46.18; H, 7.77; N, 21.48.

***N,N'*-Dimethylglutaramide (2)**

To a solution of glutaric acid (6.010 g, 45.49 mmol) in cold (ice bath) methanol (30 mL) was added acetyl chloride (8.508 g, 109.0 mmol) and the reaction mixture was stirred 3 h. It was then concentrated to a tacky syrup, which was dissolved in cold (ice bath) 10.5M methylamine (80 mL, 850 mmol) in ethanol, and the solution stirred at room temperature for 3 days. The reaction mixture was concentrated under a stream of air to a volume of 10 mL. A solid was removed by filtration and the solid rinsed with cold methanol (2 x 1 mL) to yield *N,N'*-dimethylglutaramide (**2**, 1.606 g, 10.149 mmol, 22.31%): mp 121 ºC, lit. mp 103 ºC.[19] ^{1}H NMR ($CDCl_3$) δ 7.73 (s, 2H), 2.55-2.54 (d, 6H, *J* 4.43 Hz), 2.03 (t, 4H, *J* 8.84 Hz), 1.73-1.65 (m, 2H). Crystals were obtained by dissolving *N,N'*-dimethylglutaramide (**2**) in methanol and allowing the methanol to slowly evaporate. Anal. Calcd for $C_7H_{14}N_2O_2$ (158.20): C, 53.15; H, 8.92; N, 17.71. Found C, 53.15; H, 8.93; N, 17.62.

Xylaramide (3)

To a solution of xylaric acid (1.016 g, 5.639 mmol) in cold (ice bath) methanol (25 mL) was added thionyl chloride (0.7380 g, 6.203 mmol) and the solution was stirred at room temperature for 3 h. The reaction mixture was concentrated to tacky syrup, which was then dissolved in cold (ice bath) methanol (10 mL), and 7M ammonia (50 mL, 350 mmol) in methanol was added dropwise to the solution, the resulting reaction mixture was stirred at room temperature for 2 h, solid was removed by filtration and rinsed with cold methanol (2 x 2 mL) to yield xylaramide (**3**, 0.6725 g, 3.775 mmol,

67.0%), ^{1}H NMR (DMSO-d_6) δ 7.23 (s, 2H), 7.16 (s, 2H), 3.98-3.97 (d, 2H, *J* 3.97 Hz), 3.88 (t, 1H, *J* 5.29 Hz). ^{13}C NMR (D_2O): 178.30, 73.23, 73.00 ppm. Crystals were obtained by dissolving xylaramide (**3**) in water and allowing the water to slowly evaporate. mp 191 – 193 ºC. lit mp 180 ºC.[21] Anal. Calcd for $C_5H_{10}N_2O_5$ (178.14): C, 33.71; H, 5.66; N, 15.73. Found C, 33.47; H, 5.76; N, 15.33.

***N,N'*-Dimethylxylaramide** (**4**)

To a solution of xylaric acid (2.056 g, 11.41 mmol) in cold methanol (10 mL) was added acetyl-chloride (0.3394 g, 2.852 mmol) and the solution stirred for 3 h. The reaction mixture was concentrated to syrup which was dissolved in cold (ice bath) methanol (15 mL). Methylamine 10.5M (5.209 g, 0.1677 mmol) in ethanol was added dropwise to the reaction and stirred for 3 h. A solid was removed by filtration and rinsed with cold methanol (2 x 5 mL) to yield *N,N'*-dimethylxylaramide (**4**, 1.737 g, 8.425 mmol, 73.8%): mp 191 -194 ºC, lit mp not available. ^{1}H NMR (D_2O) δ 4.266-4.256 (d, 2H, *J* 3.66 Hz), 4.097-4.079 (t, 1H), 2.749 (s, 6H). ^{13}C NMR (D_2O): 175.55, 73.34, 26.58 ppm. Crystals were obtained by dissolving *N,N'*-dimethylxylaramide (**4**) in water and allowing the water to slowly evaporate. Anal. Calcd for $C_7H_{14}N_2O_5$ (206.2): C, 40.77; H, 6.84; N, 13.59. Found C, 40.69; H, 6.84; N, 13.40.

2,3,4-Tri-*O*-acetyl-*N,N'*-dimethylxylaramide (**7**)

To a solution of *N,N'*-dimethylxylaramide (0.2442 g, 1.1849 mmol) in pyridine (4 mL) was added acetic anhydride (5.0 mL, 52.93 mmol) and the solution warmed to 50 °C for 3 h. To the reaction mixture was added cold (ice bath) water (7 mL) with stirring. The mixture was extracted with chloroform (3 x 4 mL) and the organic fractions combined. The organic fractions were concentrated under a stream of nitrogen and dried

overnight to yield crystalline 2,3,4-tri-*O*-acetyl-*N,N'*-dimethylxylaramide (**7**, 0.2731 g, 0.5779 mmol, 85.3%): mp 171 ºC, lit. MP not available ^{1}H NMR ($CDCl_3$) δ 6.26 (s, 2H), 5.70 (t, 1H, *J* 5.11 Hz), 5.40-5.38 (d, 2H, *J* 5.53 Hz), 2.81 (s, 3H), 2.80 (s, 3H), 2.16 (s, 6H), 2.05 (s, 3H). ^{13}C NMR ($CDCl_3$): 169.44, 166.85, 71.86, 70.43, 26.15, 20.65, 20.43 ppm. Crystals were obtained by dissolving 2,3,4-tri-*O*-acetyl-*N,N'*-dimethylxylaramide (**7**) in water and allowing acetone to diffuse into the water.Anal. Calcd for $C_{10}H_{14}N_2O_{11}$ (332.31): C, 46.99; H, 6.07; N, 8.43. Found C, 46.93; H, 6.12; N, 8.33.

L-Arabinaramide (**8**)

To a mixture of disodium L-arabinarate (2.9858 g, 13.325 mmol) in cold (ice bath) methanol (10 mL) was added acetyl chloride (4.8129 g, 67.96 mmol) dropwise and the reaction mixture stirred for 3 h. A white solid precipitated and was removed by centrifugation. The filtrate was concentrated, the syrupy product dissolved in cold (ice bath) methanol (10 mL), and 7M ammonia (10 ml, 69.29 mmol) in methanol was added dropwise. The reaction mixture was stirred 4 h and a white solid was removed by filtration, the solid was rinsed with cold methanol (2 x 1 mL), and dried overnight to yield L-arabinaramide (**8,** 0.9134 g, 5.1273 mmol, 64.10%): mp 196.5–200.5 ºC, lit. mp 188 ºC.[22] ^{1}H NMR (D_2O) δ 4.47 (d, 1H, *J* 1.06 Hz), 4.31 (d, 1H, *J* 7.60 Hz), 4.17-4.14 (dd, 1H).

***N,N'*-Dimethyl L-Arabinaramide** (**9**)

To a mixture of disodium L-arabinarate (4.198 g, 18.73 mmol) in methanol (10 mL) was added acetyl chloride (5.425 ml, 5.995 g, 76.81 mmol) dropwise and the reaction mixture was stirred for 3 h. A white solid was removed by centrifugation, the filtrate was concentrated, the syrupy residue dissolved in cold (ice bath) methanol (10

mL), and methylamine (10.5 M,15 mL, 127.5 mmol) in ethanol was dropwise. The reaction mixture was stirred 16 h, the solution was concentrated, the resulting solid dried, and stirred with methanol (5 mL) for 1 h. The solid was removed by filtration and rinsed with cold methanol (2 x 1 mL) to yield *N,N'* dimethyl L-arabinaramide (**9,** 1.4456 g, 6.953 mmol, 37.1%): mp 194 – 196 ºC, Lit. MP not available. ^{1}H NMR (D_2O) δ 4.316 (s, 1H), 4.172-4.154 (d, 1H, *J* 7.33 Hz), 4.044-4.026 (d, 1H, *J* 7.33 Hz), 2.749 (s, 6H). Crystals were obtained by dissolving *N,N'*-dimethyl- L-arabinaramide (**9**) in warm water and allowing the water allowed to slowly evaporate.

2,3,4-Tri-*O*-acetyl-*N,N'*-dimethyl L-arabinaramide (**11**)

To a mixture of *N,N'*-dimethyl L-arabinaramide (0.3510 g, 1.6875 mmol) in pyridine (4 mL) was added acetic anhydride (5.0 mL, 52.93 mmol) dropwise and the solution warmed to 50 °C for 3 h. Cold (ice bath) water (7 mL) was added dropwise and the solution was concentrated under a stream of nitrogen and then dried under vacuum overnight. The resulting solid was stirred with water (1.5 mL) for 30 min, isolated by filtration, and dried to yield 2,3,4-tri-*O*-acetyl-*N,N'*-dimethyl-L-arabinaramide (**11,** 0.3516 g, 1.058 mmol, 62.74%): mp 209 – 210 ºC, Lit. MP not available ^{1}H NMR ($CDCl_3$) δ 6.74 (s, 1H), 6.46 (s, 1H), 5.67-5.64 (d, 1H), 5.48-5.46 (d, *J* 7.99 Hz, 1H), 5.35-5.34 (d, 1H, *J* 4.79 Hz), 2.85-2.83 (q, 6H), 2.21 (s, 3H), 2.12 (s, 3H), 2.06 (s, 3H). ^{13}C NMR ($CDCl_3$): 169.48, 169.27, 168.65, 166.91, 166.81, 71.71, 70.57, 70.50, 26.18, 26.09, 20.62, 20.56 ppm. Crystals were obtained by dissolving 2,3,4- tri-*O*-acetyl-*N,N'*-dimethyl- L-arabinaramide (**11**) in warm methanol and allowing the diffusion of acetone into the methanol. Anal. Calcd for $C_{13}H_{20}N_2O_8$ (332.31): C, 46.99; H, 6.07; N, 8.43. Found C, 47.03; H, 6.07; N, 8.41.

***N,N'*-Dimethylribaramide (13)**

To a solution of disodium ribarate (4.839 g, 21.60 mmol) in cold (ice bath) methanol (30 mL) acetyl chloride (4.61 mL, 5.086 g, 64.79 mmol) was added dropwise and the reaction mixture was stirred for 3 h. A white solid was removed by filtration, the filtrate was concentrated, the syrupy residue dissolved in cold (ice bath) methanol (10 mL), and methylamine (10.5 M, 11.01 mL, 86.39 mmol) in ethanol was added dropwise. The reaction mixture stirred at room temperature overnight, a white solid was removed by filtration, dried overnight, stirred with methanol (5 mL), separated by filtration, rinsed with methanol (2 x 1 mL), and dried to yield *N,N'*-dimethylribaramide (**13,** 1.580 g, 7.665 mmol, 35.5%): mp 165-168 ºC, lit. mp not available ^{1}H NMR (D_2O) δ 4.233 (d, 1H, *J* 5.13 Hz), 4.112 (t, 2H, *J* 5.13 Hz), 2.73 (s, 6H). ^{13}C NMR (D_2O): 175.48, 74.37, 73.04, 26.55 ppm. Crystals were obtained by dissolving *N,N'*-dimethylribaramide (**13**) in water and allowing the water to evaporate. Anal. Calcd for $C_7H_{14}N_2O_5$ (206.2): C, 40.77; H, 6.84; N, 13.59. Found C, 40.86; H, 6.83; N, 13.58.

2,3,4-Tri-*O*-acetyl-*N,N'*-dimethylribaramide (15)

To a mixture of *N,N'*-dimethylribaramide (1.249 g, 6.2319 mmol) in pyridine (5 mL) was added acetic anhydride (11.78 mL, 124.64 mmol) dropwise and the solution was stirred overnight. Cold (ice bath) water (15 mL) was added dropwise and the mixture stirred for 30 min. The solvent was removed under a stream of nitrogen, the residue dissolved in water (3 mL), and the aqueous solution extracted with chloroform (3 x 10 mL). The organic fractions were combined, concentrated under a stream of nitrogen and dried overnight to yield 2,3,4-tri-*O*-acetyl-*N,N'*-dimethylribaramide (**15,** 2.048 g, 6.163 mmol, 79.89%): mp 166.25-169.25 ºC, lit. mp not available. ^{1}H NMR ($CDCl_3$) δ

6.33 (s, 2H), 5.66 (t, 1H, *J* 5.86 Hz), 5.45 (d, 2H, *J* 5.86 Hz), 2.81 (s, 3H), 2.80 (s, 3H), 2.13 (s, 6H), 2.03 (s, 3H). ^{13}C NMR ($CDCl_3$): 169.23, 166.73, 71.18, 70.65, 26.11, 20.68 ppm. Anal. Calcd for $C_{10}H_{14}N_2O_{11}$ (332.31): C, 46.99; H, 6.07; N, 8.43. Found C, 47.17; H, 5.97; N, 8.54.

References

1. Durig, J. R.; Compton, D.A.C. Analysis of torsional spectra of molecules with two internal C3v rotors. 12. Low frequency vibrational spectra, methyl torsional potential function, and internal rotation of n-butane. Journal of Physical Chemistry, **1979**, 83(2), 265-8

2. Wiberg, Kenneth. B.; Murko, Mark. A. Rotational barriers. 2. Energies of alkane rotamers. An examination of gauche interactions. Journal of the American Chemical Society, **1988**, 110(24), 8029-38

3. Maissara, M.; Cornut, J. C.; Devaure, J.; Lascombe, J**.** Conformational equilibrium of pentane as a function of temperature and pressure. Spectroscopy (Amsterdam, Netherlands), **1983**, 2(2), 104-19

4. Kanesaka, Isao; Snyder, Robert G.; Strauss, Herbert L. Experimental determination of the trans-gauche energy difference of gaseous n-pentane and diethyl ether**,** Journal of Chemical Physics, **1986**, 84(1), 395-7

5. Alman, C., Puiggali, J.; A quantum mechanical study of the folding of methylene units in compounds with several glutaramide units: nylon 1,5. Macromol. Theory Simul.; **1998**, 7, 367-372

6. Navarro, Eloisa; Aleman, Carlos; Puiggali, Jordi. Folding of Methylene Groups in Linear Glutaramide Analogs. Journal of the American Chemical Society, **1995**, 117(28), 7307-10.11 and references therein

7. Wendoloski, J. J.; Garndner, K. H.; Hirschinger, J.; Miura, H.; English, A. D. Molecular dynamics in ordered structure: computer simulation and experimental results for nylon 66 crystals. Science, **1990**, 247(4941), 431-6

8. Aleman, Carlos; Navarro, Eloisa; Puiggali, Jordi.; Conformational Analysis of Succinamide Analogues. Journal of Organic Chemistry, **1995**, 60, 6135-6140

9. Horton, D.; Wander, J. D.; Conformation of acyclic derivatives of sugars. Conformations of peracetylated aldose dithioacetals in solution; Carbohydrate Research,**1969**, 10, 179-288

10. Eliel, E.L.; Wilen, S.H.; Configuration and Conformation of Cyclic Molecules. Stereochemistry of Organic Compounds; Wiley: New York, **1994**; 707

11. Sweeting, L.; Coxon, B.; Varma, R.; Conformational analysis of per-acetylated hexononitriles. Carbohydrate Research, **1979**, 72, 43-55.

12. Angyal, S.; LeFur, R.; Gagnaire, D.; Conformations of acyclic sugar derivatives part II: determination of the conformations of alditol acetates in solution by the use of 250-MHZ NMR spectra. Carbohydrate Research, **1972**, 23, 121-134.

13. Chen, L.; Haraden, B.; Kane, R.W.; Kiely, D. E.; Rowland, R. S.; Molecular Modeling of Acyclic Carbohydrate Derivatives *N,N'*-dimethyl- and *N,N'*-Dihexyl xylaramide: Model Compounds for Synthetic Poly (hexamethylene xylaramide). Journal of the American Chemical Society, **1990**, 8, 141-151

14. Zhang, Jinsong; Kiely, Donald E.; Application of a model building approach to molecular mechanics (MM3) for calculating low-energy conformations of tetra-*O*-acyl-N,N'-dialkyl-*D*-glucaramides. Journal of Carbohydrate Chemistry, **2006**, 25(8-9), 697-711

15. Zhang, Jinsong; Kiely, Donald E.; Hardcastle, Kenneth I. MM3 conformational analysis and X-ray crystal structure of 2,3,4,5-tetra-*O*-acetyl-N,N'-dimethyl-D-glucaramide as a conformational model for the D-glucaryl unit of poly(alkylene 2,3,4,5-

tetra-*O*-acetyl-D-glucaramides). Journal of Carbohydrate Chemistry, **2006**, 25(8-9), 633-659

16. Styron, Susan D.; French, Alfred D.; Friedrich, Joyce D.; Lake, Charles H.; Kiely, Donald E.; MM3(96) conformational analysis of D-glucaramide and x-ray crystal structures of three D-glucaric acid derivatives-models for synthetic poly(alkylene D-glucaramides). Journal of Carbohydrate Chemistry, **2002**, 21(1 & 2), 27-51

17. Michael K. Dowd Reference

18. Haasnoot, C. A. G.; DE Leeuw, F. A. A. M.; Altona, C.; The relationship between proton-proton NMR coupling constants and substituet electronegativites-1: An empirical generalization of the Karplus equation. Tetrahedron, **1979**, 36, 2782-2792

19. Kaupp, G.; Schmeyers, J.; Boy, J.; Quantitative solid-state reactions of amines and carbonyl compounds and isothiocyanates. Tetrahedron, **2000**, 56, 6899-6911

20. Paden, Joseph H.; Adkins, Homer.; Synthesis of pyrrolidines, piperidines and hexahydroazepines. Journal of the American Chemical Society, **1936**, 58, 2487-99

21. Kiely, Donald E.; Gray, Kathy; Riordan, James M.; Six-Membered Nitrogen Heterocycles from Xylaramide and Ribaramide. Journal of Carbohydrate Chemistry, **1982**, 1(2), 191-211

22. Gall, Ruth E., Tarasoff, L.; Molecular Asymmetry in Sugar Derivatives. Australian Journal of Chemistry, **1975**, 28, 687-91

4. X-Ray Crystal Analysis of *N,N'*-dihexylglutaramide, *N,N'*-dimethylglutaramide, *N,N'*-dimethylxylaramide, 2,3,4-tri-*O*-acetyl-*N,N'*-dimethylxylaramide, *N,N'*-dimethyl-L-arabinaramide, 2,3,4-tri-*O*-acetyl-*N,N'*-dimethyl-L-arabinaramide, and *N,N'*-dimethylribaramide monohydrate

4.1 Introduction

X-ray crystal analysis is an analytical technique that allows for the direct observation of atoms within a molecule. Bond lengths and angles, crystal packing, chemical structure, and absolute configuration are all provided through x-ray crystallography analysis. There are two types of x-ray crystallography, single crystal and powder. Single crystal x-ray crystallography requires a crystal of good size and quality. Obtaining quality single crystals can be quite easy for some compounds and nearly impossible for others. All x-ray data presented here were obtained from single crystals. In an effort to further support the validity of the computational results presented in Chapter 3 and to gain a better understanding of the forces driving the conformational preferences of the aldaryl monomer unit in polyhydroxypolyamides (PHPAs), x-ray crystals of acyclic molecules **1-7** were obtained, analyzed, and compared for structural detail. Those compounds are: *N,N'*-dihexylglutaramide (**1**), *N,N'*-dimethylglutaramide (**2**), *N,N'*-dimethylxylaramide (**3**) 2,3,4-tri-*O*-acetyl-*N,N'*-dimethylxylaramide (**4**), *N,N'*-dimethyl-L-arabinaramide (**5**), 2,3,4-tri-*O*-acetyl-*N,N'*-dimethyl-L-arabinaramide (**6**), and *N,N'*-dimethylribaramide monohydrate (**7**), Figure 4.1. Glutaramides **1** and **2** were chosen because parallel amide dipoles have been shown to influence the conformational preference of small molecule diamides. Additionally, it was of interest to determine how

different terminal N- groups, hexyl and methyl, respectively, influenced the conformational preference of these molecules. Diamides **3**, **5**, and **7** are unprotected acyclic aldaramides that represent all possible stereochemical arrangements in hydroxylated pentaramides. Pentaramides **4** and **6** are the acetylated derivatives of **3** and **5**, respectively, and are of interest because the acetate groups prevent intramolecular hydrogen bonding between hydroxyl groups thereby allowing steric interactions to dominate the conformation preference.

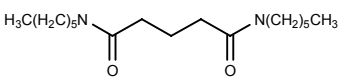

N,*N*′-dihexylglutaramide **(1)**

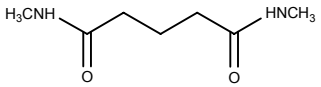

N,*N*′-dimethylglutaramide **(2)**

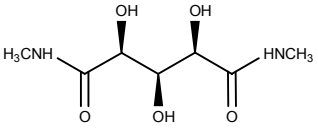

N,*N*′-dimethylxylaramide **(3)**

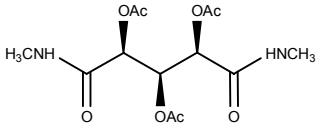

2,3,4-tri-*O*-acetyl-*N*,*N*′-dimethylxylaramide **(4)**

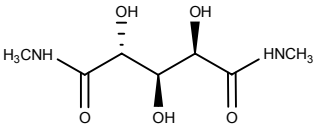

N,*N*′-dimethyl-L-arabinaramide **(5)**

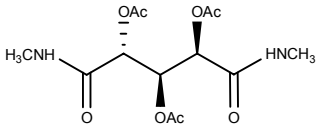

2,3,4-tri-*O*-acetyl-*N*,*N*′-dimethyl-L-arabinaramide **(6)**

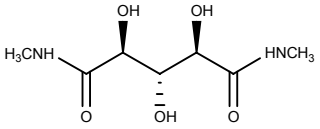

N,*N*′-dimethylribaramide **(7)**

Figure 4.1 Diamides **1-7**

Single crystals suitable for x-ray crystallographic analysis are in a regular repeating three dimensional arrangement of atoms, entitled a unit cell. The unit cell has six parameters; a, b, and c which are the lengths of the unit cell, and α, β, and γ which are the angles of the unit cell, Figure. 4.2. Crystalline **1**, **2**, **4**, **5, 7** were determined to have monoclinic crystal systems corresponding to axes of unequal length and angles of $\alpha = \gamma = 90°$; $\beta \neq 90°$. Compounds **3** and **6** had orthorhombic crystal systems with axes of unequal length but of equal α, β, γ, angles = 90°. The space group of a crystal is a mathematical description of the crystal structure's symmetry and is not the same as the internal molecular symmetry such as is present in *meso* compounds. The crystal of the *meso* compound **4** is a good example in which the molecule has symmetry through a C(3) axis but the crystal does not. Space groups, the orientation of the molecule within the unit cell, result as a combination of translational symmetry such as lattice centering and the point group symmetry operations of reflection, rotation, and rotoinversion. Interest lies in the overall conformation and hydrogen bonding network of each crystal and as such there will be no discussion of a crystal's space group. Space group data is listed along with the unit cell details in Table 4.1.

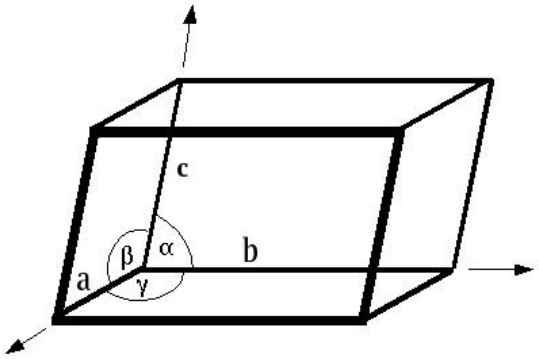

Figure 4.2 An example of a unit cell showing its six defining parameters

4.2 Results and Discussion

For all compounds examined (**1-7**), all individual bond lengths and angles fell within expected values. The results and discussion of each crystal's conformation and hydrogen bonding network are presented.

4.2.1 X-ray Crystal Analysis of Diamides 1-7

***N,N'*-Dihexylglutaramide (1)**

Figure 4.3 shows the geometry of *N,N'*-dihexylglutaramide (**1**), which forms monoclinic crystals and has a 2-fold axis of symmetry through the middle of the glutaryl segment at C(3), Figure. 4.3. The unit cell details are given in Table 4.1.

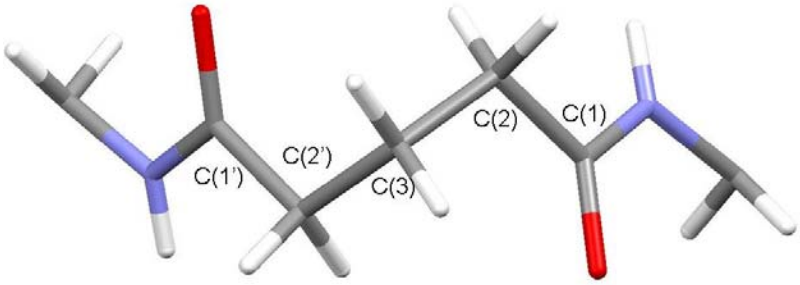

Figure 4.3 The geometry of the glutaramide portion of **1** showing an axis of symmetry through C(3)

The geometry of one half of **1** showing atom labeling and thermal ellipsoids at 30 percent probability is presented in Figure 4.4.

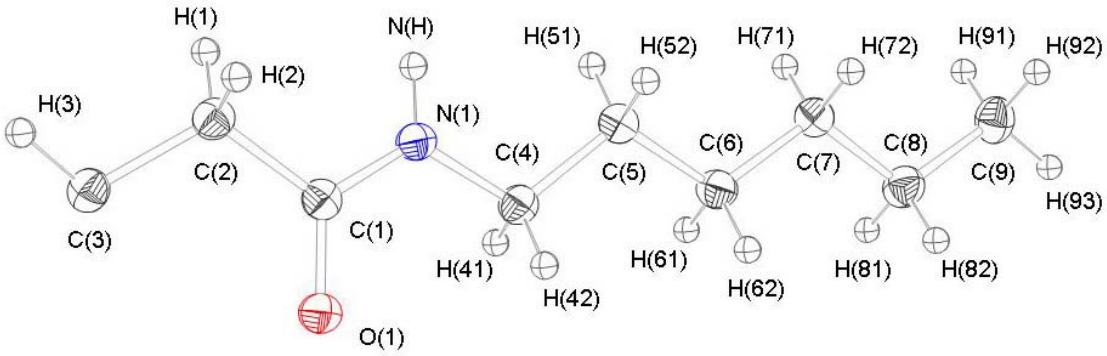

Figure 4.4 The geometry of one half of **1** showing atom labeling scheme and thermal ellipsoids at the 30 percent probability level

The glutaryl portion of **1** is in a sickle conformation with C(1)-C(2)-C(3)-C(2') in a *gauche* arrangement with a torsion angle of 68.18°. The methylene carbons of the hexyl portion, shown in Figure 4.4, are all in the expected *trans* (*anti*) conformational arrangement. The amide functionality is in a planar conformation about the atoms C(1)-C(2)-O(1)-N(1) where the average deviation from the least squares plane is 0.005Å.

Figure 4.5 shows the hydrogen bonding arrangement found in the crystal of **1** which is simple in that the crystal symmetry results in one hydrogen bond between N(1)-(N)H···O(1) 2.07Å with an angle of 171.1°. This generates doubly hydrogen bonded molecules stacked parallel to the c-axis.

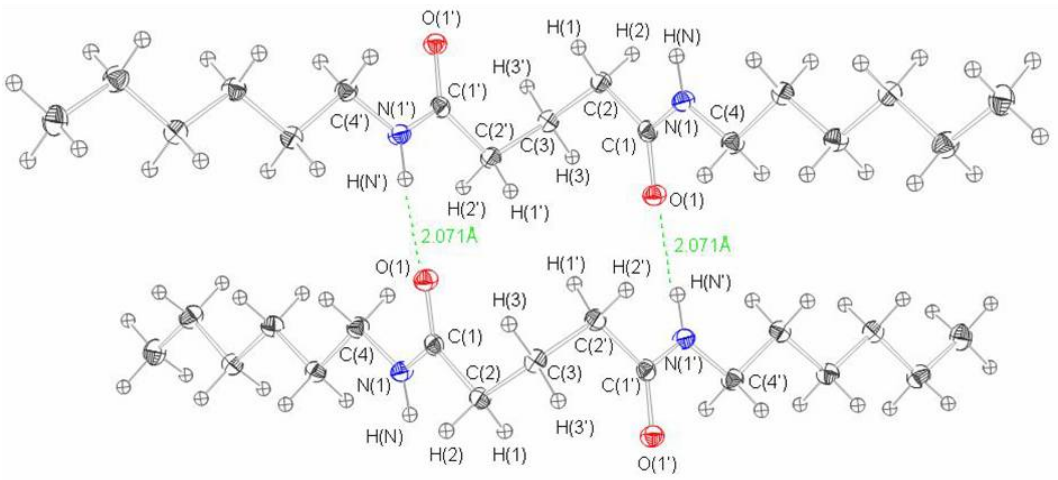

Figure 4.5 Hydrogen bonding schematic of *N,N'*-dihexylglutaramide (**1**)

***N,N'*-Dimethylglutaramide (2)**

Figure 4.6 shows the geometry of monoclinic crystal *N,N'*-dimethylglutaramide (**2**). The asymmetric unit of **2** contains half a molecule, with the other half generated by the same crystallographic 2-fold axis through C(3) as **1**, shown in Figure 4.4. The unit cell details are given in Table 4.1.

The overall conformation of the glutaryl unit of **2** is also in a sickle (*gauche*) conformation with torsion angle of 67.83° about C(1)-C(2)-C(3)-C(2'). The amide functionality of C(1)-C(2)-N(1)-O(1) atoms are planar with the average deviation from the least squares plane of 0.0077Å. The amide functionality, C(1')-C(2')-N(1')-O(1'), corresponding to the other half of the molecule generated about the crystallographic 2-fold axis through C(3) is identical. As with **1**, the hydrogen bonding of **2** is also simple in that there is only one hydrogen bond between N(1)-(N)H···O(1) 2.03Å with an angle of 172° (Figure 4.6).

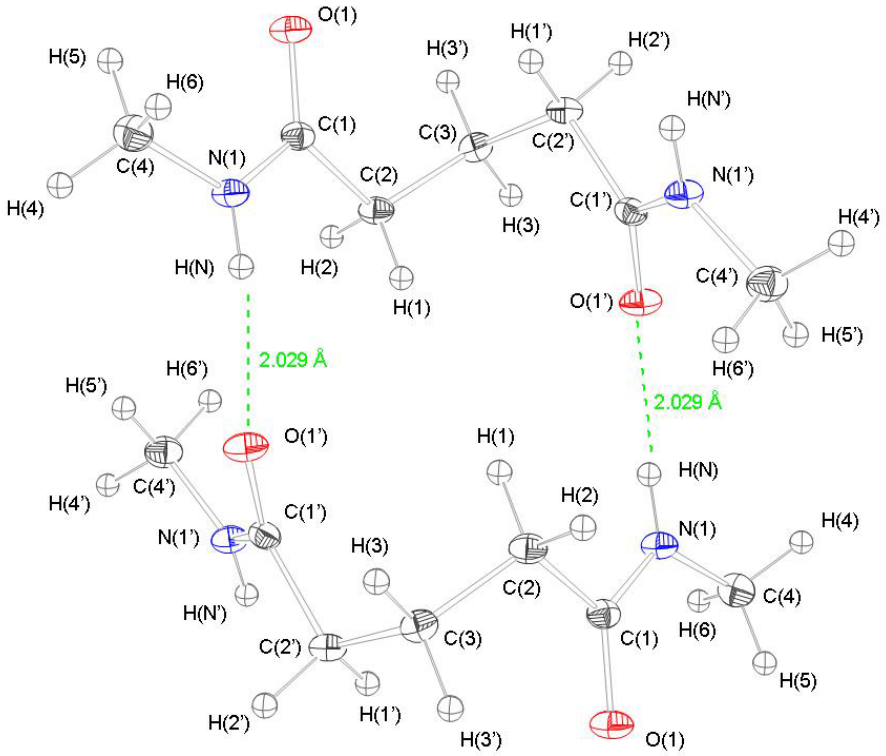

Figure 4.6 Hydrogen bonding schematic of *N,N'*-dimethylglutaramide (**2**)

N,N'-Dimethylxylaramide (**3**)

The geometry of *N,N'*-dimethylxylaramide (**3**) showing atom labeling and thermal ellipsoids at the 40 percent probability level is shown in Figure 4.7. Compound **3** forms orthorhombic crystals with a mirror plane through H(3)-C(3)-O(3)-H(4).

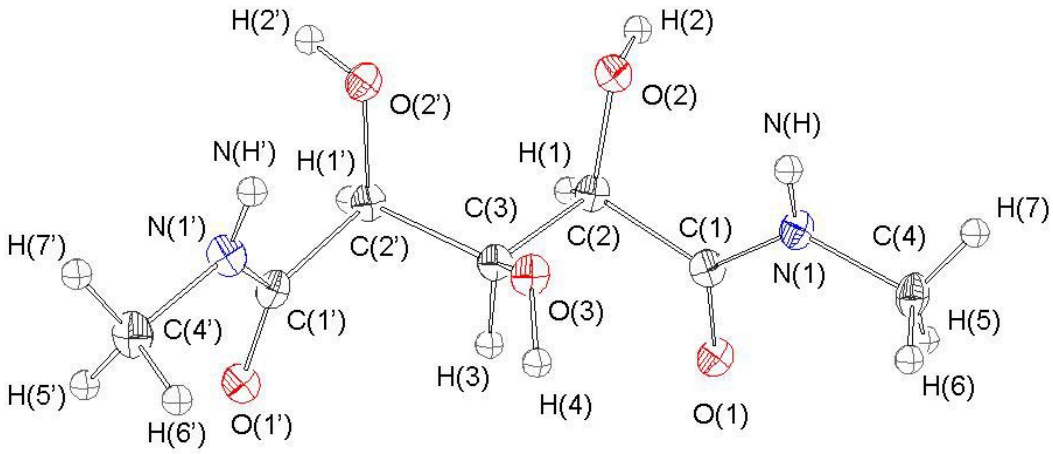

Figure 4.7 The geometry of *N,N'*-dimethylxylaramide (**3**) showing atom labeling scheme and thermal ellipsoids at the 40 percent probability level

The xylaryl unit of **3**, C(1)-C(2)-C(3)-C(2)'-C(1)', is in an extended conformation, with O(2) and O(3) atoms in a *gauche* relationship with a torsional angle of 58.97°. The planarity of the amide functionality of O(1)-C(1)-C(2)-N(1) is illustrated by an average deviation from the least squares plane of +/-0.001Å and is identical to the corresponding O(1')-C(1')-C(2')-N(1') amide functionality.

The hydrogen bonding scheme for **3** is shown in Figure 4.8 and is more complex than observed for both **1** and **2** due to the presence of pendant hydroxyl groups. There is one 2.124Å bifurcated hydrogen bond with O(2) and O(2)' of one molecule bonded to H(4) of a second molecule of **3** across the mirror plane. O(1) is involved in two separate hydrogen bonding interactions of an adjacent molecule, a very strong interaction to O(2)-H(2)···O(1), 1.87Å and a weaker interaction with N(1)-H(N) ···O(1), 2.24Å.

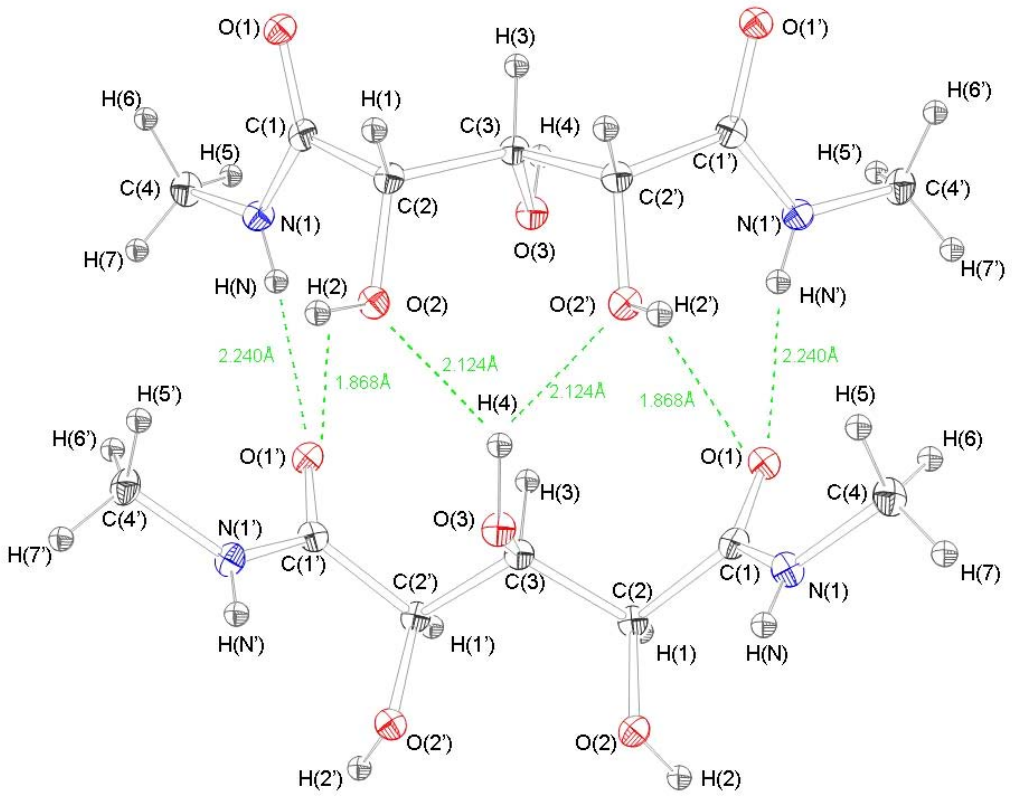

Figure 4.8 Hydrogen bonding schematic of *N,N'*-dimethylxylaramide (**3**)

2,3,4-Tri-*O*-acetyl-*N,N'*-dimethylxylaramide (**4**)

The structure of monoclinic crystalline 2,3,4-tri-*O*-acetyl-*N,N'*-dimethylxylaramide (**4**) is shown in Figure 4.9. Despite being a *meso* compound, **4** has no internal crystallographic symmetry as observed in the crystal structures of **1**-**3**. The unit cell details for **4** are given in Table 4.1.

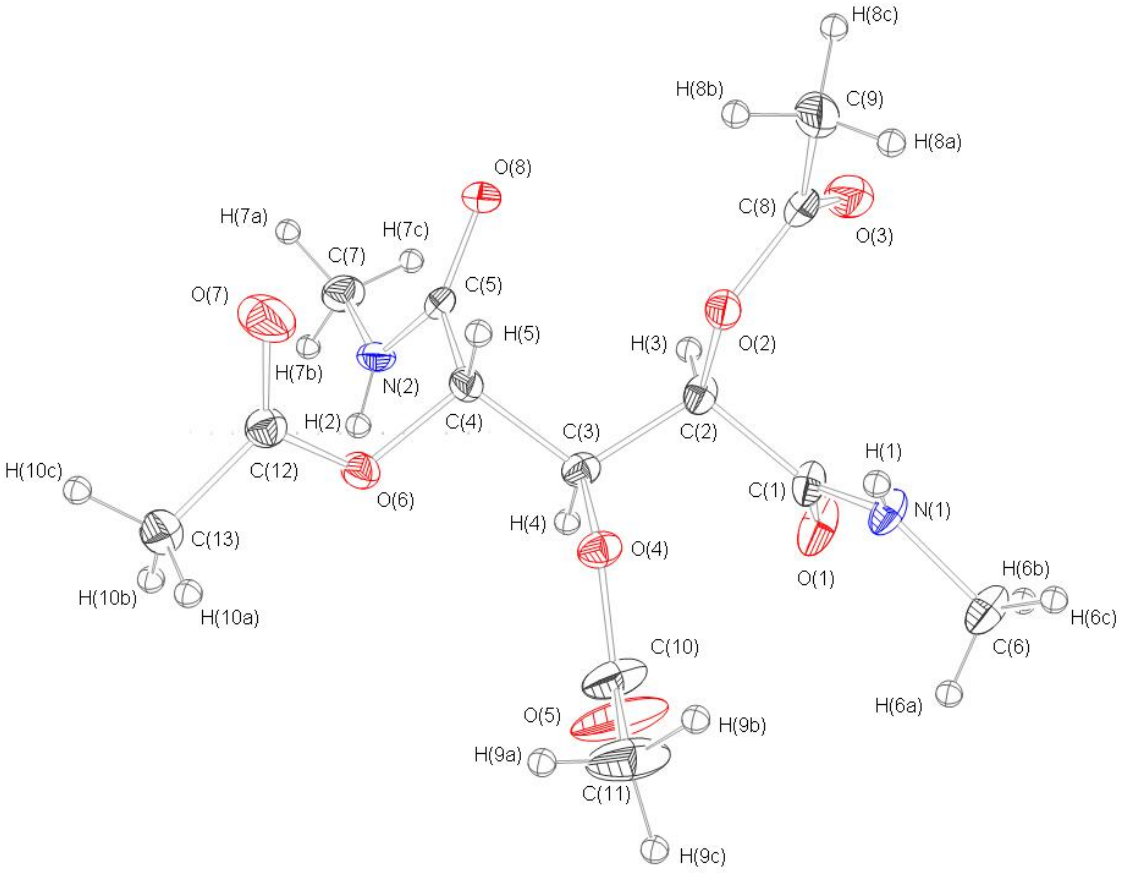

Figure 4.9 The geometry of 2,3,4-tri-*O*-acetyl-*N,N'*-dimethylxylaramide (**4**) showing atom labeling scheme and thermal ellipsoids at the 40 percent probability level

Unlike its free hydroxyl group precursor **3**, which is in an extended (*anti*) conformation, *O*-acetylated compound **4** adopts a sickle ($_3G^+$) conformation corresponding to an approximately +120º rotation around the C(3)-C(4) bond. The xylaryl unit is bent around three torsion angles, N(1)-C(1)-C(2)-C(3) at 94.32º, C(2)-C(3)-C(4)-C(5) at 61.62º, and C(3)-C(4)-C(5)-N(2) at -83.29º. The O(2) and O(4) acetate oxygens are in a *gauche* relationship as are the O(4) and O(6) acetate oxygens, with torsion angles of -61.92º and -58.31º, respectively. The planarity of the amide

functionalities of C(1)-O(1)-N(1)-C(2) and C(5)-O(8)-C(4)-N(2) are illustrated by an average deviation from the least squares plane of +/-0.03Å and +/-0.01Å, respectively.

The hydrogen bonding of crystalline *meso* **4** (Figure 4.10) is unlike that of *meso* **3** due to the asymmetry present within the molecule's bond geometries. There are two distinct amide hydrogen bonds, the stronger [N(2)-H(2)···O(8), 2.18Å] and more linear bond at 151°, and the weaker [N(1)-H(1)···O(1), 2.25Å] and the less linear bond at 138°.

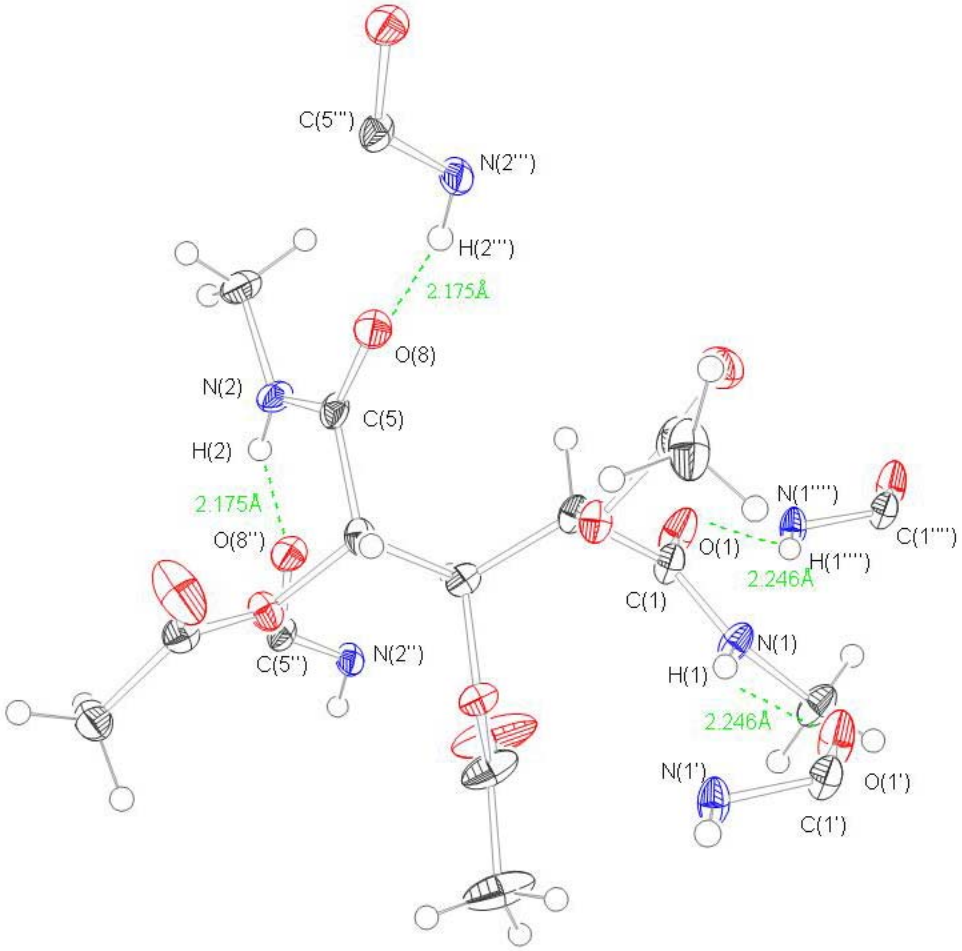

Figure 4.10 Hydrogen bonding schematic of 2,3,4-tri-*O*-acetyl-*N,N'*-dimethylxylaramide (**4**)

N,N'-Dimethyl-L-arabinaramide (**5**)

The geometries of *N,N'*-dimethyl-L-arabinaramide (**5**) showing atom labeling and thermal ellipsoids at the 40 percent probability level is shown in Figure 4.11.

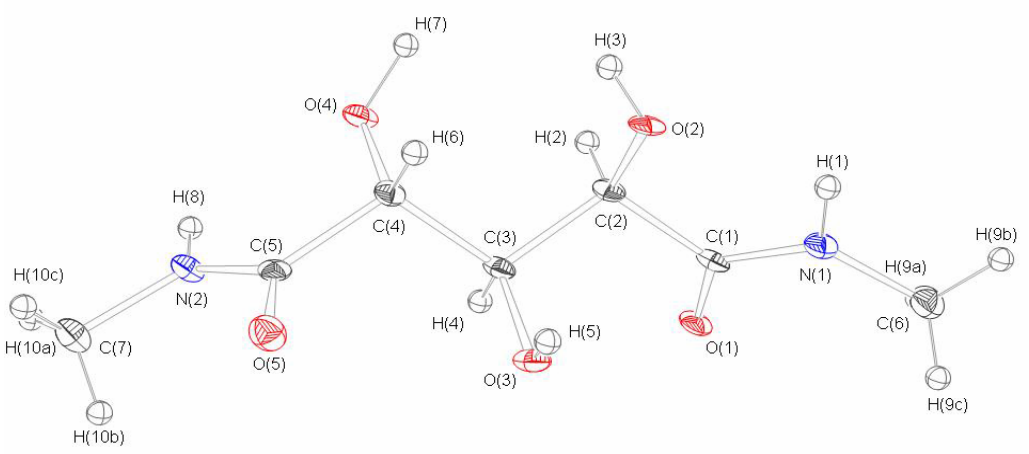

Figure 4.11 The geometry of *N,N'*-dimethyl-L-arabinaramide (**5**) showing atom labeling and thermal ellipsoids at the 40 percent probability level

Compound **5** forms monoclinic crystals and is in an extended conformation having torsion angles of 178.43º and -175.03º corresponding to C(1)-C(2)-C(3)-C(4) and C(2)-C(3)-C(4)-C(5), respectively. The extended (*anti*) conformation is also manifested in the relative orientations of the substituents. The O(2) and O(3) hydroxyl group oxygens are *gauche* with a torsion angle of -66.13º whereas the O(3) and O(4) hydroxyl group oxygens are in an *anti* relationship with a torsion angle of -175.08º. The planarity of the amide functionalities of C(1)-O(1)-N(1)-C(2) and C(5)-O(5)-C(4)-N(2) are illustrated by an average deviation from the least squares plane of +/-0.008Å and +/-0.0004Å.

Figure 4.12 shows the hydrogen bonding scheme of **5**. The N(1)-H(1)···O(2) intramolecular interaction has an uncharacteristically low bond angle of 110.49º relative to a hydrogen bond length of 2.090Å, signifying a weak hydrogen bond interaction.

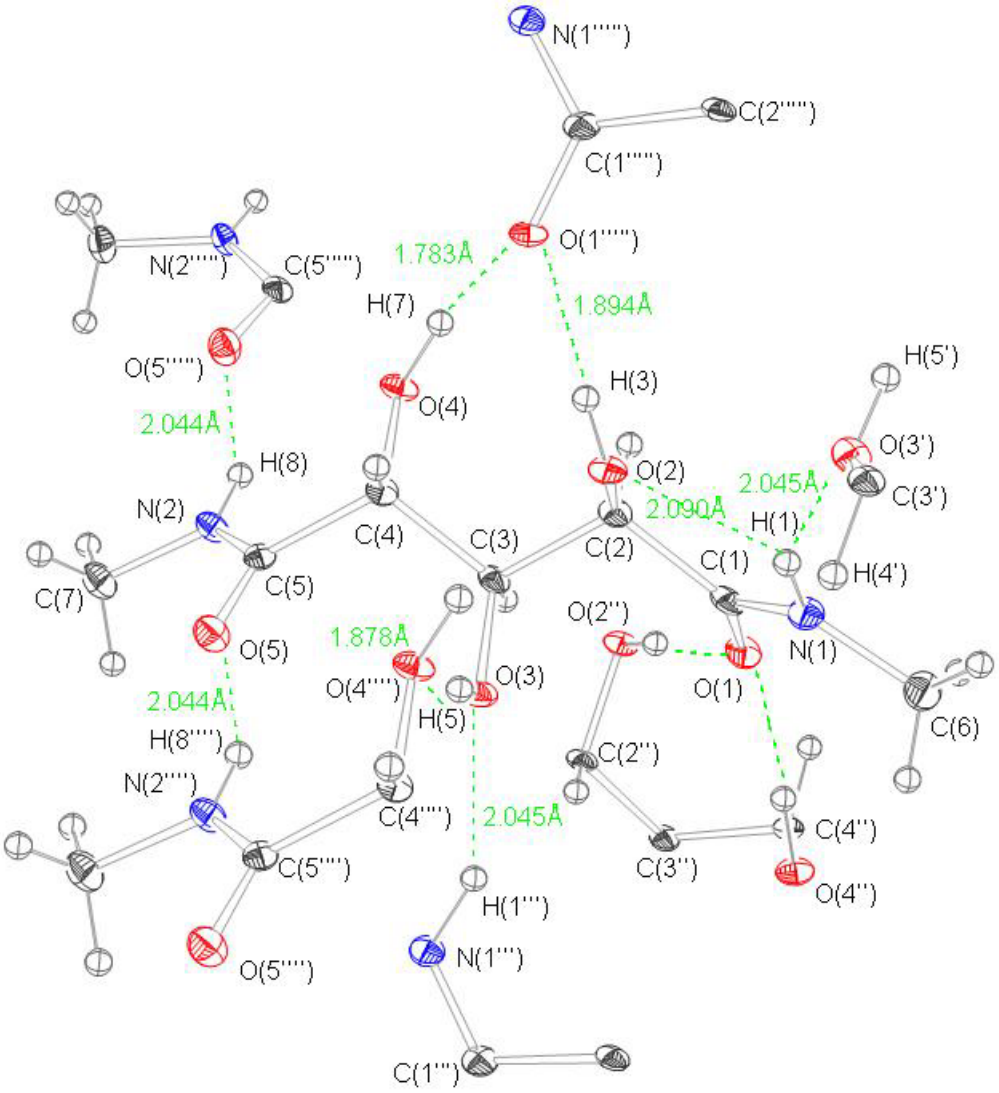

Figure 4.12 Hydrogen bonding schematic of *N,N'*-dimethyl-L-arabinaramide (**5**)

There are three amide hydrogen bonding interactions, two intermolecular amide hydrogen bonds [N(2)-H(8)···O(5) and N(1)-H(1)···O(3)] and one intramolecular [N(1)-H(1)···O(2)]. The bond length and angles of these hydrogen bonds are [2.044Å, 148.62º],

[2.045Å, 149.86°], and [2.090Å, 110.49°], respectively. The three hydroxyl groups hydrogens are also intermolecularly hydrogen bonded, O(3)-H(5)···O(4), O(4)-H(7)···O(1), O(2)-H(3)···O1, with hydroxyl hydrogen bond lengths and angles of [1.878Å, 176.24°], [1.783Å, 166.02°], and [1.894Å, 176.862°], respectively.

2,3,4-Tri-*O*-acetyl-*N,N'*-dimethyl-L-arabinaramide (6)

The geometry of crystalline 2,3,4-tri-*O*-acetyl-*N,N'*-dimethyl-L-arabinaramide (**6**) is shown in Figure 4.13.

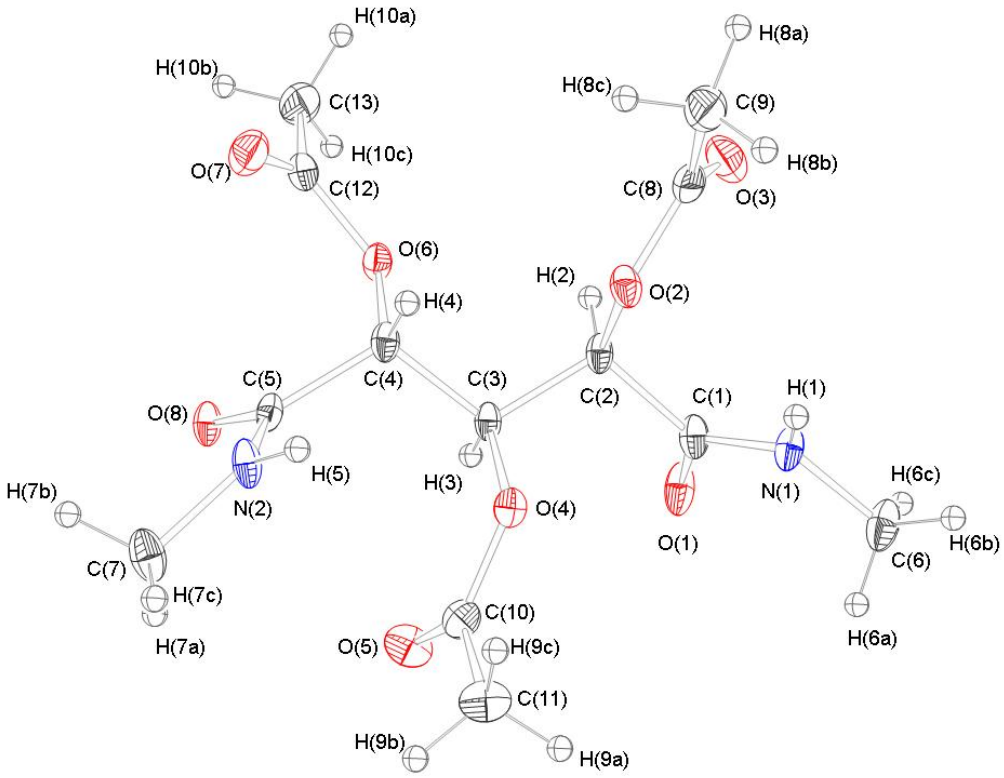

Figure 4.13 The geometry of 2,3,4-tri-*O*-acetyl-*N,N'*-dimethyl-L-arabinaramide (**6**) showing atom labeling and thermal ellipsoids at the 40 percent probability level

The arabinaryl carbon backbone of **6** is similar to that of **5** and is extended with torsion angles of 177.39° for C(1)-C(2)-C(3)-C(4) and 178.42° for C(2)-C(3)-C(4)-C(5).

The O(2) and O(4) acetate oxygens are *gauche* with a torsion angle of 63.96º and the O(4) and O(6) acetate oxygens atoms are *anti*, with a torsion angle of -176.77º. The planarity of the amide functionalities of C(1)-O(1)-N(1)-C(2) and C(5)-O(8)-C(4)-N(2) is illustrated by an average deviation from the least squares plane of +/-0.0002Å and +/-0.025Å, respectively.

As observed with diastereoisomer **4**, compound **6** has two distinct hydrogen bonds, a stronger [N1-H1···O8, 2.115Å] bond and a weaker [N2-H5···O1, 1.963Å] bond, Figure 4.14. The stronger, shorter hydrogen bond is the more linear of these bonds with a hydrogen bond angle of 176º, compared to 158º for the weaker and longer hydrogen bond.

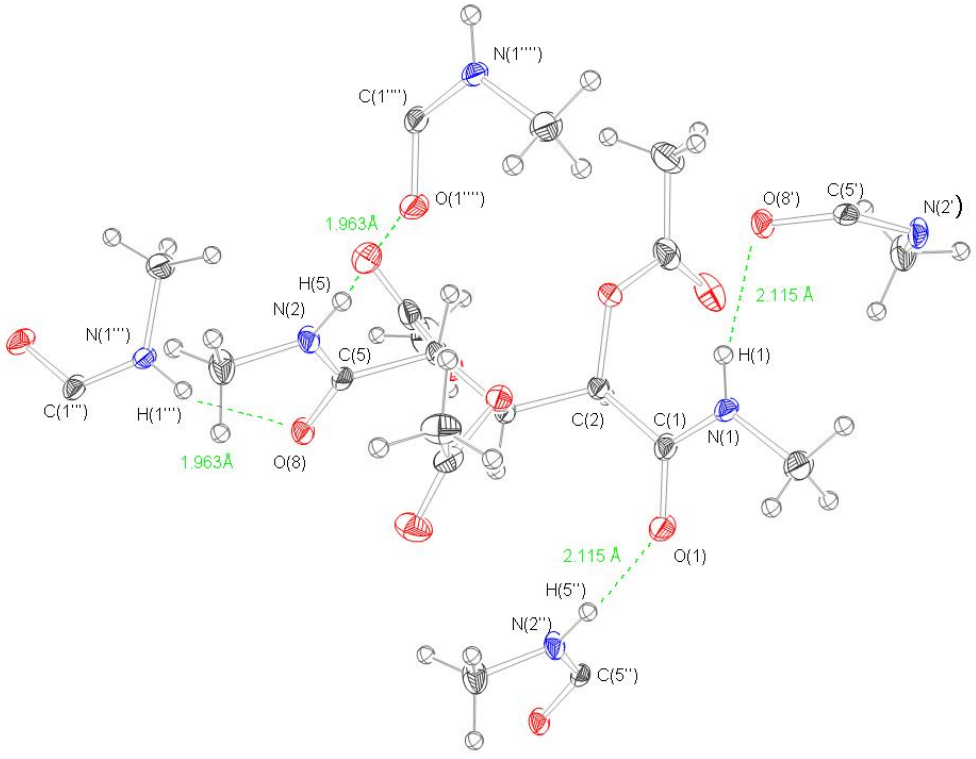

Figure 4.14 Hydrogen bonding schematic of 2,3,4-tri-*O*-acetyl-*N,N'*-dimethyl-L-arabinaramide (**6**)

***N,N'*-dimethylribaramide monohydrate (7)**

The geometry of monoclinic crystalline *N,N'*-dimethylribaramide monohydrate (**7**) showing atom labeling and thermal ellipsoids at the 40 percent probability level is shown in Figure 4.15. Unlike the conformationally extended diastereoisomer *meso* **3**, *meso* compound **7** has no internal crystallographic symmetry and is in a sickle ($_3G^-$) (*gauche*) conformation.

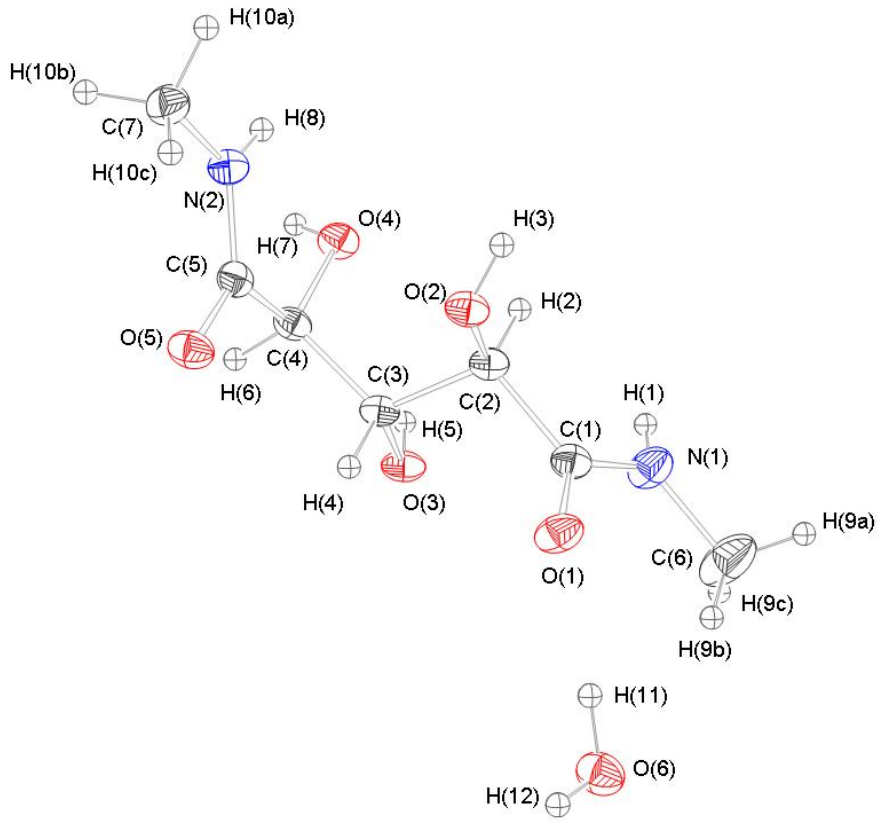

Figure 4.15 The geometry of **7** showing atom labeling and thermal ellipsoids at the 40 percent probability level

The ribaryl carbon backbone of **7** is in a sickle ($_3G^-$) (*gauche*) conformation with torsion angles of 177.39º for C(1)-C(2)-C(3)-C(4) and -74.3º for C(2)-C(3)-C(4)-C(5). The O(2) and O(3) hydroxyl group oxygens are *anti* with a torsion angle of -176.53º and the O(3) and O(4) hydroxyl group oxygens atoms are *gauche*, with a torsion angle of -

69.95º. Figure 4.16 shows the hydrogen bonding schematic of **7**. Compound **7** has one distinct amide hydrogen bond [N1-H1···O6, 2.049Å, 168.59º] bonded to the oxygen of an adjacent water molecule. The intermolecular hydrogen bonding of compounds **3** and **7** is similar in that all hydroxyl group hydrogens are intermolecularly hydrogen bonded. Compounds **3** and **7** are also similar in that O(3) acts as a hydrogen bond donor of a bifurcated H(4), although the acceptors are two hydroxyl group oxygens in **3** and a hydroxyl group oxygen [O3-H5···O2, 2.647Å, 109.88 º] and carbonyl carbon [O3-H5···O5, 2.248Å, 150.05 º] in **7**. The hydroxyl groups substituents on C(2) and C(4) are intermolecularly hydrogen bonded to a hydroxyl group oxygen acceptor [O2-H3···O3, 1.873Å, 170.80º] and a carboxyl oxygen acceptor [O4-H7···O1, 2.049Å, 151.61º]. The carboxyl oxygens on C(1) and C(5) hydrogen bond to an adjacent water molecule, [O6-H11···O1, 1.897Å, 173.27º] and [O6-H12···O5, 1.992Å, 171.41º], respectively. Thus a water molecule acts as a hydrogen bond bridge between the carboxyl oxygen on C(1) of one molecule and the carbonyl oxygen on C(5) of an adjacent molecule.

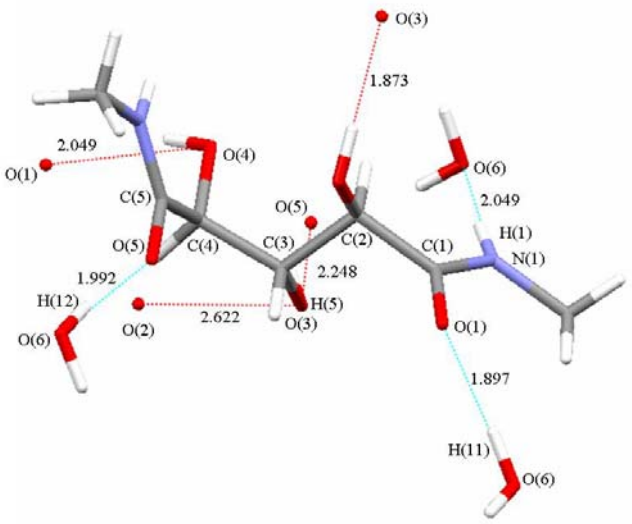

Figure 4.16 Hydrogen bonding schematic of *N,N'*-dimethylribaramide monohydrate (**7**)

4.2.2 Crystal Packing

Due to the presence of hydroxyl groups on **3** and **5** there is more potential for hydrogen bonding between adjacent molecules than between those of their acetates derivatives, compounds **4** and **6**, respectively. This additional hydrogen bonding leads to more efficient packing in the crystals as displayed in the densities of each; **3** (1.531g cm^{-3}), **5** (1.452g cm^{-3}), **7** (1.420g cm^{-3}), **4** (1.369g cm^{-3}), **6** (1.286g cm^{-3}). Because of the absence of hydroxyl and acetate groups there is decreased potential for hydrogen bonding within **1** (1.125g cm^{-3}) and **2** (1.242g cm^{-3}) relative to **3, 5, 4,** and **6**.

4.2.3 Analysis and Comparison of Crystalline *N,N'*-Dimethylglutaramide and *N,N'*-Dihexylglutaramide

Applying quantum mechanical calculations, Durig and coworkers established that the experimental energies for the *trans* (*anti*)-*gauche* (T-G) rotamers of butane differed from 0.5-0.9 kcal/mol[1] and that the T conformation is favored by 0.75 kcal/mol.[2] The same conformational result was found for *n*-pentane where the TT-to-GG energy change experimentally ranges from 0.46[3] to 0.56[4] kcal/mol, compared to 0.76 kcal/mol derived from quantum mechanical calculations.[5] An investigation of a series of X-ray crystallographic studies of oligomeric models of polyamides indicated that the central methylene carbons of the diacyl unit usually adopted a *trans* (*anti*) conformation.[6] This was reinforced in early studies of crystalline phase Nylon 6,6 that detailed the conformational preference for the methylene carbons of the adipoyl unit was an all *trans* (*anti*) conformation based upon a comparison of results from molecular dynamics computer simulations and experimental NMR spectroscopy.[7] However, Navarro *et. al.* established that the preference for an all *trans* (*anti*) conformation may decrease for some

acyclic diamides.[6-8] When fewer than six methylene carbons are present in the diacyl unit, the repulsive interactions of the amide groups can induce folding of the molecule into a *gauche* conformation resulting in a more favorable orientation of the dipoles despite the *gauche* orientation of the methylene carbon atoms. Navarro and co-workers performed ab Initio HF/6-31G* quantum mechanical calculations on the glutaramido portion of **1** and found the TTTTTT or fully extended conformation (*anti*) to be less stable than the TTGGTT or folded conformation by 2.7 kcal/mol.[6] Our findings are consistent with these observations. Crystalline **1** and **2** were observed to be in the TTGGTT or a folded (sickle) conformation, Figure 4.17.

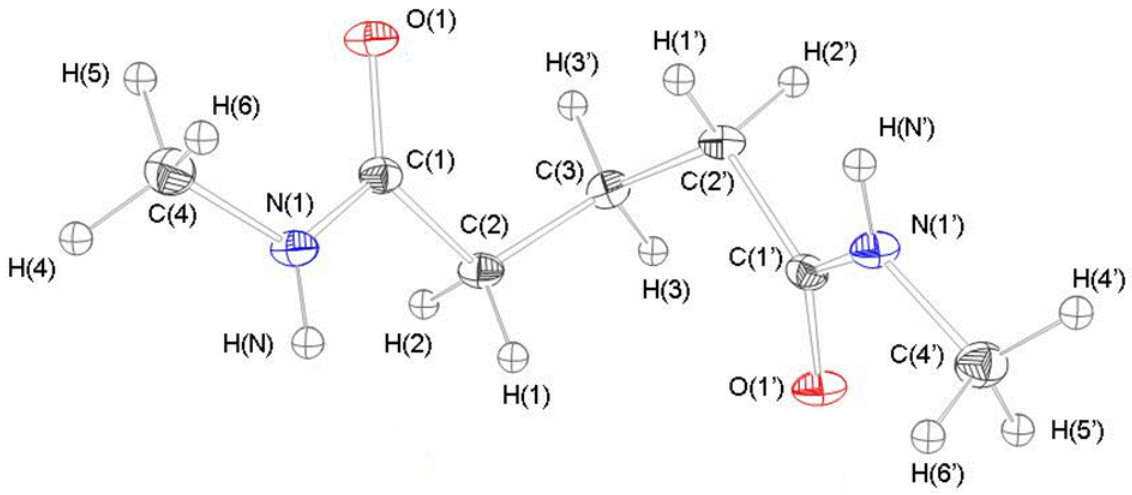

Figure 4.17 Dimethylglutaramide in a TTGGTT or sickle conformation

The hydrogen bonding network was able to accommodate the preferred folded conformation and is essentially the same for both **1** and **2**, with marginally shorter N-H and H···O distances for the **2**. This gives rise to closely similar b and c axes, with the extra chain length for **2** being accommodated by the doubling of the a axis length. Crystals of **1** and **2** are in a conformational arrangement in agreement with computed quantum mechanical and molecular mechanic calculations, the latter being reported in

Chapter 3 of this dissertation. The force driving the conformational preference in these calculations was the energetically favorable separation of parallel dipoles rather than the interactions of backbone methylene units.

4.2.4 Analysis of Crystalline *N,N'*-Dimethylxylaramide (3), *N,N'*-Dimethyl L-arabinaramide (5), *N,N'*-Dimethylribaramide Monohydrate (7), 2,3,4-Tri-*O*-acetyl-*N,N'*-dimethylxylaramide (4), and 2,3,4-Tri-*O*-acetyl-*N,N'*- dimethyl L-arabinaramide (6)

It has been suggested that unfavorable steric interactions resulting from hydroxyl group oxygens that are in eclipsed 1,3-parallel arrangements cause acyclic carbohydrates in an extended (*anti*) conformation to undergo a 120° rotation about a C-C bond to alleviate this interaction resulting in a sickle (*gauche*) conformation.[9] For such molecules these interactions are similar to a 1,3-*syn*-diaxial interaction (1.9 kcal/mol) of hydroxyl groups in chair conformations of diaxial *cis*-cyclohexane-1,3-diol.[10] In reference to simple monosaccharide derivatives, vicinal coupling constant data were used by Sweeting et al. as a means of computational comparison of six per-acetylated hexonitriles.[11] The hexononitriles conformationally preferred an extended (*anti*) conformation except when an eclipsed 1,3- parallel interaction was present, as with penta-*O*-acetyl-D-gluconononitrile, wherein a sickle (*gauche*) conformation was preferred. Hexa-*O*-acetyl-D-glucitol also preferred a sickle conformation as determined from ^{1}H NMR conformational studies carried out by Angyal and co-workers.[12] Molecular modeling of *N,N'*-dimethylxylaramide and *N,N'*-dihexyl xylaramide using MacroModel V2.0[13] found, for both molecules, that two sickle conformations were lower in energy than the extended conformation. The sickle conformations allowed for the alleviation of

the eclipsed 1,3-parallel interaction between hydroxyls at C(2) and C(4). Compounds **3** and **4** have eclipsed 1,3-hydroxyl and acetate groups, respectively, attached at C(2) and C(4). An extended conformation was observed in crystalline **3**, whereas a sickle ($_3G^+$) conformation was observed for **4**. Despite having an eclipsed 1,3-hydroxyl interaction it is not surprising that crystalline **3** is observed to be in an extended conformation because of the relative number and strength of hydrogen bonds as evidenced by the high crystal density. Compound **7**, a diastereoisomer of **3**, also has an eclipsed 1,3-hydroxyl interaction and is in a sickle ($_3G^-$) conformation unlike the extended **3**. Compound **7** has a hydrogen bonding network with individual hydrogen bonds having relatively long hydrogen bonds and/or donor-hydrogen-acceptor geometries that are less than optimal for strong hydrogen bonding as evidenced by the lower crystal density. Additionally, **7** has a water molecule acting as a hydrogen bond bridge between adjacent molecules. The inability to stabilize the 1,3-hydroxyl interaction through a strong hydrogen bonding network resulted in the observed sickle (*gauche*) conformation. Compounds **5** and **6** have no eclipsed 1,3-parallel interactions in the extended conformation and exhibit extended conformations as expected, Figures 4.10 and 4.12.

4.3 Experimental

General Methods

Colorless crystals of **1-7** were obtained from appropriate solvents [**1** (MeOH), **2** (MeOH), **3** (H_2O), **4** (H_2O/Acetone), **5** (H_2O), **6** (MeOH/acetone), **7** (H_2O)]. X-ray intensity data were collected on a Siemens SMART CCD diffractometer using Mo-Kα X-radiation. Data were corrected for absorption and other effects semi-empirically.[1] Structures were solved using direct methods and routinely developed and refined on F_o^2.

Hydrogen atoms were located from difference maps and were refined, except for the methyl hydrogen atoms for 2,3,4-tri-*O*-acetyl-*N,N'*-dimethyl-L-arabinaramide (**6**) which were included in calculated positions. All calculations were carried out using the SHELX programs[2] operating under WinGx.[3] All crystal structure graphics were generated using ORTEP-3[4] and/or Mercury. Crystal and refinement data are summarized in Table 4.1. Melting points were obtained with a Fisher-Johns melting point apparatus and are reported uncorrected.

***N,N'*-Dihexylglutaramide (1)**

Crystals were obtained by dissolving *N,N'*-dihexylglutaramide in methanol and allowing the methanol to slowly evaporate. The resulting crystals were colorless blocks, mp 143 ºC.

***N,N'*-Dimethylglutaramide (2)**

Crystals were obtained by dissolving *N,N'*-dimethylglutaramide in methanol and allowing the methanol to slowly evaporate. The resulting crystals were colorless prisms, mp 121 ºC.

***N,N'*-Dimethylxylaramide (3)**

Crystals were obtained by dissolving the *N,N'*-dimethylxylaramide in water and allowing the water to evaporate**.** The resulting crystals were colorless blocks, mp 191-194 ºC.

2,3,4-Tri-*O*-acetyl-*N,N'*-dimethylxylaramide (4)

Crystals were obtained by dissolving 2,3,4-tri-*O*-acetyl-*N,N'*-dimethylxylaramide in water and allowing acetone to diffuse into the water. The resulting crystals were colorless prisms, mp 171 ºC.

***N,N'*-Dimethyl-L-arabinaramide (5)**

Crystals were obtained by dissolving *N,N'*-dimethyl- L-arabinaramide in warm water and allowing the water allowed to slowly evaporate. The resulting crystals were colorless prisms, mp 194-196 ºC.

2,3,4-Tri-*O*-acetyl-*N,N'*-dimethyl-L-arabinaramide (6)

Crystals were obtained by dissolving 2,3,4- tri-*O*-acetyl-*N,N'*-dimethyl- L-arabinaramide in warm methanol and allowing the diffusion of acetone into the methanol. The resulting crystals were needles, mp 209-210 ºC.

***N,N'*-Dimethylribaramide Monohydrate (7)**

Crystals were obtained by dissolving *N,N'*-dimethylribaramide in water and allowing the water to evaporate. The resulting crystals were colorless blocks, mp 166-168 ºC.

Table 4.1 Crystal and refinement data

compound	MHGH (**1**)	MHGZ (**2**)	MHDM (**3**)	MHXA (**4**)	MHDA (**5**)	MHAA (**6**)
formula	$C_{17}H_{34}N_2O_2$	$C_7H_{14}N_2O_2$	$C_7H_{14}N_2O_5$	$C_{13}H_{20}N_2O_8$	$C_7H_{14}N_2O_5$	$C_{13}H_{20}N_2O_8$
Mr	298.46	158.20	206.20	332.31	206.20	332.31
crystal system	monoclinic	monoclinic	orthorhombic	monoclinic	monoclinic	orthorhombic
space group	C2/c	C2/c	Pnma	C c	$P2_1$	$P2_12_12_1$
a (Å)	37.458(13)	18.069(14)	8.2938(1)	8.9373(2)	5.0242(2)	6.2852(1)
b (Å)	5.3446(19)	5.4967(4)	21.0671(2)	21.9589(1)	8.5927(2)	16.032(2)
c (Å)	8.850(3)	8.5233(7)	5.1215(1)	9.0433(2)	10.9416(4)	17.036(3)
α	90	90	90	90	90	90
β	96.014(4)	91.400(2)	90	114.681(1)	93.129(1)	90
γ	90	90	90	90	90	90
V ($Å^3$)	1762.1(11)	846.29(11)	894.86(2)	1612.64(5)	471.66(3)	1716.65(5)
Z	4	4	4	4	2	4
F(000)	664	344	440	704	220	704
calc density (g cm^{-3})	1.125	1.242	1.531	1.369	1.452	1.286
vol per non-H atom	21.0	19.2	16.0	17.5	16.8	18.6

Table 4.1 Crystal and refinement data conti.

compound	MHGH (**1**)	MHGZ (**2**)	MHDM (**3**)	MHXA (**4**)	MHDA (**5**)	MHAA (**6**)
crystal size (mm^3)	0.58x0.44x0.18	0.42x0.24x0.18	0.38x0.26x0.22	0.36x0.24x0.12	0.34x0.26x0.10	0.42x0.36x0.28
temp (K)	93(2)	93(0)	93(2)	93(2)	93(2)	93(2)
μ(Mo-Kα) (mm^{-1})	0.073	0.091	0.130	0.114	0.123	0.107
total refl	4097	2397	4562	4797	2702	10335
θ range (deg)	1.09-25.16	2.25-26.35	1.93-25.72	1.85-26.35	1.86-25.69	1.74-26.55
unique refl	1588	871	872	2107	1704	3521
R_{int}	0.0201	0.0374	0.0555	0.0334	0.0249	0.0634
R_1 (I>2s(I))	0.0312	0.0396	0.0444	0.0299	0.0529	0.0543
wR_2 (all data)	0.1169	0.1082	0.1226	0.0787	0.1407	0.1435
GoF	1.185	1.049	1.058	1.058	1.037	1.355

Table 4.1 Crystal and refinement data conti.

compound	MHRI (**7**)
formula	$C_7H_{16}N_2O_6$
Mr	224.21
crystal system	Monoclinic
space group	P2 (1) / c
a (Å)	11. 4378(11)
b (Å)	10.2707(10)
c (Å)	9.5798(10)
α	90
β	111.25(5)
γ	90
V ($Å^3$)	1048.86(18)
Z	4
F(000)	480

Table 4.1 Crystal and refinement data conti.

compound	MHRI (**7**)
calc density (g cm^{-3})	1.420
vol per non-H atom	17.48
crystal size (mm^3)	0.27x0.24x0.09
temp (K)	173(2)
μ(Mo-Kα) (mm^{-1})	0.1072
total refl	2068
2θ range (deg)	8.63-65.22
unique refl	1281
R_{int}	0.0188
R_1 (I>2s(I))	0.0391
wR_2 (all data)	0.1098
GoF	1.027

References

1. Durig, J. R.; Compton, D.A.C. Analysis of torsional spectra of molecules with two internal C3v rotors. 12. Low frequency vibrational spectra, methyl torsional potential function, and internal rotation of n-butane. Journal of Physical Chemistry, **1979**, 83(2), 265-8

2. Wiberg, Kenneth. B.; Murko, Mark. A. Rotational barriers. 2. Energies of alkane rotamers. An examination of gauche interactions. Journal of the American Chemical Society, **1988**, 110(24), 8029-38

3. Maissara, M.; Cornut, J. C.; Devaure, J.; Lascombe, J**.** Conformational equilibrium of pentane as a function of temperature and pressure. Spectroscopy (Amsterdam, Netherlands), **1983**, 2(2), 104-19

4. Kanesaka, Isao; Snyder, Robert G.; Strauss, Herbert L. Experimental determination of the trans-gauche energy difference of gaseous n-pentane and diethyl ether**,** Journal of Chemical Physics, **1986**, 84(1), 395-7

5. Alman, C., Puiggali, J.; A quantum mechanical study of the folding of methylene units in compounds with several glutaramide units: nylon 1,5. Macromol. Theory Simul.; **1998**, 7, 367-372

6. Navarro, Eloisa; Aleman, Carlos; Puiggali, Jordi. Folding of Methylene Groups in Linear Glutaramide Analogs. Journal of the American Chemical Society, **1995**, 117(28), 7307-10.11 and references therein

7. Wendoloski, J. J.; Garndner, K. H.; Hirschinger, J.; Miura, H.; English, A. D. Molecular dynamics in ordered structure: computer simulation and experimental results for nylon 66 crystals. Science, **1990**, 247(4941), 431-6

8. Aleman, Carlos; Navarro, Eloisa; Puiggali, Jordi.; Conformational Analysis of Succinamide Analogues. Journal of Organic Chemistry, **1995**, 60, 6135-6140

9. Horton, D.; Wander, J. D.; Conformation of acyclic derivatives of sugars. Conformations of peracetylated aldose dithioacetals in solution; Carbohydrate Research,**1969**, 10, 179-288

10. Eliel, E.L.; Wilen, S.H.; Configuration and Conformation of Cyclic Molecules. Stereochemistry of Organic Compounds; Wiley: New York, **1994**; 707

11. Sweeting, L.; Coxon, B.; Varma, R.; Conformational analysis of per-acetylated hexononitriles. Carbohydrate Research, **1979**, 72, 43-55.

12. Angyal, S.; LeFur, R.; Gagnaire, D.; Conformations of acyclic sugar derivatives part II: determination of the conformations of alditol acetates in solution by the use of 250-MHZ NMR spectra. Carbohydrate Research, **1972**, 23, 121-134.

13. Chen, L.; Haraden, B.; Kane, R.W.; Kiely, D. E.; Rowland, R. S.; Molecular Modeling of Acyclic Carbohydrate Derivatives *N*,*N*'-dimethyl- and *N*,*N*'-Dihexyl xylaramide: Model Compounds for Synthetic Poly(hexamethylene xylaramide). Journal of the American Chemical Society, **1990**, 8, 141-151

Appendix 5.1 NMR Spectra of Xylaric Acid, Disodium L-Arabinarate (Disodium L-Lyxarate), Disodium D-Arabinarate (Disodium D-Lyxarate), Disodium Ribarate, and Ribaric Acid 5,2 (1,4) Lactone

Proton NMR Spectrum of Xylaric Acid in D_2O

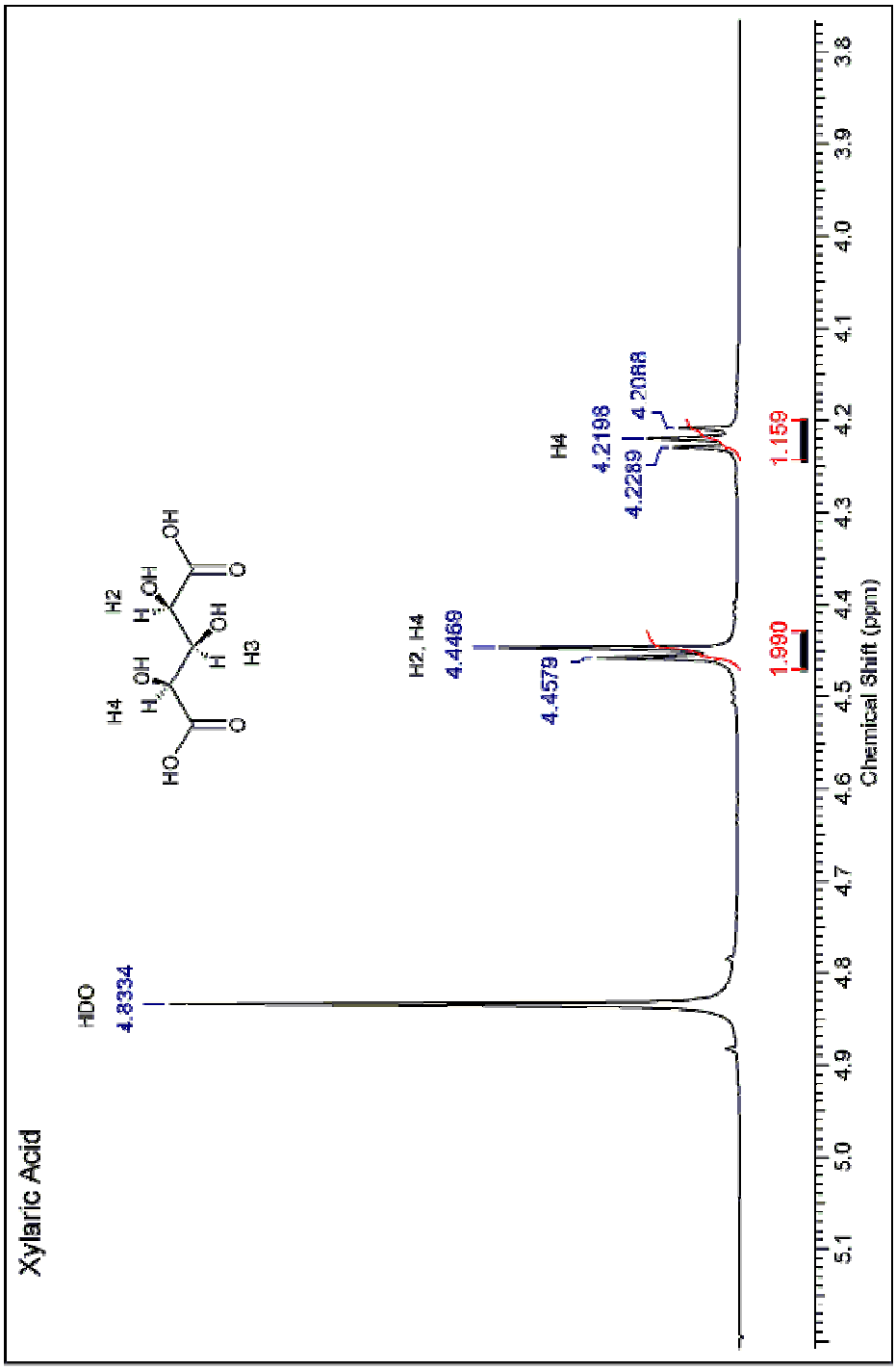

Proton NMR Spectrum of Disodium L-Arabinarate in D_2O

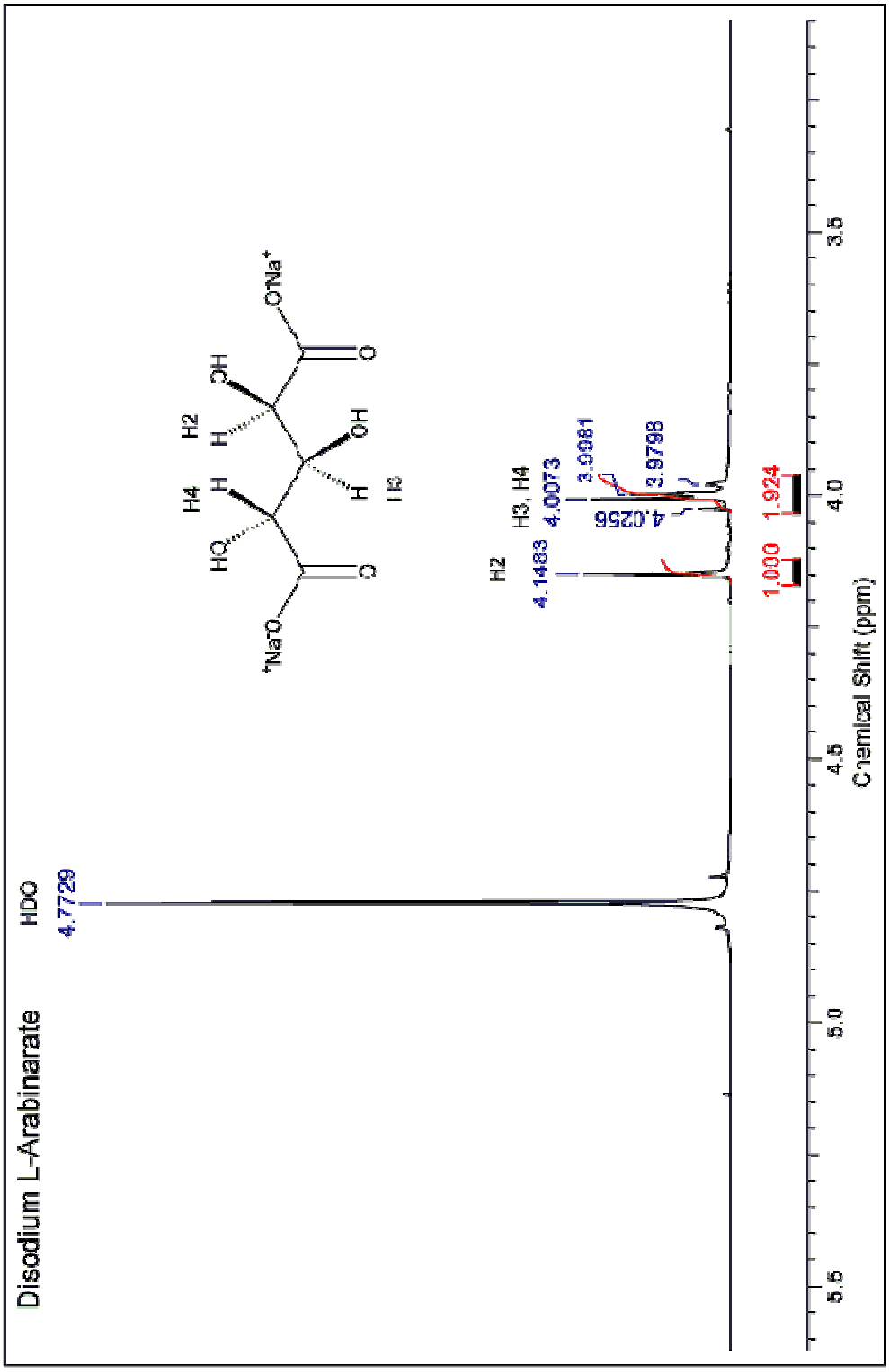

Proton NMR Spectrum of Disodium D-Arabinarate in D_2O

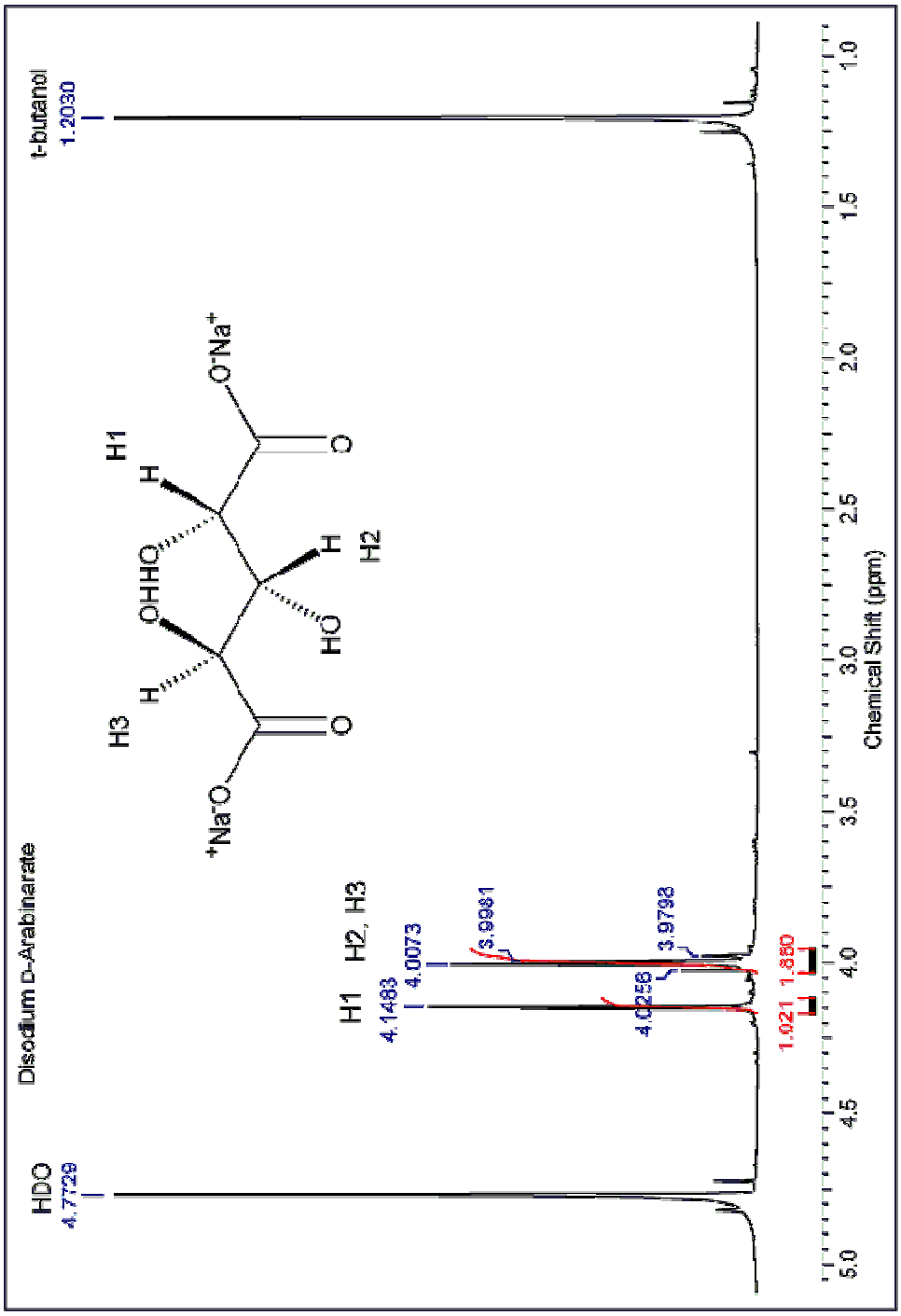

Proton NMR Spectrum of Disodium Ribarate in D_2O

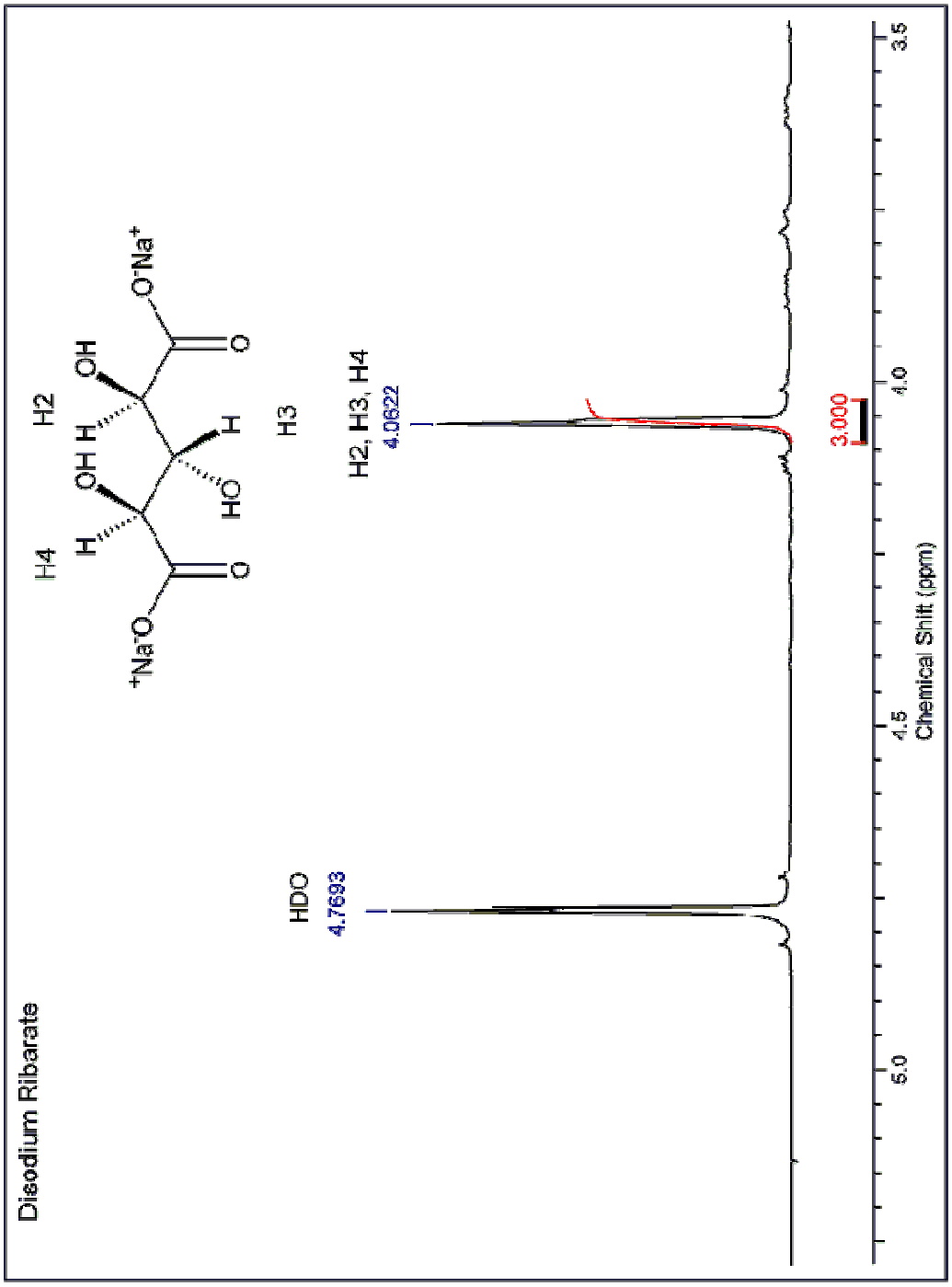

Proton NMR Spectrum of Ribaric Acid-5,2(1,4)-Lactone in D_2O

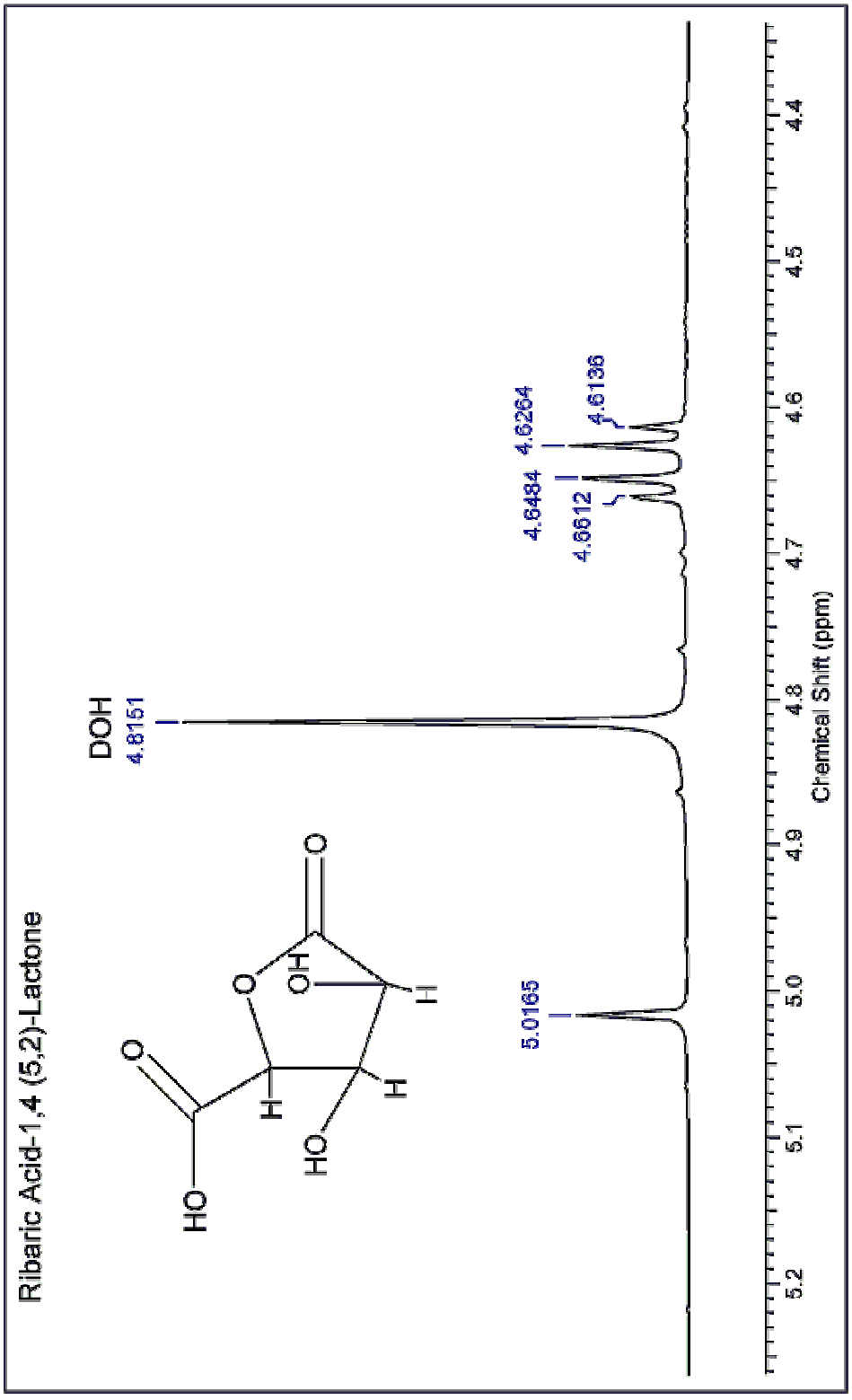

Appendix 5.2 NMR Spectra of Ethylenediammonium, Tetramethylene diammonium, Hexamethylene diammonium salts from Xylaric Acid, Disodium L-Arabinarate (Disodium L-Lyxarate), and Disodium Ribarate

Proton NMR Spectrum of Ethylenediammonium Xylarate in D_2O

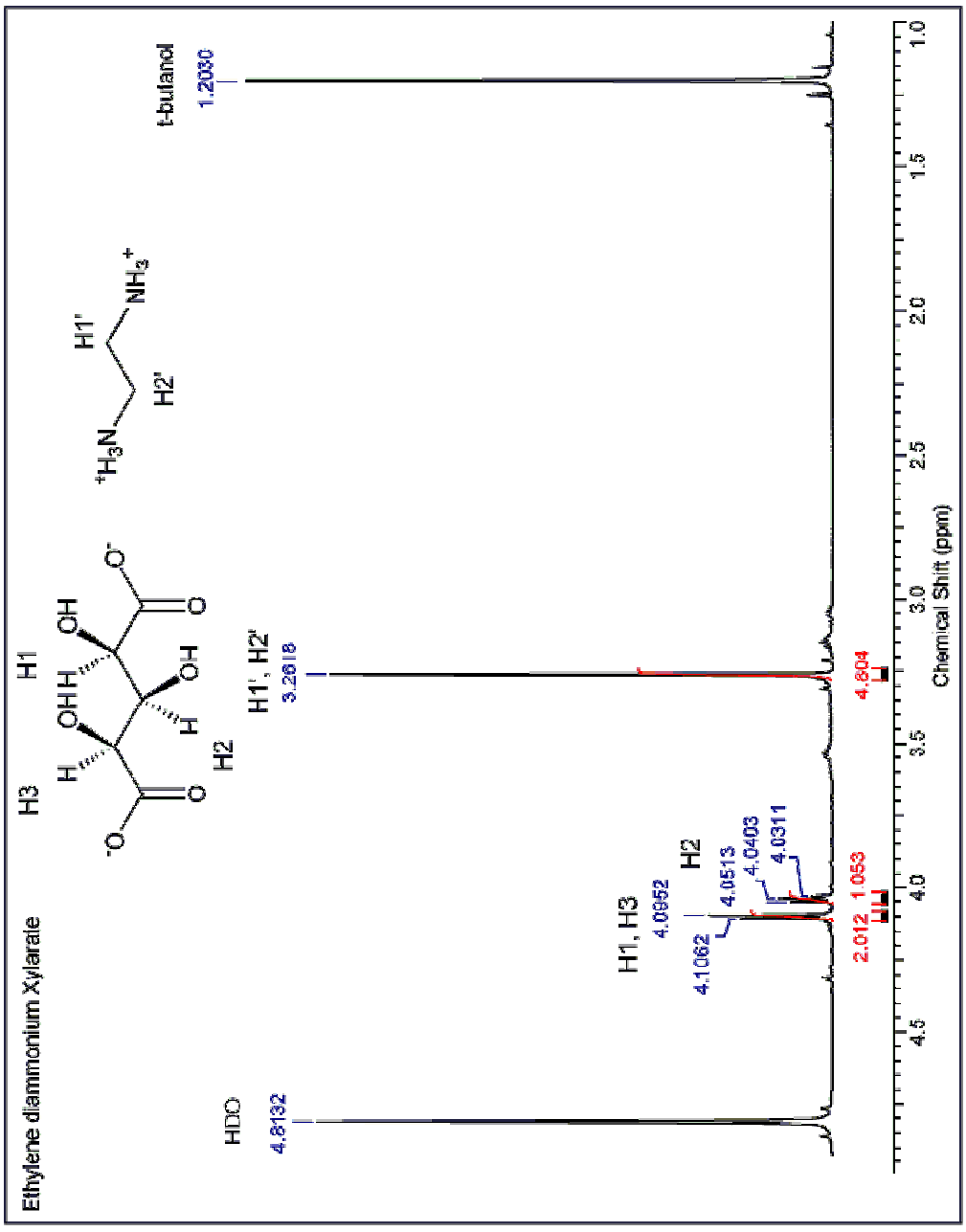

Proton NMR Spectrum of Tetramethylenediammonium Xylarate in D_2O

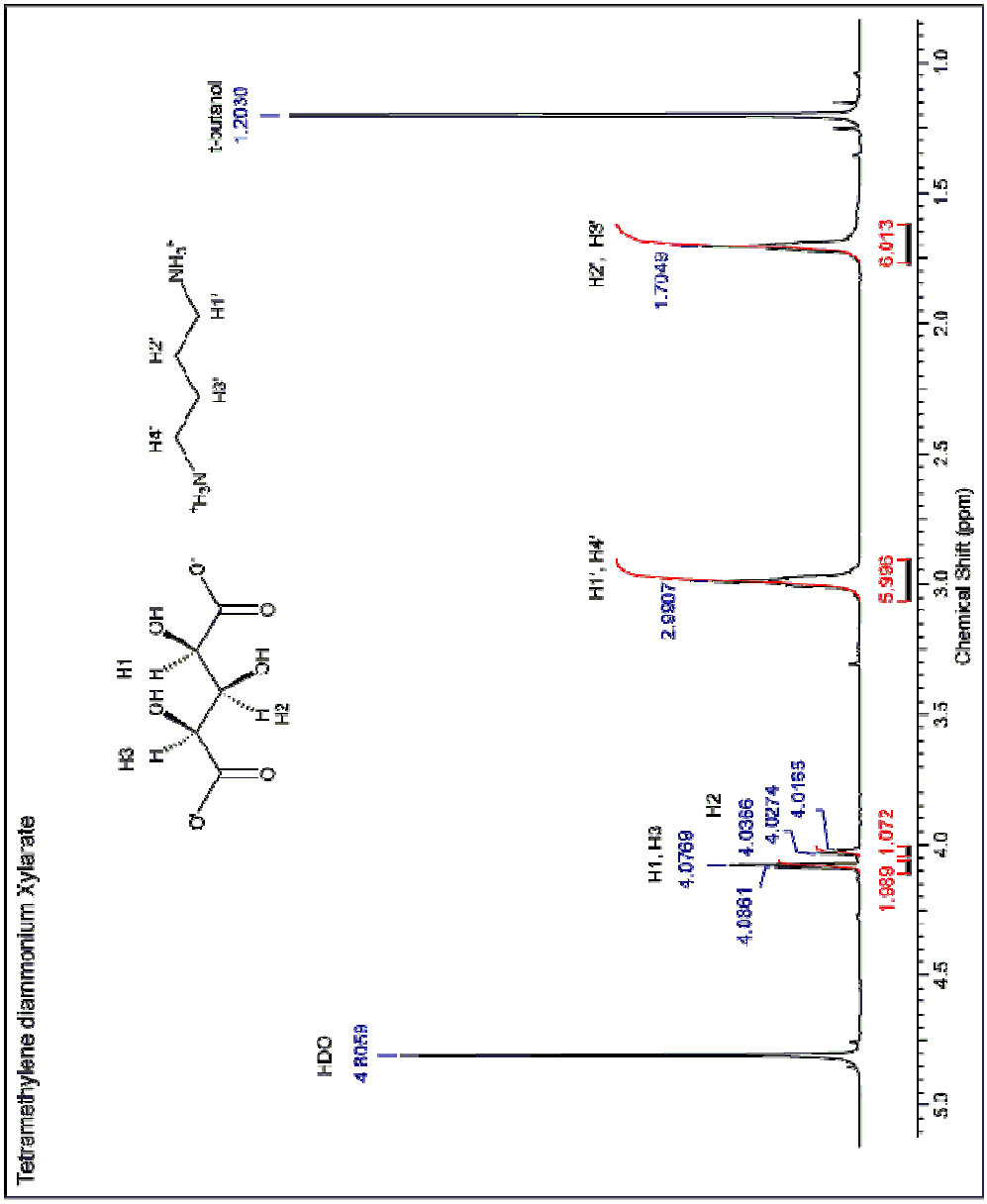

Proton NMR Spectrum of Hexamethylenediammonium Xylarate in D_2O

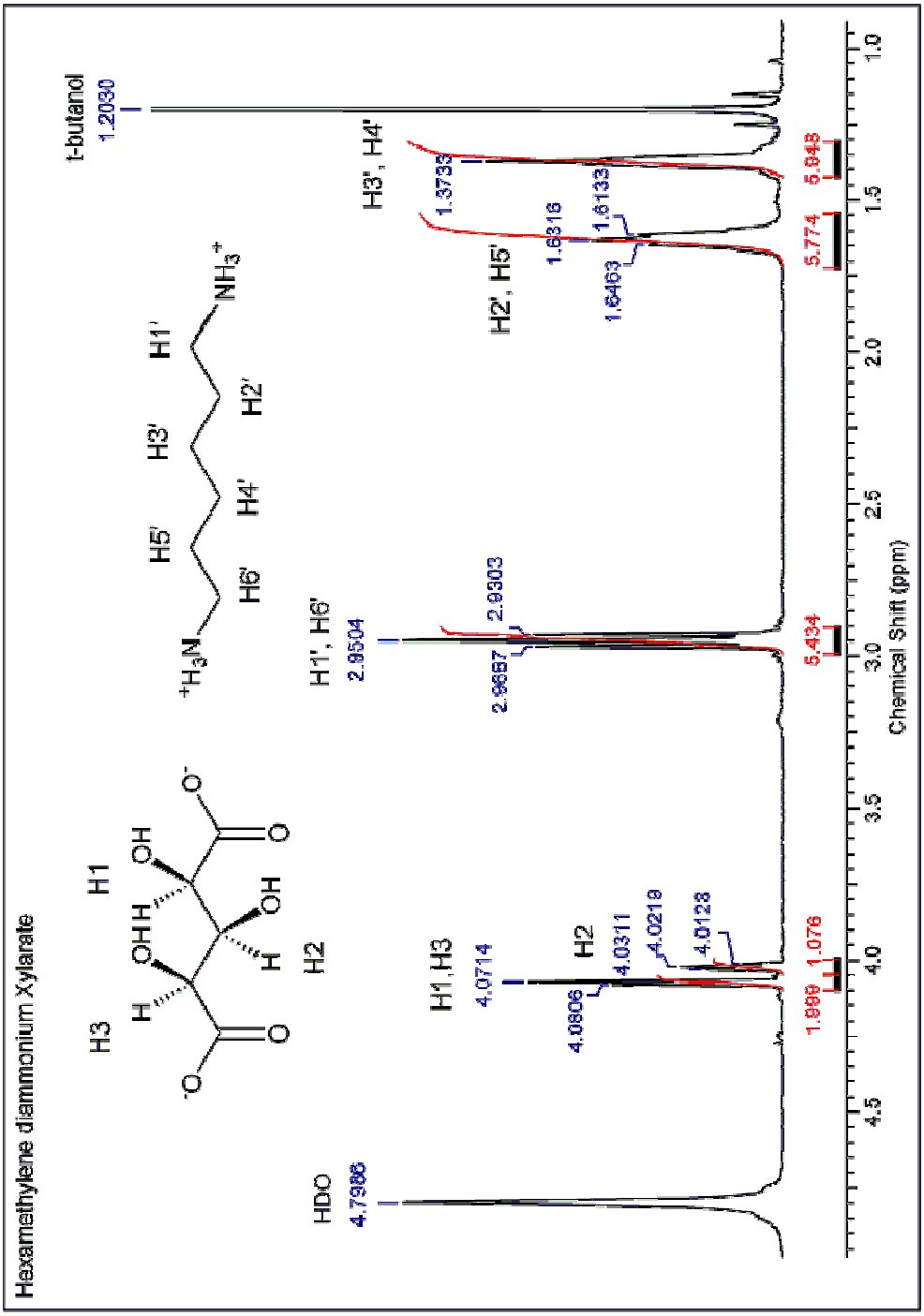

Proton NMR Spectrum of Tetramethylenediammonium L-Arabinarate in D_2O

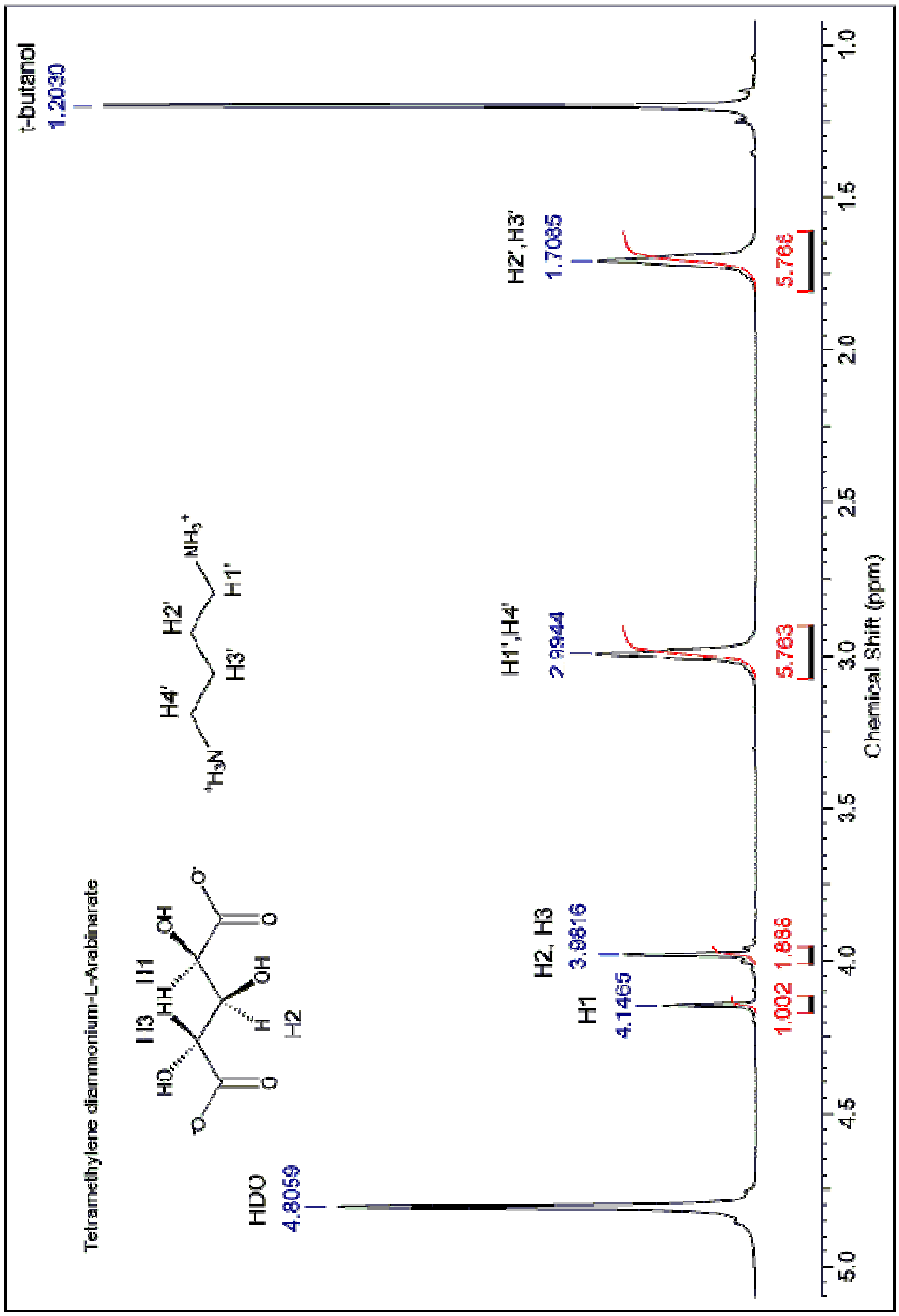

Proton NMR Spectrum of Hexamethylenediammonium L-Arabinarate in D_2O

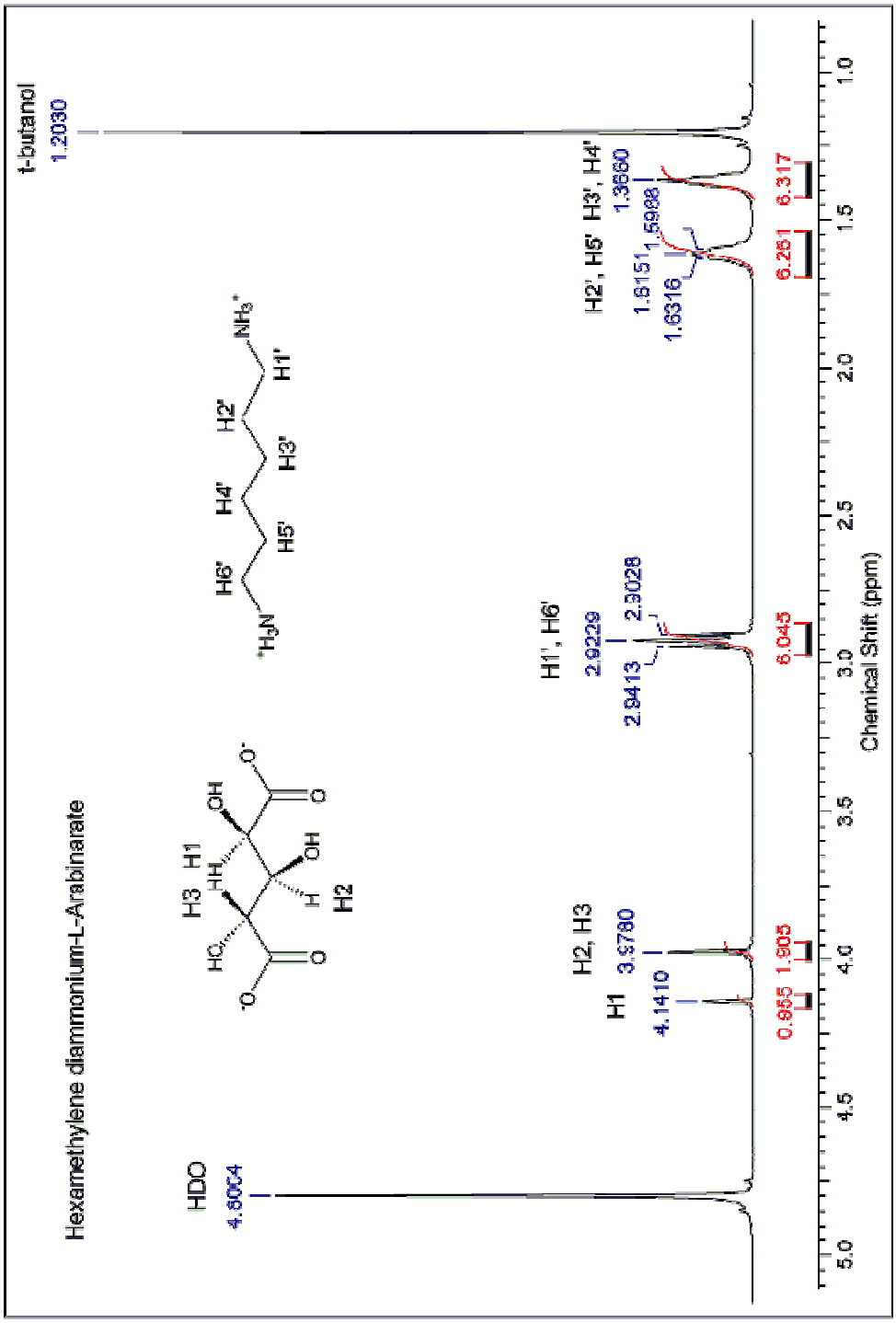

Proton NMR Spectrum of Ethylenediammonium Ribarate in D_2O

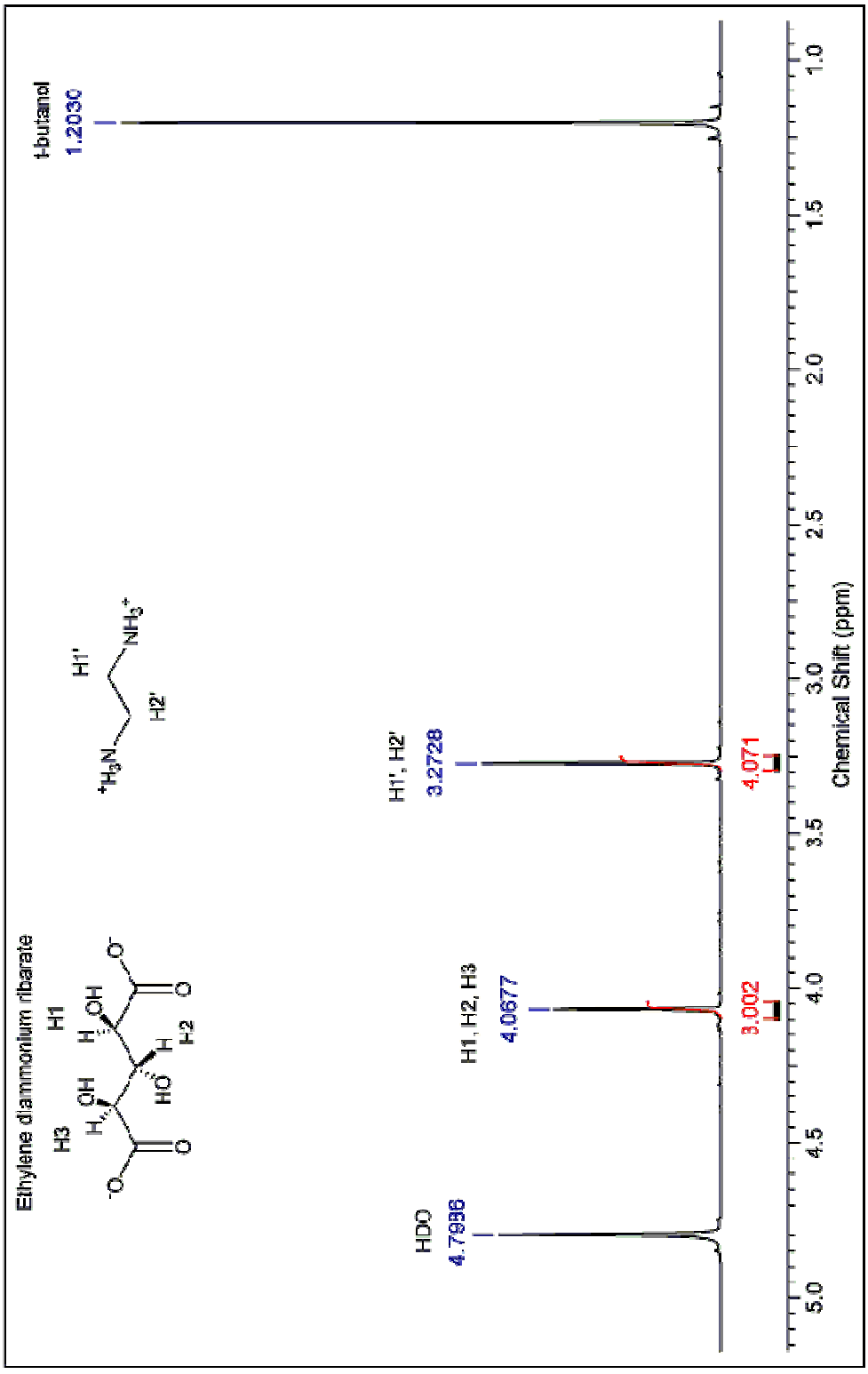

Proton NMR Spectrum of Tetramethylenediammonium Ribarate in D_2O

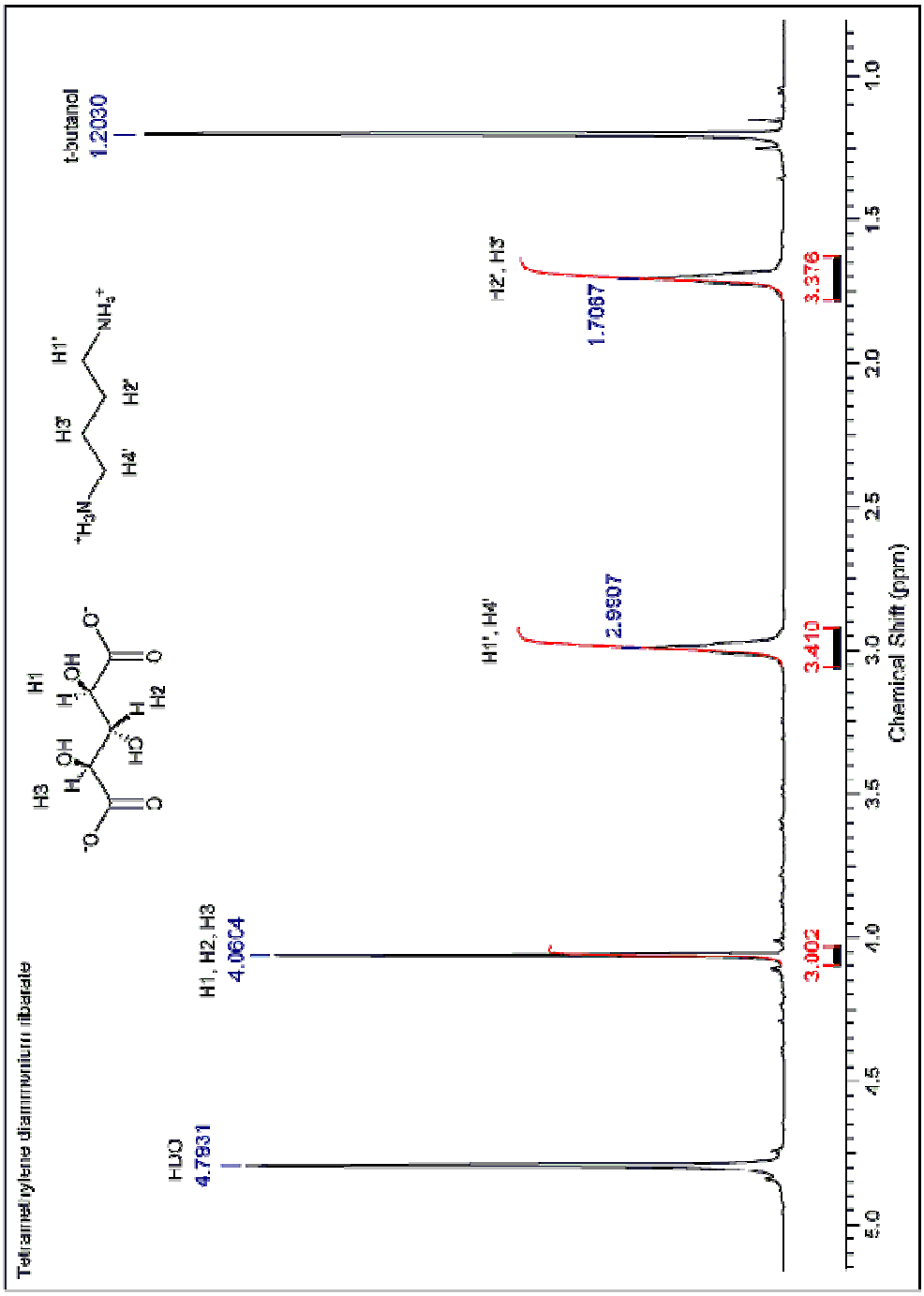

Proton NMR Spectrum of Hexamethylenediammonium Ribarate in D_2O

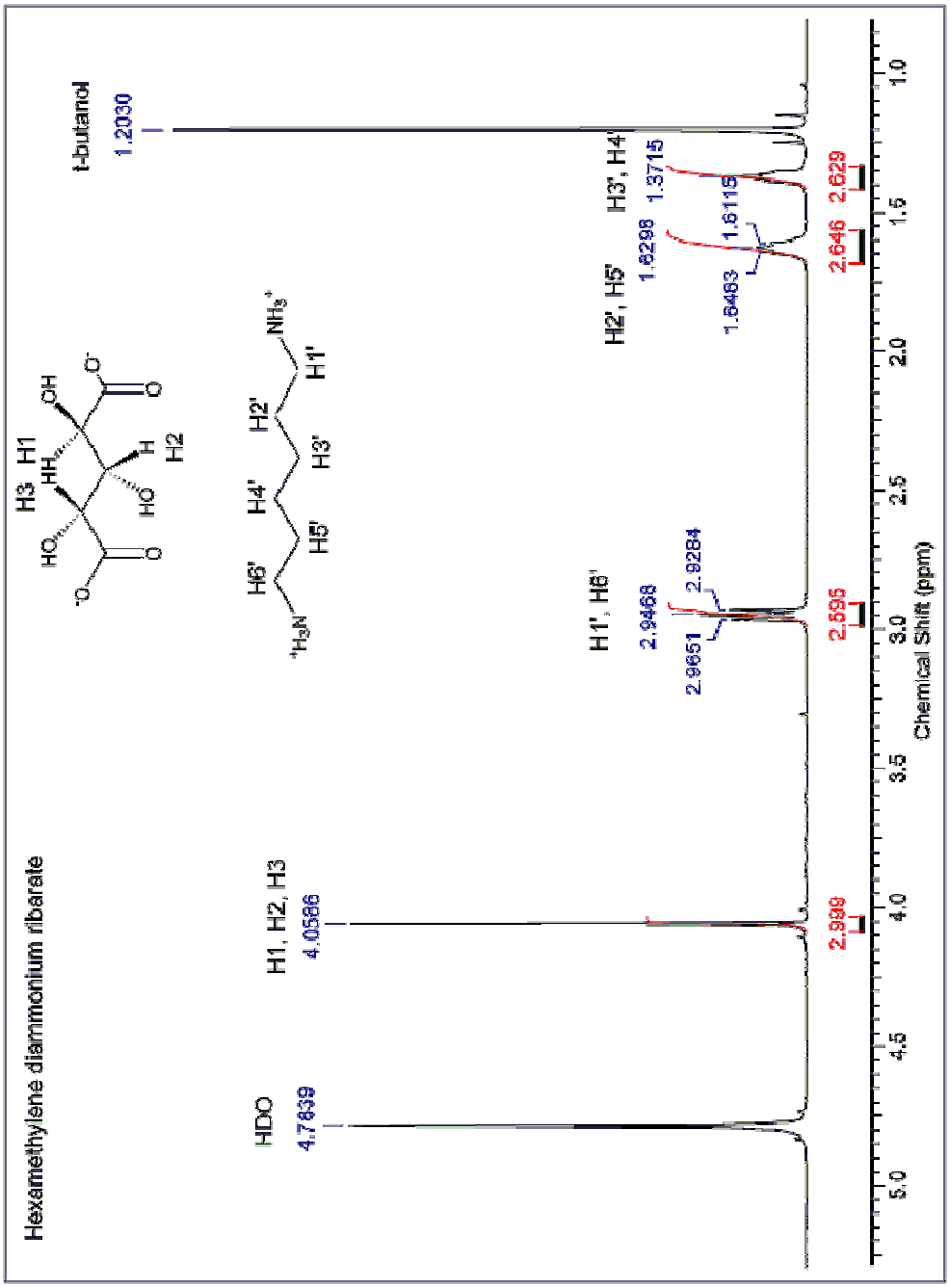

Appendix 5.3 NMR Spectra of Poly (Ethylene Aldaramides), Poly (Tetramethylene Aldaramides), and Poly (Hexamethylene Aldaramides) Prepolymers from Xylaric Acid, Disodium L-Arabinarate (Disodium L-Lyxarate), and Disodium Ribarate

Proton NMR Spectrum of poly (ethylene xylaramide) prepolymer in D_2O

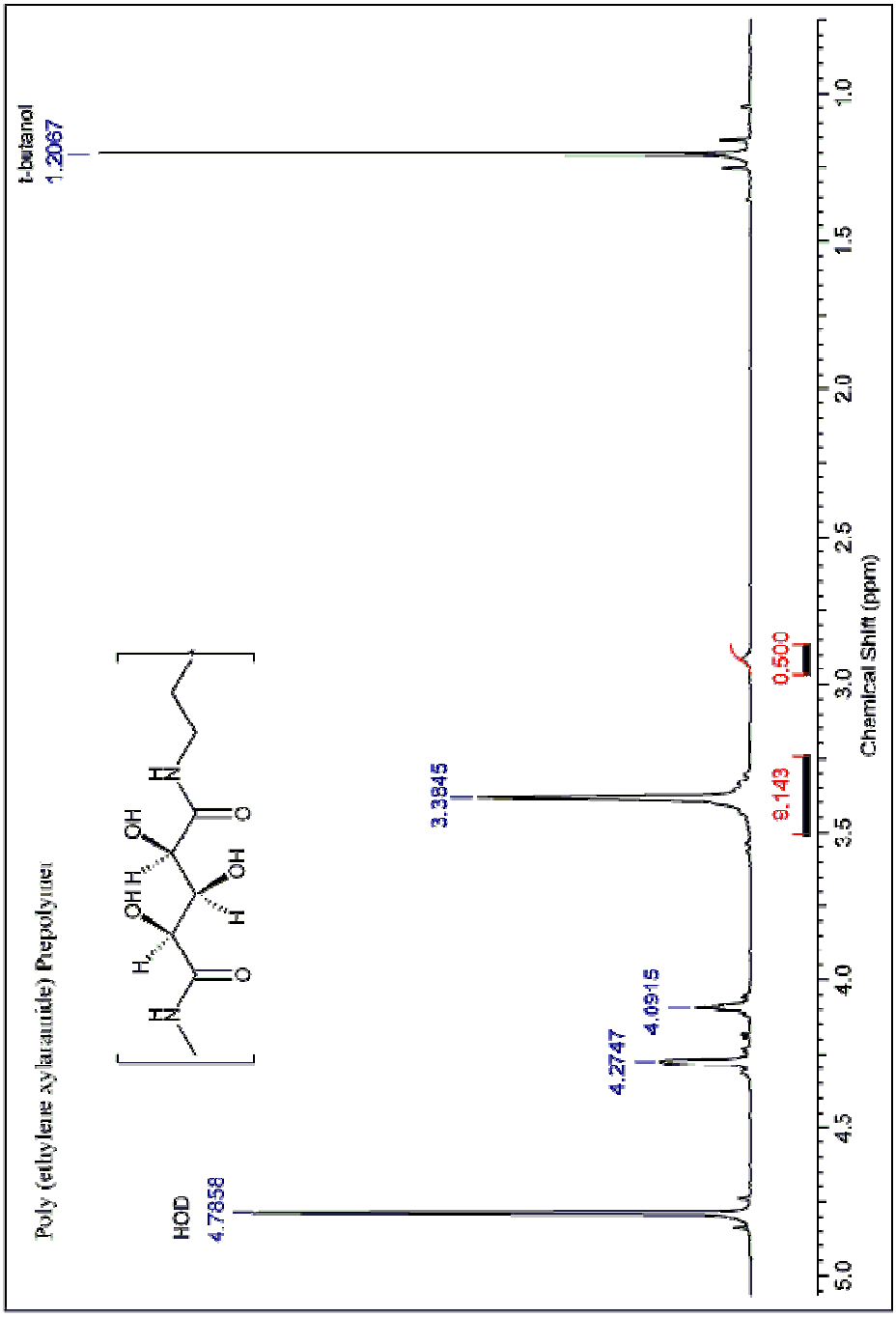

Proton NMR Spectrum of poly (Tetramethylene xylaramide) prepolymer in TFA-*d*

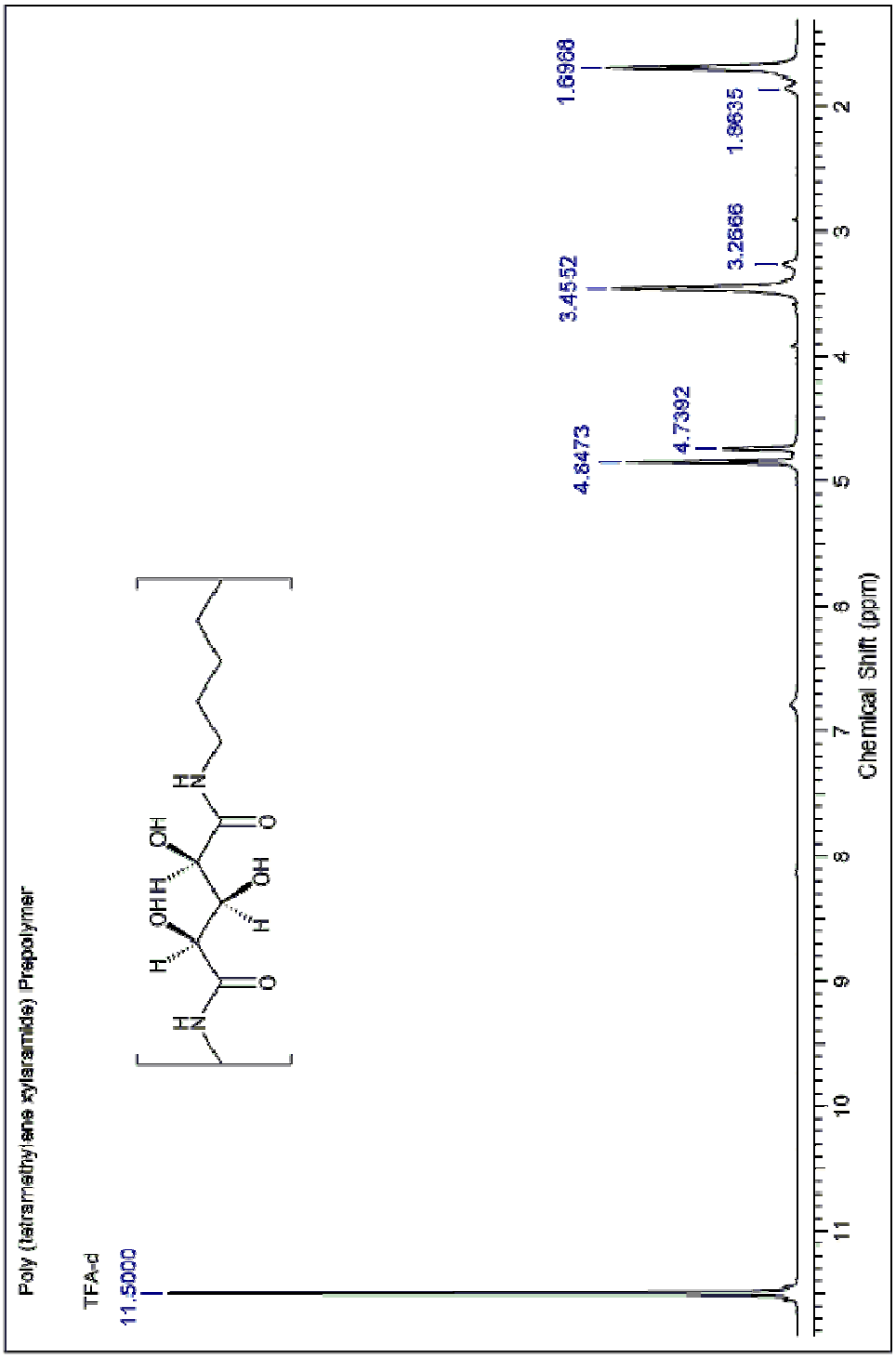

Proton NMR Spectrum of Poly (hexamethylene xylaramide) Prepolymer in DMSO-d_6 and TFA-*d*

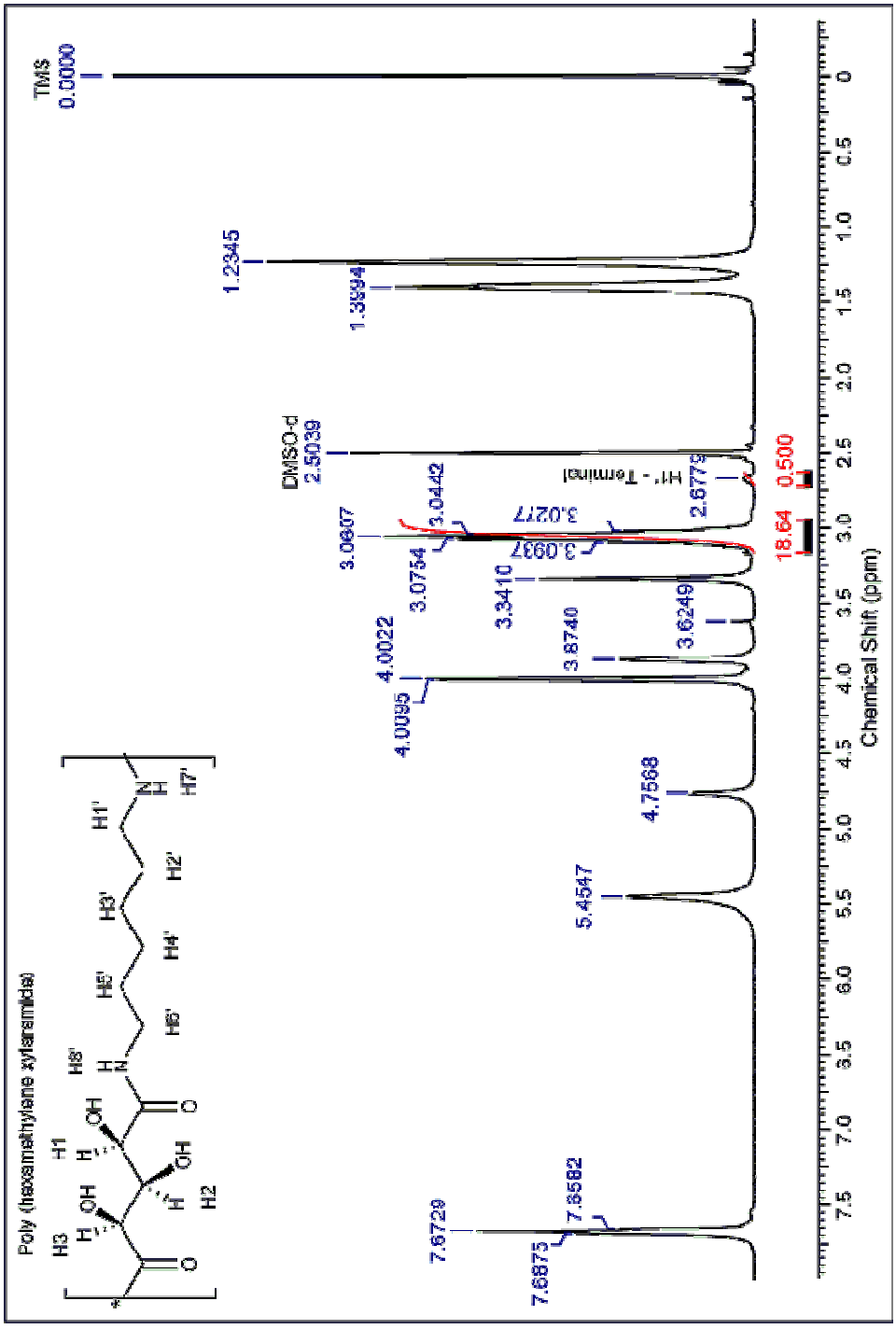

Proton NMR Spectrum of Poly (ethylene L-arabinaramide) Prepolymer in DMSO-d_6 and TFA-*d*

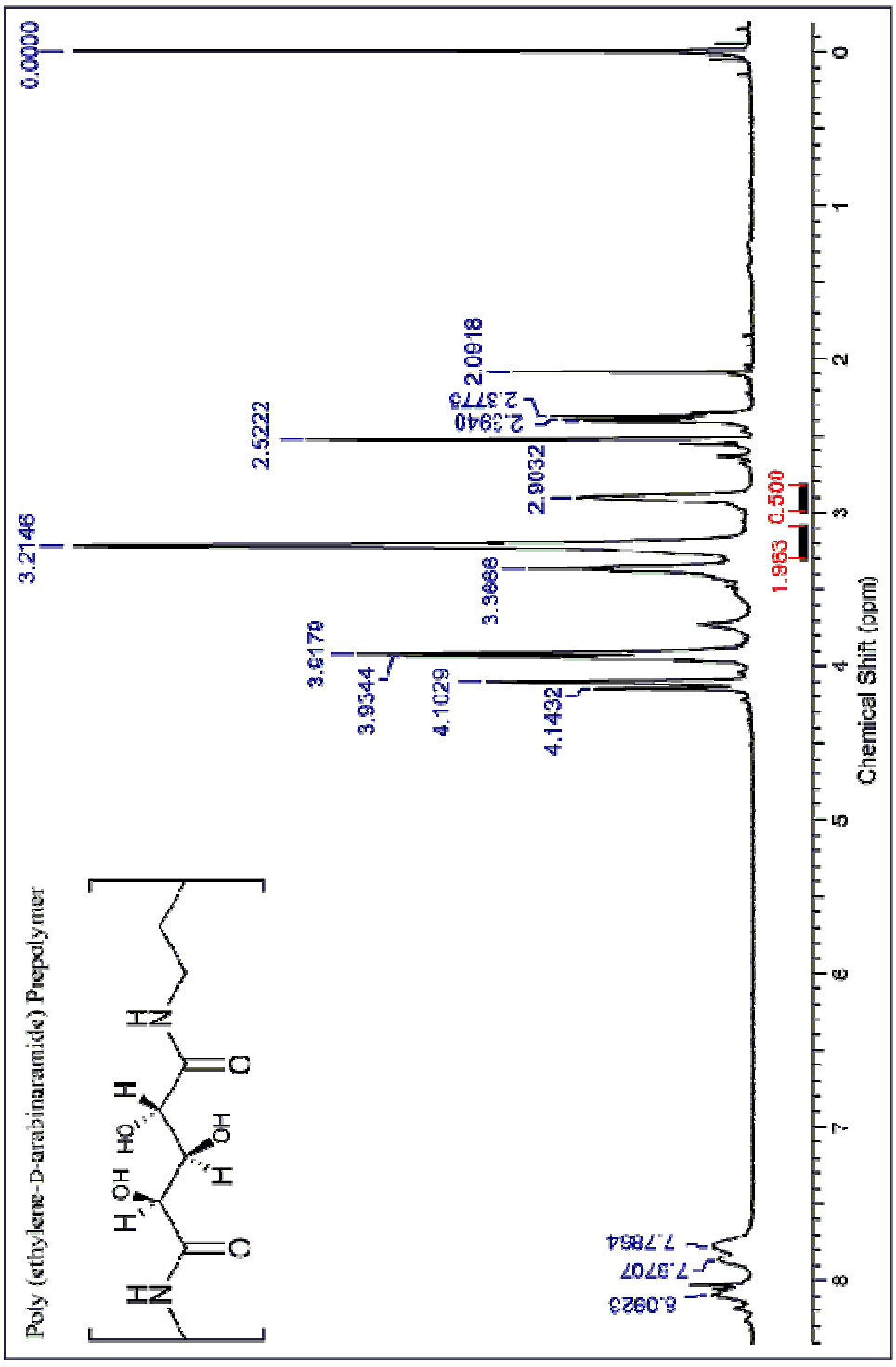

Proton NMR Spectrum of Poly (tetramethylene L-arabinaramide) Prepolymer in DMSO-d_6 and TFA-*d*

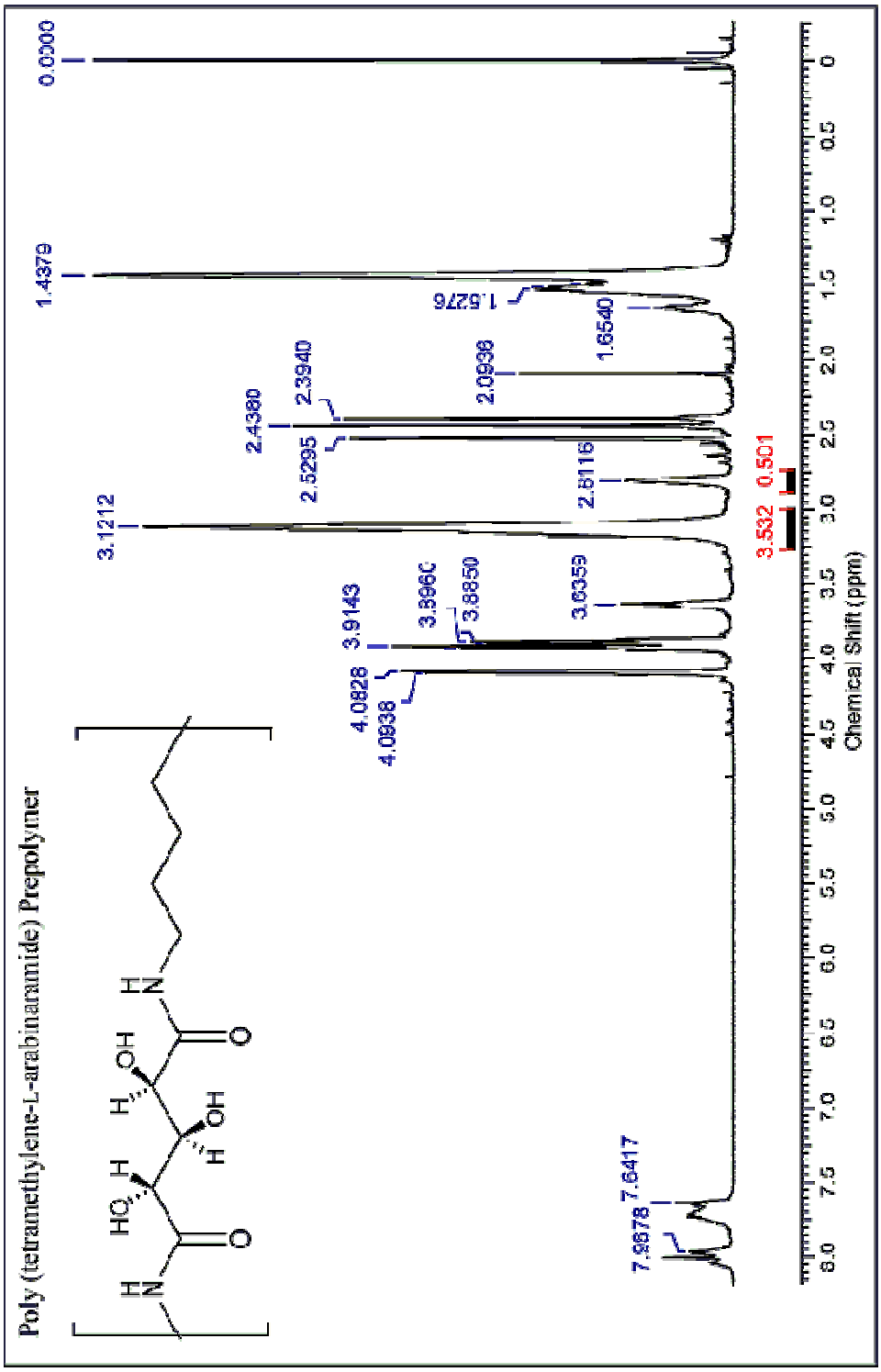

Proton NMR Spectrum of Poly (hexamethylene L-arabinaramide) Prepolymer in DMSO-d_6 and TFA-*d*

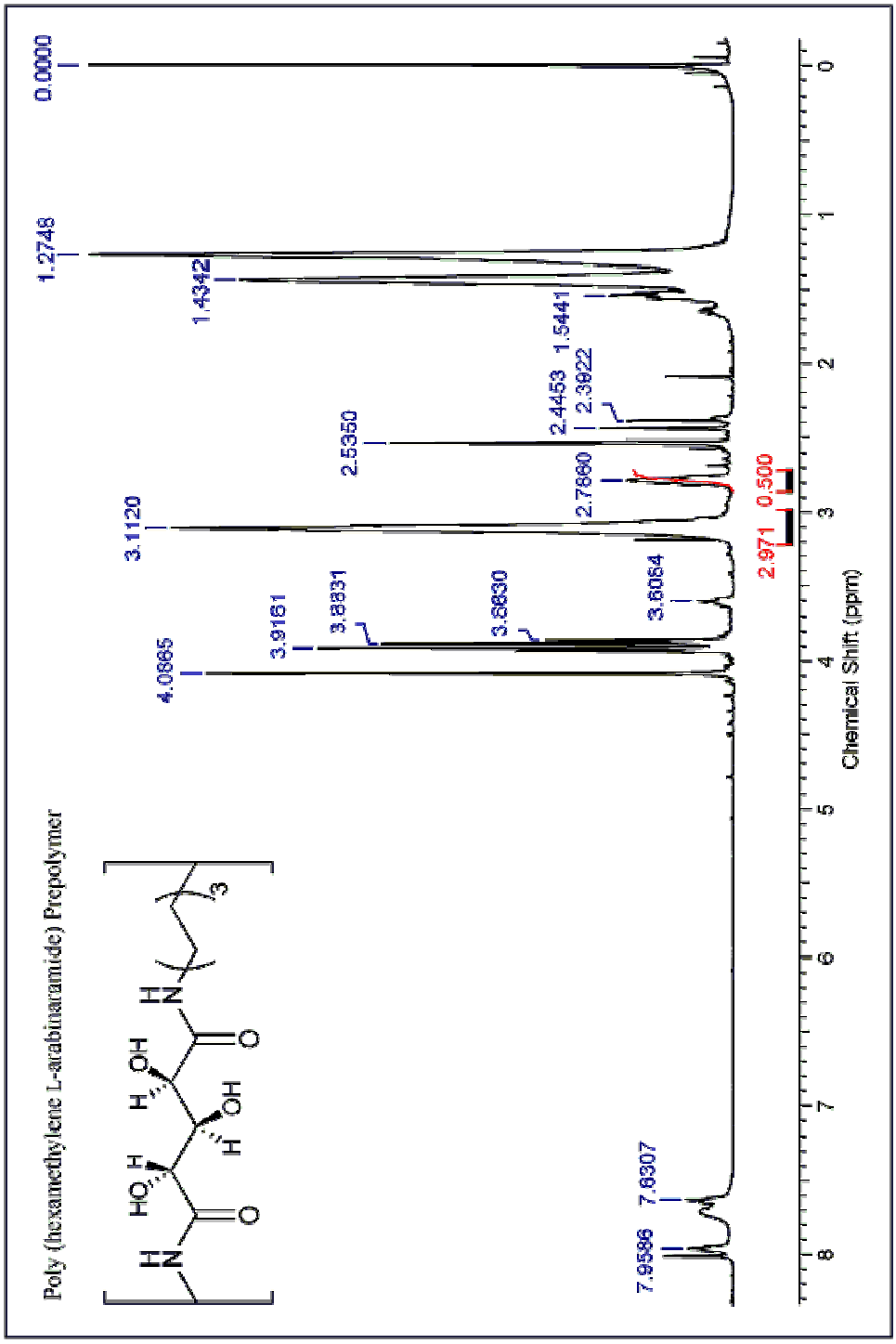

Proton NMR Spectrum of Poly (ethylene ribaramide) Prepolymer in DMSO-d_6 and TFA-*d*

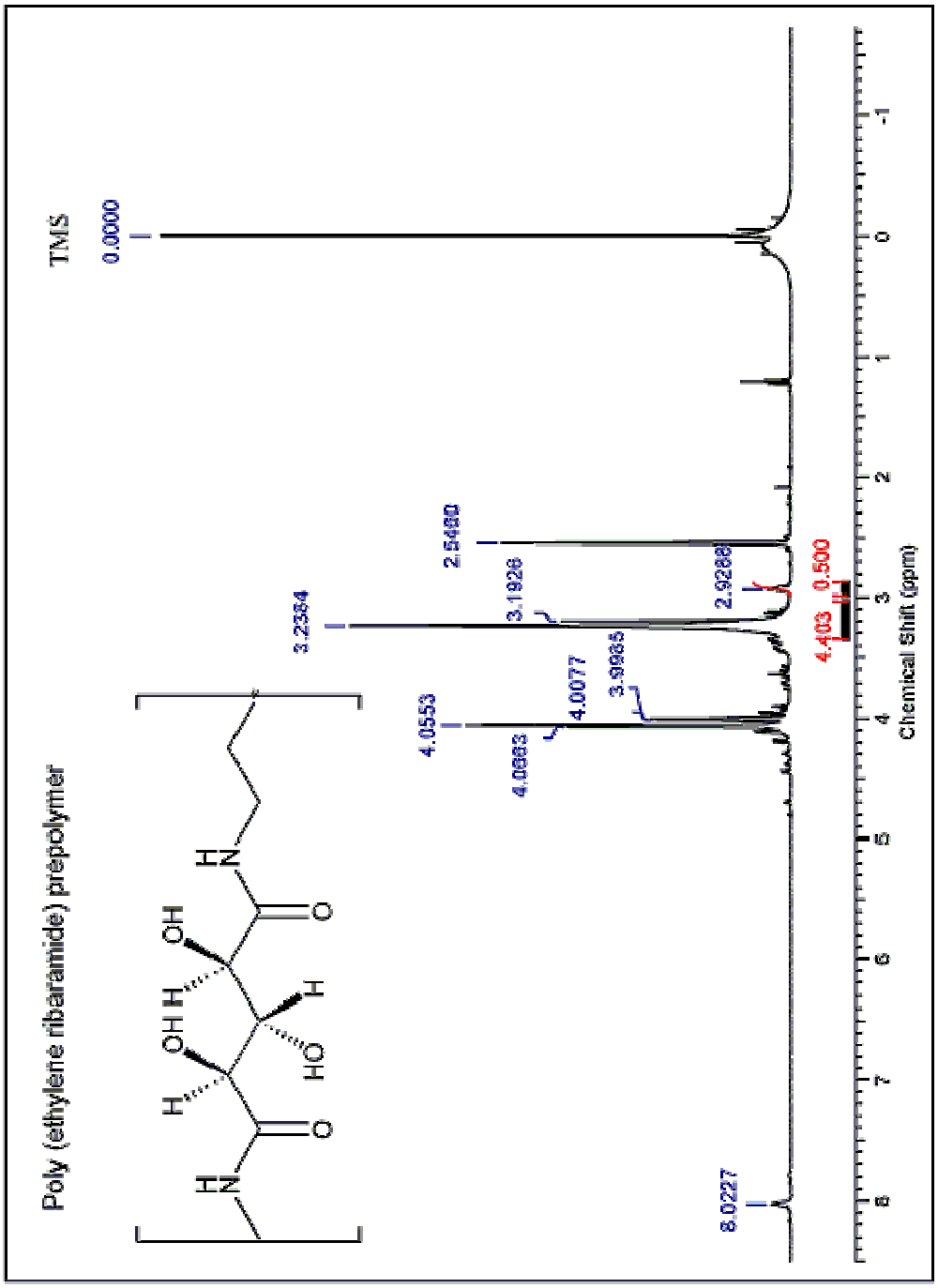

Proton NMR Spectrum of Poly (tetramethylene ribaramide) Prepolymer in DMSO-d_6 and TFA-*d*

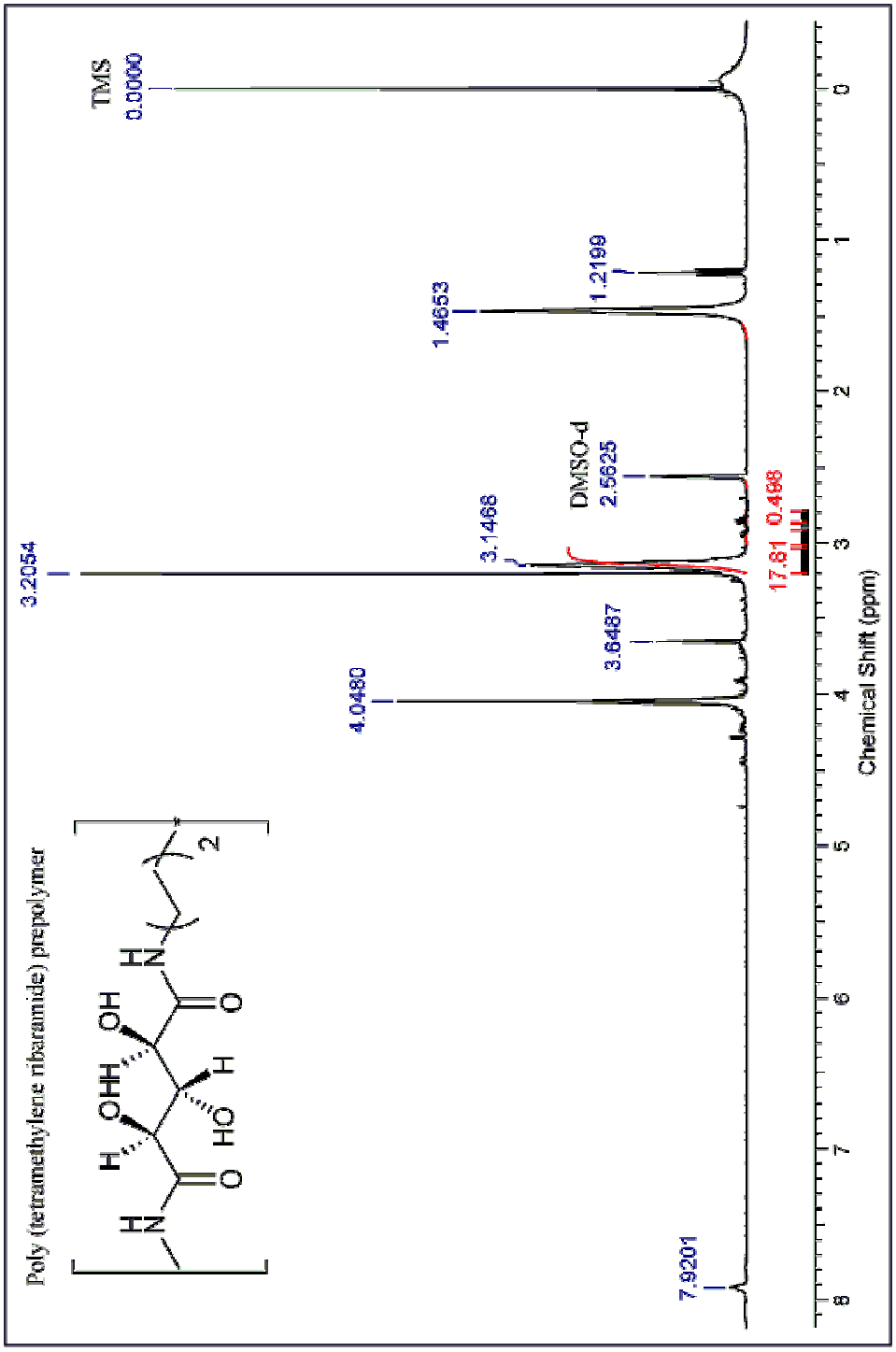

Proton NMR Spectrum of Poly (hexamethylene ribaramide) Prepolymer in DMSO-d_6 and TFA-*d*

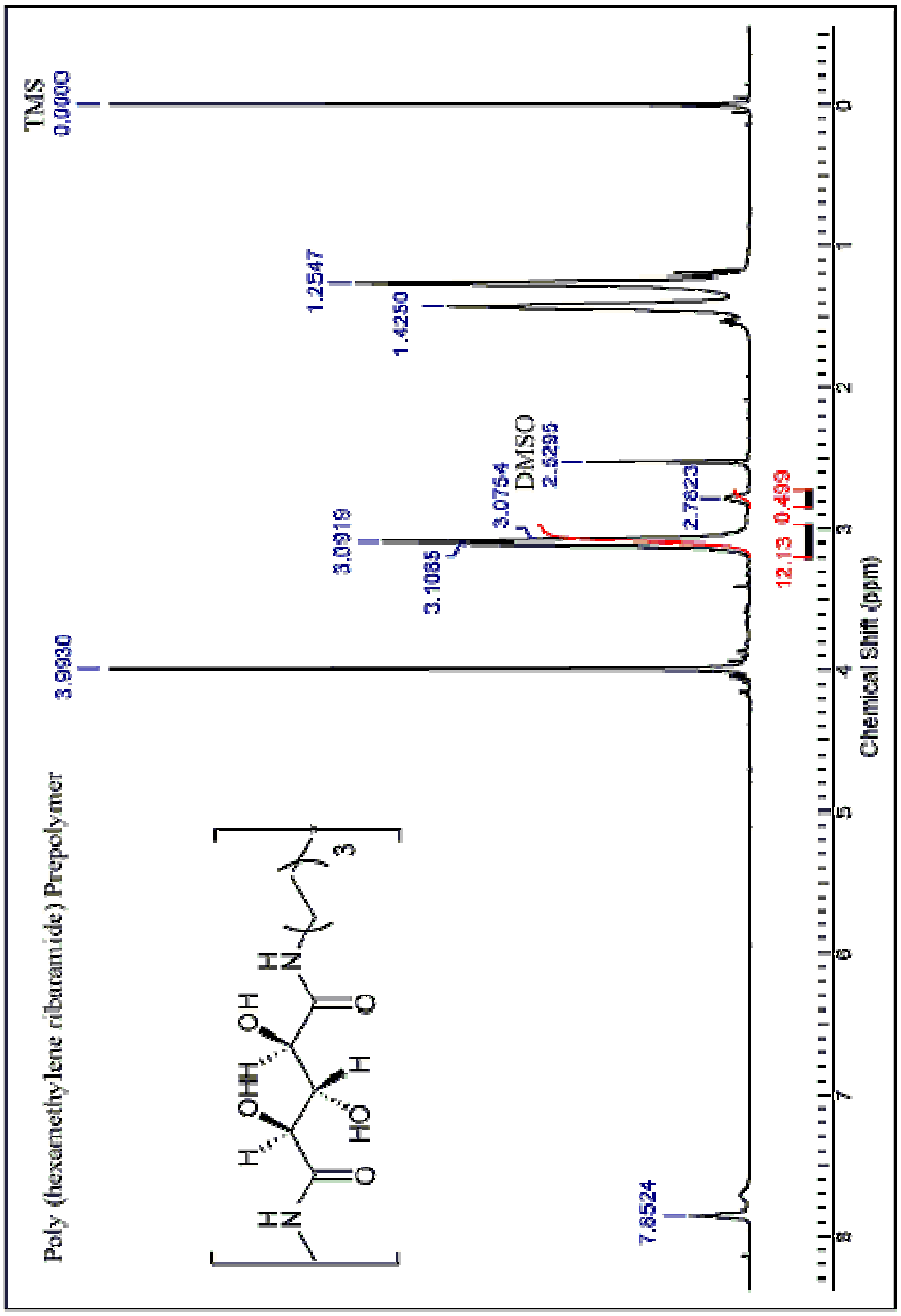

Appendix 5.4 NMR Spectra of glutaramide, *N*,*N*'-dimethylglutaramide, *N*,*N*'-dihexyl xylaramide, *N*,*N*'-dimethylxylaramide, 2,3,4-tri-*O*-acetyl-*N*,*N*'-dimethylxylaramide, *N*,*N*'-dimethyl L-arabinaramide, 2,3,4-tri-*O*-acetyl-*N*,*N*'-dimethyl L-arabinaramide, *N*,*N*'-dimethylribaramide, and 2,3,4-tri-*O*-acetyl- *N*,*N*'-dimethylribaramide

Proton NMR Spectrum of glutaramide in DMSO-d_6

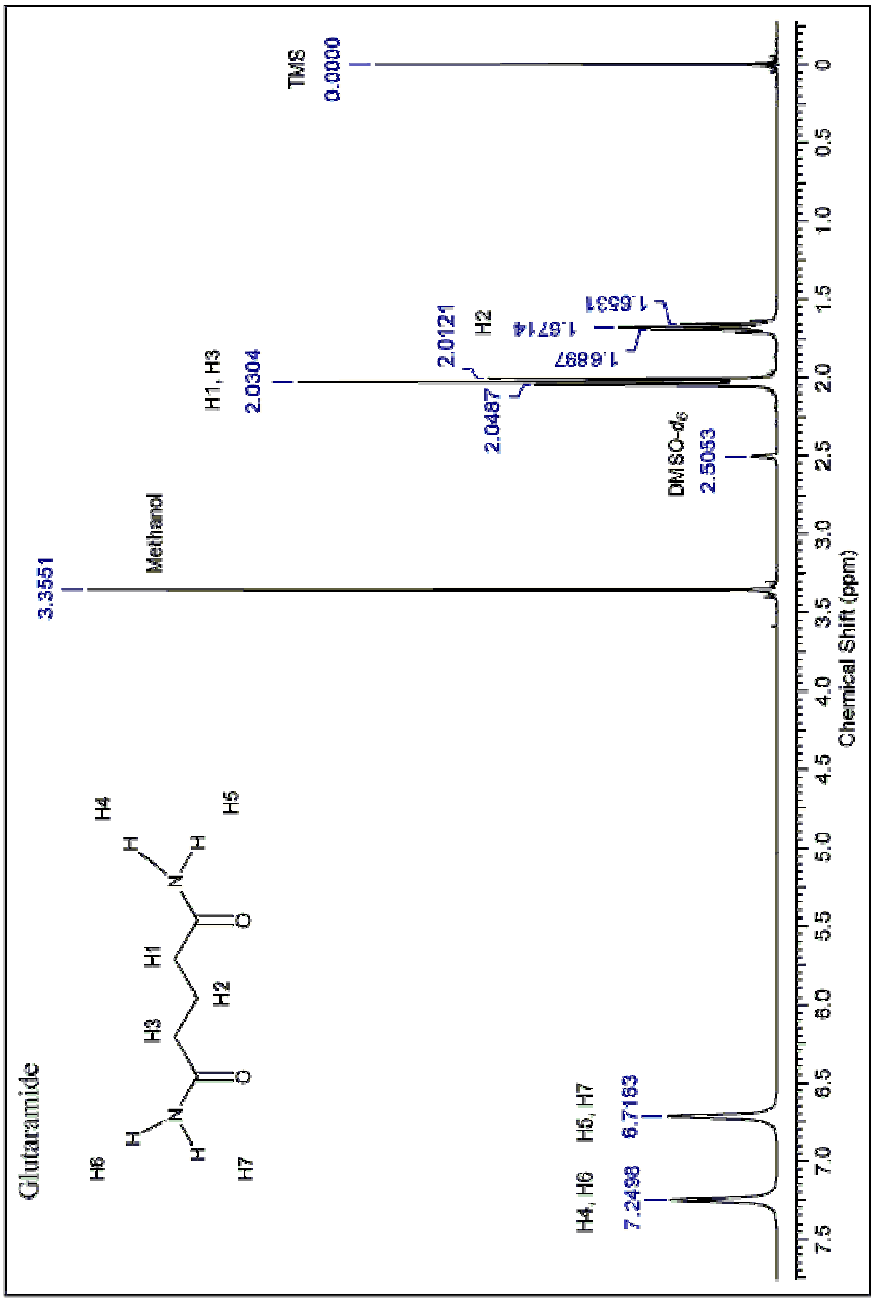

Proton NMR Spectrum of *N,N'*-dimethylglutaramide in chloroform-*d*

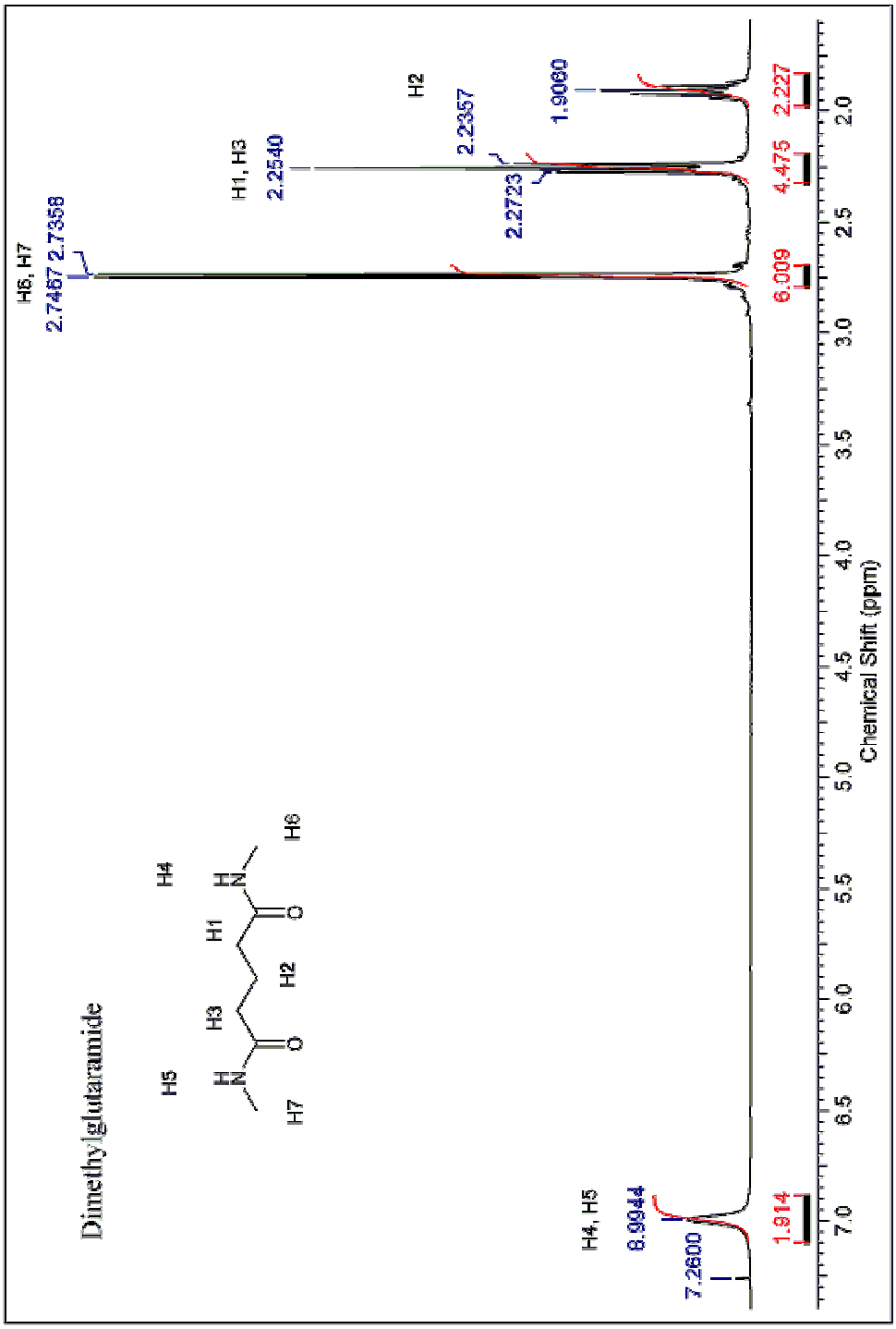

Proton NMR Spectrum of *N,N'*-dihexylglutaramide in DMSO-d_6

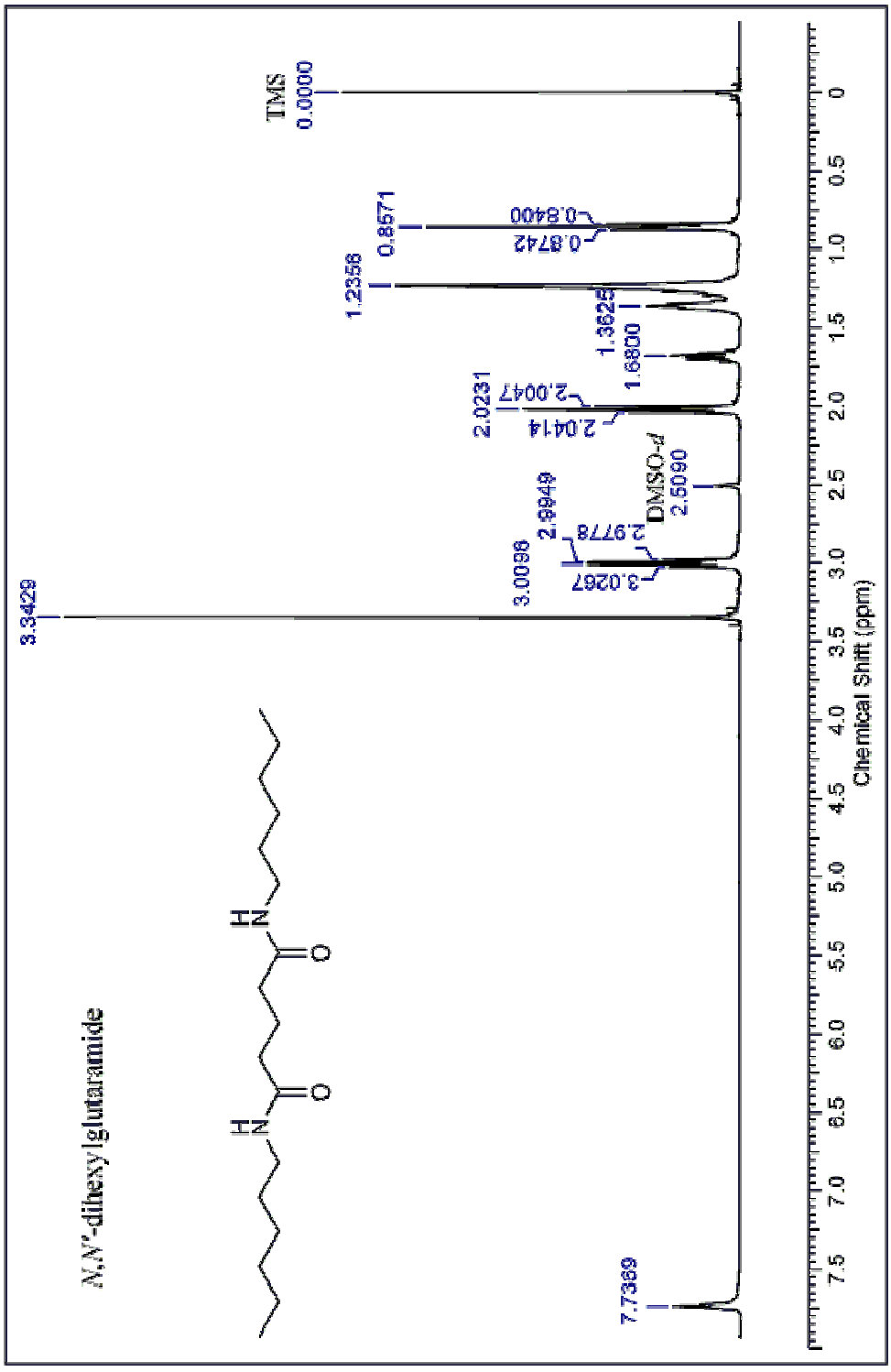

Proton NMR Spectrum of *N,N'*-dimethylxylaramide D_2O

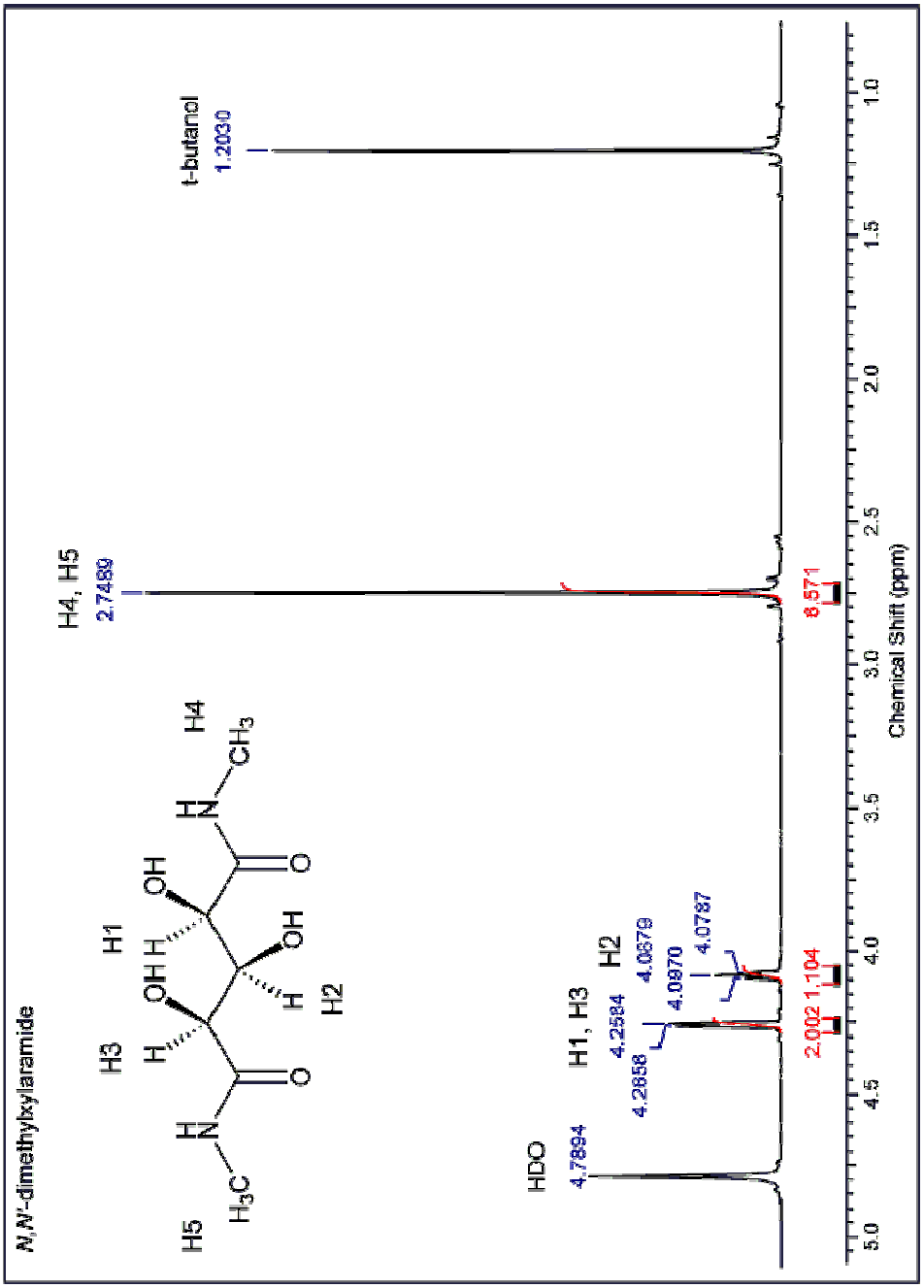

Proton NMR Spectrum of 2,3,4-Tri-*O*-acetyl-*N,N'*-dimethylxylaramide chloroform-*d*

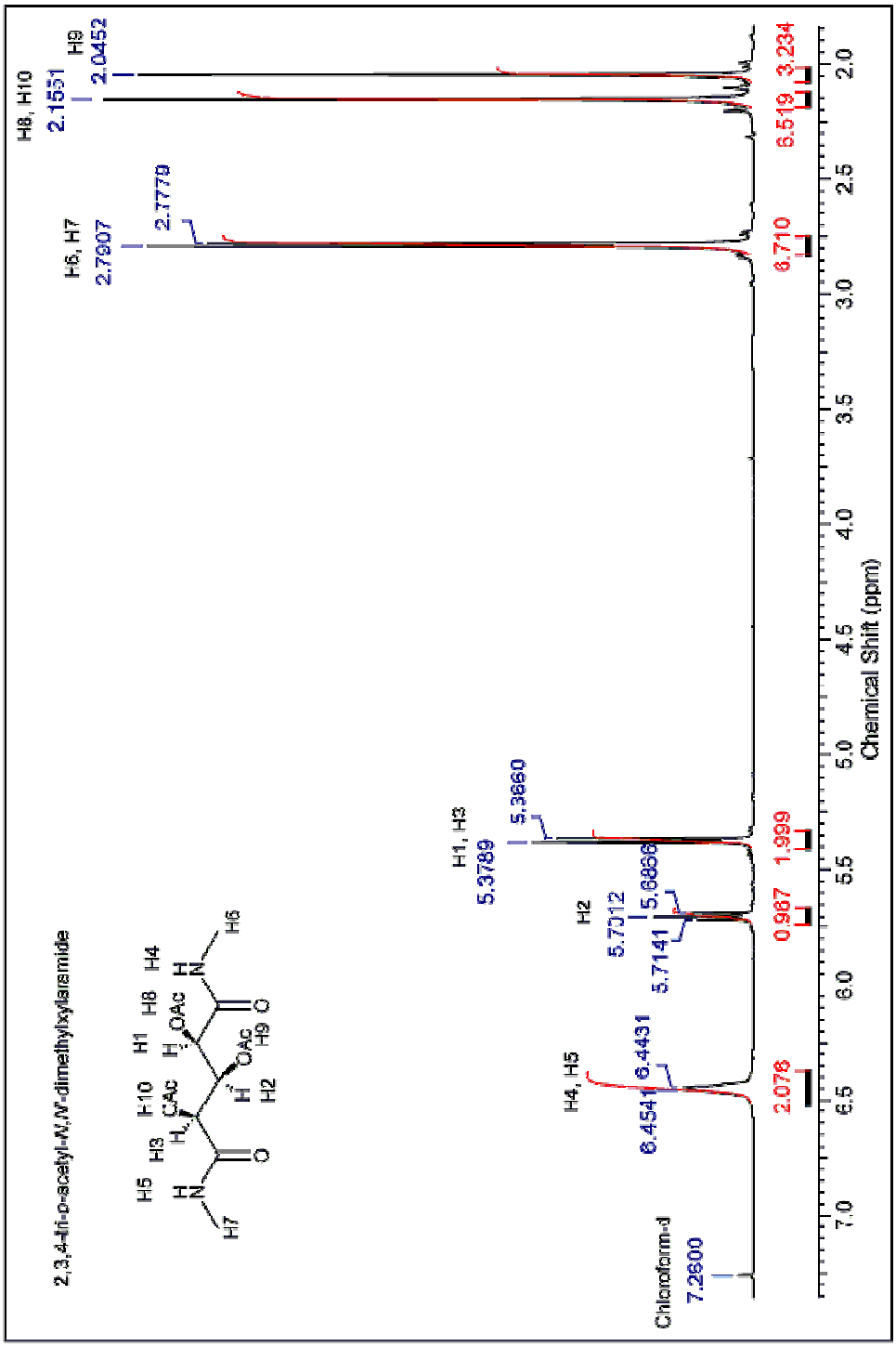

Proton NMR Spectrum of *N,N'*-dimethyl L-arabinaramide DMSO-d_6

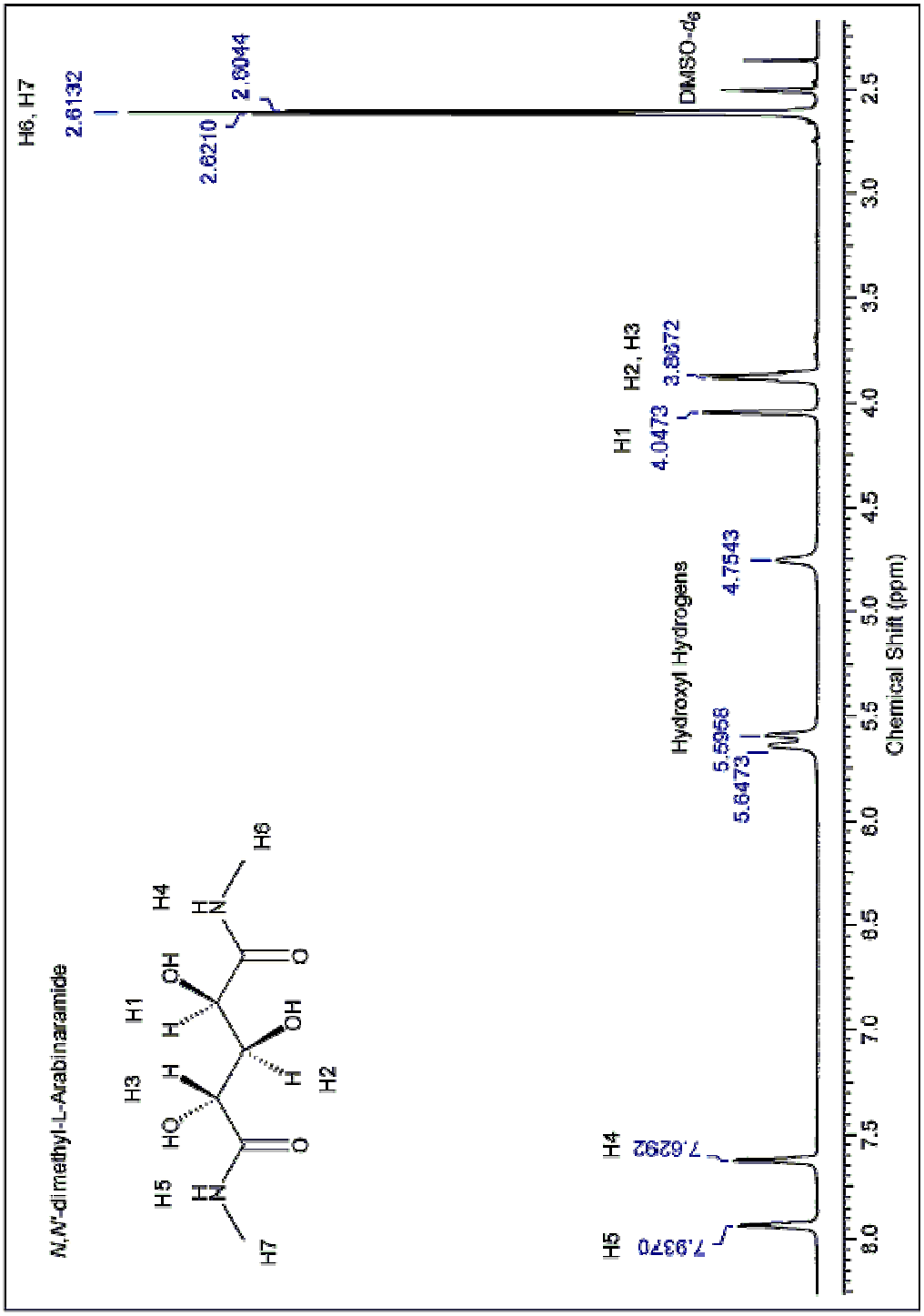

Proton NMR Spectrum of 2,3,4-Tri-*O*-acetyl-*N,N'*-dimethyl L-arabinaramide chloroform-*d*

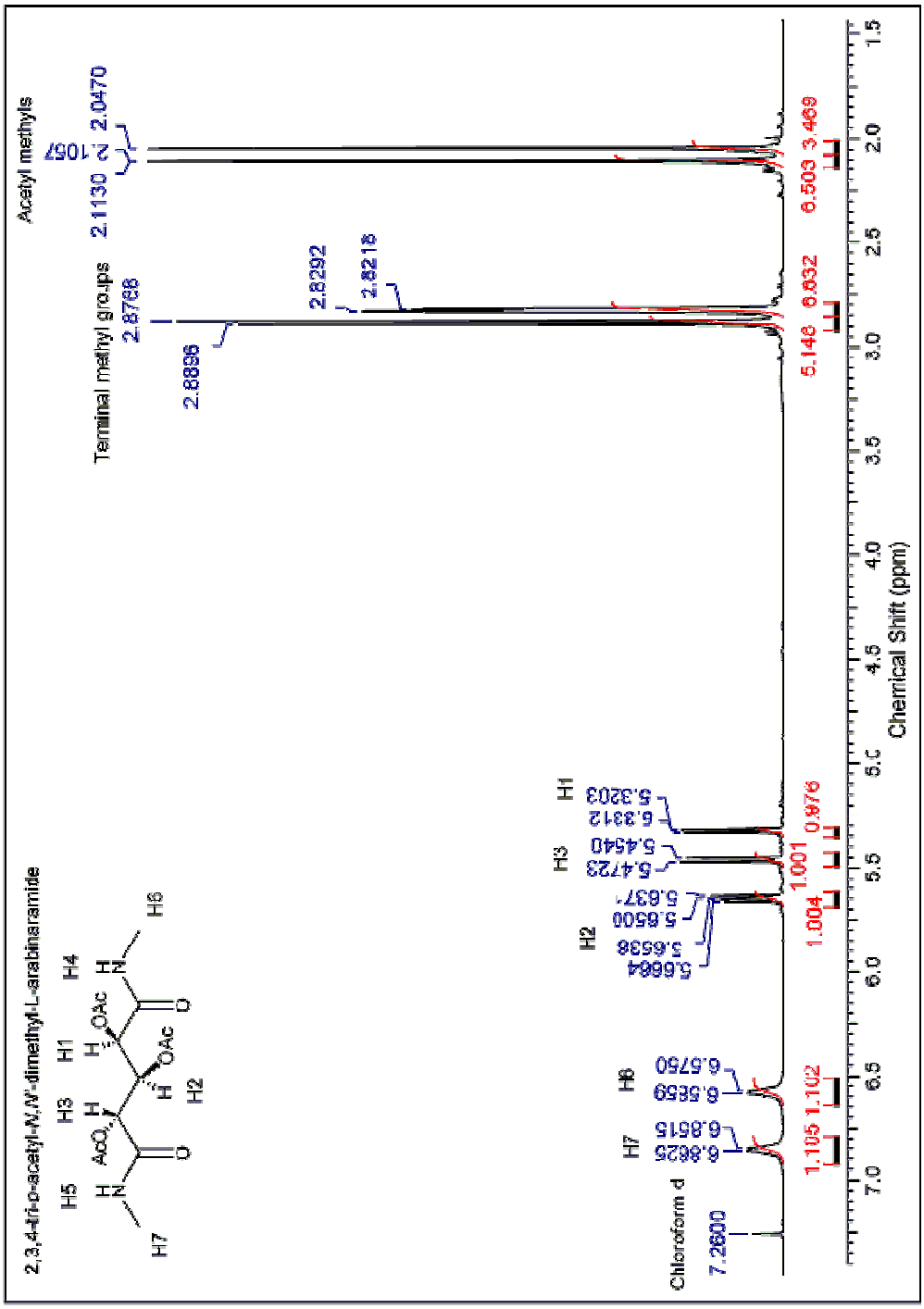

Proton NMR Spectrum of *N,N'*-dimethylribaramide D_2O

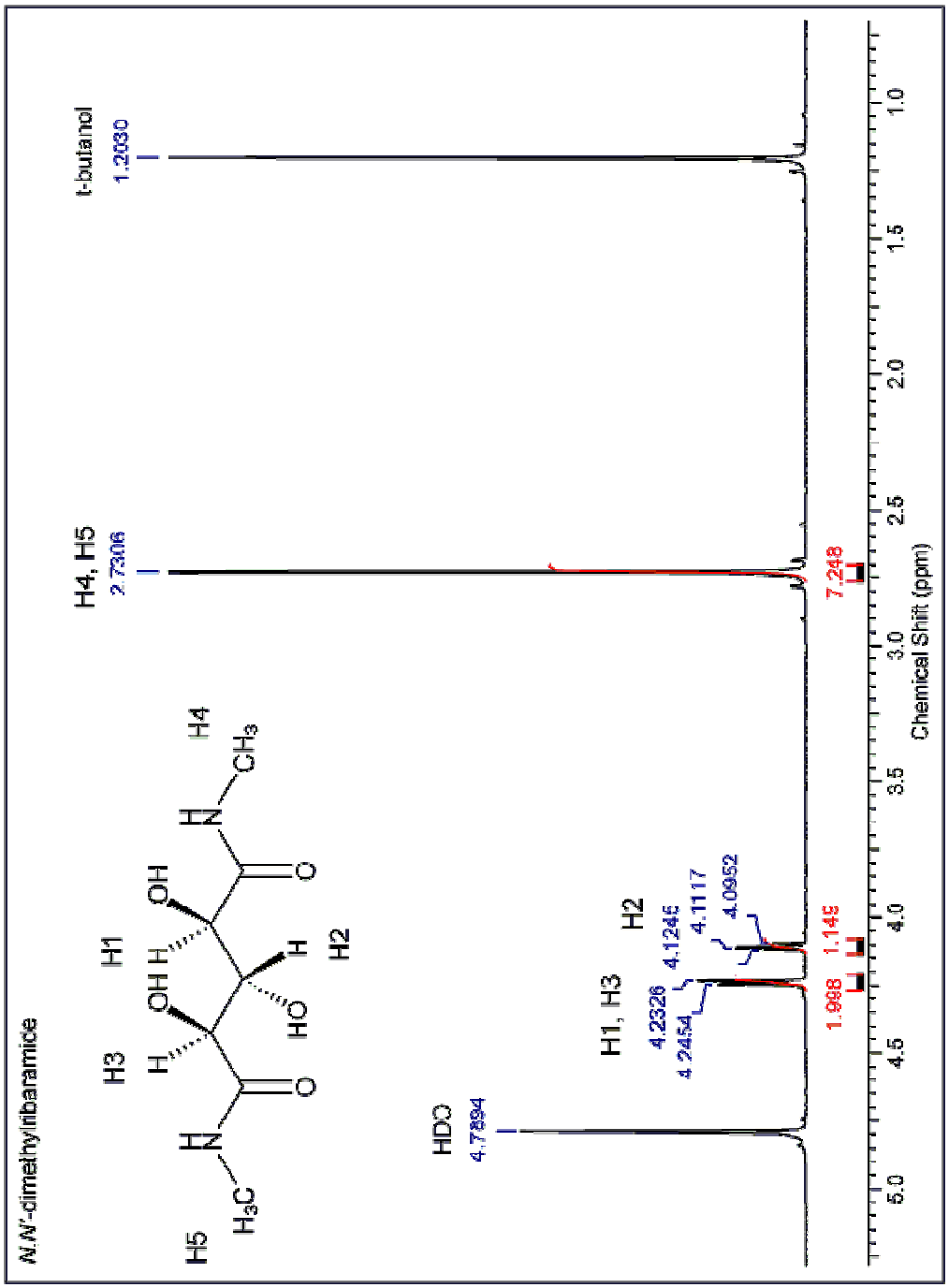

Proton NMR Spectrum of 2,3,4-Tri-*O*-acetyl-*N,N'*-dimethylribaramide chloroform-*d*

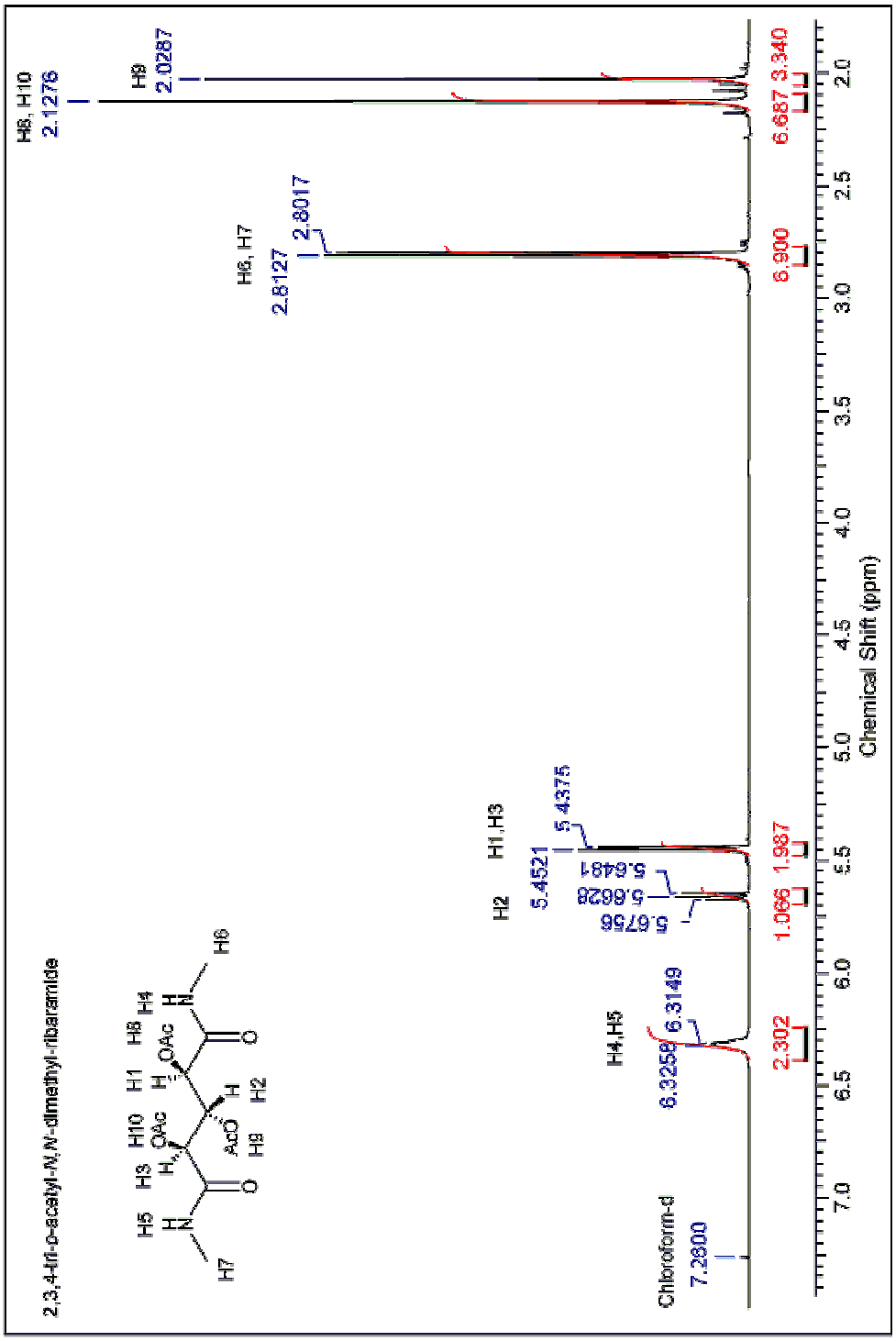

Appendix 5.5 Complete Bond Lengths, Bond Angles, Principle Torsion Angles and Thermal and Positional Parameters for *N,N'*-Dihexylglutaramide

Table 5.1 Atomic coordinates (x 10^4) and equivalent isotropic displacement parameters (Å^2 x 10^3) for *N,N'*-dihexylglutaramide. U(eq) is defined as one third of the trace of the orthogonalized Uij tensor

	x	y	z	U(eq)
O(1)	4439(1)	2180(2)	5631(1)	24(1)
N(1)	4286(1)	-313(2)	7525(1)	22(1)
C(1)	4471(1)	1585(2)	7002(1)	19(1)
C(2)	4715(1)	3019(2)	8180(1)	21(1)
C(3)	5000	4586(3)	7500	21(1)
C(4)	4041(1)	-1843(2)	6517(1)	22(1)
C(5)	3796(1)	-3424(2)	7397(1)	21(1)
C(6)	3543(1)	-5016(2)	6325(1)	24(1)
C(7)	3296(1)	-6751(2)	7102(1)	23(1)
C(8)	3046(1)	-8240(2)	5960(2)	27(1)
C(9)	2804(1)	-10071(2)	6691(2)	29(1)

Table 5.2 Bond lengths [Å] and angles [deg] for *N,N'*-dihexylglutaramide

O(1)-C(1)	1.2478(15)
N(1)-C(1)	1.3383(16)
N(1)-C(4)	1.4620(16)
N(1)-HN	0.861(16)
C(1)-C(2)	1.5193(17)
C(2)-C(3)	1.5289(15)
C(2)-H(1)	0.980(14)
C(2)-H(2)	0.986(14)
C(3)-C(2)#1	1.5289(15)
C(3)-H(3)	1.008(14)
C(4)-C(5)	1.5210(17)
C(4)-H(41)	0.984(14)
C(4)-H(42)	0.969(15)
C(5)-C(6)	1.5263(17)
C(5)-H(51)	0.970(15)
C(5)-H(52)	0.985(14)
C(6)-C(7)	1.5248(17)

Table 5.2 Cont. Bond lengths [Å] and angles [deg] for *N,N'*-dihexylglutaramide

C(6)-H(61)	0.971(15)
C(6)-H(62)	0.993(16)
C(7)-C(8)	1.5285(17)
C(7)-H(71)	0.963(14)
C(7)-H(72)	0.996(14)
C(8)-C(9)	1.5217(18)
C(8)-H(81)	0.997(16)
C(8)-H(82)	0.973(16)
C(9)-H(91)	0.984(17)
C(9)-H(92)	0.995(16)
C(9)-H(93)	0.997(18)
C(1)-N(1)-C(4)	121.90(10)
C(1)-N(1)-HN	119.9(10)
C(4)-N(1)-HN	118.1(10)
O(1)-C(1)-N(1)	121.86(11)
O(1)-C(1)-C(2)	121.95(10)
N(1)-C(1)-C(2)	116.17(10)
C(1)-C(2)-C(3)	113.61(9)
C(1)-C(2)-H(1)	109.8(8)
C(3)-C(2)-H(1)	111.1(8)
C(1)-C(2)-H(2)	107.2(8)
C(3)-C(2)-H(2)	110.6(8)
H(1)-C(2)-H(2)	104.0(11)
C(2)#1-C(3)-C(2)	113.54(14)
C(2)#1-C(3)-H(3)	109.7(8)
C(2)-C(3)-H(3)	108.2(8)
N(1)-C(4)-C(5)	111.88(10)
N(1)-C(4)-H(41)	110.0(8)
C(5)-C(4)-H(41)	108.7(8)
N(1)-C(4)-H(42)	108.7(8)
C(5)-C(4)-H(42)	109.1(8)
H(41)-C(4)-H(42)	108.5(11)
C(4)-C(5)-C(6)	111.02(10)
C(4)-C(5)-H(51)	109.8(8)
C(6)-C(5)-H(51)	110.6(8)
C(4)-C(5)-H(52)	109.3(8)
C(6)-C(5)-H(52)	110.5(8)
H(51)-C(5)-H(52)	105.5(11)
C(7)-C(6)-C(5)	115.12(11)
C(7)-C(6)-H(61)	109.1(9)

Table 5.2 Cont. Bond lengths [Å] and angles [deg] for *N,N'*-dihexylglutaramide

C(5)-C(6)-H(61)	108.9(9)
C(7)-C(6)-H(62)	108.5(9)
C(5)-C(6)-H(62)	109.5(9)
H(61)-C(6)-H(62)	105.3(12)
C(6)-C(7)-C(8)	112.23(10)
C(6)-C(7)-H(71)	108.8(8)
C(8)-C(7)-H(71)	109.2(8)
C(6)-C(7)-H(72)	110.9(8)
C(8)-C(7)-H(72)	108.6(8)
H(71)-C(7)-H(72)	106.9(11)
C(9)-C(8)-C(7)	113.88(11)
C(9)-C(8)-H(81)	109.6(8)
C(7)-C(8)-H(81)	108.5(8)
C(9)-C(8)-H(82)	109.6(9)
C(7)-C(8)-H(82)	108.5(9)
H(81)-C(8)-H(82)	106.6(13)
C(8)-C(9)-H(91)	110.8(9)
C(8)-C(9)-H(92)	112.4(9)
H(91)-C(9)-H(92)	105.3(12)
C(8)-C(9)-H(93)	111.1(9)
H(91)-C(9)-H(93)	110.3(13)
H(92)-C(9)-H(93)	106.6(12)

Symmetry transformations used to generate equivalent atoms:
#1 -x+1,y,-z+3/2

Table 5.3 Anisotropic displacement parameters (Å ^2 x 10^3) for *N*,*N*'-dihexylglutaramide. The anisotropic displacement factor exponent takes the form: -2 pi^2 [h^2 a*^2 U11 + ... + 2 h k a* b* U12]

	U11	U22	U33	U23	U13	U12
O(1)	26(1)	24(1)	20(1)	1(1)	2(1)	-3(1)
N(1)	24(1)	23(1)	18(1)	1(1)	1(1)	-3(1)
C(1)	18(1)	19(1)	22(1)	-1(1)	4(1)	3(1)
C(2)	20(1)	23(1)	21(1)	-2(1)	2(1)	1(1)
C(3)	22(1)	18(1)	23(1)	0	0(1)	0
C(4)	24(1)	23(1)	21(1)	-1(1)	2(1)	-2(1)
C(5)	22(1)	20(1)	22(1)	0(1)	3(1)	1(1)
C(6)	26(1)	23(1)	22(1)	0(1)	3(1)	-2(1)
C(7)	24(1)	21(1)	23(1)	1(1)	2(1)	0(1)
C(8)	29(1)	26(1)	27(1)	1(1)	0(1)	-4(1)
C(9)	26(1)	26(1)	36(1)	0(1)	1(1)	-4(1)

Table 5.4 Torsion angles [deg] for *N*,*N*'-dihexylglutaramide.

C(4)-N(1)-C(1)-O(1)	1.48(17)
C(4)-N(1)-C(1)-C(2)	179.79(10)
O(1)-C(1)-C(2)-C(3)	-19.46(16)
N(1)-C(1)-C(2)-C(3)	162.23(10)
C(1)-C(2)-C(3)-C(2)#1	-68.18(8)
C(1)-N(1)-C(4)-C(5)	-165.77(10)
N(1)-C(4)-C(5)-C(6)	-179.70(10)
C(4)-C(5)-C(6)-C(7)	177.71(10)
C(5)-C(6)-C(7)-C(8)	178.70(10)
C(6)-C(7)-C(8)-C(9)	177.71(11)

Symmetry transformations used to generate equivalent atoms: #1 -x+1,y,-z+3/2

Appendix 5.6 Complete Bond Lengths, Bond Angles, Principle Torsion Angles and Thermal and Positional Parameters for *N,N'*-Dimethylglutaramide

Table 5.5 Atomic coordinates and equivalent isotropic displacement parameters (Å ^2 x 10^3) for *N,N'*-dimethylglutaramide. U(eq) is defined as one third of the trace of the orthogonalized Uij tensor.

	x	y	z	U(eq)
C(1)	3923(1)	3402(2)	7066(1)	16(1)
C(2)	4398(1)	1999(2)	8250(1)	18(1)
C(3)	5000	474(3)	7500	18(1)
C(4)	3069(1)	6830(2)	6682(2)	22(1)
O(1)	3825(1)	2666(2)	5699(1)	22(1)
N(1)	3598(1)	5408(2)	7610(1)	18(1)

Table 5.6 Bond lengths [Å] and angles [deg] for *N,N'*-dimethylglutaramide

C(1)-O(1)	1.2421(14)
C(1)-N(1)	1.3376(16)
C(1)-C(2)	1.5191(15)
C(2)-C(3)	1.5263(14)
C(2)-H(1)	0.980(15)
C(2)-H(2)	0.983(17)
C(3)-C(2)#1	1.5263(14)
C(3)-H(3)	0.984(15)
C(4)-N(1)	1.4534(15)
C(4)-H(4)	0.976(18)
C(4)-H(5)	0.953(17)
C(4)-H(6)	0.978(18)
N(1)-HN	0.834(18)
O(1)-C(1)-N(1)	122.67(10)
O(1)-C(1)-C(2)	121.55(10)
N(1)-C(1)-C(2)	115.73(9)
C(1)-C(2)-C(3)	113.43(8)
C(1)-C(2)-H(1)	109.8(9)
C(3)-C(2)-H(1)	110.5(9)
C(1)-C(2)-H(2)	106.8(10)

Table 5.6 Cont. Bond lengths [Å] and angles [deg] for *N,N'*-dimethylglutaramide

C(3)-C(2)-H(2)	108.8(9)
H(1)-C(2)-H(2)	107.3(13)
C(2)-C(3)-C(2)#1	113.40(13)
C(2)-C(3)-H(3)	108.7(9)
C(2)#1-C(3)-H(3)	108.4(9)
N(1)-C(4)-H(4)	110.7(10)
N(1)-C(4)-H(5)	109.6(10)
H(4)-C(4)-H(5)	106.3(14)
N(1)-C(4)-H(6)	112.3(11)
H(4)-C(4)-H(6)	111.3(15)
H(5)-C(4)-H(6)	106.4(14)
C(1)-N(1)-C(4)	122.89(10)
C(1)-N(1)-HN	119.5(11)
C(4)-N(1)-HN	117.6(11)

Symmetry transformations used to generate equivalent atoms: #1 -x+1,y,-z+3/2

Table 5.7 Anisotropic displacement parameters (Å ^2 x 10^3) for *N,N'*-dimethylglutaramide. The anisotropic displacement factor exponent takes the form: -2 pi^2 [h^2 a*^2 U11 + ... + 2 h k a* b* U12]

	U11	U22	U33	U23	U13	U12
C(1)	19(1)	16(1)	13(1)	1(1)	2(1)	-4(1)
C(2)	24(1)	18(1)	12(1)	2(1)	0(1)	1(1)
C(3)	22(1)	15(1)	17(1)	0	-2(1)	0
C(4)	26(1)	20(1)	20(1)	2(1)	1(1)	3(1)
O(1)	33(1)	19(1)	13(1)	-1(1)	-2(1)	2(1)
N(1)	24(1)	18(1)	13(1)	-1(1)	-1(1)	1(1)

Table 5.8 Torsion angles [deg] for *N,N'*-dimethylglutaramide

O(1)-C(1)-C(2)-C(3)	27.60(15)
N(1)-C(1)-C(2)-C(3)	-154.93(10)
C(1)-C(2)-C(3)-C(2)#1	67.83(8)
O(1)-C(1)-N(1)-C(4)	3.61(18)
C(2)-C(1)-N(1)-C(4)	-173.82(10)

Symmetry transformations used to generate equivalent atoms: #1 -x+1,y,-z+3/2

Appendix 5.7 Complete Bond Lengths, Bond Angles, Principle Torsion Angles and Thermal and Positional Parameters for *N,N'*-Dimethylxylaramide

Table 5.9 Atomic coordinates and equivalent isotropic displacement parameters (Å ^2 x 10^3) for *N,N'*-dimethylxylaramide. U(eq) is defined as one third of the trace of the orthogonalized Uij tensor.

	x	y	z	U(eq)
C(1)	6410(2)	6324(1)	4683(3)	14(1)
C(2)	7372(2)	6890(1)	5734(3)	13(1)
C(3)	6639(3)	7500	4584(4)	13(1)
C(4)	6348(2)	5457(1)	1521(3)	18(1)
O(1)	5045(1)	6196(1)	5563(2)	16(1)
O(2)	9031(1)	6830(1)	5117(2)	15(1)
O(3)	6820(2)	7500	1808(2)	15(1)
N(1)	7123(2)	5992(1)	2802(3)	16(1)

Table 5.10 Bond lengths [Å] and angles [deg] for *N,N'*-dimethylxylaramide.

C(1)-O(1)	1.2484(18)
C(1)-N(1)	1.330(2)
C(1)-C(2)	1.532(2)
C(2)-O(2)	1.4169(18)
C(2)-C(3)	1.5395(17)
C(2)-H(1)	0.95(2)
C(3)-O(3)	1.430(2)
C(3)-C(2)#1	1.5395(17)
C(3)-H(3)	0.99(2)
C(4)-N(1)	1.4541(19)
C(4)-H(5)	0.98(2)
C(4)-H(6)	0.99(2)
C(4)-H(7)	0.95(2)
O(2)-H(2)	0.87(3)
O(3)-H(4)	0.93(3)
N(1)-HN	0.80(2)
O(1)-C(1)-N(1)	123.42(14)
O(1)-C(1)-C(2)	120.98(13)
N(1)-C(1)-C(2)	115.59(13)
O(2)-C(2)-C(1)	111.03(11)
O(2)-C(2)-C(3)	111.86(12)
C(1)-C(2)-C(3)	107.99(12)
O(2)-C(2)-H(1)	111.6(10)
C(1)-C(2)-H(1)	106.1(10)
C(3)-C(2)-H(1)	108.0(10)
O(3)-C(3)-C(2)#1	109.82(10)
O(3)-C(3)-C(2)	109.82(10)
C(2)#1-C(3)-C(2)	113.23(17)
O(3)-C(3)-H(3)	108.6(13)
C(2)#1-C(3)-H(3)	107.6(6)
C(2)-C(3)-H(3)	107.6(6)
N(1)-C(4)-H(5)	109.9(13)
N(1)-C(4)-H(6)	109.3(12)
H(5)-C(4)-H(6)	105.3(15)
N(1)-C(4)-H(7)	105.7(13)
H(5)-C(4)-H(7)	114.8(19)
H(6)-C(4)-H(7)	111.9(17)
C(2)-O(2)-H(2)	108.1(16)
C(3)-O(3)-H(4)	103.0(16)
C(1)-N(1)-C(4)	122.56(15)
C(1)-N(1)-HN	120.6(13)
C(4)-N(1)-HN	116.7(13)

Symmetry transformations used to generate equivalent atoms: #1 x,-y+3/2,z

Table 5.11 Anisotropic displacement parameters (Å^2 x 10^3) for *N,N'*-dimethylxylaramide. The anisotropic displacement factor exponent takes the form: -2 pi^2 [h^2 a*^2 U11 + ... + 2 h k a* b* U12]

	U11	U22	U33	U23	U13	U12
C(1)	19(1)	16(1)	5(1)	3(1)	-1(1)	1(1)
C(2)	18(1)	16(1)	5(1)	1(1)	0(1)	0(1)
C(3)	17(1)	16(1)	5(1)	0	0(1)	0
C(4)	25(1)	17(1)	12(1)	-4(1)	-1(1)	0(1)
O(1)	19(1)	19(1)	9(1)	0(1)	1(1)	-2(1)
O(2)	18(1)	17(1)	11(1)	2(1)	-1(1)	2(1)
O(3)	22(1)	19(1)	3(1)	0	-2(1)	0
N(1)	19(1)	17(1)	10(1)	-2(1)	2(1)	-1(1)

Table 5.12 Torsion angles [deg] for *N,N'*-dimethylxylaramide

O(1)-C(1)-C(2)-O(2)	161.08 (0.12)
N(1)-C(1)-C(2)-O(2)	-19.18 (0.17)
O(1)-C(1)-C(2)-C(3)	-75.95 (0.17)
N(1)-C(1)-C(2)-C(3)	103.78 (0.15)
O(2)-C(2)-C(3)-O(3)	58.97 (0.17)
C(1)-C(2)-C(3)-O(3)	-63.49 (0.17)
O(2)-C(2)-C(3)-C(2')	-64.19 (0.19)
C(1)-C(2)-C(3)-C(2')	173.35 (0.11)
O(1)-C(1)-N(1)-C(4)	2.22 (0.22)
C(2)-C(1)-N(1)-C(4)	-177.51 (0.12)

Symmetry transformations used to generate equivalent atoms: #1 -x+1,y,-z+3/2

Appendix 5.8 Complete Bond Lengths, Bond Angles, Principle Torsion Angles and Thermal and Positional Parameters for 2,3,4-Tri-*O*-acetyl-*N,N'*-Dimethylxylaramide

Table 5.13 Atomic coordinates and equivalent isotropic displacement parameters (Å ^2 x 10^3) for 2,3,4-tri-*O*-acetyl-*N,N'*-dimethylxylaramide. U(eq) is defined as one third of the trace of the orthogonalizedUij tensor.

	x	y	z	U(eq)
C(1)	5975(3)	540(1)	9074(3)	23(1)
C(2)	5393(3)	1103(1)	7982(2)	20(1)
C(3)	6830(2)	1546(1)	8359(2)	19(1)
C(4)	6340(2)	2110(1)	7261(2)	19(1)
C(5)	4997(2)	2473(1)	7495(3)	20(1)
C(6)	7218(3)	-473(1)	9400(3)	30(1)
C(7)	4397(3)	3255(1)	9070(3)	28(1)
C(10)	9484(3)	1084(1)	9371(3)	38(1)
C(11)	10732(3)	811(2)	8867(4)	53(1)
C(8)	3237(3)	723(1)	5569(3)	26(1)
C(9)	2719(3)	619(1)	3788(3)	38(1)
C(12)	7988(2)	2782(1)	6501(3)	23(1)
C(13)	9634(3)	3088(1)	7067(3)	28(1)
O(1)	6038(2)	556(1)	10457(2)	35(1)
O(2)	4786(2)	960(1)	6271(2)	22(1)
O(3)	2439(2)	620(1)	6332(2)	35(1)
O(4)	8110(2)	1248(1)	8046(2)	22(1)
O(5)	9611(3)	1142(1)	10735(2)	68(1)
O(6)	7834(2)	2463(1)	7716(2)	22(1)
O(7)	6932(2)	2798(1)	5139(2)	49(1)
O(8)	3529(2)	2390(1)	6581(2)	25(1)
N(1)	6435(2)	62(1)	8442(2)	23(1)
N(2)	5523(2)	2856(1)	8744(2)	23(1)

Table 5.14 Bond lengths [Å] and angles [deg] for 2,3,4-tri-*O*-acetyl-*N*,*N*'-dimethylxylaramide

C(1)-O(1)	1.229(3)
C(1)-N(1)	1.339(3)
C(1)-C(2)	1.531(3)
C(2)-O(2)	1.444(2)
C(2)-C(3)	1.532(3)
C(2)-H(3)	0.93(2)
C(3)-O(4)	1.444(2)
C(3)-C(4)	1.532(3)
C(3)-H(4)	0.93(3)
C(4)-O(6)	1.447(2)
C(4)-C(5)	1.529(3)
C(4)-H(5)	0.92(3)
C(5)-O(8)	1.238(2)
C(5)-N(2)	1.326(3)
C(6)-N(1)	1.454(3)
C(6)-H(6A)	0.9600
C(6)-H(6B)	0.9600
C(6)-H(6C)	0.9600
C(7)-N(2)	1.454(3)
C(7)-H(7A)	0.9600
C(7)-H(7B)	0.9600
C(7)-H(7C)	0.9600
C(10)-O(5)	1.197(3)
C(10)-O(4)	1.359(3)
C(10)-C(11)	1.496(4)
C(11)-H(9A)	0.9600
C(11)-H(9B)	0.9600
C(11)-H(9C)	0.9600
C(8)-O(3)	1.203(3)
C(8)-O(2)	1.363(3)
C(8)-C(9)	1.496(3)
C(9)-H(8A)	0.9600
C(9)-H(8B)	0.9600
C(9)-H(8C)	0.9600
C(12)-O(7)	1.199(3)
C(12)-O(6)	1.357(3)
C(12)-C(13)	1.499(3)
C(13)-H(10A)	0.9600
C(13)-H(10B)	0.9600

Table 5.14 Cont. Bond lengths [Å] and angles [deg] for 2,3,4-tri-*O*-acetyl-*N*,*N*'-dimethylxylaramide

C(13)-H(10C)	0.9600
N(1)-H(1)	0.82(3)
N(2)-H(2)	0.79(3)
O(1)-C(1)-N(1)	124.5(2)
O(1)-C(1)-C(2)	119.44(18)
N(1)-C(1)-C(2)	116.06(18)
O(2)-C(2)-C(1)	112.90(16)
O(2)-C(2)-C(3)	106.34(15)
C(1)-C(2)-C(3)	110.01(17)
O(2)-C(2)-H(3)	111.1(15)
C(1)-C(2)-H(3)	106.4(14)
C(3)-C(2)-H(3)	110.1(14)
O(4)-C(3)-C(4)	105.93(16)
O(4)-C(3)-C(2)	109.12(15)
C(4)-C(3)-C(2)	112.51(16)
O(4)-C(3)-H(4)	108.8(15)
C(4)-C(3)-H(4)	112.5(16)
C(2)-C(3)-H(4)	107.8(15)
O(6)-C(4)-C(5)	111.39(15)
O(6)-C(4)-C(3)	105.62(15)
C(5)-C(4)-C(3)	111.12(16)
O(6)-C(4)-H(5)	107.5(15)
C(5)-C(4)-H(5)	110.3(15)
C(3)-C(4)-H(5)	110.7(16)
O(8)-C(5)-N(2)	124.18(19)
O(8)-C(5)-C(4)	120.35(18)
N(2)-C(5)-C(4)	115.44(17)
N(1)-C(6)-H(6A)	109.5
N(1)-C(6)-H(6B)	109.5
H(6A)-C(6)-H(6B)	109.5
N(1)-C(6)-H(6C)	109.5
H(6A)-C(6)-H(6C)	109.5
H(6B)-C(6)-H(6C)	109.5
N(2)-C(7)-H(7A)	109.5
N(2)-C(7)-H(7B)	109.5
H(7A)-C(7)-H(7B)	109.5
N(2)-C(7)-H(7C)	109.5
H(7A)-C(7)-H(7C)	109.5
H(7B)-C(7)-H(7C)	109.5
O(5)-C(10)-O(4)	122.8(2)

Table 5.14 Cont. Bond lengths [Å] and angles [deg] for 2,3,4-tri-*O*-acetyl-*N*,*N*'-dimethylxylaramide

O(5)-C(10)-C(11)	126.5(2)
O(4)-C(10)-C(11)	110.6(2)
C(10)-C(11)-H(9A)	109.5
C(10)-C(11)-H(9B)	109.5
H(9A)-C(11)-H(9B)	109.5
C(10)-C(11)-H(9C)	109.5
H(9A)-C(11)-H(9C)	109.5
H(9B)-C(11)-H(9C)	109.5
O(3)-C(8)-O(2)	122.3(2)
O(3)-C(8)-C(9)	126.7(2)
O(2)-C(8)-C(9)	110.9(2)
C(8)-C(9)-H(8A)	109.5
C(8)-C(9)-H(8B)	109.5
H(8A)-C(9)-H(8B)	109.5
C(8)-C(9)-H(8C)	109.5
H(8A)-C(9)-H(8C)	109.5
H(8B)-C(9)-H(8C)	109.5
O(7)-C(12)-O(6)	122.93(19)
O(7)-C(12)-C(13)	125.2(2)
O(6)-C(12)-C(13)	111.83(18)
C(12)-C(13)-H(10A)	109.5
C(12)-C(13)-H(10B)	109.5
H(10A)-C(13)-H(10B)	109.5
C(12)-C(13)-H(10C)	109.5
H(10A)-C(13)-H(10C)	109.5
H(10B)-C(13)-H(10C)	109.5
C(8)-O(2)-C(2)	115.87(16)
C(10)-O(4)-C(3)	116.45(17)
C(12)-O(6)-C(4)	116.10(16)
C(1)-N(1)-C(6)	122.35(19)
C(1)-N(1)-H(1)	121.5(17)
C(6)-N(1)-H(1)	115.3(17)
C(5)-N(2)-C(7)	121.69(18)
C(5)-N(2)-H(2)	118.9(18)
C(7)-N(2)-H(2)	119.4(18)

Table 5.15 Anisotropic displacement parameters (Å ^2 x 10^3) for 2,3,4-tri-*O*-acetyl-*N,N'*-dimethylxylaramide.The anisotropic displacement factor exponent takes the form: -2 pi^2 [h^2 a*^2 U11 + ... + 2 h k a* b* U12]

	U11	U22	U33	U23	U13	U12
C(1)	35(1)	16(1)	20(1)	0(1)	14(1)	0(1)
C(2)	29(1)	16(1)	15(1)	-1(1)	10(1)	1(1)
C(3)	21(1)	20(1)	15(1)	-1(1)	6(1)	3(1)
C(4)	20(1)	18(1)	16(1)	-1(1)	4(1)	-4(1)
C(5)	21(1)	14(1)	19(1)	4(1)	3(1)	1(1)
C(6)	43(1)	21(1)	27(1)	7(1)	16(1)	10(1)
C(7)	24(1)	25(1)	31(1)	-2(1)	8(1)	7(1)
C(10)	38(1)	44(1)	24(1)	-1(1)	4(1)	23(1)
C(11)	38(2)	72(2)	36(2)	-12(1)	4(1)	32(1)
C(8)	28(1)	16(1)	28(1)	6(1)	4(1)	3(1)
C(9)	43(1)	31(1)	25(1)	3(1)	-1(1)	-10(1)
C(12)	22(1)	23(1)	23(1)	0(1)	9(1)	1(1)
C(13)	25(1)	29(1)	29(1)	2(1)	11(1)	-3(1)
O(1)	66(1)	20(1)	25(1)	2(1)	27(1)	7(1)
O(2)	27(1)	18(1)	17(1)	0(1)	6(1)	-2(1)
O(3)	26(1)	38(1)	37(1)	5(1)	10(1)	1(1)
O(4)	22(1)	23(1)	20(1)	-1(1)	7(1)	5(1)
O(5)	63(1)	107(2)	19(1)	2(1)	4(1)	59(1)
O(6)	20(1)	26(1)	18(1)	1(1)	5(1)	-5(1)
O(7)	37(1)	72(1)	27(1)	16(1)	1(1)	-20(1)
O(8)	19(1)	24(1)	23(1)	2(1)	-1(1)	-1(1)
N(1)	37(1)	16(1)	17(1)	4(1)	14(1)	7(1)
N(2)	16(1)	20(1)	25(1)	-3(1)	1(1)	3(1)

Table 5.16 Torsion angles [deg] for 2,3,4-tri-*O*-acetyl-*N*,*N*'-dimethylxylaramide

O(1)-C(1)-C(2)-O(2)	-157.75 (0.20)
N(1)-C(1)-C(2)–O(2)	24.29 (0.26)
O(1)-C(1)-C(2)-C(3)	83.63 (0.25)
N(1)-C(1)-C(2)-C(3)	-94.32 (0.22)
O(2)-C(2)-C(3)-O(4)	-61.92 (0.19)
C(1)-C(2)–C(3)-O(4)	60.65 (0.21)
O(2)-C(2)-C(3)-C(4)	55.35 (0.21)
C(1)-C(2)-C(3)-C(4)	177.93 (0.16)
O(4)-C(3)-C(4)-O(6)	-58.31 (0.19)
C(2)-C(3)-C(4)-O(6)	-177.46 (0.16)
O(4)-C(3)-C(4)-C(5)	-179.23 (0.16)
C(2)-C(3)-C(4)-C(5)	61.62 (0.21)
O(6)-C(4)-C(5)-O(8)	147.67 (0.18)
C(3)-C(4)-C(5)-O(8)	-94.86 (0.22)
O(6)-C(4)-C(5)-N(2)	-34.17 (0.24)
C(3)-C(4)-C(5)-N(2)	83.29 (0.21)
O(3)-C(8)-O(2)-C(2)	-2.47 (0.28)
C(9)-C(8)-O(2)-C(2)	177.52 (0.18)
C(1)-C(2)–O(2)-C(8)	78.06 (0.21)
C(3)-C(2)-O(2)-C(8)	-161.22 (0.16)
O(5)-C(10)-O(4)-C(3)	4.88 (0.40)
C(11)-C(10)-O(4)-C(3)	-177.10 (0.23)
C(4)-C(3)-O(4)-C(10)	131.63 (0.20)
C(2)-C(3)-O(4)-C(10)	-107.01 (0.21)
O(7)-C(12)-O(6)-C(4)	3.36 (0.30)
C(13)-C(12)-O(6)-C(4)	-175.08 (0.17)
C(5)-C(4)-O(6)-C(12)	-92.36 (0.20)
C(3)-C(4)-O(6)-C(12)	146.89 (0.16)
O(1)-C(1)-N(1)-C(6)	-6.20 (0.36)
C(2)-C(1)-N(1)-C(6)	171.64 (0.20)
O(8)-C(5)-N(2)-C(7)	-5.17 (0.32)
C(4)-C(5)-N(2)-C(7)	176.76 (0.18)

Appendix 5.9 Complete Bond Lengths, Bond Angles, Principle Torsion Angles and Thermal and Positional Parameters for *N,N'*-Dimethyl L-arabinaramide

Table 5.17 Atomic coordinates and equivalent isotropic displacement parameters (Å ^2 x 10^3) for *N,N'*-dimethyl L-arabinaramide. U(eq) is defined as one third of the trace of the orthogonalized Uij tensor.

	x	y	z	U(eq)
C(7)	6264(7)	2155(4)	-34(3)	21(1)
N(2)	6375(5)	3172(3)	1033(2)	16(1)
C(5)	4148(6)	3728(3)	1461(3)	14(1)
O(5)	1923(4)	3405(3)	1022(2)	19(1)
C(4)	4462(6)	4832(3)	2564(3)	13(1)
O(4)	7148(4)	5371(3)	2710(2)	16(1)
C(3)	3672(6)	4037(3)	3749(3)	14(1)
O(3)	1095(4)	3361(3)	3629(2)	17(1)
C(2)	3784(6)	5230(4)	4802(3)	13(1)
O(2)	2078(5)	6505(3)	4502(2)	16(1)
C(1)	2932(6)	4482(4)	5984(3)	16(1)
O(1)	4039(4)	3262(2)	6373(2)	18(1)
N(1)	1050(5)	5213(3)	6558(2)	17(1)
C(6)	137(8)	4675(4)	7726(3)	22(1)

Table 5.18 Bond lengths [Å] and angles [deg] for *N,N'*-dimethyl L-arabinaramide.

C(7)-N(2)	1.457(4)
C(7)-H(10A)	1.00(4)
C(7)-H(10B)	0.94(5)
C(7)-H(10C)	0.85(4)
N(2)-C(5)	1.326(4)
N(2)-H(8)	0.84(4)
C(5)-O(5)	1.224(4)
C(5)-C(4)	1.536(4)
C(4)-O(4)	1.427(4)
C(4)-C(3)	1.537(4)
C(4)-H(6)	0.97(4)
O(4)-H(7)	0.99(5)

Table 5.18 Cont. Bond lengths [Å] and angles [deg] for *N*,*N*'-dimethyl L-arabinaramide

C(3)-O(3)	1.419(4)
C(3)-C(2)	1.541(4)
C(3)-H(4)	0.96(4)
O(3)-H(5)	0.90(5)
C(2)-O(2)	1.418(4)
C(2)-C(1)	1.526(4)
C(2)-H(2)	0.98(4)
O(2)-H(3)	0.79(5)
C(1)-O(1)	1.250(4)
C(1)-N(1)	1.323(4)
N(1)-C(6)	1.456(4)
N(1)-H(1)	0.96(4)
C(6)-H(9A)	0.98(4)
C(6)-H(9B)	0.94(5)
C(6)-H(9C)	1.01(5)

N(2)-C(7)-H(10A)	104(2)
N(2)-C(7)-H(10B)	104(3)
H(10A)-C(7)-H(10B)	117(4)
N(2)-C(7)-H(10C)	110(3)
H(10A)-C(7)-H(10C)	105(4)
H(10B)-C(7)-H(10C)	115(4)
C(5)-N(2)-C(7)	120.2(3)
C(5)-N(2)-H(8)	126(3)
C(7)-N(2)-H(8)	114(3)
O(5)-C(5)-N(2)	123.4(3)
O(5)-C(5)-C(4)	120.0(3)
N(2)-C(5)-C(4)	116.6(3)
O(4)-C(4)-C(5)	110.1(2)
O(4)-C(4)-C(3)	109.6(2)
C(5)-C(4)-C(3)	111.6(2)
O(4)-C(4)-H(6)	113(2)
C(5)-C(4)-H(6)	106(2)
C(3)-C(4)-H(6)	107(2)
C(4)-O(4)-H(7)	105(2)
O(3)-C(3)-C(4)	112.4(2)
O(3)-C(3)-C(2)	109.7(2)
C(4)-C(3)-C(2)	109.6(2)
O(3)-C(3)-H(4)	108(2)
C(4)-C(3)-H(4)	110(2)
C(2)-C(3)-H(4)	106(2)

Table 5.18 Cont. Bond lengths [Å] and angles [deg] for *N,N'*-dimethyl L-arabinaramide

C(3)-O(3)-H(5)	117(3)
O(2)-C(2)-C(1)	109.1(2)
O(2)-C(2)-C(3)	110.1(2)
C(1)-C(2)-C(3)	110.7(2)
O(2)-C(2)-H(2)	113(3)
C(1)-C(2)-H(2)	106(3)
C(3)-C(2)-H(2)	108(3)
C(2)-O(2)-H(3)	96(3)
O(1)-C(1)-N(1)	123.5(3)
O(1)-C(1)-C(2)	120.1(3)
N(1)-C(1)-C(2)	116.3(3)
C(1)-N(1)-C(6)	122.3(3)
C(1)-N(1)-H(1)	116(3)
C(6)-N(1)-H(1)	122(3)
N(1)-C(6)-H(9A)	108(2)
N(1)-C(6)-H(9B)	113(2)
H(9A)-C(6)-H(9B)	113(4)
N(1)-C(6)-H(9C)	105(2)
H(9A)-C(6)-H(9C)	115(3)
H(9B)-C(6)-H(9C)	104(3)

Table 5.19 Anisotropic displacement parameters (Å ^2 x 10^3) for *N,N'*-dimethyl L-arabinaramide. The anisotropic displacement factor exponent takes the form:
-2 pi^2 [h^2 a*^2 U11 + ... + 2 h k a* b* U12]

	U11	U22	U33	U23	U13	U12
C(7)	23(2)	19(2)	21(2)	-7(2)	0(1)	0(1)
N(2)	17(1)	12(1)	18(1)	-5(1)	0(1)	0(1)
C(5)	20(2)	6(1)	15(1)	3(1)	0(1)	0(1)
O(5)	17(1)	21(1)	20(1)	-4(1)	0(1)	-1(1)
C(4)	13(1)	10(2)	16(2)	-1(1)	1(1)	2(1)
O(4)	16(1)	9(1)	24(1)	-3(1)	2(1)	-1(1)
C(3)	18(2)	7(1)	16(2)	-1(1)	-1(1)	0(1)
O(3)	20(1)	10(1)	20(1)	1(1)	0(1)	-4(1)
C(2)	17(2)	6(1)	17(2)	1(1)	-1(1)	2(1)
O(2)	24(1)	4(1)	21(1)	1(1)	2(1)	1(1)
C(1)	20(2)	7(1)	19(2)	-4(1)	-1(1)	0(1)
O(1)	26(1)	7(1)	21(1)	-1(1)	2(1)	3(1)

Table 5.19 Cont. Anisotropic displacement parameters (Å ^2 x 10^3) for *N,N'*-dimethyl L-arabinaramide. The anisotropic displacement factor exponent takes the form:
-2 pi^2 [h^2 a*^2 U11 + ... + 2 h k a* b* U12]

	U11	U22	U33	U23	U13	U12
N(1)	24(1)	9(1)	19(1)	1(1)	3(1)	1(1)
C(6)	28(2)	16(2)	21(2)	-1(1)	5(1)	3(2)

Table 5.20 Torsion angles [deg] for *N,N'*-dimethyl L-arabinaramide

O(1) - C(1) - C(2) - O(2)	174.72 (0.26)
N(1) - C(1) - C(2) - O(2)	-6.75 (0.37)
O(1) - C(1) - C(2) - C(3)	53.41 (0.37)
N(1) - C(1)- C(2) - C(3)	-128.06 (0.28)
O(2) - C(2) - C(3)- O(3)	-66.13 (0.31)
C(1) - C(2) - C(3) - O(3)	54.62 (0.32)
O(2) - C(2) - C(3) - C(4)	57.68 (0.31)
C(1) - C(2) - C(3) - C(4)	178.43 (0.23)
O(3) - C(3) - C(4) - O(4)	175.08 (0.24)
C(2) - C(3) - C(4) - O(4)	62.67 (0.30)
O(3) - C(3) - C(4) - C(5)	-52.78 (0.31)
C(2) - C(3) - C(4) - C(5)	-175.03 (0.24)
O(4) - C(4) - C(5) - O(5)	-164.33 (0.25)
C(3) - C(4) - C(5) - O(5)	73.66 (0.34)
O(4) - C(4) - C(5) - N(2)	15.59 (0.36)
C(3) - C(4) - C(5) - N(2)	-106.42 (0.29)
O(1) - C(1) - N(1) - C(6)	1.61 (0.48)
C(2)- C(1) - N(1) - C(6)	-176.87 (0.28)
O(5) - C(5) - N(2) - C(7)	1.81 (0.48)
C(4) - C(5) - N(2) - C(7)	-178.11 (0.27)

Appendix 5.10 Complete Bond Lengths, Bond Angles, Principle Torsion Angles and Thermal and Positional Parameters for 2,3,4-Tri-*O*-acetyl-*N*,*N*'-Dimethyl L-arabinaramide

Table 5.21 Atomic coordinates and equivalent isotropic displacement parameters (Å ^2 x 10^3) for 2,3,4-tri-*O*-acetyl-*N*,*N*'-dimethyl L-arabinaramide. U(eq) is defined as one third of the trace of the orthogonalized Uij tensor.

	x	y	z	U(eq)
C(1)	4154(3)	9369(1)	2401(1)	21(1)
C(2)	2584(3)	8884(1)	2902(1)	19(1)
C(3)	1488(3)	8233(1)	2396(1)	17(1)
C(4)	-198(3)	7744(1)	2853(1)	19(1)
C(5)	-1244(3)	7076(1)	2344(1)	18(1)
C(6)	5338(4)	10665(1)	1836(2)	31(1)
C(10)	435(3)	8328(1)	1042(1)	23(1)
C(12)	-286(4)	6996(1)	4045(1)	26(1)
N(1)	3842(3)	10171(1)	2294(1)	21(1)
N(2)	-2895(3)	7350(1)	1926(1)	21(1)
O(1)	5675(2)	8987(1)	2113(1)	30(1)
O(2)	933(2)	9395(1)	3235(1)	22(1)
O(3)	3111(3)	9732(1)	4235(1)	37(1)
O(4)	440(2)	8671(1)	1772(1)	19(1)
O(5)	1369(2)	7697(1)	880(1)	31(1)
O(6)	945(2)	7366(1)	3488(1)	22(1)
O(7)	-2191(3)	7024(1)	4021(1)	34(1)
O(8)	-544(2)	6363(1)	2316(1)	22(1)
C(8)	1382(4)	9764(1)	3934(1)	28(1)
C(7)	-3875(4)	6857(1)	1308(1)	28(1)
C(9)	-514(4)	10216(2)	4238(2)	40(1)
C(13)	1037(4)	6592(2)	4661(1)	38(1)
C(11)	-895(4)	8835(2)	500(1)	30(1)

Table 5.22 Bond lengths [Å] and angles [deg] for 2,3,4-tri-*O*-acetyl-*N*,*N*'-dimethyl L-arabinaramide.

C(1)-O(1)	1.237(2)
C(1)-N(1)	1.313(3)
C(1)-C(2)	1.519(3)
C(2)-O(2)	1.439(2)
C(2)-C(3)	1.519(3)
C(2)-H(2)	0.99(2)
C(3)-O(4)	1.434(2)
C(3)-C(4)	1.531(3)
C(3)-H(3)	0.93(2)
C(4)-O(6)	1.432(2)
C(4)-C(5)	1.527(3)
C(4)-H(4)	0.95(2)
C(5)-O(8)	1.225(2)
C(5)-N(2)	1.332(3)
C(6)-N(1)	1.457(3)
C(6)-H(6A)	0.9600
C(6)-H(6B)	0.9600
C(6)-H(6C)	0.9600
C(10)-O(5)	1.201(2)
C(10)-O(4)	1.359(2)
C(10)-C(11)	1.487(3)
C(12)-O(7)	1.199(3)
C(12)-O(6)	1.361(3)
C(12)-C(13)	1.487(3)
N(1)-H(1)	0.82(3)
N(2)-C(7)	1.453(3)
N(2)-H(5)	0.83(2)
O(2)-C(8)	1.360(3)
O(3)-C(8)	1.203(3)
C(8)-C(9)	1.487(3)
C(7)-H(7A)	0.9600
C(7)-H(7B)	0.9600
C(7)-H(7C)	0.9600
C(9)-H(8A)	0.9600
C(9)-H(8B)	0.9600
C(9)-H(8C)	0.9600
C(13)-H(10A)	0.9600
C(13)-H(10B)	0.9600
C(13)-H(10C)	0.9600
C(11)-H(9A)	0.9600

Table 5.22 Cont. Bond lengths [Å] and angles [deg] for 2,3,4-tri-*O*-acetyl-*N*,*N*'-dimethyl L-arabinaramide.

C(11)-H(9B)	0.9600
C(11)-H(9C)	0.9600
O(1)-C(1)-N(1)	122.97(19)
O(1)-C(1)-C(2)	118.18(18)
N(1)-C(1)-C(2)	118.85(17)
O(2)-C(2)-C(1)	113.47(15)
O(2)-C(2)-C(3)	106.75(15)
C(1)-C(2)-C(3)	109.10(17)
O(2)-C(2)-H(2)	107.1(12)
C(1)-C(2)-H(2)	108.4(12)
C(3)-C(2)-H(2)	112.1(11)
O(4)-C(3)-C(2)	107.06(15)
O(4)-C(3)-C(4)	108.09(15)
C(2)-C(3)-C(4)	112.10(17)
O(4)-C(3)-H(3)	113.2(14)
C(2)-C(3)-H(3)	106.7(13)
C(4)-C(3)-H(3)	109.8(13)
O(6)-C(4)-C(5)	110.41(15)
O(6)-C(4)-C(3)	104.70(15)
C(5)-C(4)-C(3)	111.53(16)
O(6)-C(4)-H(4)	112.0(14)
C(5)-C(4)-H(4)	111.6(14)
C(3)-C(4)-H(4)	106.3(14)
O(8)-C(5)-N(2)	124.50(18)
O(8)-C(5)-C(4)	121.39(18)
N(2)-C(5)-C(4)	114.08(16)
N(1)-C(6)-H(6A)	109.5
N(1)-C(6)-H(6B)	109.5
H(6A)-C(6)-H(6B)	109.5
N(1)-C(6)-H(6C)	109.5
H(6A)-C(6)-H(6C)	109.5
H(6B)-C(6)-H(6C)	109.5
O(5)-C(10)-O(4)	123.31(19)
O(5)-C(10)-C(11)	126.3(2)
O(4)-C(10)-C(11)	110.43(17)
O(7)-C(12)-O(6)	121.9(2)
O(7)-C(12)-C(13)	126.7(2)
O(6)-C(12)-C(13)	111.3(2)
C(1)-N(1)-C(6)	120.73(18)
C(1)-N(1)-H(1)	121.0(16)

Table 5.22 Cont. Bond lengths [Å] and angles [deg] for 2,3,4-tri-*O*-acetyl-*N*,*N*'-dimethyl L-arabinaramide.

C(6)-N(1)-H(1)	118.0(16)
C(5)-N(2)-C(7)	122.56(17)
C(5)-N(2)-H(5)	117.3(16)
C(7)-N(2)-H(5)	119.7(16)
C(8)-O(2)-C(2)	116.38(17)
C(10)-O(4)-C(3)	118.78(15)
C(12)-O(6)-C(4)	115.18(17)
O(3)-C(8)-O(2)	122.8(2)
O(3)-C(8)-C(9)	126.6(2)
O(2)-C(8)-C(9)	110.5(2)
N(2)-C(7)-H(7A)	109.5
N(2)-C(7)-H(7B)	109.5
H(7A)-C(7)-H(7B)	109.5
N(2)-C(7)-H(7C)	109.5
H(7A)-C(7)-H(7C)	109.5
H(7B)-C(7)-H(7C)	109.5
C(8)-C(9)-H(8A)	109.5
C(8)-C(9)-H(8B)	109.5
H(8A)-C(9)-H(8B)	109.5
C(8)-C(9)-H(8C)	109.5
H(8A)-C(9)-H(8C)	109.5
H(8B)-C(9)-H(8C)	109.5
C(12)-C(13)-H(10A)	109.5
C(12)-C(13)-H(10B)	109.5
H(10A)-C(13)-H(10B)	109.5
C(12)-C(13)-H(10C)	109.5
H(10A)-C(13)-H(10C)	109.5
H(10B)-C(13)-H(10C)	109.5
C(10)-C(11)-H(9A)	109.5
C(10)-C(11)-H(9B)	109.5
H(9A)-C(11)-H(9B)	109.5
C(10)-C(11)-H(9C)	109.5
H(9A)-C(11)-H(9C)	109.5
H(9B)-C(11)-H(9C)	109.5

Table 5.23 Anisotropic displacement parameters (Å ^2 x 10^3) for 2,3,4-tri-*O*-acetyl-*N*,*N'*-dimethyl L-arabinaramide. The anisotropic displacement factor exponent takes the form: -2 pi^2 [h^2 a*^2 U11 + ... + 2 h k a* b* U12]

	U11	U22	U33	U23	U13	U12
C(1)	13(1)	16(1)	35(1)	-1(1)	-2(1)	0(1)
C(2)	14(1)	12(1)	30(1)	-1(1)	1(1)	0(1)
C(3)	13(1)	11(1)	26(1)	0(1)	-1(1)	1(1)
C(4)	17(1)	12(1)	28(1)	-1(1)	1(1)	0(1)
C(5)	14(1)	14(1)	26(1)	0(1)	4(1)	-3(1)
C(6)	26(1)	17(1)	50(2)	3(1)	12(1)	1(1)
C(10)	17(1)	26(1)	25(1)	1(1)	4(1)	0(1)
C(12)	35(1)	17(1)	26(1)	-3(1)	2(1)	-6(1)
N(1)	14(1)	13(1)	37(1)	1(1)	6(1)	1(1)
N(2)	16(1)	10(1)	38(1)	-3(1)	-4(1)	2(1)
O(1)	19(1)	15(1)	58(1)	-1(1)	10(1)	2(1)
O(2)	19(1)	16(1)	32(1)	-5(1)	4(1)	0(1)
O(3)	52(1)	26(1)	35(1)	-7(1)	-10(1)	1(1)
O(4)	16(1)	16(1)	25(1)	1(1)	-1(1)	2(1)
O(5)	29(1)	32(1)	31(1)	-5(1)	-1(1)	11(1)
O(6)	23(1)	16(1)	25(1)	1(1)	-1(1)	-4(1)
O(7)	32(1)	32(1)	38(1)	1(1)	8(1)	-7(1)
O(8)	19(1)	11(1)	35(1)	-1(1)	-1(1)	0(1)
C(8)	41(1)	16(1)	28(1)	3(1)	6(1)	-4(1)
C(7)	23(1)	19(1)	41(1)	-3(1)	-12(1)	1(1)
C(9)	53(2)	24(1)	42(1)	-6(1)	21(1)	-3(1)
C(13)	50(2)	32(1)	30(1)	8(1)	-4(1)	-7(1)
C(11)	28(1)	36(1)	26(1)	1(1)	1(1)	8(1)

Table 5.24 Torsion angles [deg] for 2,3,4-tri-*O*-acetyl-*N*,*N*'-dimethyl L-arabinaramide

O(1) – C(1) – C(2) – O(2)	177.44 (0.18)
N(1) – C(1) – C(2) – O(2)	-2.49 (0.27)
O(1) – C(1) – C(2) – C(3)	-63.69 (0.24)
N(1) – C(1) – C(2) – C(3)	116.39 (0.20)
O(2) – C(2) – C(3) – O(4)	63.96 (0.19)
C(1) – C(2) – C(3) – O(4)	-59.02 (0.20)
O(2) – C(2) – C(3) – C(4)	-54.40 (0.21)
C(1) – C(2) – C(3) – C(4)	-177.39 (0.16)
O(4) – C(3) – C(4) – O(6)	-176.77 (0.14)
C(2) – C(3) – C(4) – O(6)	-59.01 (0.19)
O(4) – C(3) – C(4) – C(5)	63.83 (0.20)
C(2) – C(3) – C(4) – C(5)	-178.42 (0.16)
O(6) – C(4) – C(5) – O(8)	-24.64 (0.26)
C(3) – C(4) – C(5) – O(8)	91.32 (0.22)
O(6) – C(4) – C(5) – N(2)	157.47 (0.16)
C(3) – C(4) – C(5) – N(2)	-86.57 (0.21)
O(1) – C(1) – N(1) – C(6)	-1.59 (0.33)
C(2) – C(1) – N(1) – C(6)	178.33 (0.20)
O(8) – C(5) – N(2) – C(7)	-8.68 (0.32)
C(4) – C(5) – N(2) – C(7)	169.14 (0.19)
C(1) – C(2) – O(2) – C(8)	-87.04 (0.21)
C(3) – C(2) – O(2) – C(8)	152.74 (0.16)
O(5) – C(10) – O(4) – C(3)	-4.41 (0.28)
C(11) – C(10) – O(4) – C(3)	174.70 (0.17)
C(2) – C(3) – O(4)- C(10)	141.64 (0.16)
C(4) – C(3) – O(4) – C(10)	-97.42 (0.19)
O(7) – C(12) – O(6) – C(4)	-3.58 (0.28)
C(13) – C(12) – O(6) – C(4)	177.64 (0.17)
C(5) – C(4) – O(6) – C(12)	-69.11 (0.20)
C(3) – C(4) – O(6) – C(12	170.73 (0.15)
C(2) – O(2) – C(8) – O(3	6.17 (0.28)
C(2) – O(2) – C(8) – C(9)	-175.56 (0.17)

Appendix 5.11 Complete Bond Lengths, Bond Angles, Principle Torsion Angles and Thermal and Positional Parameters for *N,N'*-Dimethylribaramide

Table 5.25 Atomic coordinates and equivalent isotropic displacement parameters ($Å^2 x\ 10^3$) for *N,N'*-dimethylribaramide. U(eq) is defined as one third of the trace of the orthogonalized U^{ij} tensor.

	x	y	z	U(eq)
C(1)	2522(2)	8365(2)	3659(2)	26(1)
C(2)	1361(2)	7906(2)	2369(2)	23(1)
C(3)	489(2)	7228(2)	3029(2)	22(1)
C(4)	-720(2)	6742(2)	1850(2)	24(1)
C(5)	-1634(2)	7841(2)	1137(2)	23(1)
C(6)	4730(2)	7978(3)	5158(4)	58(1)
C(7)	-3049(2)	8840(2)	-1170(3)	32(1)
N(1)	3573(2)	7720(2)	3887(2)	36(1)
N(2)	-2125(2)	7877(2)	-338(2)	26(1)
O(1)	2441(1)	9301(1)	4449(2)	33(1)
O(2)	710(1)	8990(1)	1533(2)	26(1)
O(3)	1161(1)	6176(1)	3953(2)	27(1)
O(4)	-430(1)	5978(1)	789(2)	28(1)
O(5)	-1919(1)	8611(1)	1969(2)	30(1)
O(1S)	3673(2)	9750(2)	7517(2)	35(1)

Table 5.26 Bond lengths [Å] and angles [°] for *N*,*N*'-dimethylribaramide

C(1)-O(1)	1.247(2)
C(1)-N(1)	1.320(3)
C(1)-C(2)	1.524(3)
C(2)-O(2)	1.416(2)
C(2)-C(3)	1.529(3)
C(2)-H(2)	1.0000
C(3)-O(3)	1.432(2)
C(3)-C(4)	1.518(3)
C(3)-H(4)	1.0000
C(4)-O(4)	1.416(2)
C(4)-C(5)	1.522(3)
C(4)-H(6)	1.0000
C(5)-O(5)	1.247(2)
C(5)-N(2)	1.319(3)
C(6)-N(1)	1.461(3)
C(6)-H(9A)	0.9800
C(6)-H(9B)	0.9800
C(6)-H(9C)	0.9800
C(7)-N(2)	1.457(3)
C(7)-H(10A)	0.9800
C(7)-H(10B)	0.9800
C(7)-H(10C)	0.9800
N(1)-H(1)	0.84(3)
N(2)-H(8)	0.87(3)
O(2)-H(3)	0.8400
O(3)-H(5)	0.8400
O(4)-H(7)	0.8400
O(1S)-H(1S)	0.81(3)
O(1S)-H(2S)	0.91(4)
O(1)-C(1)-N(1)	123.4(2)
O(1)-C(1)-C(2)	119.76(18)

Table 5.26 Cont. Bond lengths [Å] and angles [°] for *N*,*N*'-dimethylribaramide

N(1)-C(1)-C(2)	116.85(18)
O(2)-C(2)-C(1)	109.91(15)
O(2)-C(2)-C(3)	107.63(15)
C(1)-C(2)-C(3)	108.22(16)
O(2)-C(2)-H(2)	110.3
C(1)-C(2)-H(2)	110.3
C(3)-C(2)-H(2)	110.3
O(3)-C(3)-C(4)	110.58(15)
O(3)-C(3)-C(2)	108.35(15)
C(4)-C(3)-C(2)	113.40(17)
O(3)-C(3)-H(4)	108.1
C(4)-C(3)-H(4)	108.1
C(2)-C(3)-H(4)	108.1
O(4)-C(4)-C(3)	109.23(16)
O(4)-C(4)-C(5)	113.00(16)
C(3)-C(4)-C(5)	112.46(16)
O(4)-C(4)-H(6)	107.3
C(3)-C(4)-H(6)	107.3
C(5)-C(4)-H(6)	107.3
O(5)-C(5)-N(2)	123.97(19)
O(5)-C(5)-C(4)	118.68(18)
N(2)-C(5)-C(4)	117.26(17)
N(1)-C(6)-H(9A)	109.5
N(1)-C(6)-H(9B)	109.5
H(9A)-C(6)-H(9B)	109.5
N(1)-C(6)-H(9C)	109.5
H(9A)-C(6)-H(9C)	109.5
H(9B)-C(6)-H(9C)	109.5
N(2)-C(7)-H(10A)	109.5
N(2)-C(7)-H(10B)	109.5
H(10A)-C(7)-H(10B)	109.5
N(2)-C(7)-H(10C)	109.5

Table 5.26 Cont. Bond lengths [Å] and angles [°] for *N,N'*-dimethylribaramide

H(10A)-C(7)-H(10C)	109.5
H(10B)-C(7)-H(10C)	109.5
C(1)-N(1)-C(6)	122.8(2)
C(1)-N(1)-H(1)	116.7(18)
C(6)-N(1)-H(1)	119.1(18)
C(5)-N(2)-C(7)	123.23(18)
C(5)-N(2)-H(8)	116.0(17)
C(7)-N(2)-H(8)	120.8(17)
C(2)-O(2)-H(3)	109.5
C(3)-O(3)-H(5)	109.5
C(4)-O(4)-H(7)	109.5
H(1S)-O(1S)-H(2S)	104(3)

Table 5.27 Anisotropic displacement parameters ($Å^2 x\ 10^3$) for *N,N'*-dimethylribaramide. The anisotropic displacement factor exponent takes the form: $-2^2[h^2 a^{*2} U^{11} + ... + 2 h k a^* b^* U^{12}]$

U^{11}	U^{22}	U^{33}	U^{23}	U^{13}	U^{12}	
C(1)	31(1)	23(1)	23(1)	-1(1)	10(1)	0(1)
C(2)	29(1)	18(1)	20(1)	-1(1)	8(1)	2(1)
C(3)	30(1)	18(1)	18(1)	1(1)	8(1)	3(1)
C(4)	31(1)	19(1)	22(1)	-1(1)	13(1)	-1(1)
C(5)	27(1)	21(1)	24(1)	-1(1)	11(1)	-5(1)
C(6)	34(2)	65(2)	60(2)	-28(2)	-2(1)	13(1)
C(7)	30(1)	35(1)	28(1)	4(1)	7(1)	2(1)
N(1)	30(1)	36(1)	37(1)	-14(1)	7(1)	4(1)
N(2)	29(1)	26(1)	22(1)	-1(1)	8(1)	0(1)
O(1)	35(1)	30(1)	30(1)	-10(1)	5(1)	4(1)
O(2)	35(1)	21(1)	22(1)	3(1)	10(1)	1(1)

Table 5.27 Cont. Anisotropic displacement parameters ($Å^2 x\ 10^3$) for *N,N'*-dimethylribaramide. The anisotropic displacement factor exponent takes the form: $-2\pi^2[h^2 a^{*2} U^{11} + ... + 2 h k a^* b^* U^{12}]$

	U^{11}	U^{22}	U^{33}	U^{23}	U^{13}	U^{12}
O(3)	39(1)	20(1)	19(1)	1(1)	8(1)	2(1)
O(4)	36(1)	20(1)	28(1)	-8(1)	12(1)	-3(1)
O(5)	38(1)	28(1)	26(1)	-2(1)	14(1)	7(1)
O(1S)	39(1)	36(1)	32(1)	1(1)	15(1)	8(1)

Table 5.28 Torsion angles [°] for *N,N'*-dimethylribaramide.

O(1)-C(1)-C(2)-O(2)	45.5(2)
N(1)-C(1)-C(2)-O(2)	-135.27(19)
O(1)-C(1)-C(2)-C(3)	-71.7(2)
N(1)-C(1)-C(2)-C(3)	107.5(2)
O(2)-C(2)-C(3)-O(3)	-176.53(14)
C(1)-C(2)-C(3)-O(3)	-57.79(19)
O(2)-C(2)-C(3)-C(4)	60.3(2)
C(1)-C(2)-C(3)-C(4)	179.04(15)
O(3)-C(3)-C(4)-O(4)	-69.95(19)
C(2)-C(3)-C(4)-O(4)	52.0(2)
O(3)-C(3)-C(4)-C(5)	163.76(15)
C(2)-C(3)-C(4)-C(5)	-74.3(2)
O(4)-C(4)-C(5)-O(5)	-177.16(16)
C(3)-C(4)-C(5)-O(5)	-52.9(2)
O(4)-C(4)-C(5)-N(2)	6.2(2)
C(3)-C(4)-C(5)-N(2)	130.39(19)
O(1)-C(1)-N(1)-C(6)	4.6(4)
C(2)-C(1)-N(1)-C(6)	-174.6(2)
O(5)-C(5)-N(2)-C(7)	0.9(3)
C(4)-C(5)-N(2)-C(7)	177.44(17)